Phenomenology Of Sterile Neutrinos At Different Mass Scales: Neutrinoless Double Beta Decay And Neutrino Oscillations

CHAN FAI WONG

Phenomenology Of Sterile Neutrinos At Different Mass Scales:

Neutrinoless Double Beta Decay And Neutrino Oscillations

Student: Chan-Fai Wong

Institute for Particle Physics Phenomenology, Durham University

A thesis submitted for the degree of Doctor of Philosophy

Supervisor: Silvia Pascoli

September 11, 2012

Abstract

The existence of neutrino oscillation is the first evidence of physics beyond the Standard Model. It proves that neutrinos are massive and motivates the study of the neutrino nature, mixings and mass generation models. To have a better understanding of neutrino masses and mixings, the existence and character of sterile neutrinos would be an important factor. In this thesis, we will describe the phenomena of neutrinoless double beta decay and sterile neutrino oscillations. The studies of these two topics will contribute to understanding the properties of sterile neutrinos in the heavy and light mass regime.

We first study the neutrinoless double beta decay process to tackle the issue about the nature of neutrino. Establishing the nature of neutrinos, whether they are Dirac or Majorana particles is one of the fundamental questions we need to answer in particle physics, and is related to the conservation of lepton number. Neutrinoless double beta decay ($(\beta\beta)_{0\nu}$) is the tool of choice for testing the Majorana nature of neutrinos. However, up to now, this process has not been observed, but a wide experimental effort is taking place worldwide and soon new results will become available.

Different mechanisms can induce $(\beta\beta)_{0\nu}$-decay and might interfere with each other, potentially leading to suppressed contributions to the decay rate. This possibility would become of great interest if upcoming neutrino mass measurements from KATRIN and cosmological observations found that $m_\nu > 0.2$ eV but no positive signal was observed in $(\beta\beta)_{0\nu}$-decay experiments. We focus on the possible interference between light Majorana neutrino exchange with other mechanisms, such as heavy sterile neutrinos and R-parity violating supersymmetric models. We show that in some cases the use of different nuclei would allow to disentangle the different contributions and allow to test the hypothesis of destructive interference. Finally, we present a model in which such interference can emerge and we discuss the range of parameters which would lead to a significant suppression of the decay rate.

Heavy sterile neutrino is involved in the studies of neutrinoless double beta decay and mass generation involve. On the other hand, the effect of light sterile neutrino may be present in the oscillation experiments. To measure the light sterile neutrino mixing, high statistics measurements are necessary. A neutrino factory has been suggested as a powerful tool for

studying new physics, for example, sterile neutrinos, exploiting its near detectors. Here, we use the new version of GLoBES to study the potential of a low energy neutrino factory (LENF) in constraining the sterile mixing angles and the mass-square difference. Unlike in conventional long baseline neutrino experiments, the $\nu_\mu \to \nu_e$ and $\nu_e \to \nu_e$ channels are also included, since they have been proved helpful in constraining some of the mixing angles.

We will explore the dependence of the performance of the LENF depending on different experimental setups, such as the detector type (TASD and LiAr), the energy range, the systematic errors. etc. Moreover, the re-analysis of reactor neutrino experiments suggests the presence of neutrino oscillations due to large sterile neutrino mixing with ν_e. We show that, with a near detector, LENF can constrain the sterile parameter values in a very small range and helps us to check the recent Reactor Anomaly.

Declaration

This thesis is the result of my own work as a research student at Durham University, except where explicit reference is made to the work of others. This work has not been submitted for any other degree at the University of Durham or any other University.

The research in Chapter 3 was carried out in collaboration with Jacobo Lopez-Pavon and Silvia Pascoli, both in the Department of Physics at the Durham University, and this work will be submitted for publication at a later date.

The work in Chapter 4 was carried out in collaboration with Silvia Pascoli, has been presented in '24th Rencontres de Blois—Particle Physics and Cosmology" and will later be submitted for publication.

The work in Chapter 5 and 6 was carried out in collaboration with Silvia Pascoli and will be submitted for publication later.

Acknowledgements

Getting the doctoral degree would not have been possible without the assistance and encouragement of my supervisor, colleagues and friends. I am sincerely grateful to them.

First, I would like to thank my supervisor, Silvia Pascoli, for offering me such a great opportunity to work with her in such a wonderful institute. I sincerely appreciate her supervision, great enthusiasm, patience, guidance, and help. Besides physics, she also has given me suggestions for the right attitude to do research. It is really enjoyable working with her. I would also like to thank my collaborator, Jacobo Lopez-Pavon, for inspiration and invaluable suggestions for my work in 'Neutrinoless Double Beta Decay'. Through the discussion with Silvia and Jacobo, my passion for particle physics and understanding on neutrino physics have been brought up to a level that I could not have reached on my own.

Then I have to thank Professor Chong Sun Chu and Professor Lin Guey Lin, for the encouragements and suggestions for my career. I would also like to thank my colleagues here at the Department of Physics, for contributing to the friendly environment which has made my time here enjoyable.

Finally I want to thank my friends in UK, Macau, Taiwan and my family for years of unending encouragement, heartening words and incalculable practical support. I would like to share with my family and my friends my pleasure of finishing up this thesis.

Contents

Chapter 1

Introduction

Neutrinos are the Standard Model particles about which we have the least information, despite being the most abundant in the Universe. They hardly interact with other particles and therefore their observation requires very specific experiments and detectors.
In the past 15 years, our understanding of neutrinos has changed dramatically. Thanks to neutrino oscillation experiments, it has been shown that neutrinos have non-zero masses. The first model-independent indication of neutrino oscillation was announced by the Super-Kamiokande collaboration in 1998 [1], after several indications of an "atmospheric neutrino anomaly" were reported by Kamiokande [2], IMB [3], Soudan-2 [4] etc. On the other hand, the solar neutrino experiments like Homestake [5], Super-Kamiokande [1], SAGE [6], GALLEX [7] and SNO [8] also reported deficits with respect to the predictions of the standard solar model. All these experiments imply that neutrinos oscillate, i.e. they can change from one flavour to another while traveling. In all these experiments, neutrinos are produced and detected via charged current weak interactions, i.e. they are detected in the flavour eigenstates. Neutrino oscillation occurs because, due to mixing, the neutrinos produced in the experiments are superpositions of massive eigenstates, which propagate in space with different phases. At detection, there will be a different superposition of massive states and conversion from one flavour to another will be possible. This concept was first proposed in 1957 by Pontecorvo [9], 30 years before the oscillation experiments.

Besides the experiments mentioned above, the LSND experiment [10, 11] also suggests the existence of neutrino oscillation. However, it provokes the unsettled question in neutrino physics beyond the Standard Model: the number of neutrino species. Standard Model expects that there are only three light neutrinos, but the data of LSND suggest that there may exist four or even more light neutrinos. More details about the LSND anomaly will be discussed later.

The origin of neutrino masses has emerged as one of the hot topics in neutrino physics after the observations of neutrino oscillation. Previously, neutrinos were thought to be massless, according to the Standard Model of electroweak interactions, but the existence of neutrino oscillations implies that the mass eigenstates of neutrinos exist. The explanation of non-zero neutrino mass requires new physics beyond the Standard Model. In the minimal extension of the Standard Model, one can introduce a right-handed neutrino field, which will couple with the left-handed leptonic doublet and the Higgs. Once the Higgs field obtains a vacuum expectation value, a Dirac mass term for the neutrinos is produced. This mass term is analogous to the one of the other fermions and there is no special reason why the right-handed neutrino is not introduced. Previously, the Standard Model did not include right-handed neutrinos just in order to avoid neutrino masses. However, simply introducing right-handed ν cannot naturally explain the lightness of neutrinos. In fact, one of the compelling questions concerning the mass of neutrinos is why neutrino masses are so small, a few orders smaller than any other fermion of the Standard Model. A natural explanation can be obtained by introducing heavy extra neutrinos, which are not included in the Standard Model. According to the traditional model of ν mass generation (Seesaw Mechanism), the mass scale of the heavy neutrino could be as large as 10^{15} GeV, which is much heavier than any other elementary particle. Light neutrino masses emerge thanks to the coupling of these heavy neutrinos to the Standard Model ones. Other mechanisms of neutrino mass generation are also possible, which might require new physics at different scales, such as TeV scale (R-parity violation, inverse see-saw models, see-saw type II and others). Thus, the existence of neutrino masses will possibly lead to a new direction in particle physics. This will be discussed in detail in the rest of this chapter.

The neutrino mass generation is closely related to the question about the nature of neutrino and of the fundamental symmetries of particle interactions. In Seesaw models, neutrinos are Majorana particles, which means that neutrinos are indistinguishable from anti-neutrinos. This implies the existence of Lepton Number Violation (LNV), which is beyond the expectation of the Standard Model and is crucial in explaining the origin of the matter-antimatter asymmetry in the Early Universe. Thus, the nature of the neutrino and the possibility of LNV are crucial issues in neutrino physics. The conspicuous consequence of the existence of Majorana neutrino is neutrinoless double beta decay ($(\beta\beta)_{0\nu}$), which will be described in detail in subsequent chapters.

Besides the neutrino oscillation, neutrino mass generation and nature of neutrino, **sterile neutrino** is the other topic which is important in neutrino physics. As just mentioned, the

LSND anomaly suggests that there may exist more than three species of neutrinos. The result of LSND experiment reports the value of Δm^2 is around 1 eV^2, which is much larger than the Δm^2 measured by the atmospheric and solar neutrino experiments. If the data of LSND are correct, than there should exist at least three Δm^2 and four light neutrinos. Previously, the measurement of Z fermionic decay widths in LEP-SLC experiment determined that the number of light species $N_\nu = 2.9841 \pm 0.0083$ [12]. However, the LSND experiment suggests that other neutrino species may exist. Moreover, the neutrino mass generation model also predicts the existences of heavy extra neutrinos. If extra neutrinos really exist, they must not have significant interactions with W and Z, hence they are difficult to be detected and called 'sterile neutrinos'. The historical profile and the properties of sterile neutrinos will be discussed in *Chapter 2*.

Physics beyond the simple three neutrino picture has become an important topic for particle physics. This thesis is intended as an investigation of the roles of sterile neutrinos at different mass scales. This would involve the issues about the nature of neutrino and the light neutrino oscillation. The rest of this chapter will put the main work of this thesis into context by discussing neutrino oscillation, neutrino nature and neutrino mass generation models, and then briefly describe the experimental progress of these issues. At the end of the chapter, we will provide an outline of the remainder of the thesis.

1.1 Neutrino Oscillation

Neutrino oscillation is a quantum mechanical phenomenon, which is generated by the interference of the neutrino mass eigenstates. The very reason of neutrino oscillation is because the flavour states (the states interacting with other Standard Model particles) do not coincide with the mass states (the states propagating). The transformation relating the flavour and mass eigenstates can be written as

$$|\nu_\alpha\rangle = \sum_k U_{\alpha k} |\nu_k\rangle,$$

where $\alpha = e, \mu, \tau$, denotes the active neutrino flavours and k denotes the light mass eigenstates. Before sterile neutrinos are taken into account, the number of flavour states and light mass states considered here are assumed to be three, and U is a 3×3 unitary matrix ($UU^\dagger = 1$) which is called the Pontecorvo-Maki-Nakagawa-Sakata (PMNS) matrix [13]. In the three

neutrino mass scheme, the mixing can be expressed as

$$\begin{pmatrix} \nu_e \\ \nu_\mu \\ \nu_\tau \end{pmatrix} = \begin{pmatrix} U_{e1} & U_{e2} & U_{e3} \\ U_{\mu 1} & U_{\mu 2} & U_{\mu 3} \\ U_{\tau 1} & U_{\tau 2} & U_{\tau 3} \end{pmatrix} \begin{pmatrix} \nu_1 \\ \nu_2 \\ \nu_3 \end{pmatrix}$$
$$= \begin{pmatrix} c_{12}c_{13} & s_{12}c_{13} & s_{13}e^{i\delta} \\ -s_{12}c_{23} - c_{12}s_{23}s_{13}e^{-i\delta} & c_{12}c_{23} - s_{12}s_{23}s_{13}e^{-i\delta} & s_{23}c_{13} \\ s_{12}s_{23} - c_{12}c_{23}s_{13}e^{-i\delta} & c_{12}s_{23} - s_{12}c_{23}s_{13}e^{-i\delta} & c_{23}c_{13} \end{pmatrix} \begin{pmatrix} e^{-i\phi_1} & 0 & 0 \\ 0 & e^{-i\phi_2} & 0 \\ 0 & 0 & 1 \end{pmatrix} \begin{pmatrix} \nu_1 \\ \nu_2 \\ \nu_3 \end{pmatrix}, \tag{1.1}$$

where $s_{ij} \equiv \sin\theta_{ij}$, $c_{ij} \equiv \cos\theta_{ij}$. The angles θ_{ij} characterise the mixing between massive and flavour states. δ is the CP-phase (for antineutrinos the mixing is described by U^*.). CP violation takes place if δ does not equal 0 or π. On the other hand, ϕ_1 and ϕ_2 are the Majorana CP phases, which will not play any roles in neutrino oscillations.

Now we are going to investigate the propagation of the flavour states, keeping in mind that the flavour state is a superposition of different mass states. According to the Schrodinger equation, in vacuum, the massive state $|\nu_k\rangle$ evolves in time as

$$i\frac{d}{dt}|\nu_k\rangle = \hat{H}|\nu_k\rangle = E_k|\nu_k\rangle,$$
$$|\nu_k\rangle(t) = e^{-iE_k t}|\nu_k\rangle.$$

Here, $\hat{H}$ is the Hamiltonian operator in vacuum. Therefore, at time t, the evolution of the initial flavour state $|\nu_\alpha\rangle$ is given by

$$|\nu_\alpha\rangle(t) = \sum_k U_{\alpha k} e^{-iE_k t}|\nu_k\rangle.$$

From the equation above, the probability of neutrino oscillation from flavour α to flavour β can be derived and is given by

$$P_{\nu_\alpha \to \nu_\beta} = \delta_{\alpha\beta} - 4\sum_{k>j} \mathrm{Re}[U_{\alpha k}U^*_{\beta k}U^*_{\alpha j}U_{\beta j}]\sin^2(\frac{\Delta m^2_{kj}L}{2E}) + 2\sum_{k>j} \mathrm{Im}[U_{\alpha k}U^*_{\beta k}U^*_{\alpha j}U_{\beta j}]\sin(\frac{\Delta m^2_{kj}L}{2E}) \tag{1.2}$$

where $\Delta m^2_{kj} = m^2_k - m^2_j$ is the neutrino mass square difference and $\Phi \equiv \dfrac{\Delta m^2_{kj}L}{2E}$ is the oscillation phase. The details of this derivation are reported in Appendix A..

The equation above shows that the measurement of oscillation probabilities can give information about the mixing matrix [consisting of the mixing angles θ_{kj} and the CP phase δ, as shown in Eq. (1.1)] and the mass square differences. It is noteworthy that the measurements of the oscillation parameters also depend on the values of E and L. The ratio of L/E is

the key factor in the oscillation measurements. If L/E is small, then the terms with small Δm^2 will become insignificant, as the oscillation phase Φ will become too small to produce any measurable oscillation effects; on the contrary, large L/E would lead to large Φ, which means the resolution of the detector is not good enough to detect such fast oscillation, and the value of $\sin^2\left(\frac{\Delta m^2_{kj}L}{2E}\right)$ will average 1/2. Therefore, it is necessary to have different oscillation experiments with different energy scales and baselines to effectively measure all the oscillation parameters.

In this thesis, we are particularly interested in a proposed program of neutrino oscillation measurement, i.e. neutrino factory, which will be described in *Section 1.4* of this chapter and used to study the sterile ν oscillation in *Chapter 5 and 6*. The values of the active neutrino oscillation parameters have been measured by a lot of experiments. We will briefly introduce these oscillation experiments in *Section 1.4*. The global neutrino oscillation data from the current measurements can be summarised as Table. 1.1.

Table 1.1 Neutrino oscillation parameters summary [14, 15][1]. For Δm^2_{31}, $\sin^2\theta_{23}$, the upper (lower) row corresponds to normal (inverted) neutrino mass hierarchy.

mass squared difference	best fit $\pm$ 1 σ	mixing angles	best fit $\pm$ 1σ
Δm^2_{21}	$7.54^{+0.26}_{-0.22} \times 10^{-5}$ eV^2	$\sin^2\theta_{12}$	$0.307^{+0.018}_{-0.016}$
Δm^2_{31}	$2.43^{+0.06}_{-0.1} \times 10^{-3}$ eV^2	$\sin^2\theta_{23}$	$0.386^{+0.024}_{-0.021}$
	$2.42^{+0.07}_{-0.11} \times 10^{-3}$ eV^2		$0.392^{+0.039}_{-0.022}$
		$\sin^2 2\theta_{13}$	$0.092 \pm 0.016(\text{stat}) \pm 0.005(\text{sys})$

Δm^2_{21} is called as solar mass-squared difference since it affects the oscillations relevant in solar neutrino experiments, while Δm^2_{31} is the atmospheric mass-squared difference and is measured by the atmospheric neutrino experiments.

Table 1.1 shows that the values of Δm^2_{31} and $\sin^2\theta_{23}$ depend on the neutrino mass hierarchy, or, the sign of Δm^2_{31}. At this moment, we are still not sure if Δm^2_{31} is positive or negative. Thus the ordering of neutrino mass states is not known yet. **Normal Hierarchy** corresponds to positive Δm^2_{31} with ν_1 as the lightest mass state. **Inverted Hierarchy** corresponds to negative Δm^2_{31} with ν_3 as the lightest mass state. They are described diagrammatically in Fig. 1.1.

At present, there are still a lot of open questions about neutrino oscillations: (1) The CP phase δ, which is related to CP-invariance, i.e. whether $P_{\nu_\alpha\to\nu_\beta} = P_{\bar{\nu_\alpha}\to\bar{\nu_\beta}}$;
(2) The precise value of θ_{13}, which is smaller than θ_{12} and θ_{23}. Recently the oscillation exper-

[1]Except θ_{13}, the values of all other parameters are from Ref. [14]. The value of θ_{13} corresponds to the recent result of the Daya-Bay Experiment [15].

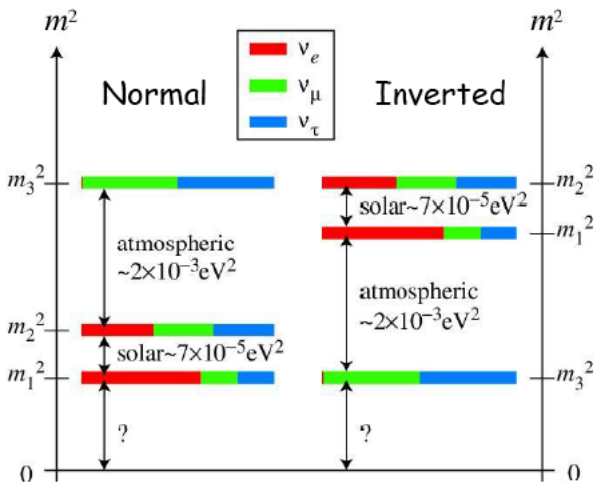

Figure 1.1: The Normal and Inverted Hierarchy of neutrino (taken from Ref. [16]).

iments Tokai-to-Kamioka (T2K) [17], Main Injector Neutrino Oscillation Search (MINOS) [18], Daya Bay [15] and RENO [19] have measured a non-zero θ_{13}. The implication and precise measurement of large θ_{13} is still important for neutrino physics [20];
(3) The precision measurement of θ_{23}, which is the other goal of long baseline experiments. Table 1.1 shows that the atmospheric mixing angle (θ_{23}) is nearly 45°, which means that $\sin^2 2\theta_{23} \approx 1$. This is the 'maximal mixing problem' in neutrino oscillation. The deviation of θ_{23} from its maximal value (45°) is related to the model of neutrino mass matrix [21, 22]. More experiments and effort are still necessary for verifying the value of the atmospheric angle.
(4) The neutrino mass hierarchy problem, which is mentioned above. Neutrino oscillations in matter are sensitive to the sign of Δm^2_{31}. This parameter has important theoretical implications and consequences for neutrinoless double beta decay, which will be discussed in Chapter 4.
(5) The number of light neutrino species, which may be > 3 if there exist light sterile neutrinos. Chapter 2 will discuss this issue more in detail. The sterile ν measurements are referred to *Chapters 5 and 6*.

1.2 Neutrino Nature and $(\beta\beta)_{0\nu}$-Decay

All known fundamental fermions, except neutrinos, must be Dirac particles (which means that the particle could be distinguished from its anti-particle) since they are charged particles and their anti-particles must have opposite charges. On the other hand, neutrinos do

not carry any electric charge, therefore they may be Majorana spinors, which means that a neutrino is equivalent to its anti-neutrino, hence Lepton Number Violation (LNV) exists. If this is true, the fundamental distinction between neutrino and anti-neutrino has to be abandoned. LNV may create an imbalance between matter and anti-matter in the early universe and consequentially explain the excess of matter today. Therefore, the study of neutrino nature may be necessary to explain our existence.[2]

After the discovery of neutrino oscillation, the search of the nature of neutrino has gained new momentum. It has been shown that the observation of neutrinoless double beta decay [$(\beta\beta)_{0\nu}$-decay] will prove the Majorana nature of neutrinos [24]. This process, (A,Z) $\rightarrow$ (A,Z+2) + 2 e^-, happens in middle-heavy to heavy nuclei, which have large binding energies and ordinary (single) β decay is energetically forbidden [25, 26]. Obviously, in this process, the lepton number of L.H.S. is different with R.H.S. This means that the existence of $(\beta\beta)_{0\nu}$-decay implies LNV. The Feynman diagram of this process is shown in Fig. 1.2.

Moreover, $(\beta\beta)_{0\nu}$-decay is also related to the estimation of the absolute value of neutrino

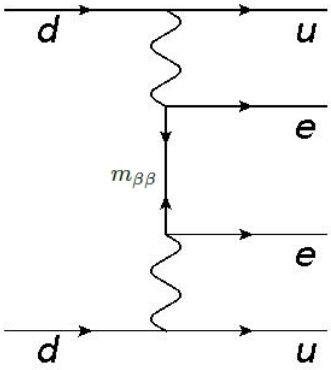

Figure 1.2: Feynman diagram of $(\beta\beta)_{0\nu}$-decay.

mass, as we are going to show in the following:
Here we denote a Majorana field by $\chi(x)$. Similar to the Dirac field $\psi(x)$, $\chi(x)$ has to obey the Dirac equation and the following equation,

$$\langle 0|T[\chi(x)\bar{\chi}(y)]|0\rangle = i\int \frac{d^4p}{(2\pi)^4}\frac{p_\mu\gamma^\mu + m}{p^2 - m^2}e^{ip(x-y)}, \tag{1.3}$$

but $\chi(x)$ also satisfies the Majorana condition,

$$\chi^c = \chi,$$

where $\chi^c = C\bar{\chi}^T$ is the charge conjugate of the field χ, and C is the charge conjugation operator. As we work with the *Weyl representation*, $C = i\gamma^2\gamma^0$, thus $\chi^c = i\gamma^2\chi^*$. Charge

[2]However, it has been shown that Dirac neutrino can also produce the leptogenesis and matter asymmetry [23].

conjugation implies 'changing the sign of the charge', i.e. converts a particle of a given helicity to an anti-particle with the same helicity. This implies that we can rewrite a Majorana propagator as:

$$\langle 0|T[\chi(x)\bar{\chi^c}(y)]|0\rangle = \langle 0|T[\chi(x)\chi^T(y)]|0\rangle,$$

thus if neutrino is a Majorana particle, the propagator in Fig. 1.2 can be rewritten as

$$\begin{aligned}
\langle 0|T[\nu_{eL}(x)\nu_{eL}^T(y)]|0\rangle &= \frac{1-\gamma_5}{2}\sum_k (U_{ek})^2\langle 0|T[\chi_k(x)\chi_k^T(y)]|0\rangle\left(\frac{1-\gamma_5}{2}\right)^T, \\
&= -\frac{1-\gamma_5}{2}\sum_k (U_{ek})^2\langle 0|T[\chi_k(x)\bar{\chi_k}(y)]|0\rangle C\frac{1-(\gamma_5)^T}{2}, \\
&= -\frac{1-\gamma_5}{2}\sum_k (U_{ek})^2 i\int \frac{d^4p}{(2\pi)^4}\frac{p_\mu\gamma^\mu + m_k}{p^2-m_k^2}e^{ip(x-y)}\frac{1-\gamma_5}{2}C, \\
&\qquad\qquad\qquad\qquad\qquad\qquad \text{[from Eq. (1.3)]} \\
&= -i\sum_k (U_{ek})^2\int \frac{d^4p}{(2\pi)^4}\frac{m_k}{p^2-m_k^2}e^{ip(x-y)}\frac{1-\gamma_5}{2}C, \\
&\propto \sum_k (U_{ek})^2 m_k, \qquad (1.4)
\end{aligned}$$

where we have used $(1-\gamma_5)p_\mu\gamma^\mu(1-\gamma_5) = 0$ and $(1-\gamma_5)m_k(1-\gamma_5) = m_k(1-\gamma_5)$. More details about the calculation of $(\beta\beta)_{0\nu}$-decay can be found in *Appendix B*.

The calculation above shows that the decay rate is proportional to the square of effective light neutrino mass $|\langle m_\nu\rangle| \equiv \sum_k^{\text{light}}(U_{ek})^2 m_k$. Thus by measuring the decay rate of neutrinoless double beta decay, we not only prove the Majorana nature of neutrino, but also are able to measure the absolute value of neutrino mass. Therefore, the study of $(\beta\beta)_{0\nu}$-decay plays an important role in neutrino physics.

However, also because of the smallness of the effective neutrino mass (or the cancellation between different mechanisms), the amplitude of this process is very small and it has not yet been observed. Neither can we identify the underlying mechanism of the process, but a wide experimental programs are under way [27], including GERDA [28, 29], CUORE [30, 31], MAJORANA [32, 33], SuperNEMO [34, 35] and EXO [36, 37]. Different experiments use various nuclei to induce the neutrinoless double beta decay, but all of them are expected to achieve the sensitivity of measuring the effective neutrino mass, $|\langle m_{\beta\beta}\rangle| = |\langle m_\nu\rangle| \equiv \sum_k^{\text{light}}(U_{ek})^2 {m_k}^3$, around 10-100 meV. More details of the neutrinoless double beta decay will be discussed in

[3] In *Chapter 4*, $|\langle m_{\beta\beta}\rangle|$ will be redefined as what we measured in the experiments only, but we always define $|\langle m_\nu\rangle|$ as the effective light neutrino mass ($\sum_k^{\text{light}}(U_{ek})^2 m_k$) in the whole thesis.

Chapters 3 and 4.

The other reason for the importance of the Majorana nature of neutrino is that it affects the model of neutrino mass generation. It is straightforward to obtain a Dirac mass term $m_D(\bar{\nu_L}\nu_R + h.c.)$ for a neutrino by including the right-handed neutrino ν_R, just like the treatment for other fermions through Yukawa couplings to the Higgs doublet in standard model. However, as ν_R is a gauge singlet, there is no reason to forbid the Majorana mass term $M\bar{\nu_R}\nu_R$, which suggests the existence of Majorana neutrinos. In fact, as we are going to discuss in the next section, the Type I Seesaw Mechanism predicts the existence of the Majorana neutrino and expects that the Majorana mass term can naturally explain the lightness of active neutrinos. Therefore, the observation of $(\beta\beta)_{0\nu}$-decay or other LNV processes will put Seesaw in favour.

1.3 Neutrino Mass Generation

The Standard Model contains left and right chiral projections of all fermions except neutrinos. This seems unnatural, especially after the presence of neutrino masses is revealed. The simplest way to introduce neutrino masses without violating the Standard Model, is to add right-handed neutral fields that correspond with every charged lepton, i.e. three families of right-handed neutrinos. Unlike the active left-handed neutrinos, right-handed neutrinos are singlets under the electro-weak gauge group, since they do not interact with the gauge bosons. Introducing right-handed neutrinos would lead to new Yukawa couplings

$$-\mathcal{L}_Y = Y_{\alpha\beta} H \bar{\psi}_{L\alpha} \nu_{R\beta} + h.c., \tag{1.5}$$

where Y is the new coupling matrix, H is the Higgs multiplet, ψ_L is the lepton doublet[4]. After electro-weak symmetry breaking, $< H > = v/\sqrt{2}$, $M_D = Yv/\sqrt{2}$ is the Dirac mass matrix. If we diagonalise the mass matrix with the relation

$$\begin{aligned} \nu_{Lk} &\equiv \sum_k U_{\alpha k} \nu_{L\alpha}, \\ \nu_{Rk} &\equiv \sum_k V_{\beta k} \nu_{R\beta}, \\ U^\dagger M_D V &= m, \end{aligned}$$

where m is the diagonal mass matrix, Eq. (1.5) can be re-written as

$$-\mathcal{L}_{\text{Dirac}} = \bar{\nu}_{L\alpha} M_{D_{\alpha\beta}} \nu_{R\beta} + h.c. = \bar{\nu}_{Lk} m_{kk} \nu_{Rk} + h.c. = m\bar{\nu}_L \nu_R + h.c. \tag{1.6}$$

[4] $\psi_L = \begin{pmatrix} \nu_{eL} \\ e_L \end{pmatrix}$

The equation above gives the mass term of neutrinos. Therefore, the addition of right-handed ν leads to the generation of the neutrino masses and the model above is simple, since it simply treats neutrino as the other fermions.
However, this scenario cannot explain the lightness of neutrinos. Since $v = \sqrt{2}M_w/g \simeq 174$ GeV, which means that $M_D \sim Y \cdot$ 100 GeV. The cosmological bounds of active neutrinos reveal that neutrino masses are smaller than 1 eV, which means $O(M_D)$ is required to be smaller than 1 eV. In this case, the Yukawa coupling Y has to be $< 10^{-11}$, but there is no good reason why the coupling must be so small in the model. Moreover, this weak coupling implies that right-handed neutrinos are hardly involved in any process or coupling with other particles. Therefore they are not likely to be observed in any collider experiments.

The scenario above assumes neutrinos are Dirac particles. However, as the previous section commented, neutrinos can be Majorana particles and equivalent to their own anti-particles. In this case, the lepton number would be violated; this is beyond the Standard Model. But in the presence of black holes, lepton number or baryon number cannot be an exact symmetry since any lepton (or baryon) dropping into a black hole would just lead to a net change in the number of lepton (baryon) in the universe but nothing else. This means that we cannot define the number of leptons or baryons in our universe. Hence it is not guaranteed that the global lepton symmetry will be respected, and there is no reason to reject the existence of Majorana neutrinos in the mass generation model [38].

If right-handed neutrino is a Majorana particle, then besides the Dirac mass term in Eq. (1.5), there also exist a Majorana mass term,

$$-\mathcal{L}_{\text{Majorana}} = \frac{1}{2}\overline{\nu^c}_{R\alpha} M_{R_{\alpha\beta}} \nu_{R\beta} + h.c. \tag{1.7}$$

Different to ν_L, ν_R is defined as a gauge singlet. It does not carry any color, weak isospin, or hypercharge; the Majorana mass term in the equation above is therefore consistent with the gauge symmetries.
Including both the Dirac and Majorana mass terms, the mass terms of neutrino are given by

$$\begin{aligned} -\mathcal{L}_{\text{Mass}} &= \bar{\nu}_{L\alpha} M_{D_{\alpha\beta}} \nu_{R\beta} + \frac{1}{2}\overline{\nu^c}_{R\alpha} M_{R_{\alpha\beta}} \nu_{R\beta} + h.c. \\ &= \frac{1}{2}\begin{pmatrix} \bar{\nu}_L & \overline{\nu^c}_R \end{pmatrix} \begin{pmatrix} 0 & M_D^T \\ M_D & M_R \end{pmatrix} \begin{pmatrix} \nu_L \\ \nu_R \end{pmatrix} + h.c. \\ &= \bar{\nu} M \nu \end{aligned} \tag{1.8}$$

If the number of left-handed lepton doublets, right-handed neutrino singlets are denoted as n_L, n_R, then M_D is a $(n_R + n_L) \times n_L$ matrix, M_R is a $(n_R + n_L) \times (n_R + n_L)$ matrix. In the

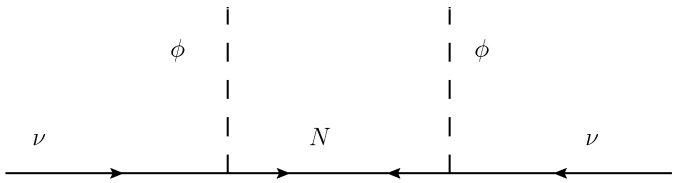

Figure 1.3: Seesaw Mechanism that gives the active (left-handed) neutrino a tiny Majorana mass.

simple case of one generation, $n_L = n_R = 1$, M_D and M_R are just numbers. The eigenvalues of the mass matrix M are then given by

$$m_{1,2} = \frac{1}{2}|M_R \pm \sqrt{4M_D^2 + M_R^2}|.$$

Moreover, $M_D = Yv/\sqrt{2}$, is suppressed by the Yukawa coupling and the symmetry breaking value, but M_R does not carry any gauge quantum number, which means that it would not suffer from any gauge symmetry constraints and could be as large as the unification scale of unified theories. If it is assumed that $M_R \gg M_D$, than the eigenvalues can be rewritten as

$$m_1 \simeq M_D \frac{1}{M_R} M_D, \qquad m_2 \simeq M_R.$$

Generally, it is assumed that $O(M_R) \sim 10^{15}$ GeV, $O(M_D) \sim 100$ GeV. In this case, $m_1 \simeq 10^{-2}$ eV, which is consistent with the present experimental range of active neutrino mass.

This model explains the lightness of active neutrinos and is widely discussed in neutrino physics. It is called Seesaw Mechanism [39, 40], or more specifically, Type I Seesaw. The corresponding Feynman Diagram is shown in Fig. 1.3.

There are also other Seesaw Mechanisms to generate light neutrino masses without relying on the right-handed state ν_R. Depending on the scheme in generating the new heavy intermediate states, there are two more possible Seesaw Mechanisms:
(ii) Type II Seesaw [41, 42], which expands the Standard Model and explains the lightness of neutrinos by the addition of a scalar $SU(2)$ triplet.
(iii)Type III Seesaw [43, 44], by the addition of a fermionic $SU(2)$ triplet.
Since the Type I Seesaw has been studied in depth in the literature, and a detailed discussion of Type II and III Seesaw would be outside of the scope of this thesis. We will focus on the Type I Seesaw in the following discussions.

Besides the traditional Type I, II and III Seesaw Mechanisms, there are also some other models to explain the light neutrino masses. In *Chapter 3*, we will discuss two examples,

Extended Seesaw and trilinear R-parity violation, and study their relationships with **neutrinoless double beta decay**.

1.4 Neutrino Experiments

1.4.1 Experiments for double beta decay

The importance of neutrinoless double beta decay has been mentioned in *Section 1.2*. In this section, the results of current experiments and plans for future experiments will be summarised.

The crucial issue in double beta decay experiments is the suppression of backgrounds. In the past 25 years, the background reduction in the measurements of the two neutrinos mode ($(\beta\beta)_{2\nu}$-decay, see *Appendix C* for more details) has improved greatly. Based on this success, physicists are now focusing on the measurements of the neutrinoless mode ($(\beta\beta)_{0\nu}$-decay).

The sensitivities of $(\beta\beta)_{0\nu}$-decay experiments are always expressed in terms of effective neutrino mass $|< m_{\beta\beta} >|$ since the decay rate $\Gamma \propto |< m_{\beta\beta} >|$ and $|< m_{\beta\beta} >|$ relates to the absolute scale of neutrino mass[5]. Over the past two decades, a wide effort has been made to improve the sensitivity to Γ or $|< m_{\beta\beta} >|$. For the best sensitivity, the detector has to increase the $(\beta\beta)_{0\nu}$-decay count rate and reduce the background, and the source has to be massive in order to produce more events[6]. Various nuclei have been chosen to induce $(\beta\beta)_{0\nu}$-decay in different experiments, but the existence of this process has not been confirmed yet. Table 1.2 lists the best present results on $(\beta\beta)_{0\nu}$-decay measurements [45].

Table 1.2 The best present measurements on the $T_{1/2}$ of $(\beta\beta)_{0\nu}$-decay (except the last experiment, all data taken from Ref. [45]).

Experiments	Isotope	The limit of $T_{1/2}$ (years)
HM	^{76}Ge	$> 1.9 \times 10^{25}$
NEMO-3	^{100}Mo	$> 5.8 \times 10^{23}$
	^{82}Se	$> 2.1 \times 10^{23}$
CUORICINO	^{130}Te	$> 3 \times 10^{24}$
DAMA	^{136}Xe	$> 4.5 \times 10^{23}$
EXO [46]	^{136}Xe	$> 1.6 \times 10^{25}$

Due to the absence of observation in the current/past experiments, next generation and next-to-next generation experiments are being planned. In Table 1.3, five of the most promising

[5] *Chapter 3 and Appendix B* will show why $\Gamma \propto |< m_{\beta\beta} >|$ and the exceptional cases which are involved with new physics.
[6] In most of the double beta decay experiments, the source nuclei are also used as the detector.

and developed experiments are listed [45]. Notice that the values of $< m_{\beta\beta} >$ depend on the values of the common phase space factor and nuclear matrix elements (NMEs), which will be discussed in detail in *Chapters 3 and 4*. Here, all the sensitivities of $< m_{\beta\beta} >$ correspond to the NMEs calculated through Quasiparticle Random Phase Approximation (QRPA) [47]. All experiments are expected to achieve the sensitivity of measuring $< m_{\beta\beta} >$ around 10 -100 meV [27]. The goals and current progresses of these experiments are referred to Refs. [28, 29, 30, 31, 32, 33, 34, 35, 36, 37].

Table 1.3 The next-generation and next-to-next generation neutrinoless double beta decay experiments.

Experiments	Isotope	Mass of Isotope (kg)	Sensitivity of $T_{1/2}$ (years)	Sensitivity of $< m_{\beta\beta} >$ (meV)
CUORE	^{130}Te	200	6.5×10^{26}	20 - 50
			2.1×10^{26}	35 - 90
GERDA	^{76}Ge	40	2×10^{26}	70 - 300
		1000	6×10^{27}	10 - 40
MAJORANA	^{76}Ge	30-60	$1 - 2 \times 10^{26}$	70 - 300
		1000	6×10^{27}	10 - 40
EXO	^{136}Xe	200	6.4×10^{25}	95 - 220
		1000	8×10^{26}	27 - 63
SuperNEMO	^{82}Se	100-200	$1 - 2 \times 10^{26}$	40 - 100

Heidelberg-Moscow experiment

As just mentioned, the observation of $(\beta\beta)_{0\nu}$-decay is still absent. However, a fraction of the Heidelberg-Moscow Collaboration, once claimed that they managed to observe this process and measured the decay rate. The Heidelberg-Moscow experiment, using a large source strength of 11 kg of enriched ^{76}Ge, was run in the Gran Sasso Underground Laboratory (Italy) from 1990 to 2003. After the conclusion of the experiment, part of the collaboration analysed the data and claimed a 4σ evidence for $(\beta\beta)_{0\nu}$-decay with a lifetime $\simeq 1.2 \times 10^{25}$ years, corresponding to $< m_{\beta\beta} >$ of about 0.44 eV [48]. However, the Moscow part of the collaboration disagreed with this result [49], and there are also others who are critical of the measurement [50] since the signal is indeed faint and close to other unexplained peaks. At the moment, the Heidelberg-Moscow "positive" result is not accepted and new experiments are necessary for verifying it.

1.4.2 Experiments for oscillations

The neutrino oscillation probability is basically a sinusoidal function of the ratio $\frac{\Delta m^2 L}{E}$. The transitions to different flavours would be too small to be measured if $\frac{\Delta m^2 L}{E} \ll 1$. On the other hand, if $\frac{\Delta m^2 L}{E} \gg 1$, the probability will be averaged and only the information of the mixing angle can be measured (refer to *subsection 1.1*). Since the value of Δm^2 is fixed by nature, different oscillation experiments choose different values of L/E[7] and aim at measuring different values of Δm^2.

In the following, I list some examples of oscillation experiments:

Solar and atmospheric experiment

The solar neutrino experiments were the first to indicate that neutrino oscillation may exist [5]. The goal of these experiments was to detect the electron neutrinos generated in the core of the Sun. Since the distance between the Sun and Earth is about 1.5×10^8 km, and the energy of solar neutrinos take values up to 10^7 eV, the sensitivity to Δm^2 in these experiments can be as good as $\gtrsim 10^{-12}$ eV^2. Several solar neutrino oscillation experiments have been performed: Homestake in USA [5], SAGE in Russia [6], the GALLEX [7] and GNO [51] in Italy, Kamiokande [2] and Super-Kamiokande [1] in Japan, and SNO in Canada [8]. These experiments are sensitive to the oscillation corresponding to small Δm^2. They can constrain the parameter region of Δm^2_{21}-θ_{12}, but they can not precisely measure the mass square difference when Δm^2 is large.

On the other hand, Δm^2_{31} ($\approx \Delta m^2_{32}$) and θ_{23} are constrained by the atmospheric neutrino experiments. The atmospheric neutrinos are produced from the interactions between cosmic rays and nuclei in the upper atmosphere. Primary cosmic rays collide with the upper layers of the atmosphere and a lot of pions and kaons are produced. These particles will further decay into ν_μ and muons in the atmosphere. A large fraction of these muons will further decay via $\mu^+ \to \bar{\nu_\mu} e^+ \nu_e$ (or $\mu^- \to \bar{\nu_e} e^- \nu_\mu$). The energy of detectable atmospheric neutrinos is in the range of 500 MeV to 100 GeV. The source-detector distance is around 10 km (distance between the upper atmosphere and the Earth's surface) for the neutrinos coming from above, and $\sim 10^4$ km for neutrinos coming from below (these neutrinos travel through the Earth to reach the detector). The typical values of $L/E \precsim 10^4$ km/GeV, and the associated sensitivity to $\Delta m^2 \gtrsim 10^{-4}$ eV^2. The atmospheric experiments include Kamiokande [2],

[7] For solar and atmospheric neutrino experiments, both L and E are fixed. These experiments instead change the size and material of the detector in order to enhance the number of events being detected.

Super-Kamiokande [1], IMB [3] and Soudan-2 [4]. Besides, the MINOS detector is also sensitive to atmospheric neutrinos [52].

Reactor neutrino experiment

The neutrino sources for reactor neutrino experiments are nuclear reactors. In the reactor, electron anti-neutrinos are produced and emitted from the beta decay of radiative products. The energy scale of these experiments is around a few MeV, with flexible baselines. All the reactor neutrino experiments consist of identical near detector and far detector. Both are located deep underground to reduce the background from cosmic muons. The distances of the detectors for the Double Chooz [53], Daya Bay [54] and Reno [19] experiments are around a few hundred meters for near detectors and 1-2 km for far detectors. They are sensitive to Δm^2 around 10^{-3} eV^2 and their goal is to measure the small θ_{13}. On the other hand, there also exists long baseline reactor experiments like KamLAND [55]. The corresponding distance for the far detector is of the order of 100 km, which is sensitive to Δm^2 around 10^{-5} eV^2.

Neutrino factory

Modern accelerator technologies offer the possibility of accumulating 10^{20} - 10^{21} muons per year for the neutrino oscillation experiments. A Neutrino Factory (NF) is a proposed long baseline experiment intended to create a fairly focused beam of neutrinos at one site on the Earth and fire it downwards until the beams resurface at other points. It is expected to be able to precisely measure the mixing angles and matter effects, determine the neutrino mass hierarchy, observe or place limits on CP violation, etc. In this thesis, its ability to measure the sterile neutrino mixing is quantitatively analyzed in *Chapter 5 and 6*.

At NF, muons are produced by pions and stored in a long storage ring which is called a decay straight, as shown in Fig. 1.4. The muons in the decay straight will produce an equal number of muon neutrinos and electron neutrinos. The muon and electron neutrinos will be measured in order to study the oscillation effects. It is also possible to produce and store anti-muons to study the CP-conjugated oscillations.

Since higher energy means higher statistics and better sensitivity for studying neutrino oscillation, the energy scale of NF is proposed to be very high, around 20 - 50 GeV. However, an NF with low energy ($<$ 10 GeV, called LENF) has been proposed and discussed for a few years [56, 57, 58]. It has been shown that LENF can be compared with the high energy factory in measuring active neutrino parameters and there is a significant cost advantage. Recently, a Very Low Energy Neutrino Factory (VLENF; the energy scale is around 2 GeV)

has also been proposed [59]. It is claimed that with a combination of very near detectors (20 meters to a few hundred meters), VLENF can provide excellent sensitivity in measuring eV-scale neutrinos. However, for such considerations, the geometry effect and decoherence effect should be considered. More details are included in *Chapter 5*.

With different energy scales, the detector considerations of NFs are different. Traditionally, a Magnetized Iron Neutrino Detector (MIND) is favored in the high energy neutrino factory. It offers excellent resolution for the high energy scale, and is expected to contribute in avoiding the potential background from pion to muon decay and pion/muon mis-identification. However, it requires a threshold of muon energy, which is about 4 GeV, and it further leads to the loss of ν events for E_μ = 4 - 20 GeV. Thus, it is not favored in the LENF. Generally, LENF is proposed to use a magnetized Totally Active Scintillator Detector (TASD), which is suitable for measuring the charge of low momentum particles, and the corresponding charge mis-identification rate is expected to be negligible ($O(10^{-5})$) for muons above 0.4 GeV/c. Recently, the possibility of constructing a kton scale Liquid Argon Detector (LAr) is also considered [60]. If a large LAr can be magnetized, it could also be used in LENF to detect the neutrino beams. Both TASD and LAr are good at measuring neutrinos with a few GeV and are also supposed to offer good resolution. More discussion about the detector performance and characteristics can be found in Ref. [61].

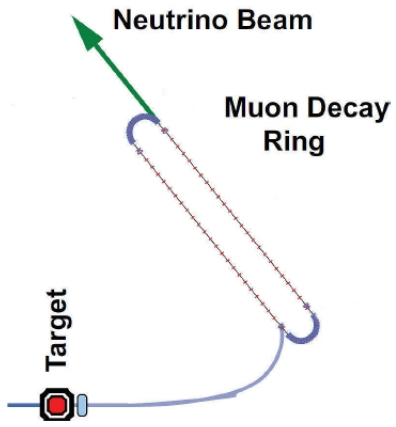

Figure 1.4: Schematic of the neutrino beam production in Neutrino Factory [62].

1.5 Outline Of The Thesis

The previous sections introduced the issues about neutrino oscillations, nature and mass generations. Basically they can all be related to sterile neutrinos. In the rest of this thesis

we will focus the attention on physics involved with sterile neutrinos. We will investigate the roles of sterile neutrinos in the phenomena of neutrinoless double beta decay and neutrino oscillation experiments. Since the mass scales of sterile neutrinos could be from sub eV to the Grand Unified Theory (GUT) scale, they could affect the neutrino phenomena in different ways. In *Chapter 2* we will briefly introduce sterile neutrinos and describe their character in different mass regions.

Then in *Chapter 3 and 4*, the roles of heavy sterile neutrinos in neutrino mass generations and $(\beta\beta)_{0\nu}$-decay will be revealed. *Chapter 3* will discuss the $(\beta\beta)_{0\nu}$-decay in detail and show how do heavy sterile neutrino affect this process. Since the heavy sterile neutrino is closely related to the neutrino mass generation, we can estimate the amplitudes of $(\beta\beta)_{0\nu}$-decay by studying ν mass generation models carefully. Then in *Chapter 4* we will further discuss the possible explanation of absence of observing the $(\beta\beta)_{0\nu}$-decay experimentally. We will make an assumption and analysis how does our assumption affect the future measurements. To make the study of the $(\beta\beta)_{0\nu}$-decay more complete, in *Chapter 3 and 4* we will not only tackle heavy sterile neutrino, but also discuss R-parity violation as the other example of new physics source of the $(\beta\beta)_{0\nu}$-decay.

The role of light sterile neutrinos in neutrino oscillations will be studied in *Chapter 5 and 6*. *Chapter 5* will focus on the simulation of the light sterile neutrino oscillations in Low Energy Neutrino Factory (LENF). The experimental setup and the potential of LENF for measuring sterile neutrinos will be discussed in detail. All the oscillation formulas and simulation results in this chapter correspond to the '3+1' mass scheme. Then in *Chapter 6*, we will extend the study to '3+2' mass scheme and compare the performance of LENF with the Reactor Anomaly [63]. *Chapter 6* will show that LENF is an excellent candidate for verifying the values of sterile oscillation parameters.

At last, we will draw the conclusions of the thesis in *Chapter 7*.

Chapter 2

Sterile Neutrinos with Different Mass Scales

As mentioned in *Chapter 1*, in the framework of the Standard Model, there are only three neutrinos, which correspond to the electron, muon and tau flavor. However, one could naturally imagine additional sterile neutrinos, which are neutral leptons with no ordinary weak interactions except those induced by mixing. They are present in most extensions of the Standard Model, and in principle can have any mass.

Sterile neutrinos do not contribute to the number of active neutrinos determined by the measurement of the decay width of Z boson in LEP-SLC experiment, $N_\nu = 2.9841 \pm 0.0083$ [12]. They only interact with the active neutrinos through mixing. As Fig. 2.1 shows, the existence of sterile neutrinos would modify the typical picture of three-neutrino mixing.

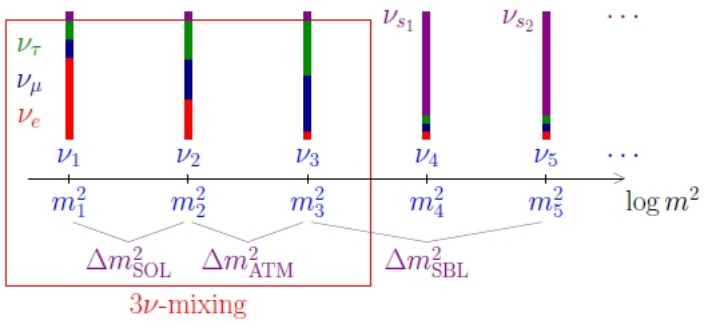

Figure 2.1: The mixing between flavour and mass states of neutrino in presence of sterile neutrinos [64].

If the sterile neutrinos are light, they may have relatively large mixing with active neutrinos

and thus affect the ν oscillation experiments. Actually, light sterile neutrinos ($O(m_s) \sim 0.1$ - 10 eV) have attracted more attention since the LSND experiment [10, 11] announced their data. They observed $\bar{\nu_\mu} \to \bar{\nu_e}$ transitions at very short baseline, which could be explained by ν oscillations in presence of a sterile neutrino. A decade later, the MiniBooNE experiment [65, 66], which is an independent test of the LSND result, also found hints of the existence of sterile neutrinos. Nevertheless, their results suggested that there may exist more than one light sterile neutrino [64]. There are many hints [67, 66, 68] suggesting that the mass scheme may be '3+2' or even '3+3'. Thus, the study of the sterile neutrino and its measurement has become more and more important in neutrino physics.

On the other hand, the mass of sterile neutrinos can also be around TeV or even the GUT scale. As mentioned in the previous chapter, the Seesaw mechanism favours the existence of heavy sterile neutrinos (or heavy neutral leptons), which may also play an important role in cosmology. Sterile neutrinos of mass $\sim$ keV are also one of the dark matter candidates [69]. However, sterile neutrinos whose masses are larger than 100 eV are not involved in the neutrino oscillation phenomenology, since they would lead to very fast oscillation which are averaged over. The observation of 100 eV - 1 MeV sterile neutrinos relies on the β decay spectrum [70], while the extremely heavy (over 1 MeV) neutrinos should be searched through peak searches and heavy neutrino decay [71].

In the rest of this chapter, sterile neutrino will be discussed in two different cases, heavy sterile neutrino (with mass larger than 100 eV) and light sterile neutrino (with mass smaller than 100 eV, involved in oscillation experiments).

2.1 Search of Heavy Sterile Neutrino and Its Mixing with Active Neutrinos

In this section we are going to discuss the phenomenology of heavy neutrinos.

One of the strong theoretical motivation for the existence of heavy neutrinos is the explanation of the lightness of light neutrinos. As mentioned in *Chapter 1*, the Type I Seesaw Mechanism is one of the favoured mechanisms for neutrino mass generation and requires the existences of right-handed partners of the known neutrinos, which gives the light neutrino mass as

$$m_\nu \simeq \frac{m_D^2}{M_R}, \tag{2.1}$$

where M_R is the mass of right-handed neutrino. According to Type I Seesaw, the right-handed neutrino is superheavy ($10^8 - 10^{16}$ GeV) and contributes one class of sterile neutrinos.
With the existence of heavy neutrinos, the mixing relation between the flavour and mass

eigenstates is given by

$$\nu_\alpha = \sum_{k=1}^{3} U_{\alpha k}\nu_k + \sum_{l=4}^{3+n} V_{\alpha l} N_k, \tag{2.2}$$

$$UU^\dagger + VV^\dagger = I, \tag{2.3}$$

where N_k are the heavy neutrinos, $M_N \simeq M_R$. The typical scale of light ν mixing (U) and heavy ν mixing (V) are given by

$$U^\dagger U \approx I,$$
$$V_{\alpha i} = \left(\frac{m_D}{M_N}\right)_{\alpha i} \Rightarrow V^\dagger V \approx \frac{m_\nu}{M_N}, \tag{2.4}$$

Therefore, the heavy ν mixing V is very small in order to generate sub-eV scale m_ν in the typical Seesaw. For example, if there is only one heavy neutrino and no cancellation between different mixing matrix elements, in order to generate 0.1 eV m_ν, Eq. (2.4) will give the following approximation

$$|V_{\alpha 4}| \sim \sqrt{\frac{m_\nu}{M_4}} \lesssim 10^{-6}\sqrt{\left(\frac{100\text{GeV}}{M_4}\right)}. \tag{2.5}$$

If $O(M_4)$ is around $10^8 - 10^{16}$ GeV as typical Seesaw model assumes, the mixing will be very tiny and hardly to be measured in experiments. However, Eq. (2.5) is only a generic bound on the heavy ν mixing. It assumes the absence of cancellations among different contributions to ν masses. Moreover, as we are going to study in this thesis, there are several scenarios in which it is possible to lower the mass scale M_N [or M_R in Eq. (2.1)]. Thus in reality, the bound on the mixing may be weaker than Eq. (2.5).

For simplicity, in the rest of this subsection, we will focus on the case in which only one heavy sterile neutrino is kinematically accessible, which is denoted by N_4. N_4 is expected to hardly interact with other particles, but theoretically it still can indirectly interact with gauge bosons and Higgs through its mixing with the light left-handed neutrinos [72],

$$\mathcal{L}_W = -\frac{g}{\sqrt{2}} V_{l4}\bar{l}\gamma^\mu \frac{1-\gamma_5}{2} N_4 W_\mu^- + h.c.,$$
$$\mathcal{L}_Z = -\frac{g}{2\cos\theta_w} V_{l4}\bar{\nu}_l\gamma^\mu \frac{1-\gamma_5}{2} N_4 Z_\mu + h.c.,$$
$$\mathcal{L}_H = -\frac{g m_{N_4}}{2m_w} V_{l4}\bar{\nu}_l\gamma^\mu \frac{1+\gamma_5}{2} N_4 H^0 + h.c., \tag{2.6}$$

where l represents a charged lepton. Eq. (2.6) shows that the interaction lagrangian of heavy neutrino depends on the mixing V. Therefore, besides the mass m_{N_4}, it is also important to determine the bound on the mixing V in order to study the phenomena of heavy neutrino.

One of the powerful strategies to constrain the heavy neutrino mass and mixing is called 'peak searches'. The mixing of heavy sterile neutrinos with ν_e and ν_μ can be measured in the leptonic decays of pions and kaons [73, 74, 75]. These decays could produce light or heavy neutrino

$$M^+ \to l^+ \nu_l,$$
$$M^+ \to l^+ N_4,$$

where M is the meson, l represents the lepton (e or μ). When a heavy neutrino is produced in the meson decays, the lepton spectrum would show a peak at [73]

$$E_l = \frac{m_M^2 + m_l^2 - m_{N_4}^2}{2m_M},$$

where E_l is the lepton energy. m_l and m_M are the mass of lepton and meson. The branching fraction of this process depends on the mixings U and V,

$$\frac{\Gamma(M^+ \to l^+ N_4)}{\Gamma(M^+ \to l^+ \nu_l)} = \frac{|V_{l4}|^2}{\sum_{k=1}^{3} |U_{lk}|^2} \rho \approx \frac{|V_{l4}|^2}{1} \rho = |V_{l4}|^2 \rho, \tag{2.7}$$

where ρ is the kinematical factor,

$$\rho = \frac{\sqrt{1 + \mu_l^2 + \mu_4^2 - 2(\mu_l + \mu_4 + \mu_l \mu_4)}[\mu_l + \mu_4 - (\mu_l - \mu_4)^2]}{\mu_l (1 - \mu_l)^2},$$
$$\mu_l = m_l^2 / m_M^2, \quad \mu_4 = m_{N_4}^2 / m_M^2.$$

Therefore, the branching ratio of the meson decays provide constraints on N_4 mass and mixing.

Besides the pion [74] and kaon [75] decays, there are also other probes of the mixing of heavy neutrino. Since the main interest of this thesis is neutrinoless double beta decay (and light sterile ν oscillation), in the following, we will focus on the mixing V_{e4}, especially in the mass range $>$ 100 MeV (the nuclear scale of $(\beta\beta)_{0\nu}$-decay). The searches of $V_{\mu 4}$ and $V_{\tau 4}$ are discussed in Ref. [71].

Fig. 2.2 (taken from Ref. [71]) shows the constraints of $|V_{e4}|^2$ versus m_{N_4} for 10 MeV $\leq m_{N4} \leq$ 100 GeV. In this mass range, the beam dump experiments and Z decay experiments could also be used to determine the bound of $|V_{e4}|^2$. The beam dump experiments like 'CHARM' [76], 'PS191' [77] and 'NA3' [78] are used in the mass range 10 MeV - 1 GeV. The experiments for Z decay (DELPHI [79] and L3 [80]) are used in the mass range 1 GeV - 100 GeV. Similar to the pion and kaon deccays, Z decays can also produce light and heavy

neutrinos. Actually, heavy neutrinos would be produced in all processes (whenever kinematically allowed) in which active neutrinos are emitted with the branching ratio proportional to $|V_{l4}|^2$. By determining the decay rates, the bound on the $|V_{e4}|^2$ can be achieved. It is interesting that in reality, the heavy neutrinos could not be detected. The search of heavy neutrinos, relies on the products from the subsequent decays of heavy neutrinos. After the heavy neutrinos are produced in the decays of heavy particles, it would further decay into active neutrinos and other detectable particles. By measuring these subsequent decay products the 'invisible' heavy neutrinos is searched and thus the mixing $|V_{l4}|^2$ is constrained.

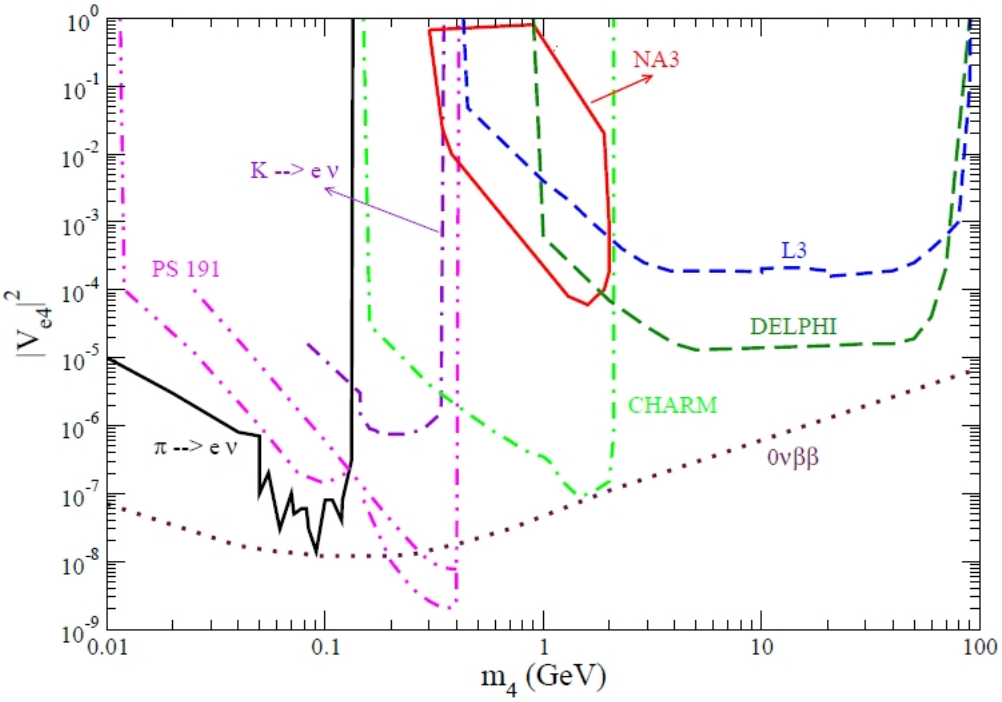

Figure 2.2: Bounds on $|V_{e4}|^2$ versus m_{N_4} in the mass range 10 MeV - 100 GeV. Figure is taken from Ref. [71] where all details can be found. However, it is important to note that the contour of neutrinoless double beta decay (dotted, maroon) is based on the assumptions that only one heavy ν exists and its contribution dominates the LNV process.

It is noteworthy that in Fig. 2.2, the contour of neutrinoless double beta decay (dotted, maroon) is based on the assumptions that only heavy ν mechanism dominates the process. Also, Ref. [71] assumes that only one heavy ν exists. In *Chapter 3*, it is revealed that the heavy ν mechanism may not dominate the process, and there may exist more than one heavy ν, whose masses may be beyond the range in Fig. 2.2. Thus in Ref. [71], the bound from neutrinoless double beta decay may not be applicable.

Besides the experiments mentioned above, the decay of heavy neutrino itself can also lead to rich phenomena and depends on $|V_{l4}|$. There are a few decay modes of heavy neutrino via the charged and neutral current interactions. Their decay widths are listed in Eq. (2.8) [71],

$$\begin{aligned}
\Gamma^{lP} &\equiv \Gamma(N_4 \to l^- P^+) \propto |V_{q\bar{q}}|^2 |V_{l4}|^2 f_1(m_{N_4}), \\
\Gamma^{\nu_l P} &\equiv \Gamma(N_4 \to \nu_l P^0) \propto |V_{l4}|^2 f_2(m_{N_4}), \\
\Gamma^{lV} &\equiv \Gamma(N_4 \to l^- V^+) \propto |V_{q\bar{q}}|^2 |V_{l4}|^2 f_3(m_{N_4}), \\
\Gamma^{\nu_l V} &\equiv \Gamma(N_4 \to \nu_l V^0) \propto |V_{l4}|^2 f_4(m_{N_4}), \\
\Gamma^{l_1 l_2 \nu_{l_2}} &\equiv \Gamma(N_4 \to l_1^- l_2^+ \nu_{l_2}) \propto |V_{l_1 4}|^2 f_5(m_{N_4}), \\
\Gamma^{l_2 l_2 \nu_{l_1}} &\equiv \Gamma(N_4 \to l_2^- l_2^+ \nu_{l_1}) \propto |V_{l_1 4}|^2 f_6(m_{N_4}), \\
\Gamma^{\nu_{l_1} \nu\nu} &\equiv \Gamma(N_4 \to \nu_{l_1} \nu_{l_2} \bar{\nu_{l_2}}) \propto |V_{l_1 4}|^2 f_7(m_{N_4}),
\end{aligned} \tag{2.8}$$

where P^+ and P^0 are the charged and neutral pseudoscalar mesons (e.g. pion), V^+ and V^0 are the charged and neutral vector mesons (e.g. kaon), and $V_{q\bar{q}}$ is the CKM matrix. $f_i(m_{N_4})$ represent different functions of m_{N_4}, for example,

$$\begin{aligned}
f_1(m_{N_4}) &= m_{N_4}^3 \left[\left(1 + \frac{m_l^2}{m_{N_4}^2} - \frac{m_{P^+}^2}{m_{N_4}^2} \right) \left(1 + \frac{m_l^2}{m_{N_4}^2} \right) - 4 \frac{m_l^2}{m_{N_4}^2} \right] \lambda^{1/2} \left(1, \frac{m_l^2}{m_{N_4}^2}, \frac{m_{P^+}^2}{m_{N_4}^2} \right), \\
\lambda(a,b,c) &= a^2 + b^2 + c^2 - 2ab - 2ac - 2bc.
\end{aligned}$$

The definition of other $f_i(m_{N_4})$ can be found in Ref. [71]. With increasing mass of the sterile neutrino, there will be more decay channels. If the heavy neutrino is heavier than W and H, it can also decay into the gauge bosons and Higgs with decay rates [81]

$$\begin{aligned}
\Gamma^{lW} &\equiv \Gamma(N_4 \to l^- W^+) = \Gamma(N_4 \to l^+ W^-) \propto |V_{l4}|^2 m_{N_4}^3 (1 + 2\frac{m_W^2}{m_{N_4}^2})(1 - \frac{m_W^2}{m_{N_4}^2})^2, \\
\Gamma^{\nu_l Z} &\equiv \Gamma(N_4 \to \nu_l Z) \propto |V_{l4}|^2 m_{N_4}^3 (1 + 2\frac{m_Z^2}{m_{N_4}^2})(1 - \frac{m_Z^2}{m_{N_4}^2})^2, \\
\Gamma^{\nu_l H^0} &\equiv \Gamma(N_4 \to \nu_l Z) \propto |V_{l4}|^2 m_{N_4}^3 (1 - \frac{m_H^2}{m_{N_4}^2})^2.
\end{aligned} \tag{2.9}$$

By detecting the decay (or subsequent decay) products, the decay rate of heavy neutrinos and the mixing $|V_{l4}|^2$ can be determined.

Notice that if heavy neutrino is Majorana particle, then some of the decays will lead to lepton number violation. For example, if N_4 is Majorana, then both $(N_4 \to l^- P^+)$ and $(N_4 \to l^+ P^-)$ are possible and have the same decay width, but the second process is a $\Delta L = 2$ process.

Furthermore, as we will discuss in *Chapter 3*, the heavy neutrino and its mixing V are closely related to neutrinoless double beta decay. The mass and mixing of heavy neutrinos would provide constraints on the contribution from heavy neutrino mechanism. Thus the heavy neutrino is very important in the study of Lepton Number Violation processes.

Besides, if $O(m_{N_4}) \sim$ MeV to GeV, the heavy Majorana neutrino can provide resonant contribution to the lepton number violating tau decay and rare mesons decays, which are also related to the mixing V_{l4}. Detailed discussion of these processes are referred to Refs. [71, 82, 83].

On the other hand, if TeV scale heavy neutrino exists, the search of heavy neutrino and even $(\beta\beta)_{0\nu}$-decay may be achievable at the LHC [84, 85, 86, 87, 88, 89]. According to the Type I Seesaw, since small Yukawa coupling is not in favor, the Majorana mass of heavy neutrino turns out to be of order $10^8 - 10^{16}$ GeV. In this case a direct verification of Seesaw Mechanism would be impossible. However, by modifying the model of Seesaw[1], the mass scale of the heavy neutrino could be reduced to (100 GeV $\sim$ 10 TeV), which is within the energy reach of the LHC. In this case, collider signatures of heavy ν would become possible. More importantly, it may offer the possibility of measuring the Majorana character of heavy neutrino in LHC. Left-right symmetry theories suggest that heavy neutrinos have right-handed interactions with charged leptons through W_R. Provided that W_R is in the TeV region while heavy neutrino mass is in 100 GeV to TeV region, then N can be produced at the LHC through the following process,

$$pp \Rightarrow W_R \Rightarrow lN,$$

where l represents e, μ, τ and N is the heavy neutrino. Then the heavy neutrino can further decay via off-shell W_R

$$N \Rightarrow ljj,$$

where jj represent two jets from this subsequent decay. The Feynman diagram of this process is shown in Fig. 2.2. Obviously this is similar to $(\beta\beta)_{0\nu}$-decay and it is also a lepton number violation (LNV) process. Thus the existence of 'lighter' heavy neutrinos could lead to signatures of LNV processes in LHC. More detailed discussions can be found in Refs. [86, 87, 91, 92].

Last but not least, heavy neutrinos have also been investigated for their roles in cosmology [93, 94, 95]. If $O(m_{N_4}) \sim$ keV, it could be a viable dark matter candidate [69]. It is

[1] One of the example is Extended Seesaw [90], which will be introduced in *Section 3.2.3*.

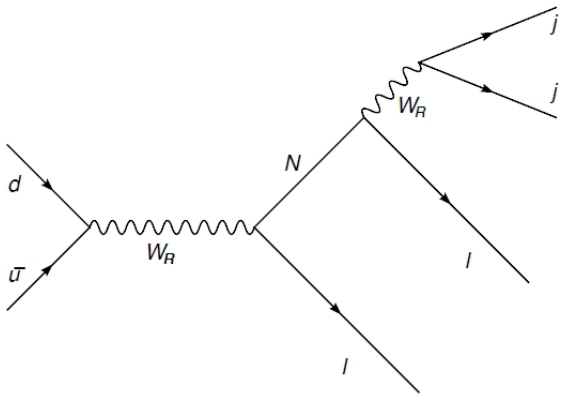

Figure 2.3: Same sign charged lepton pairs production in colliders. This is the collider analog of $(\beta\beta)_{0\nu}$-decay.

also suggested that the coupling between sterile neutrinos and light dark matter scalars can be the neutrino mass origination and reveal the missing mass problem of the universe [96]. More details about the relation between sterile neutrinos and dark matter are referred to Refs. [97, 69, 98, 96].

In this section we have studied the rich phenomena of heavy sterile neutrinos. To sum up, by the introduction of heavy sterile neutrinos, the lightness of usual active neutrinos can be explained. Besides neutrino mass generation, heavy neutrino are also involved in a lot of phenomena of neutrino physics. The fuller study of heavy sterile neutrino lies outside the scope of this thesis. More details about the physics implication of heavy neutrino can be found in Refs. [99, 100]. There are strong theoretical and phenomenological motivations for the study of heavy sterile neutrino.

2.2 The Implication of Existence of Light Sterile Neutrino

The previous section discussed the physics of heavy sterile neutrino. However, it is not necessary that all sterile neutrinos are heavy. If a light sterile neutrino (ν_s) exists and mixes significantly with the active neutrinos, there would be anomalies in the results of oscillation experiments. For example, if the mixing between ν_μ and ν_s is large enough, the ν_e appearance experiments would be fruitless since parts of the neutrino beam change to sterile neutrinos which is not detectable, the ν_e production rate will become small due to the existence of sterile neutrinos. For the disappearance experiments, they will measure a larger deficit of

the ν beam.

The mass scheme of three light neutrinos is consistent with most neutrino oscillation experiments. The first exception is the LSND anomaly. In the LSND experiment, $\bar{\nu}_\mu \to \bar{\nu}_e$ is detected by the Liquid Scintillator Neutrino Detector (LSND). The value of L/E in LSND is in the order 1 m/MeV, which is too small for Δm^2_{21} and Δm^2_{31} to produce any significant oscillation at the observed level. However, the experiment found a 3.8σ excess of $\bar{\nu}_e$ candidate events. This anomaly indicates that there may exist an eV scale Δm^2, which indicates the existence of fourth light neutrino.
If there are four species of neutrinos, then the possible mass scheme may be '3+1' or '2+2' [101], as shown in Fig. 2.4. The '2+2' scenario suggests that ν_μ and ν_τ form a heavier pair, while the pair of ν_e and ν_s is lighter, and the space between these two pairs is equal to $\sqrt{\Delta m^2_{\rm new}}$. In this case, the sterile state must have a significant contribution to either the solar or atmospheric oscillation, or even to both, which means that $|U_{\alpha 4}|$ should be large. However, the solar neutrino oscillation data require large $(|U_{e1}|^2 + |U_{e2}|^2)$, while the atmospheric neutrino experiment results imply that $(|U_{\mu 1}|^2 + |U_{\mu 2}|^2 + |U_{\mu 3}|^2)$ is large. Since the values of mixing matrix elements are subject to the unitarity constraints,

$$\sum_k |U_{\alpha k}|^2 = 1,$$

large $|U_{e4}|$ and $|U_{\mu 4}|$ contradict the experimental data. Thus the '2+2' scheme has already been ruled out by the disagreement between the latest solar and atmospheric neutrino data [102].

On the other hand, according to '3+1' scenario, the three active neutrinos are bunched together. This scenario is not affected by the tension between solar and atmospheric constraints, since if the sterile-active mixing is small, this mass-scheme can be referred to a limiting scenario as the traditional three-flavor framework. '3+1' is somewhat more acceptable but still has difficulties in conforming with the experimental data and has to be tested by other experiments.

In the '3+1' neutrino mixing, the **short-baseline** approximations (neglecting the terms with Δm^2_{31} and Δm^2_{21}) of flavour transition and survival probabilities are given by

$$P_{\alpha\beta} \simeq \sin^2 2\theta_{\alpha\beta} \sin^2 \frac{\Delta m^2_{41} L}{4E}, \tag{2.10}$$

$$P_{\alpha\alpha} \simeq 1 - \sin^2 2\theta_{\alpha\alpha} \sin^2 \frac{\Delta m^2_{41} L}{4E}, \tag{2.11}$$

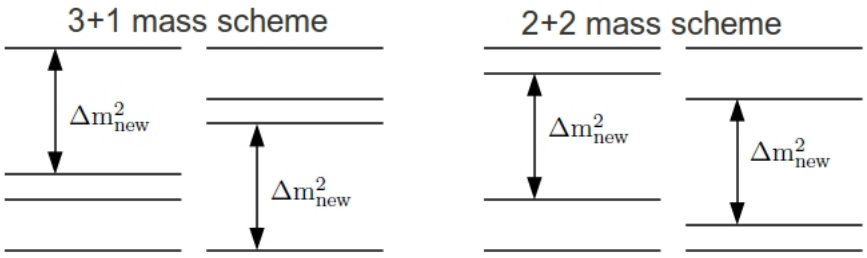

Figure 2.4: '3+1' and '2+2' mass spectrum suggested by the LSND anomaly.

where

$$\sin^2 2\theta_{\alpha\beta} = 4|U_{\alpha 4}|^2|U_{\beta 4}|^2,$$
$$\sin^2 2\theta_{\alpha\alpha} = 4|U_{\alpha 4}|^2(1-|U_{\alpha 4}|^2) \approx 4|U_{\alpha 4}|^2.$$

These mixing parameters are constrained by different experiments:
(i) Bugey [103], Chooz [104]: $\sin^2 2\theta_{ee} = 4|U_{e4}|^2(1-|U_{e4}|^2)$;
(ii) CDHS [105]: $\sin^2 2\theta_{\mu\mu} = 4|U_{\mu 4}|^2(1-|U_{\mu 4}|^2)$;
(iii) KARMEN [106], NOMAD [107], LSND: $\sin^2 2\theta_{\mu e} = 4|U_{\mu 4}|^2|U_{e4}|^2$.

In '3+1' scenario, there is strong tension between these experimental results because Bugey, CHOOZ, CDHS, KARMEN, and NOMAD favors small U_{e4} and $U_{\mu 4}$, but LSND suggests nonzero values [108].

In fact, the neutrino mass scheme could be more complicated than '3+1'. It is also possible that there exist two (or even more) light sterile neutrinos. The existence of fifth light neutrino is in favour after the MiniBooNE experiment. Around ten years after LSND, the MiniBooNE experiment [65, 66, 109] searched for both $\nu_\mu \to \nu_e$ and $\bar{\nu}_\mu \to \bar{\nu}_e$. At first, no excess of ν_e was observed above 475 MeV, but in 2010, in the $\bar{\nu}_e$ search, an excess was found above 475 MeV [109]. The result of MinoBooNE provides hints of the existence of sterile neutrinos but disfavors the '3+1' model. In fact, it has been shown that in the framework of '3+1', there is strong tension between LSND and MiniBooNE antineutrino data and disappearance, KARMEN, NOMAD and MiniBooNE neutrino data[110, 68], as shown in Fig. 2.5 .

Furthermore, MiniBooNE data suggest no-oscillation for ν but find excess in the $\bar{\nu}$ measurement, which is probably related to CP violation. However, as shown in Eq. (2.10) and (2.11), in '3+1' scenario, the sterile neutrino oscillations in short-baseline limit do not involve the CP-violation phases and are the same for neutrinos and antineutrinos. This means that

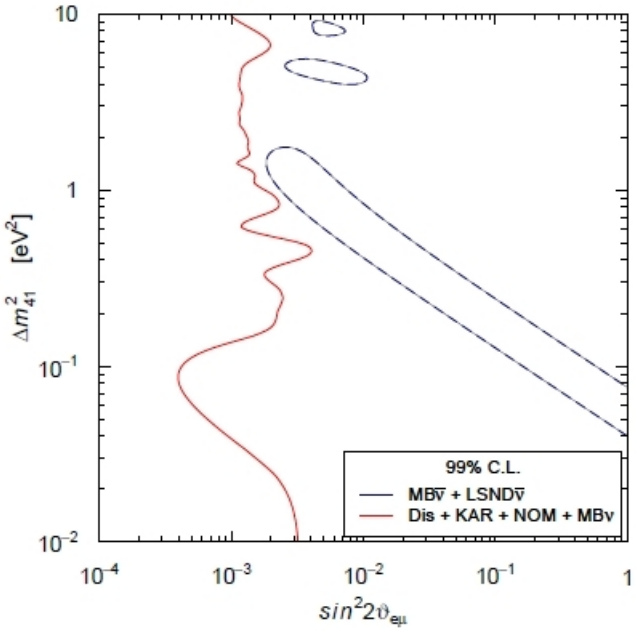

Figure 2.5: The exclusion contour in the $\sin^2 2\theta_{e\mu} - \Delta m^2_{41}$ plane under '3+1' mass scheme [68]. The regions allowed by the LSND and MiniBooNE antineutrino data are enclosed by the dashed blue contours. The red line describes the excluded area after considering the data from disappearance experiments, KARMEN [106], NOMAD [107] and the MiniBooNE neutrino experiment (which did not observe $\nu_\mu \to \nu_e$ signal). This plot shows the strong tension in the framework of '3+1'.

the difference between neutrino and antineutrino measurements in MiniBooNE[2] can not be explained in the framework of '3+1' [109].

The addition of one or more light sterile neutrinos may be able to solve these problems. It has been shown that in the '3+2' framework, the tension is reduced with respect to the '3+1' fit (but not completely removed) [3]. Also, the CP violation is expected to be observable in '3+2' mass-scheme. Therefore, it is suggested that the mass scheme may be more complicated as it may be '3+2' or even '3+3'. In this thesis, both the '3+1' and '3+2' mass-schemes will be discussed.

The tension between the data from LSND, MiniBooNE becomes stronger after taking the

[2]Nevertheless, after the discovery of reactor anomaly, the recent analysis of the combined ν_e and $\bar{\nu_e}$ appearance data reported observation for ν_e as well. Ref. [111] reports that the allowed regions from a 3+1 fit to the data are consistent with both $\nu_\mu \to \nu_e$ and $\bar{\nu}_\mu \to \bar{\nu}_e$ oscillations for $\Delta^2_m = 0.01$ to 1 eV^2, and the recent result is also consistent with the data of LSND.

[3]However, the '3+2' fit is better than the '3+1' fit may be due to the existences of more oscillation parameters. The improvement may be just a statistical effect [68]. The interpretation of the indications of short-baseline oscillations is still uncertain and new experiments are needed in order to clarify the reasons of the tensions in the data.

short-baseline experiments into account. Sterile neutrino oscillation has not been observed by the short baseline oscillation experiments and their results lead to a further constraint to the allowed region from LSND and MiniBooNE $\bar{\nu}$ signal. However, the anomaly found by Ref. [63] suggests that previous short-baseline experiments are misinterpreted.

Around two years ago, the reactor anti-neutrino flux was re-evaluated and the new calculation reveals that the flux is 3% higher than what was previously expected [63]. This implies that all reactor neutrino experiments with baseline < 100 m have observed a deficit of $\bar{\nu}_e$ of 6%. This result further favors the existence of $\Delta m^2_{\text{new}} \sim 1\text{eV}^2$. The reactor anti-neutrino anomaly will be discussed in detail in *Chapter 6*.

The existence of light sterile neutrinos will be further tested by the future oscillation experiments (one of the proposals is to measure the sterile neutrino oscillation in the NF, which will be discussed in *Chapter 5 and 6*). If eV scale sterile neutrinos really exist, a theoretical challenge will arise: "What is responsible for the ultra-lightness of sterile neutrinos? [112]" By definition, sterile neutrinos do not feel standard gauge interactions, therefore the gauge symmetry does not constrain their masses and the sterile neutrinos are expected to be very heavy. It is the reason that right-handed neutrinos are expected to be heavy and able to explain the lightness of active neutrinos through the Seesaw Mechanism.
One of the theories to explain the lightness of sterile neutrinos is Singular Seesaw[4] [114]. As mentioned in *Section 1.3*, the mass matrix of traditional Type I Seesaw is given by

$$M = \begin{pmatrix} 0 & M_D^T \\ M_D & M_R \end{pmatrix} \begin{pmatrix} \nu_L \\ \nu_R \end{pmatrix} + h.c.. \tag{2.12}$$

If M_R is not singular, the mass matrix of light active neutrinos is

$$M_\nu \simeq M_D^T \frac{1}{M_R} M_D.$$

However, if M_R is singular, which means that M_R has one or more zero eigenvalues, this formula does not apply. In this case, it turns out that at least one right-handed neutrino is massless at tree level and picks up a small mass from loop diagrams. The massless right-handed neutrino(s) in this model can be seen as the light sterile neutrino(s) playing role(s) in neutrino oscillation phenomenology. To discuss Singular Seesaw as a whole is beyond the scope of this thesis. More detail can be found in Ref. [114]. In *Chapter 3*, we will discuss Extended Seesaw and more about loop-level neutrino mass calculations, which are also beyond the Type I Seesaw and can generate light sterile neutrinos.

[4]Except Singular Seesaw, the other popular theory of explaining the ultra-lightness of sterile neutrinos is the Mirror Universe (refer to references [113, 112]).

The phenomenological implication of the existence of light sterile neutrinos is that they may appear in the oscillation experiments. Although the 3-active neutrino model is consistent with most of the neutrino experimental data, it is still worth investigating scenarios in which sterile neutrinos are involved in the oscillation and constrain the corresponding parameter space. As mentioned before, Reactor Anomaly implies that sterile neutrinos may appear in the reactor oscillation experiments. Basically, it is believed that short baseline experiments and high statistics study could exhibit the sterile neutrino oscillation and measure the sterile parameters. In *Chapter 5 and 6*, searching sterile neutrino oscillation in Low Energy Neutrino Factory (LENF) will be studied. We will show that with a near detector, LENF is a good candidate to reveal the possible active sterile neutrino oscillation.

Chapter 3

Different Mechanisms For $(\beta\beta)_{0\nu}$-decay And Their Relations to Neutrino Mass

As mentioned in *Chapter 1 and 2*, the heavy sterile neutrino can be related to the nature of neutrino and Lepton Number Violation.

Lepton Number Violation (LNV) is one of the convincing manifestations of incompleteness of Standard Model, and it is also the key factor of understanding the nature of neutrino and the matter-antimatter asymmetry [115]. Thus LNV is one of the typical issues in neutrino research which can lead to physics beyond standard model. To prove the existence of LNV, neutrinoless double beta decay is the most promising process [26].

Neutrinoless double beta decay ($(\beta\beta)_{0\nu}$) can be induced by various lepton-number violating mechanisms: (a) light Majorana neutrino exchange [26, 25, 116, 117]; (b) heavy Majorana neutrino exchange [118, 119]; (c) R-parity violation (RPV) with short-range exchange [120, 121] and long-range exchange [122]; (d) right-handed leptonic and hadronic currents coupling [123]; (e) Kaluza-Klein neutrino exchange via extra dimension [124] and other LNV mechanisms. Except for (a), (b) - (e) are all related to new physics.

In the past 10 years, efforts have been made to determine the dominant mechanism for $(\beta\beta)_{0\nu}$-decay. It is typically assumed that there is one mechanism dominating the process. To determine the leading mechanism, various techniques have been discussed, e.g. analysis of the angular distribution [125] or comparison of the nuclear matrix elements between different nuclei [126], [127]. However, due to the absence of observation in $(\beta\beta)_{0\nu}$-decay experiments, the exact contributions from different mechanisms and which one is the dominant one is not known yet.

In this chapter, we will investigate the relation between these mechanisms and the value of neutrino masses. We will see that the neutrino mass generation adds constraints on different

LNV parameters and thus suppresses their contributions to neutrinoless double beta decay. By studying different models of neutrino mass generation, we have a clearer idea of the constraints on $(\beta\beta)_{0\nu}$-decay.

In the following, the mechanisms of "light Majorana neutrinos exchange", "heavy Majorana neutrinos exchange", "trilinear RPV with short-range exchange" and "trilinear RPV with long-range exchange" will be taken into account. If they all contribute, then the decay rate of $(\beta\beta)_{0\nu}$-decay is [128]

$$\Gamma_i \equiv [T^{0\nu}_{1/2}]^{-1}_i = G_i \mid \eta_\nu \mathcal{M}_{\nu,i} + \eta_N \mathcal{M}_{N,i} + \eta_\lambda \mathcal{M}_{\lambda,i} + \eta_q \mathcal{M}_{q,i} \mid^2, \tag{3.1}$$

where G_i is the common phase space factor. $\mathcal{M}_{\nu,i}$, $\mathcal{M}_{N,i}$, $\mathcal{M}_{\lambda,i}$, $\mathcal{M}_{q,i}$ are the corresponding nuclear matrix elements (NME), which describe the nuclear effects in $(\beta\beta)_{0\nu}$-decay (the subscripts ν, N, λ, q refer to light neutrino, heavy neutrino, short-range and long-range $\not{R}_p$ mechanisms, and i represents different nuclei). η_ν, η_N and η_λ, η_q are the light neutrino, heavy neutrino, $\not{R}_p$ short-range, and $\not{R}_p$ long-range lepton number violating parameters, respectively. They are defined as

$$\eta_\nu = \frac{1}{m_{\rm e}} \sum_k^{\rm light} (U_{ek})^2 m_k, \tag{3.2a}$$

$$\eta_N = m_{\rm p} \sum_j^{\rm heavy} (V^L_{ej})^2 \frac{1}{M_j}, \tag{3.2b}$$

$$\eta_\lambda \simeq \frac{\pi\alpha_s}{6} \frac{\lambda'^2_{111}}{G_F^2 m^4_{\tilde{d}_R}} \frac{m_{\rm p}}{m_{\tilde{g}}} \cdot [1 + (\frac{m_{\tilde{d}_R}}{m_{\tilde{u}_L}})^2]^2, \tag{3.2c}$$

$$\eta_q = \sum_k \frac{\lambda'_{11k}\lambda'_{1k1}}{2\sqrt{2}G_F} [\sin 2\theta^d_{(k)} (\frac{1}{m^2_{\tilde{d}_1(k)}} - \frac{1}{m^2_{\tilde{d}_2(k)}})]. \tag{3.2d}$$

In Eq.(3.2a), η_ν corresponds to the standard light neutrino mass mechanism, where $m_{\rm e}$ is the electron mass. m_k, U^L_{ek} are the light ν masses and the elements of mixing matrix between light ν mass and flavour state, respectively.

The other LNV parameters η_N, η_λ and η_q correspond to the heavy sterile neutrino, short-range and long-range $\not{R}_p$ mechanisms. In Eq. (3.2b), M_j is the heavy sterile neutrino mass and V^L_{ej} is the mixing between the heavy mass states and electron neutrinos. On the other hand, in Eq. (3.2 c-d), G_F is the Fermi constant, α_s is the SU(3) gauge coupling constant, λ'_{ijk} is the trilinear coupling constant in the $\not{R}_p$ (R-parity violation) superpotential. $m_{\tilde{u}_L}$, $m_{\tilde{d}_R}$ and $m_{\tilde{g}}$ are the masses of u-squark, d-squark and gluino, respectively. The definitions of $m_{\tilde{d}_1(k)}$, $m_{\tilde{d}_2(k)}$ and $\sin 2\theta^d_{(k)}$ can be referred to Ref.[122]. The physical meaning or more

detailed explanations of these SUSY parameters can be found in Ref. [129].

All the parameters in Eqs. (3.2) are independent of the nuclear structure. In fact, the parameters η_ν, η_N, η_λ and η_q could be complex, see Eqs. (3.2), in presence of CP-violation, and cancellations in the decay rate can take place, making the half-life time much longer than expected.

Sterile neutrinos with masses M_j much larger than the average propagating momentum, around 100 MeV, correspond to the LNV parameter in Eq. (3.2b). When the exchange neutrino mass is larger than 100 MeV, the process becomes 'short-range' and we have to calculate both the propagator and the nuclear current in different ways. The contribution from heavy sterile neutrinos is given by the second term in Eq. (3.1). The heavy ν is related to the neutrino mass generation, thus the mixing V_{ej}^L and also the contribution from heavy ν mechanism are constrained by the Seesaw relation. We will discuss this issue in detail in *Section 3.2*.

On the other hand, supersymmetry with R-parity violation can also induce $(\beta\beta)_{0\nu}$-decay. There are two possible **trilinear $\not{R}_p$ contributions**. The first case is the short-range mechanism, simply exchanging the heavy super-particles [120] to induce the LNV process [Fig 3.1 (left panel)]. This scenario is recognised as 'short-range'. The corresponding contribution to the decay rate can be parameterized by η_λ, which is defined by Eq. (3.2c).

The other possibility is the squark-neutrino mechanism [122], which suggests that the

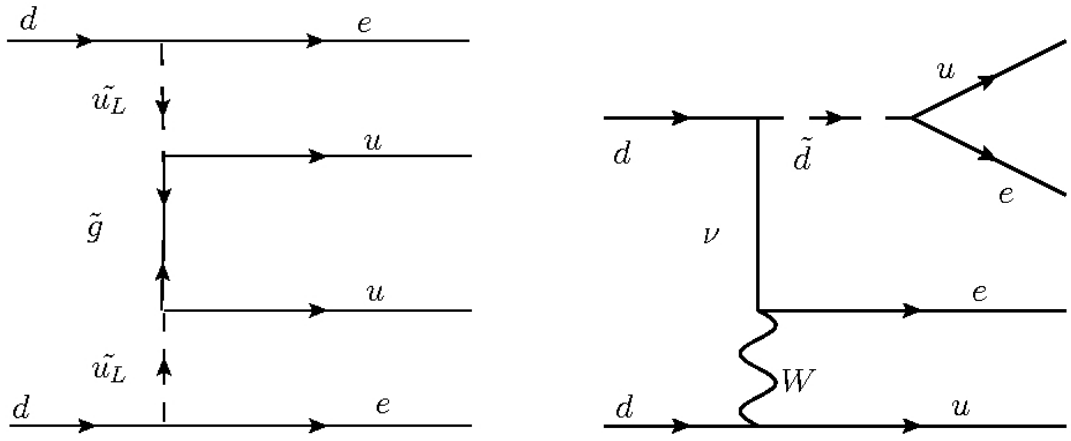

Figure 3.1: The short-range and long-range R-parity violating contribution to $(\beta\beta)_{0\nu}$-decay.

neutrino mediated $(\beta\beta)_{0\nu}$-decay originates from $\not{R}_p$ interactions [Fig 3.1 (right panel)]. This mechanism is comparatively long-range and the corresponding LNV parameter η_q is described

by Eq. (3.2d).

Both short-range and long-range $\not{R}_p$ mechanisms are dominated and enhanced by pion-exchange [121, 122]. At the hadron level, the one-pion and two-pion exchange are supposed to dominate [121, 130]. This further enhances the values of the nuclear matrix elements, which will be shown and discussed in detail in *Chapter 4 and Appendix D.*

Moreover, it is important to note that the $\not{R}_p$ superpotential can lead to generation of the Majorana neutrino masses, which can give us hints about the trilinear coupling constant limits. Different to the heavy ν mechanism, the trilinear $\not{R}_p$ is not related to right-handed neutrino nor Seesaw, thus it will not suffer the same constraint as heavy ν mechanism, but it is sensitive to the masses of squarks and gluinos, which will be discussed in detail in *Section 3.3.*

3.1 The Standard Light Neutrino Exchange Mechanism

The most discussed intermediate mechanism of neutrinoless double beta decay is the light Majorana ν exchange. As ν have masses, if they are Majorana particles, the process will proceed according to the diagram in Fig. 3.2.

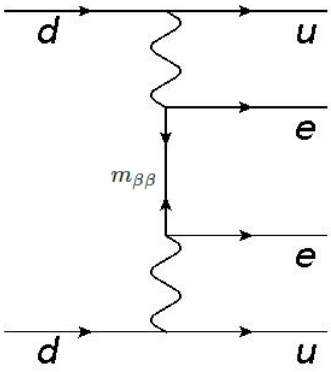

Figure 3.2: Feynman diagram giving rise to the standard light ν mechanism contribution to $(\beta\beta)_{0\nu}$-decay.

The amplitude of this diagram is [25]

$$M = -2G_F^2(\bar{u}(P_1)\gamma_\mu\nu_L)(-\bar{\nu_L^c}\gamma_\nu v(P_2)) \times \int\int \langle f|T[J^\mu(x)J^\nu(y)]|i\rangle \exp(-iP_1x - iP_2y)d^4xd^4y$$

where P_1 and P_2 are the momentum of the emitted electrons; J is the hadronic current; $|f\rangle$ and $|i\rangle$ are the final and initial nuclear states. The equation above shows that the amplitude involves the Majorana mass term of neutrino: $\nu_L\bar{\nu_L^c}$ and it will lead to the effective

neutrino mass $\langle m_\nu \rangle \equiv \sum_k^{\text{light}} (U_{ek})^2 m_k$. The detailed calculations of the equation above and the amplitude of $(\beta\beta)_{0\nu}$-decay can be referred to the *Appendix B*.
As the propagator in the diagram of Fig 3.2 is the light Majorana neutrino, this process will take place only if at least one light neutrino is Majorana particle. Besides, the corresponding decay-rate is proportional to the effective neutrino mass, $\langle m_\nu \rangle$. The decay rate of this process is supposed to be as the following:

$$\Gamma_i = G_i \mid \eta_\nu \mathcal{M}_{\nu,i} \mid^2,$$

where $\eta_\nu = \langle m_\nu \rangle / m_e$. This is just the simplified Eq. (3.1), where the contributions from the other mechanisms are neglected.
From this equation, it follows that the measurement of Γ_i should also reveal the value of η_ν or $\langle m_\nu \rangle$. Thus, traditionally, it is believed that if the $(\beta\beta)_{0\nu}$-decay can be measured, the absolute scale of the effective ν mass from the decay rate of the process can also be extracted. However, there are two problems in transferring the measured decay-rate to the value of effective ν mass.

The first problem is that the evaluation of nuclear matrix elements (i.e. $\mathcal{M}_{\nu,i}$ in the previous equation) suffers from large uncertainties. This in turn affects the predictions for the half-life time of the decay and the extraction of information on neutrino masses and mixing parameters from future measurements. Nuclear matrix elements (NMEs) depend on the nuclear structure of the reaction, the adjustment of parameters like strength parameter g_{ph}, g_{pp}, the choice of the coupling constant g_A, the measurements of Two-neutrino double beta decay[1] and the exchange mechanism considered for the process [126, 131, 132]. The details of NMEs and their uncertainties will be discussed in the next chapter.

The second problem, as mentioned previously, is that $(\beta\beta)_{0\nu}$-decay can also be induced by other "Lepton Number Violating" mechanisms. Eq. (3.1) shows that the decay-rate may be constructed from the interferences between different mechanisms. Actually, there may also exist "Extra-dimension", "Left-Right" or other LNV mechanisms which contribute to $(\beta\beta)_{0\nu}$-decay, but they are out of the scope in this thesis.

Theoretically, the contributions from the new-physics mechanisms are assumed to be small. It is because the couplings of the 'new-physics' particles must not be large, otherwise they should have been observed in other experiments. Recently, the possibility of large contributions from these mechanisms have been explored with interesting implications for $(\beta\beta)_{0\nu}$-decay [133, 134, 84]. If the magnitude of other mechanisms are large enough to interfere

[1] Two-neutrino double beta decay is described in detail in *Appendix C*.

significantly with the standard light neutrino mechanism (which means that the contributions of different mechanisms are of the same order), then the extraction of the value of effective neutrino mass may not be that easy and direct. Moreover, it is interesting to tackle the possible destructive interference between different mechanisms inducing the $(\beta\beta)_{0\nu}$-decay. If this cancellation takes place, then it may explain the absence of the observation of $(\beta\beta)_{0\nu}$-decay so far. Since the decay-rate (or the amplitude) is suppressed by the cancellation among different mechanisms, the current experimental sensitivity is not enough for measuring this process.

First of all, we need to verify whether the new-physics mechanisms could have significant contributions to $(\beta\beta)_{0\nu}$-decay. In the rest of this chapter, we will investigate how the **new physics** (mainly the heavy sterile ν and R-parity violation) is related to the light ν mass, and analyse under which circumstances they would have large contributions to double beta decay. Then in *Chapter 4*, we will further analyse the potential cancellation among different mechanisms and see how it relates to the absence of observations in the experiments.

3.2 Heavy Sterile ν And Its Relation to $(\beta\beta)_{0\nu}$-Decay

Besides the lepton number violating decays mentioned in *Chapter 2*, the heavy neutrino is also related to the other lepton number violation (LNV) process, $(\beta\beta)_{0\nu}$-decay. The typical (Type I) Seesaw predicts the Majorana nature of the heavy neutrino. If it is true, then heavy Majorana neutrino can also induce neutrinoless double beta decay.

Theoretically, besides the standard light neutrino mechanism mentioned in the previous section, $(\beta\beta)_{0\nu}$-decay can also be mediated by heavy intermediate particles, such like heavy neutrino or SUSY particles. If heavy neutrinos[2] are Majorana particles as predicted by Type I Seesaw, they can also induce this LNV process. In this case, the amplitude would be proportional to the heavy neutrino inverse mass mixings,

$$A_{\text{heavy}} \propto \sum_{j}^{\text{heavy}} (V_{ej})^2 \frac{1}{M_j}.$$

Here M_j represents the mass of the heavy neutrino and V_{ej} is the heavy sterile neutrino mixing. The values of M_j and V_{ej} are constrained by various experiments (as mentioned in *Chapter 2* and Ref. [71]). This mechanism is important because the heavy neutrino and other models like supersymmetry, offer a variety of mechanisms which allow the $(\beta\beta)_{0\nu}$-decay to take place. The LNV process may be more complicated than the traditional model

[2]The definition of heavy neutrinos means that the corresponding mediating neutrino have masses > 100 MeV. In this case, the nucleons are not point-like and the calculation of the decay rate and corresponding nuclear currents would be very different with the traditional model, namely, the standard mechanism.

(light Majorana ν exchange) expected. Since cosmology keeps pushing down the neutrino masses (≤ 0.58 eV [135]), the observation of large $|\langle m_{\beta\beta}\rangle|$ from the traditional $(\beta\beta)_{0\nu}$ model becomes more and more unfavorable. The new physics source of the $(\beta\beta)_{0\nu}$-decay becomes more strongly motivated. This is why heavy sterile neutrino is interested in this thesis. The numbers and mass scale of heavy sterile neutrino are not only related to mass generation model of neutrinos, but also the measurement of $(\beta\beta)_{0\nu}$-decay. In this section, the roles of heavy sterile neutrino in neutrino mass generation models and neutrinoless double beta decay will be further discussed. We will reveal that Seesaw Mechanism and heavy neutrinos not only are related to the neutrino mass generation, but also provide constraints on the amplitude of $(\beta\beta)_{0\nu}$-decay.

3.2.1 Heavy ν mechanism

We first assume that in $(\beta\beta)_{0\nu}$-decay, the contributions from R-parity violation mechanisms [the third and fourth terms in Eq. (3.1)] are negligible and focus on the "light and heavy ν exchange" mechanisms. We will estimate the contribution from "heavy ν exchange" and check if it can dominate over the "light ν exchange" (the standard mechanism) contribution.

Reference [136] pointed out that the contribution of "heavy ν exchange" decays as M_j^{-2} (the mass of heavy neutrino), thus the corresponding amplitude would be strongly suppressed. To get a better idea, in this section we focus on the exchange of Majorana light neutrinos and heavy neutrinos. In this case, Eq (3.1) changes to:

$$\Gamma_i \equiv [T^{0\nu}_{1/2}]^{-1}_i = G_i \mid \eta_\nu \mathcal{M}_{\nu,i} + \eta_N \mathcal{M}_{N,i} \mid^2 . \tag{3.3}$$

From the Seesaw mechanism, we know that

$$\sum_k^{\text{light}} (U_{ek})^2 m_k + \sum_j^{\text{heavy}} (V_{ej})^2 M_j = 0, \tag{3.4}$$

since there is no $\bar{\nu^c_L}\nu_L$ mass term [136].
Eq (3.2) gave us the relation between η_ν and η_N and thus Eq (3.1) can be rewritten as

$$\begin{aligned}
\Gamma_i &= G_i \mid \frac{1}{m_{\rm e}} \sum_k^{\text{light}} (U_{ek})^2 m_k \mathcal{M}_{\nu,i} + m_{\rm p} \sum_j^{\text{heavy}} (V_{ej})^2 \frac{1}{M_j} \mathcal{M}_{N,i} \mid^2 \\
&= G_i \mid (-\sum_j (V_{ej})^2 M_j) \frac{\mathcal{M}_{\nu,i}}{m_{\rm e}} + \sum_j (V_{ej})^2 M_j \frac{m_{\rm p}}{M_j^2} \mathcal{M}_{N,i} \mid^2 \\
&= G_i \mid \frac{\sum_j (V_{ej})^2 M_j}{m_{\rm e}} \mathcal{M}_{\nu,i} \cdot (-1 + \frac{m_{\rm e} m_{\rm p}}{M_j^2} \frac{\mathcal{M}_{N,i}}{\mathcal{M}_{\nu,i}}) \mid^2
\end{aligned}$$

The second term corresponds to the contribution from heavy neutrino exchange. We can see that if M_j is very large (all M_j are assumed to be larger than 100 MeV in this scenario), the second term $\ll 1$ and the light neutrino exchange dominates $(\beta\beta)_{0\nu}$-decay. To make it more clear, we simply assume only one generation for the heavy neutrino, i.e. j = 1, $M_j = m_N$, and we use this simple case as an example to reveal the contribution from heavy neutrinos.

$$\Gamma_i = G_i \mid \frac{\langle m_\nu \rangle}{m_{\rm e}} \mathcal{M}_{\nu,i} \cdot (1 - \frac{m_{\rm e} m_{\rm p}}{m_N^2} \frac{\mathcal{M}_{N,i}}{\mathcal{M}_{\nu,i}}) \mid^2 \tag{3.5}$$

$$(\because \sum_j^{\rm heavy} (V_{ej})^2 M_j = (V_{e1})^2 m_N = -\sum_k^{\rm light} (U_{ek})^2 m_k = - < m_\nu >)$$

While under the traditional assumption (i.e. no interference, only light ν exchange exists), the decay rate is

$$\Gamma_i^0 = G_i \mid \frac{\langle m_\nu \rangle}{m_{\rm e}} \mathcal{M}_{\nu,i} \mid^2,$$

in Eq. (3.5), when m_N is very large, Γ_i will just reduce to Γ_i^0, which means that the heavy ν exchange is negligible and there is no cancellation. Fig 3.3 shows the decay rate of ^{76}Ge as an example to compare Γ_{Ge} with Γ_{Ge}^0. It shows that when m_N is larger than a few hundred MeV, $\Gamma_{Ge}/\Gamma_{Ge}^0 \approx 1$, which means that **light ν exchange** dominates. This plot will change slightly for different nuclei as the NME changes, but the conclusion is similar.

Thus, we conclude that interference between light and heavy neutrino exchange is significant only when all the heavy neutrino masses approach 100 MeV. Otherwise the contribution from exchange of heavy sterile neutrinos would be negligible.

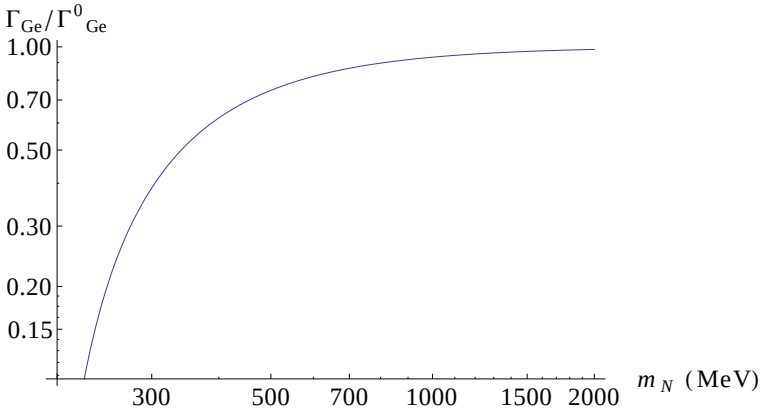

Figure 3.3: The ratio of Γ_{Ge} (considering both light and heavy ν contributions) to Γ_{Ge}^0 (considering light ν exchange only).

All extra neutrinos lighter than 100 MeV

It is interesting to study the case that all the neutrino mass eigenstates are lighter than the nuclear scale (100 MeV). In this case, the "heavy" neutrino contribution would not be suppressed by the heavy neutrino mass and the process is still so-called "long-range" (which means the nucleons can be treated as point-like). The decay rate should be rewritten as

$$\begin{aligned}\Gamma_i &= G_i \mid \frac{1}{m_{\rm e}} \sum_{k}^{\rm light} (U_{ek})^2 m_k \mathcal{M}_{\nu,i} + \frac{1}{m_{\rm e}} \sum_{j}^{\rm heavy} (V_{ej})^2 M_j \mathcal{M}'_{\nu,i} \mid^2 \\ &= G_i \mid (-\sum_{j} (V_{ej})^2 M_j) \frac{\mathcal{M}_{\nu,i}}{m_{\rm e}} + \sum_{j}^{\rm heavy} (V_{ej})^2 M_j \frac{\mathcal{M}'_{\nu,i}}{m_{\rm e}} \mid^2 \\ &\approx 0. \end{aligned} \tag{3.5a}$$

Please notice that if the masses of exchange neutrinos are smaller than the nuclear scale, than the nuclear matrix element of the "heavy" neutrino mechanism should not be $\mathcal{M}_N$. Here we used $\mathcal{M}'_\nu$ to represent the corresponding NME, which is expected to be $\approx \mathcal{M}_\nu$. This is why the decay rate ≈ 0 in Eq. (3.5a) [136].

Therefore if all heavy neutrinos are lighter than 100 MeV, a full cancellation between standard light ν and heavy ν mechanisms is possible. However, this scenario cannot explain the lightness of neutrino masses through the naive seesaw mechanism. Although basically the masses of sterile neutrinos are not restricted, the possibility of "all neutrinos being lighter than 100 MeV" is still not in favor. Here we just mentioned it as one of the possibilities of significant cancellation in the $(\beta\beta)_{0\nu}$-decay.

The other exception

The discussions above suggest that the contribution from heavy sterile neutrino is subdominant in the $(\beta\beta)_{0\nu}$-decay. A similar argument also applies in the models of Type II and Type III Seesaw [136]. However, there is a relevant exception studied in Refs. [133, 84]. The heavy neutrinos might trivially dominate the process (at tree level) if the light neutrino mass

mixing is extremely tiny, i.e.

$$\sum_{k}^{\text{light}}(U_{ek})^2 m_k \approx 0, \quad \Rightarrow \sum_{j}^{\text{heavy}}(V_{ej})^2 M_j \approx 0,$$

but the heavy neutrino contribution,

$$\sum_{j}(V_{ej})^2 M_j \frac{m_{\rm p}}{M_j^2}\mathcal{M}_{N,i}$$
$$= m_{\rm p}\sum_{j}^{\text{heavy}}(V_{ej})^2 \frac{1}{M_j}\mathcal{M}_{N,i} \neq 0.$$

In this case, the heavy ν mechanism can dominate the process.

$$\Gamma_i = G_i \mid \frac{1}{m_{\rm e}}\sum_{k}^{\text{light}}(U_{ek})^2 m_k \mathcal{M}_{\nu,i} + m_{\rm p}\sum_{j}^{\text{heavy}}(V_{ej})^2 \frac{1}{M_j}\mathcal{M}_{N,i} \mid^2$$
$$\approx G_i \mid \sum_{j}(V_{ej})^2 \frac{m_{\rm p}}{M_j}\mathcal{M}_{N,i} \mid^2 . \tag{3.5b}$$

Nevertheless, since the heavy neutrino contribution is suppressed by $\sum_j (V_{ej})^2 \frac{1}{M_j}$, it is not easy a *priori* to obtain both a measurable effect of the heavy neutrinos and a cancellation for the light ones. We will discuss this in more detail in the *Subsection 3.2.3* and give the example of Extended Seesaw.

3.2.2 Other mechanisms related to tree-level ν mass generation

Except for the heavy neutrino exchange, $(\beta\beta)_{0\nu}$-decay can also be induced by other mechanisms like KK neutrino (extra-dimension), bilinear R-parity violation. These two cases are similar to heavy ν exchange since they are also constrained by tree-level neutrino mass generation. Similar to the traditional Type I Seesaw Mechanism, the singlet ν in extra-dimension [124, 137] and bilinear R-parity violation [138] can also generate neutrino mass through tree-level diagrams. However the exchange particles of these mechanisms are not the heavy sterile neutrinos, but the KK neutrino in extra dimensions, or neutralinos which relate to the bilinear R-parity violation.

In a word, extra-dimension and bilinear $\not{R}_p$ mechanisms will suffer from the similar constraint as Eq. (3.4) and thus their contributions to $(\beta\beta)_{0\nu}$-decay will be negligible, unless the exchange particles are around $O(100$ MeV). However, such light KK neutrinos or SUSY particles are not in favor. So in the following, extra-dimension will not be discussed, since it is just similar to the heavy ν mechanism. We will just focus on the models which generate ν masses differently with the typical Seesaw.

Within R-parity violation, besides the bilinear terms, there also exist trilinear terms, which are related to the loop-level mass generation of neutrino and different to the traditional Type I Seesaw. This mechanism will be discussed in detail in *Section 3.3*.

In the next subsection, Extended Seesaw at loop level will be discussed. It is interesting because it is an exceptional model which allows heavy ν mechanism to dominate in the $(\beta\beta)_{0\nu}$-decay.

3.2.3 Extended Seesaw and its relation with $(\beta\beta)_{0\nu}$-decay

In *Subsection 3.2.1*, the relation between Seesaw and "heavy ν mechanism" contribution to $(\beta\beta)_{0\nu}$-decay has been studied. Due to Eq. (3.4), the heavy ν contribution is constrained and supposed to be subdominant. However, if the neutrino mass is generated at loop-level rather than tree level, then Eq. (3.4) will not apply anymore. In the following, the possibility that "$m_\nu = 0$ at tree level but $m_\nu \neq 0$ at loop level" will be investigated.

In the typical Seesaw Mechanism as stated above, the neutrino mass matrix is given by

$$M = \begin{pmatrix} 0 & M_D^T \\ M_D & M_R \end{pmatrix}.$$

Customarily, in 1-generation simplified scenario, M_R is assumed to be $\sim O(10^{15}$ GeV), and thus cannot be searched in the experiments. However, it is not necessary for the scale of M_R to be so high. One of the models which have been considered to reduce the Seesaw scale is the Extended Seesaw [3]. Theoretically, there could be two types of sterile neutrino states, which have different coupling with the active neutrinos. Assume that there are m-generation of sterile neutrino states N and m'-generation of sterile neutrino states S, then M_R becomes a (m+m')×(m+m') matrix. In the Extended Double Seesaw framework [90, 84], M_R, M_D are seen as two matrices,

$$M_R = \begin{pmatrix} \mu' & \Lambda^T \\ \Lambda & \mu \end{pmatrix}, \quad M_D = \begin{pmatrix} m_D \\ \epsilon m'_D \end{pmatrix},$$

then the mass matrix becomes,

$$M = \begin{pmatrix} 0 & m_D^T & \epsilon m_D'^T \\ m_D & \mu' & \Lambda^T \\ \epsilon m'_D & \Lambda & \mu \end{pmatrix}, \tag{3.6}$$

[3]This model is called as Extended Seesaw [90] or Inverse Seesaw [139], depending on the values of the parameter. In this thesis, the model is called as Extended Seesaw as our discussion of the parameters is based on the Refs. [90, 84].

where $m_D = vY$, $\epsilon m'_D = \epsilon v Y'$, Y and Y' are the Yukawa couplings. Notice that the mass matrix given above is general. A particularly interesting set of models included in Eq. (3.6) are the ones studied and summarized in Ref. [140]. In those models, which include the frequently called inverse or multiple seesaw models, Lepton Number is assumed to be a global symmetry only broken in the neutrino sector through different Lepton Number Violation terms. These terms are driven by ϵ and/or μ and/or μ' .
The corresponding mixing of this mass matrix is,

$$U = \begin{pmatrix} U_L \\ U_N^* \\ U_S^* \end{pmatrix},$$

where

$$U^T M U = \hat{M} = diag(m_1, m_2, ..., m_{n_L+n_N+n_S}).$$

Since U is unitarity, the relations between U_L, U_N and U_S are

$$\begin{aligned} U_N U_L^T = 0, \quad U_L U_N^T = 0; \\ U_S U_L^T = 0, \quad U_L U_S^T = 0; \\ U_N U_S^T = 0, \quad U_S U_N^T = 0. \end{aligned}$$

Moreover, since $U^* \hat{M} U^\dagger = M$,

$$\begin{aligned} & U_L^* \hat{M} U_L^\dagger = 0, \quad U_N \hat{M} U_N^T = \mu, \quad U_S \hat{M} U_S^T = \mu'; \\ & U_L^* \hat{M} U_N^T = m_D^T, \quad U_N \hat{M} U_L^\dagger = m_D; \\ & U_L^* \hat{M} U_S^T = \epsilon m_D'^T, \quad U_S \hat{M} U_L^\dagger = \epsilon m'_D; \\ & U_N \hat{M} U_S^T = \Lambda^T, \quad U_S \hat{M} U_N^T = \Lambda; \end{aligned} \tag{3.7}$$

In this model, the light neutrino mass at tree level is,

$$M_\nu^{\text{tree}} = m_D^T \frac{\mu}{\Lambda^T \Lambda + \mu\mu'} m_D - (\epsilon m_D'^T \frac{1}{\Lambda^T} m_D + m_D^T \frac{1}{\Lambda} \epsilon m'_D). \tag{3.8}$$

The physical implication of this model is that, if μ, μ' and ϵ are zero, the Dirac nature of neutrino can be recovered and the lepton number symmetry is protected, which is the Inverse Seesaw discussed in Ref. [139]. It is remarkable that in general, for the Seesaw limit '$O(M_R)$ $\gg$ $O(M_D)$', the light active neutrino masses are proportional to ϵ and μ. In this case the smallness of the neutrino masses can be explained by considering ϵ and μ as small parameters that break a lepton symmetry. The scale of Λ can therefore be below TeV, allowing sizable

New Physics effects to be detected by the collider experiments [140].

In the following, we assume μ and $\epsilon \ll \mu'$, Λ, m_D in order to suppress the tree-level light neutrino mass, but there is no constraint on μ' (lepton number symmetry is not implemented). In this case, the masses of the two heavy neutrinos are (neglecting the terms with μ and ϵ)[4],

$$M_4 \sim \frac{\mu' - \sqrt{\mu'^2 + 4(\Lambda^2 + m_D^2)}}{2}, \tag{3.9}$$

$$M_5 \sim \frac{\mu' + \sqrt{\mu'^2 + 4(\Lambda^2 + m_D^2)}}{2}. \tag{3.10}$$

Meanwhile, $\hat{M}$ and the mixing matrices are (ignoring those terms with μ and ϵ)

$$\hat{M} = \begin{pmatrix} 0 & 0 & 0 \\ 0 & M_4 & 0 \\ 0 & 0 & M_5 \end{pmatrix},$$

$$U = \begin{pmatrix} U_L \\ U_N^* \\ U_S^* \end{pmatrix} = \begin{pmatrix} \frac{\Lambda}{\sqrt{m_D^2+\Lambda^2}} & \frac{2m_D}{\sqrt{4(m_D^2+\Lambda^2)+4M_1^2}} & \frac{2m_D}{\sqrt{4(m_D^2+\Lambda^2)+4M_2^2}} \\ 0 & \frac{2M_1}{\sqrt{4(m_D^2+\Lambda^2)+4M_1^2}} & \frac{2M_2}{\sqrt{4(m_D^2+\Lambda^2)+4M_2^2}} \\ -\frac{m_D}{\sqrt{m_D^2+\Lambda^2}} & \frac{2\Lambda}{\sqrt{4(m_D^2+\Lambda^2)+4M_1^2}} & \frac{2\Lambda}{\sqrt{4(m_D^2+\Lambda^2)+4M_2^2}} \end{pmatrix}.$$

The mass matrix in Eq. (3.6) corresponds to 3-generation of standard ν_L, m-generation of sterile ν state N and m'-generation of sterile ν state S. For simplicity, here we focus on the case m = m' = 1, and there is only 1 generation of standard ν_L. Then all m_D, μ', Λ are just simply numbers.

In this case, the effective light neutrino mass $|< m_\nu >|$ would be[5]

$$|< m_\nu >| = (m_D \Lambda^{-1} \mu \Lambda^{-1} m_D) - (\epsilon m'_D \frac{1}{\Lambda} m_D + m_D \frac{1}{\Lambda} \epsilon m'_D). \tag{3.11}$$

The contribution of heavy neutrino mechanism to $(\beta\beta)_{0\nu}$-decay will also change, since two heavy sterile states are considered now. The decay rate will be changed to (i stands for the type of nuclei)

$$[T_{1/2}^{0\nu}]_i^{-1} = G_i \mid \frac{< m_\nu >}{m_{\rm e}} \mathcal{M}_{\nu,i} + m_{\rm p} \sum_j (\frac{V_{en_j}^2}{m_{n_j}} + \frac{V_{es_j}^2}{m_{s_j}}) \mathcal{M}_{N,i} \mid^2, \tag{3.12}$$

[4]From Eq.(3.9) we can see that if $\mu' \gg \Lambda$ and m_D, $M_1 \approx 0$, which gives us the light sterile neutrino mass.

[5]The neutrino mass m_ν is mainly supressed by the smallness of μ and largeness of Λ. Different from the typical Seesaw, here Λ is supposed to be just $O(1 \sim 10$ TeV) [133], thus this kind of models may be tested in future experiments like LHC.

where V_{en_j} and V_{es_j} are the mixings corresponding to the heavy sterile states N and S. In the one-generation case,

$$\sum_j V_{en_j} = V_{e4} = \frac{2m_D}{\sqrt{4(m_D^2+\Lambda^2)+4M_1^2}},$$
$$\sum_j V_{es_j} = V_{e5} = \frac{2m_D}{\sqrt{4(m_D^2+\Lambda^2)+4M_2^2}}.$$

Then

$$\sum_j \left(\frac{V_{en_j}^2}{m_{n_j}} + \frac{V_{es_j}^2}{m_{s_j}}\right) = -\frac{m_D^2\mu'}{(m_D^2+\Lambda^2)^2}.$$

Now, Eq. (3.10) can be rewritten as

$$[T_{1/2}^{0\nu}]_i^{-1} = G_i \left| \frac{m_D\Lambda^{-1}\mu\Lambda^{-1}m_D - (\epsilon m_D'\frac{1}{\Lambda}m_D + m_D\frac{1}{\Lambda}\epsilon m_D')}{m_{\rm e}}\mathcal{M}_{\nu,i} - m_{\rm p}\frac{m_D^2\mu'}{(m_D^2+\Lambda^2)^2}\mathcal{M}_{N,i}\right|^2. \tag{3.12a}$$

Eq. (3.12a) shows why Extended Seesaw (or Inverse Seesaw) is interesting. If μ and ϵ are negligible, then the smallness of active neutrino mass can be explained and $(\beta\beta)_{0\nu}$-decay is dominated by the heavy sterile neutrinos contributions,

$$[T_{1/2}^{0\nu}]_i^{-1} = G_i|m_{\rm p}\frac{m_D^2\mu'}{(m_D^2+\Lambda^2)^2}\mathcal{M}_{N,i}|^2.$$

This is also discussed in ref. [84]. However, the light neutrino contribution from loop-level should be noticed. Eq. (3.11) shows that the effective mass goes to 0 if both μ and ϵ are 0, but the light neutrino mass can also be generated through radiative corrections. In the rest of this section, we are going to calculate the radiative correction. We will prove that in certain parameter regions of Extended Seesaw, the light neutrino contribution from loop level can be much smaller than or comparable to heavy neutrinos contribution. This would lead to an exception of the discussion in *Subsection 3.2.1* and the possible cancellation in $(\beta\beta)_{0\nu}$-decay.

3.2.4 One-loop correction of light ν mass

In this subsection, the estimation of one loop correction of light ν mass will be shown. Then in the next subsection, we will further analyse the possibility of "dominant heavy ν contribution in $(\beta\beta)_{0\nu}$-decay" after the radiative mass is considered.

The radiative neutrino mass has been widely discussed [141, 142, 143, 144, 145]. In fact,

neutrino mass models beyond leading order are always well motivated due to the loop suppression, which allows us to lower the scale of mass generation. Here we basically follow the calculations in [143, 144], but develop it in the Extended Seesaw case.

After electro-weak symmetry breaking, the one-loop diagrams generate corrections to each element in the mass matrix M,

$$M = \begin{pmatrix} 0 & m_D^T & \epsilon m_D'^T \\ m_D & \mu' & \Lambda^T \\ \epsilon m_D' & \Lambda & \mu \end{pmatrix} + \begin{pmatrix} \delta M_L & \delta m_D^T & \delta(\epsilon m_D'^T) \\ \delta m_D & \delta\mu' & \delta\Lambda^T \\ \delta(\epsilon m_D') & \delta\Lambda & \delta\mu \end{pmatrix}.$$

Most importantly, due to the finite one-loop correction, the upper left-hand corner of M is not zero but δM_L. This Majorana mass term is not allowed at tree-level. Henceforth Eq. (3.4) does not apply in the following discussion.

Then, including the loop corrections, the mass of light neutrino is,

$$\begin{aligned} M_\nu =& m_D^T \frac{\mu}{\Lambda^T\Lambda + \mu\mu'} m_D - \epsilon(m_D'^T \frac{1}{\Lambda^T} m_D + m_D^T \frac{1}{\Lambda} m_D') \\ &+ \delta M_L \\ &+ [(\delta m_D^T \frac{\mu}{\Lambda^T\Lambda + \mu\mu'} m_D + m_D^T \frac{\mu}{\Lambda^T\Lambda + \mu\mu'} \delta m_D + m_D^T \frac{\delta\mu}{\Lambda^T\Lambda + \mu\mu'} m_D \\ &- m_D^T \frac{\mu}{\Lambda^T\Lambda + \mu\mu'} \mu' \delta\mu \frac{1}{\Lambda^T\Lambda + \mu\mu'} m_D - m_D^T \frac{\mu}{\Lambda^T\Lambda + \mu\mu'} \mu \delta\mu' \frac{1}{\Lambda^T\Lambda + \mu\mu'} m_D \\ &- 2 m_D^T \frac{\Lambda}{\Lambda^T\Lambda + \mu\mu'} \delta\Lambda \frac{\mu}{\Lambda^T\Lambda + \mu\mu'} m_D) \\ &- (\delta(\epsilon m_D'^T) \frac{1}{\Lambda^T} m_D + m_D^T \frac{1}{\Lambda} \delta(\epsilon m_D') + \epsilon m_D'^T \frac{1}{\Lambda^T} \delta(m_D) + \delta(m_D^T) \frac{1}{\Lambda} (\epsilon m_D') \\ &- \epsilon m_D'^T \frac{1}{\Lambda^2} \delta(\Lambda) m_D - m_D^T \frac{1}{\Lambda^2} \delta(\Lambda) \epsilon m_D')] \end{aligned} \tag{3.13}$$

The correction terms in the bracket [ ] are supposed to be negligible comparing with δM_L. In fact, in order to discuss the case when tree-level mass is much smaller than one-loop correction, we simply set μ and $\epsilon = 0$, or, small enough to be negligible. Then Eq (3.13) becomes

$$M_\nu = \delta M_L + m_D^T \frac{\delta\mu}{\Lambda^T\Lambda + \mu\mu'} m_D. \tag{3.13a}$$

From the diagonalization relation of the mass matrix in Eq. (3.6), we can see that

$$\delta M_L = U_L^* \Sigma(p^2) U_L^\dagger \tag{3.14a}$$

$$\delta\mu = U_S \Sigma(p^2) U_S^T, \tag{3.14b}$$

where $\Sigma(p^2)$ is the self-energy in mass-states.

To evaluate Eq.(3.14a) and Eq.(3.14b), the diagrams contributing to neutrino self-energy

have to be calculated in the Extended Seesaw model. The neutrino self energy involves the exchange of Z, neutral Goldstone boson G^0, neutral higgs h^0 and other charged particles, as shown in Figure 3.4. However, as discussed in Ref. [144], the charged particles diagrams just have irrelevant contributions to the ν mass corrections. The self-energy function $\Sigma(p^2)$ can be separated as,

$$\Sigma(p^2) = \Sigma^Z(p^2) + \Sigma^{G^0}(p^2) + \Sigma^{h^0}(p^2)$$

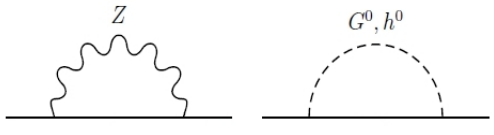

Figure 3.4: Self energy diagrams contributing to the neutrino mass correction.

The calculation of the self-energy diagrams in Fig 3.4 involves the coupling between Z, G^0, h^0 with the Majorana neutrino states χ [144]:

$$\mathcal{L}_Z = \frac{g}{4\cos\theta_w} Z_\mu \bar{\chi}\gamma^\mu[\gamma_L(U_L^\dagger U_L) - \gamma_R(U_L^T U_L^*)]\chi, \tag{3.15a}$$

$$\mathcal{L}_{G^0} = \frac{i}{2\sqrt{2}} G^0 \bar{\chi}[(U_R^\dagger \lambda U_L + U_L^T \lambda^T U_R^*)\gamma_L + (U_L^\dagger \lambda^\dagger U_R + U_R^T \lambda^* U_L^*)\gamma_R]\chi, \tag{3.15b}$$

$$\mathcal{L}_{h^0} = \frac{-1}{2\sqrt{2}} h^0 \bar{\chi}[(U_R^\dagger \lambda U_L + U_L^T \lambda^T U_R^*)\gamma_L + (U_L^\dagger \lambda^\dagger U_R + U_R^T \lambda^* U_L^*)\gamma_R]\chi. \tag{3.15c}$$

Then, we can get the self-energy function as

$$\begin{aligned}
\Sigma^Z(p^2) &= \Sigma^Z(0) \quad (p^2 = m_\nu \approx 0) \\
&= \frac{ig^2}{4c_w^2} \int \frac{d^d k}{(2\pi)^d} \sum_j \frac{\not{k} + m_j}{k^2 - m_j^2} (U_L^T U_L^*)(U_L^\dagger U_L) \\
&\quad \times \{\frac{d}{(k-p)^2 - m_z^2} + \frac{1}{m_z^2}(\frac{(k-p)^2}{(k-p)^2 - \xi m_z^2} - \frac{(k-p)^2}{(k-p)^2 - m_z^2})\},
\end{aligned}$$

where ξ is the gauge parameter in general R_ξ gauge[6]. g is the SU(2) coupling constant, which satisfies $\sqrt{2}M_w/g = v \simeq 174$ GeV.

Since the terms proportional to $\not{k}$ vanish due to symmetry, the equation above can be further

[6]The result of mass corrections should be gauge-independent, therefore the terms with ξ are expected to cancel each other or vanish.

simplified as,

$$\Sigma^Z(0) = i\frac{g^2}{4c_w^2}\int \frac{d^dk}{(2\pi)^d}\sum_j \frac{m_j}{k^2-m_j^2}(U_L^T U_L^*)(U_L^\dagger U_L)\times\{\frac{d}{k^2-m_z^2}+\frac{1}{m_z^2}(\frac{k^2}{k^2-\xi m_z^2}-\frac{k^2}{k^2-m_z^2})\}. \tag{3.16}$$

Similarly, the contributions from goldstone boson and neutral higgs are

$$\Sigma^{G^0}(0) = \frac{-ig^2}{4c_w^2 m_z^2}\int \frac{d^dk}{(2\pi)^d}\frac{k^2}{k^2-\xi m_z^2}\sum_j \frac{m_j}{k^2-m_j^2}\times(\hat{M}U_L^\dagger U_L + U_L^T U_L^*\hat{M})(\hat{M}U_L^\dagger U_L + U_L^T U_L^*\hat{M}), \tag{3.17}$$

$$\Sigma^{h^0}(0) = \frac{ig^2}{4c_w^2 m_z^2}\int \frac{d^dk}{(2\pi)^d}\frac{k^2}{k^2-m_h^2}\sum_j \frac{m_j}{k^2-m_j^2}\times(\hat{M}U_L^\dagger U_L + U_L^T U_L^*\hat{M})(\hat{M}U_L^\dagger U_L + U_L^T U_L^*\hat{M}). \tag{3.18}$$

Substitute Eqs. (3.16 - 3.18) into Eq. (3.14a) and (3.14b). We first tackle δM_L. From Eq. (3.14a), we know that $\delta M_L = U_L^*(\Sigma^Z(0)+\Sigma^{G^0}(0)+\Sigma^{h^0}(0))U_L$, using the relations of the mixing matrix in Eqs. (3.7), we can get

$$\begin{aligned}\delta M_L = {} & \frac{ig^2}{4c_w^2}\int\frac{d^dk}{(2\pi)^d}(\frac{d}{k^2-m_z^2}U_L^*\frac{\hat{M}}{k^2-\hat{M}^2}U_L^\dagger - \frac{1}{m_z^2}\frac{1}{k^2-m_z^2}U_L^*\frac{\hat{M}^3}{k^2-\hat{M}^2}U_L^\dagger)\\ & + \frac{ig^2}{4c_w^2}\int\frac{d^dk}{(2\pi)^d}\frac{1}{m_z^2}\frac{1}{k^2-m_h^2}U_L^*\frac{\hat{M}^3}{k^2-\hat{M}^2}U_L^\dagger.\end{aligned}$$

After integration (substituting $d = 4$ - ϵ), we get

$$\begin{aligned}\delta M_L = {} & \frac{-4g^2}{(64\pi^2)c_w^2}U_L^*\hat{M}(\frac{1}{\epsilon}-\gamma+\mathrm{Ln}(4\pi)+\frac{1}{2}-\mathrm{Ln}\hat{M}^2-\frac{\mathrm{Ln}(\frac{\hat{M}^2}{m_z^2})}{\frac{\hat{M}^2}{m_z^2}-1})U_L^\dagger\\ & + \frac{g^2}{(64\pi^2)c_w^2}U_L^*\hat{M}^3(\frac{1}{\epsilon}-\gamma+\mathrm{Ln}(4\pi)+\frac{1}{2}-\mathrm{Ln}\hat{M}^2-\frac{\mathrm{Ln}(\frac{\hat{M}^2}{m_z^2})}{\frac{\hat{M}^2}{m_z^2}-1})U_L^\dagger\\ & - \frac{g^2}{(64\pi^2)c_w^2}U_L^*\hat{M}^3(\frac{1}{\epsilon}-\gamma+\mathrm{Ln}(4\pi)+\frac{1}{2}-\mathrm{Ln}\hat{M}^2-\frac{\mathrm{Ln}(\frac{\hat{M}^2}{m_z^2})}{\frac{\hat{M}^2}{m_z^2}-1})U_L^\dagger\\ & = \mathrm{I}+\mathrm{II}+\mathrm{III},\end{aligned} \tag{3.19}$$

where

$$\mathrm{I} \equiv \frac{-4g^2}{(64\pi^2)c_w^2}U_L^*\hat{M}U_L^\dagger(\frac{1}{\epsilon}-\gamma+\mathrm{Ln}(4\pi)+\frac{1}{2})+\frac{4g^2}{(64\pi^2)c_w^2}U_L^*\hat{M}(\mathrm{Ln}(\hat{M}^2)+\frac{\mathrm{Ln}(\frac{\hat{M}^2}{m_z^2})}{\frac{\hat{M}^2}{m_z^2}-1})U_L^\dagger.$$

Since $U_L^* \hat{M} U_L^\dagger = 0$ (refer to Eq. (3.7)), the first term of I vanishes, which means that the divergent term of I = 0. Only the finite term is left

$$\begin{aligned}
\mathrm{I} &= \frac{4g^2}{(64\pi^2)c_w^2} U_L^* \hat{M} (\mathrm{Ln}(\hat{M}^2) + \frac{\mathrm{Ln}(\frac{\hat{M}^2}{m_z^2})}{\frac{\hat{M}^2}{m_z^2} - 1}) U_L^\dagger \\
&= \frac{4g^2}{(64\pi^2)c_w^2} U_L^* \hat{M} (\mathrm{Ln}(m_z^2) + \frac{(\frac{\hat{M}^2}{m_z^2})\mathrm{Ln}(\frac{\hat{M}^2}{m_z^2})}{\frac{\hat{M}^2}{m_z^2} - 1}) U_L^\dagger \\
&= \frac{4g^2}{(64\pi^2)c_w^2} U_L^* \hat{M}^3 \frac{\mathrm{Ln}(\frac{\hat{M}^2}{m_z^2})}{\frac{\hat{M}^2}{m_z^2} - 1} U_L^\dagger.
\end{aligned}$$

For the terms II and III, the divergent terms cancel each other as we can see from Eq.(3.19), thus

$$\begin{aligned}
\mathrm{II} + \mathrm{III} &= \frac{g^2}{(64\pi^2)c_w^2} U_L^* \hat{M}^3 (-\frac{\mathrm{Ln}(\frac{\hat{M}^2}{m_z^2})}{\frac{\hat{M}^2}{m_z^2} - 1} + \frac{\mathrm{Ln}(\frac{\hat{M}^2}{m_h^2})}{\frac{\hat{M}^2}{m_h^2} - 1}) U_L^\dagger \\
\therefore \delta M_L &= \mathrm{I} + \mathrm{II} + \mathrm{III} \\
&= \frac{g^2}{(64\pi^2)c_w^2} U_L^* \hat{M}^3 (\frac{3\mathrm{Ln}(\frac{\hat{M}^2}{m_z^2})}{\frac{\hat{M}^2}{m_z^2} - 1} + \frac{\mathrm{Ln}(\frac{\hat{M}^2}{m_h^2})}{\frac{\hat{M}^2}{m_h^2} - 1}) U_L^\dagger. \qquad (3.20)
\end{aligned}$$

The calculation of $\delta\mu$ is similar to the calculation above. We have

$$\begin{aligned}
\delta\mu(Z) &= U_S \Sigma^Z(0) U_S^T \\
&= i\frac{g^2}{4c_w^2} \int \frac{d^dk}{(2\pi)^d} U_S (U_L^T U_L^*) \sum_j \frac{m_j}{k^2 - m_j^2} (U_L^\dagger U_L) U_S^T \times \{\frac{d}{k^2 - m_z^2} + \frac{1}{m_z^2}(\frac{k^2}{k^2 - \xi m_z^2} - \frac{k^2}{k^2 - m_z^2})\} \\
&\propto U_L U_S^T \\
&= 0.
\end{aligned}$$

Thus, Z boson does not contribute to the correction of $\delta\mu$. Furthermore, since the contribution from Z boson is absent in this case, the goldstone boson is not involved in the radiative correction of $\delta\mu$ as well.
Similarly,

$$\begin{aligned}
\delta\mu(h^0) &= U_S \Sigma^{h^0}(0) U_S^T \\
&= \frac{ig^2}{4c_w^2 m_z^2} \int \frac{d^dk}{(2\pi)^d} \frac{k^2}{k^2 - m_h^2} \times U_S (\hat{M} U_L^\dagger U_L + U_L^T U_L^* \hat{M}) \sum_j \frac{m_j}{k^2 - m_j^2} (\hat{M} U_L^\dagger U_L + U_L^T U_L^* \hat{M}) U_S^T \\
&= 0,
\end{aligned}$$

due to the relations between U_S and U_L in Eq. (3.7).
Hence we conclude that the finite correction of $\delta\mu = 0$. Eq. (3.13a) can be rewritten as

$$\begin{aligned} M_\nu &= \delta M_L + m_D \frac{\delta\mu}{\Lambda^2 + \mu\mu'} m_D, \\ &= \delta M_L, \\ &= \frac{g^2}{(64\pi^2)c_w^2} U_L^* \hat{M}^3 \left(\frac{3\mathrm{Ln}(\frac{\hat{M}^2}{m_z^2})}{\frac{\hat{M}^2}{m_z^2} - 1} + \frac{\mathrm{Ln}(\frac{\hat{M}^2}{m_h^2})}{\frac{\hat{M}^2}{m_h^2} - 1}\right) U_L^\dagger, \\ &= \frac{g^2}{(64\pi^2)c_w^2} [(U_{L_2}^*)^2 M_1^3 \left(\frac{3\mathrm{Ln}(\frac{M_1^2}{m_z^2})}{\frac{M_1^2}{m_z^2} - 1} + \frac{\mathrm{Ln}(\frac{M_1^2}{m_h^2})}{\frac{M_1^2}{m_h^2} - 1}\right) + (U_{L_3}^*)^2 M_2^3 \left(\frac{3\mathrm{Ln}(\frac{M_2^2}{m_z^2})}{\frac{M_2^2}{m_z^2} - 1} + \frac{\mathrm{Ln}(\frac{M_2^2}{m_h^2})}{\frac{M_2^2}{m_h^2} - 1}\right)] \\ &\text{(in the case of 1-generation),} \end{aligned} \tag{3.21}$$

where $\hat{M}$ and U_L are defined as before.

Thus, δM_L (or M_ν) can be expressed as a function of (Λ, μ') under different values of Yukawa coupling (or m_D). As we assume δM_L dominates over the tree level contribution, the values of Λ, μ' and Yukawa coupling (Y) have to be confined by the light ν mass constraints, $\sqrt{\Delta m_\odot^2}$ eV $\leq \delta M_L \leq 0.58$ eV. The upper bound is from 95% C.L allowed region from the cosmological constraint [135], which requires that light neutrino mass being smaller than 0.58 eV; The lower bound corresponds to the square root of the solar neutrino mass difference. These constraints restrict the values of Λ and μ' in particular regions.
For example, in the cases of Yukawa coupling $Y = 10^{-3}$ and $Y = 10^{-4}$, the allowed values of Λ, μ' are shown as the following region-plots.

Previously we have proved that the radiative correction of the light neutrino mass could dominate over the tree level mass. Now in Fig. 3.5 we further show that in which parameter regions, this finite correction satisfies the constraints of light ν mass ($\sqrt{\Delta m_\odot^2}$ eV $\leq M_\nu \leq$ 0.58 eV).
It is interesting to note that in Fig. 3.5, there are two limits arising in the allowed parameter regions (assume that Λ, $\mu' \gg m_D$ in both limits).
i) $\mu' \ll \Lambda$, we call it as the Inverse Seesaw Limit (ISL).
In this limit, the ν mass matrix is similar to the Inverse Seesaw one discussed in Ref. [139]. The two eigenvalues of heavy neutrino mass $M_1 \simeq \mu'/2 - \Lambda$, $M_2 \simeq \mu'/2 + \Lambda$ [Eq. (3.9) and Eq. (3.10)], i.e., $|M_1| \simeq |M_2|$, which means that the heavy neutrino spectrum is quasi-degenerate.

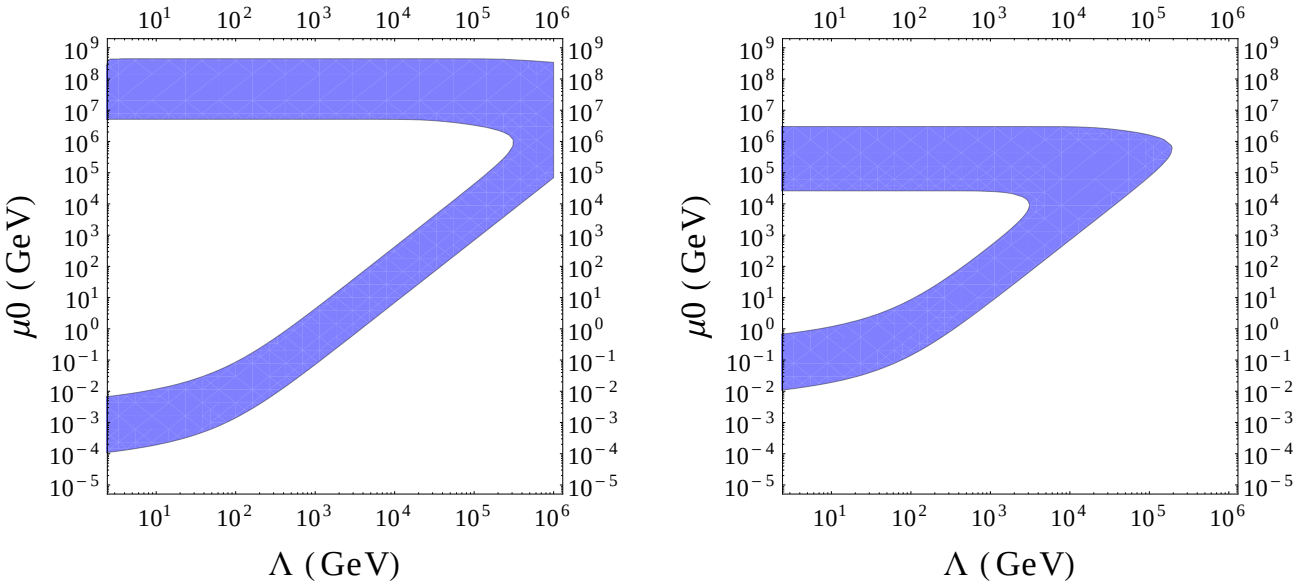

Figure 3.5: The allowed parameter regions (blue) which satisfy $\sqrt{\Delta m^2_\odot}$ eV $\leq \delta M_L \leq 0.58$ eV. Left panel corresponds to $Y = 10^{-3}$ ($m_D = 0.174$ GeV); Right panel corresponds to $Y = 10^{-4}$ ($m_D = 0.0174$ GeV).

On the other hand, the mixings of the two heavy ν states are given by

$$V_{en} \equiv U_{L_2} \simeq \frac{m_D}{\sqrt{2}\Lambda}, \qquad V_{es} \equiv U_{L_3} \simeq \frac{m_D}{\sqrt{2}\Lambda},$$

which means that the two heavy neutrino have similar mixings. In addition, they will also have similar contributions to neutrinoless double beta decay, as we will discuss in the next subsection. This limit corresponds to the lower parts in Fig. 3.5

ii) $\mu' \gg \Lambda$, we call it as the Extended Seesaw Limit (ESL).

In this limit, the ν mass matrix is similar to the Extended Seesaw one discussed in Refs. [90, 84]. $M_1 \simeq -\dfrac{\Lambda^2}{\mu'}$, $M_2 \simeq \mu'$. This scenario leads to $|M_1| \ll |M_2|$, corresponding to a hierarchical heavy neutrino spectrum. In this case, the mixings of the two heavy ν states are given by

$$V_{en} \equiv U_{L_2} \simeq \frac{m_D}{\Lambda}, \qquad V_{es} \equiv U_{L_3} \simeq \frac{m_D}{\mu'}.$$

Substitute these approximations back to Eq. (3.21), since $|M_1| \ll |M_2|$, the light ν mass

could be rewritten as

$$M_\nu = \delta M_L \simeq \frac{g^2}{(64\pi^2)c_w^2}(U_{L_3}^*)^2 M_2^3\left(\frac{3\mathrm{Ln}(\frac{M_2^2}{m_z^2})}{\frac{M_2^2}{m_z^2}-1}+\frac{\mathrm{Ln}(\frac{M_2^2}{m_h^2})}{\frac{M_2^2}{m_h^2}-1}\right),$$
$$\simeq \frac{g^2}{(64\pi^2)c_w^2}\left(\frac{m_D^*}{\mu'^*}\right)^2\mu'^3\left(\frac{3\mathrm{Ln}(\frac{\mu'^2}{m_z^2})}{\frac{\mu'^2}{m_z^2}-1}+\frac{\mathrm{Ln}(\frac{\mu'^2}{m_h^2})}{\frac{\mu'^2}{m_h^2}-1}\right),$$

which is independent of Λ, this explains to the upper parts in Fig. 3.5.
However, in this limit, the "lighter" heavy neutrino ($M_1 \simeq -\frac{\Lambda^2}{\mu'}$) contributes more to $(\beta\beta)_{0\nu}$-decay. We will discuss about it in the next subsection.

Once the one-loop ν mass correction is taken into account, the previous estimation of $(\beta\beta)_{0\nu}$-decay has to be changed and Eq. (3.12a) is no longer correct. The contribution from light ν cannot be neglected even if the tree level mass approximates to zero. In the next subsection we will study in what conditions may (or may not) be possible to have a dominant heavy neutrino contribution in $(\beta\beta)_{0\nu}$-decay, if the loop level ν mass dominates over tree-level one. We will pay special attention to the one-loop correction impact and the experimental constraints on the parameters of the model.

3.2.5 Dominant heavy ν contribution in $(\beta\beta)_{0\nu}$-decay

Now, we are going to discuss in which circumstances the heavy neutrino mechanism would be dominant in $(\beta\beta)_{0\nu}$-decay but the process would be still measurable.
The previous subsections showed that if ν mass generation is dominated by tree-level, then due to Eq. (3.5) the $(\beta\beta)_{0\nu}$ will be dominated by standard (light ν) mechanism. The interesting question is "what happens when ν mass is mainly generated through one-loop diagrams". In this scenario, Eq. (3.12) is rewritten as

$$[T_{1/2}^{0\nu}]_i^{-1} = G_i|\frac{\delta M_L}{m_\mathrm{e}}\mathcal{M}_{\nu,i} + m_\mathrm{p}\sum_j\left(\frac{V_{en_j}^2}{m_{n_j}}+\frac{V_{es_j}^2}{m_{s_j}}\right)\mathcal{M}_{N,i}|^2$$
$$= G_i|\left\{\frac{g^2}{(64\pi^2)c_w^2}U_L^*\hat{M}^3\left(\frac{3\mathrm{Ln}(\frac{\hat{M}^2}{m_z^2})}{\frac{\hat{M}^2}{m_z^2}-1}+\frac{\mathrm{Ln}(\frac{\hat{M}^2}{m_h^2})}{\frac{\hat{M}^2}{m_h^2}-1}\right)U_L^\dagger\right\}\frac{1}{m_\mathrm{e}}\mathcal{M}_{\nu,i} - m_\mathrm{p}\frac{m_D^2\mu'}{(m_D^2+\Lambda^2)^2}\mathcal{M}_{N,i}|^2. \quad (3.22)$$

The first term represents the contribution from light ν mechanism (A_light), the second one corresponds to the heavy ν contribution (A_heavy). Both contributions depend strongly on μ', Λ and Yukawa coupling Y. Therefore, A_light and A_heavy are still related even once the one-loop corrections are considered. In this chapter, we are interested in the possibility that heavy ν

contribution dominating the $(\beta\beta)_{0\nu}$-decay. Thus in the following, we assume that $A_{\rm light}$ is negligible and just focus on the contribution from $A_{\rm heavy}$, and check if this assumption agrees with the results of different neutrino experiments. We will discuss the significant interference between $A_{\rm light}$ and $A_{\rm heavy}$ in the next chapter. This means that Eq. (3.22) is rewritten as

$$[T^{0\nu}_{1/2}]^{-1}_i \approx G_i |m_{\rm p} \frac{m_D^2 \mu'}{(m_D^2+\Lambda^2)^2} \mathcal{M}_{N,i}|^2 \tag{3.23}$$

Meanwhile, the parameters of the model should be constrained by the results of various neutrino experiments. To illuminate the interplay among all this factors, we will show our results as in Fig. 3.6, and 3.7.

In Fig. 3.6, Yukawa coupling $Y = 10^{-3}$ and 10^{-4} are used as examples to show the allowed parameter regions corresponding to the following constraints. First of all, the radiative neutrino mass correction δm_L should satisfy the condition "$\sqrt{\Delta m^2_\odot}$ eV $\leq \delta M_L \leq 0.58$ eV" (refer to the discussion in the previous subsection and Fig. 3.5). This constraint is shown in the blue areas. Second, the mixing limit between active and heavy neutrinos from weak decay has to be respected, as mentioned in *Chapter 2* and Ref. [71], which further constrains the parameters. The allowed regions corresponding to the mixing limit are represented by the red areas, which means that the white regions are ruled out by the mixing limit. Moreover, if heavy ν contribution dominates in $(\beta\beta)_{0\nu}$-decay, the corresponding result should respect the current experimental bound. In addition, in order to be phenomenologically interesting, a hypothetically dominant heavy contribution should be also inside the sensitivity limit of the future $(\beta\beta)_{0\nu}$-decay experiments[7]. The orange bands represent the $\langle m_{\beta\beta}\rangle$ bounds.

The intersections of the blue, red and orange areas in Fig. 3.6 are the allowed regions. It is important to note that the allowed regions exist not only when $Y = 10^{-3}$, 10^{-4}. For other values of Yukawa couplings, significant contribution from heavy ν mechanism are also possible. Fig. 3.7 summarizes all the allowed regions corresponding to Yukawa couplings in the order of 10^{-2} (red) ,10^{-3} (green), 10^{-4} (blue), 10^{-5} (orange) and 3×10^{-6} (purple). For Yukawa couplings larger than 10^{-2} or smaller than 10^{-6}, no significant contribution from heavy neutrinos can be possible[8].

Moreover, to show the allowed regions more clearly, only the intersections are shown in Fig. 3.7. Besides, as a reference, Fig. 3.7 also shows the lines corresponding to the ratio of $r \equiv |A_{\rm heavy}/A_{\rm light}| = 1$. This line is presented in order to show in which region $A_{\rm heavy}$ starts to

[7]According to Ref.[27], the sensitivities of next-to-next generation experiments would be $\langle m_{\beta\beta}\rangle \simeq 27$ - 41 meV. Here we conservatively require that $\langle m_{\beta\beta}\rangle \geq 50$ meV.

[8]We have checked that, between 10^{-6} and 10^{-8} a measurable contribution of the heavy neutrinos may still be possible in a very small region of the parameter space, but the light neutrino masses can not be generated in the context of the model.

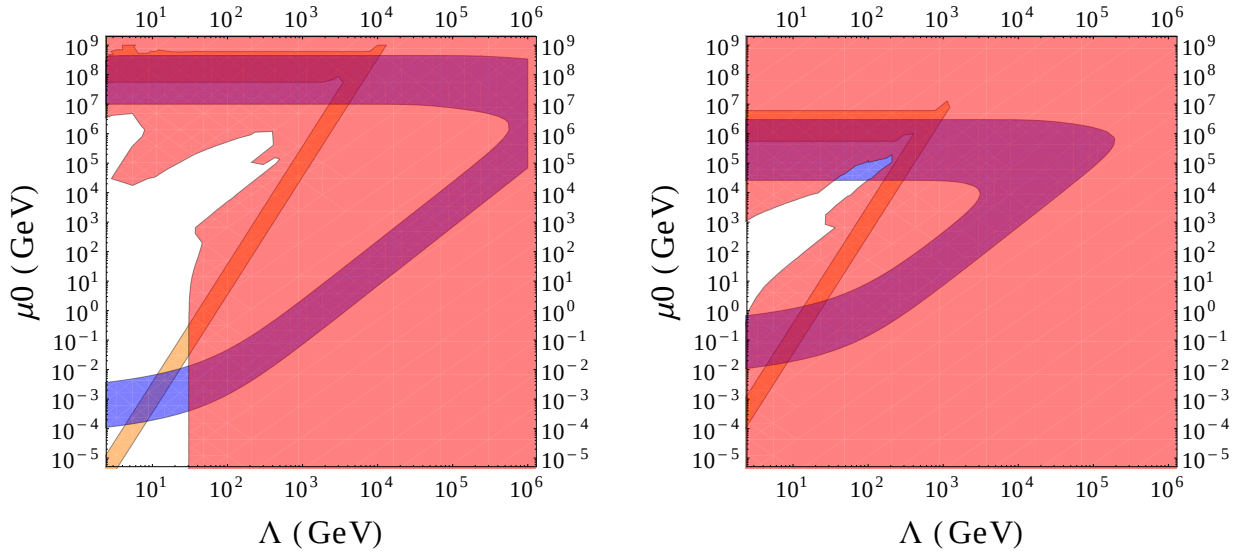

Figure 3.6: The allowed parameter regions (colored areas) which satisfy the constraints of light neutrino mass (blue), active-heavy neutrino mixing (red), current and future $(\beta\beta)_{0\nu}$-decay experimental results (orange). Details are given in the text. Left panel corresponds to $Y = 10^{-3}$ ($m_D = 0.174$ GeV); Right panel corresponds to $Y = 10^{-4}$ ($m_D = 0.0174$ GeV).

be larger than $A_{\rm light}$. We notice that the ratio r is hardly dependent on the Yukawa couplings. This is because in the Seesaw limit (Λ or $\mu' \gg m_D$), $A_{\rm light} \propto \delta M_L \propto Y^2$ and $A_{\rm heavy} \propto Y^2$ [146]. On the other hand, r depends on the ratio of the Nuclear Matrix Elements (NMEs). Since the NMEs of different nuclei are different, for simplicity, here we generally assumed the ratio of M_N/M_ν is 100. The ratio of M_N/M_ν will slightly affect the location of the green line in Fig. 3.7 but would not make a significant difference in the plots. A more detailed discussion concerning the precise values of different NMEs will be presented in the next chapter. Basically the L.H.S. of the green line is the area where heavy ν mechanism is larger than the traditional (light ν) mechanism in $(\beta\beta)_{0\nu}$-decay.

Similar to Fig. 3.5, in Fig. 3.7, the allowed regions appear the Inverse Seesaw and Extended Seesaw limits:

i) $\mu' \ll \Lambda$, ISL.

As discussed in the previous subsection, this limit corresponds to the Inverse Seesaw discussed in Ref. [139]. The two eigenvalues of heavy neutrino mass $|M_1| \sim |M_2|$, which means that the heavy neutrino spectrum is quasi-degenerate. Moreover, the two heavy ν mixings U_{L_2},

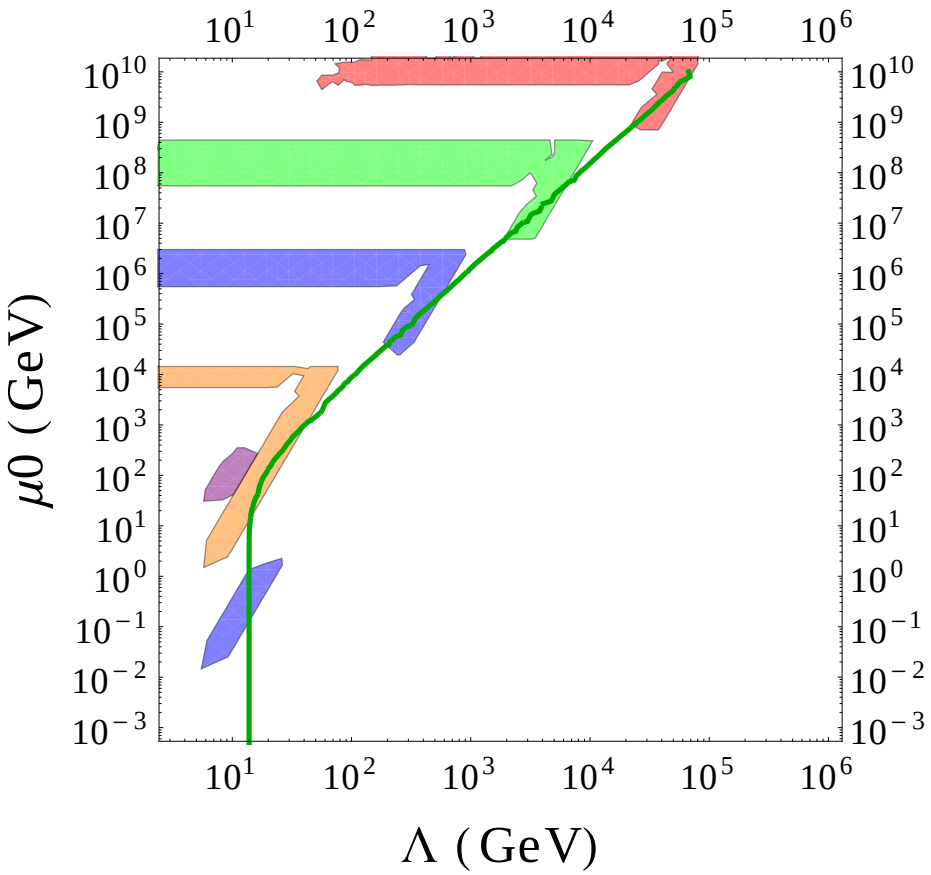

Figure 3.7: The allowed parameter regions (colored areas) which satisfy the constraints of different neutrino experimental results (refer to the text). Red, green, blue, orange and purple areas stand for $Y = 10^{-2}$, 10^{-3}, 10^{-4}, 10^{-5} and 3×10^{-6} respectively. The green line correspond to the ratio of $r \equiv |A_{\rm heavy}/A_{\rm light}| = 1$.

U_{L_3} are similar. Therefore,

$$\frac{V_{en}^2}{m_n} \equiv \frac{U_{L_2}^2}{M_1} \simeq \frac{U_{L_3}^2}{M_2} \equiv \frac{V_{es}^2}{m_s},$$

which means that they have similar contributions to neutrinoless double beta decay. Furthermore, it is important to notice that in the ISL, the dominant contribution from the heavy neutrinos can take place only in a very confined area. For $Y = 10^{-2}$ and 10^{-3}, the allowed region of ISL is even ruled out (by the active-heavy neutrino mixing limit);

ii) $\mu' \gg \Lambda$, ESL.

This limit corresponds to the Extended Seesaw one discussed in Refs. [90, 84]. In this scenario, $|M_1| \ll |M_2|$, corresponding to a hierarchical heavy neutrino spectrum. The "lighter" heavy neutrino (M_1) contributes more to $(\beta\beta)_{0\nu}$-decay. The heavier one due to the suppres-

sion of the factor $1/M_2$, only contributes irrelevantly to the process. Moreover, the heavier state also has a smaller mixing ($U_{L_2} \simeq \frac{m_D}{\Lambda}$, $U_{L_3} \simeq \frac{m_D}{\mu'}$, i.e., $U_{L_2} \gg U_{L_3}$). Therefore,

$$\frac{V_{en}^2}{m_n} \equiv \frac{U_{L_2}^2}{M_1} \gg \frac{U_{L_3}^2}{M_2} \equiv \frac{V_{es}^2}{m_s}.$$

Thus the 'lighter' sterile neutrino has larger contribution to $(\beta\beta)_{0\nu}$-decay. In addition, it is interesting to note that in this limit $|M_1|$ could be $\lesssim 100$ MeV, thus its contribution may not be suppressed by the factor of $1/M_1$ in certain ranges of μ'. In the ESL, the dominant contribution from the heavy neutrinos can take place in larger regions and is allowed for all values of Yukawa couplings.

The calculations above are made under the assumption of one generation of sterile neutrino. However, it is straightforward to extend it to the general case with three standard model neutrinos. The calculation above shows that theoretically it is possible that loop diagrams dominate over the tree-level contribution in the light neutrino mass generation. In this case, it is possible that the heavy neutrino contribution to neutrinoless double beta decay is not negligible. More details can be referred to Ref. [146].

To conclude, if the neutrino mass is generated at tree-level, the standard mechanism would be likely the leading contribution in $(\beta\beta)_{0\nu}$-decay due to the reasons discussed in *Subsection 3.2.1*. However, the above discussion shows that, in particular Seesaw models, it is allowed that $|\langle m_\nu \rangle| = 0$ at tree-level and the loop level contribution dominates. In this case, Eq. (3.4) and (3.5) are not satisfied. Then it would be possible for heavy ν mechanism to dominate the $(\beta\beta)_{0\nu}$-decay even if the masses of sterile neutrinos are very large. Moreover, since heavy neutrinos contribution can dominate over $(\beta\beta)_{0\nu}$-decay, it is also possible that $|A_{\text{heavy}}| = |A_{\text{light}}|$ and they have different signs. Therefore the heavy neutrino mechanism could make a significant destructive interference with the standard light ν mechanism and effectively reduce the decay rate. The potential cancellation effect will be discussed in detail in the next chapter.

3.3 The Other Example of New Physics—Trilinear R-parity Violation

The previous section has studied the heavy neutrino exchange mechanisms, which involve different kinds of **Seesaw models**. The discussion in *Section 3.2* suggests that the new physics source can dominate over the traditional mechanism (light ν exchange) under certain circumstances. To make the analysis of $(\beta\beta)_{0\nu}$-decay more complete, we will further

investigate the other potential leading mechanism in the $(\beta\beta)_{0\nu}$-decay. Since the trilinear R-parity violation (RPV) can also induce the light neutrino mass through loop diagrams, theoretically it could also dominate the process. Hence it is worth studying this mechanism though it is not related to sterile neutrinos. In the rest of this section, we will briefly analyse the possibility of dominant RPV mechanisms in $(\beta\beta)_{0\nu}$-decay.

In supersymmetry, R-parity is defined as $R = (\text{-}1)^{3B+L+2S}$, with B, L being the baryon and lepton numbers, and S the spin. R-parity violation may trigger LNV process and allows additional terms in superpotential as

$$W_{\not{R}_p} = \lambda_{ijk} L_i L_j E^c_k + \lambda'_{ijk} L_i Q_j D^c_k + \mu_i L_i H_2. \tag{3.24}$$

Once RPV is allowed, the $\not{R}_p$ coupling parameters lead to the automatic generation of neutrino masses and mixings. RPV can lead to lepton number violation and Majorana neutrino masses in the absence of right-handed neutrino and Seesaw mechanism.
The last term in Eq. (3.24) is the bilinear term. It can also induce the ν mass and $(\beta\beta)_{0\nu}$-decay [120, 138]. However, as stated in *Subsection 3.2.2*, the bilinear RPV terms generate the light ν mass in a similar way as Type I Seesaw mechanism. Following the similar derivation in Ref. [136], we can prove that it is sub-dominant.
For simplicity, from now on we focus on the trilinear λ' coupling and its contribution to $(\beta\beta)_{0\nu}$-decay. Similar to heavy sterile neutrino, trilinear R-parity violation is related to the LNV process $(\beta\beta)_{0\nu}$-decay, thus it may be an alternative way to explain the neutrino mass generation. In fact, similar to the discussion of Extended Seesaw in previous section, the trilinear RPV terms are involved with neutrino mass matrix at loop-level (Fig. 3.8) and thus they would not suffer from the constraint such as Eq. (3.4). From the relation between λ'_{ijk} and the neutrino mass matrix, the upper limits of λ'_{ijk} can be revealed. Therefore we can check that in $(\beta\beta)_{0\nu}$-decay, whether the contributions from **R-parity violation mechanisms** are significant.

3.3.1 The trilinear contribution to ν mass matrix

Eqs. (3.2c) and (3.2d) show that both η_λ and η_q depend on the trilinear coupling λ'_{ijk}. To compare the contributions from light ν and $\not{R}_p$ mechanism, the range of different λ'_{ijk} has to be estimated. Similar to the study of **heavy neutrino mechanism**, the estimation of λ'_{ijk} will be achievable through the relation between trilinear coupling and neutrino mass matrix. The R-parity violation can lead to neutrino mass generation through tree-level and loop self-energy diagrams. The tree-level contributions come from the bilinear terms in Eq. (3.24),

which we are not considering in this thesis (as we discussed previously). The loop diagram, as shown in Fig. 3.8, involves the quark-squark mixing and the trilinear coupling λ'. The particles that propagate inside the loops are quarks and squarks. For the sake of simplicity, in

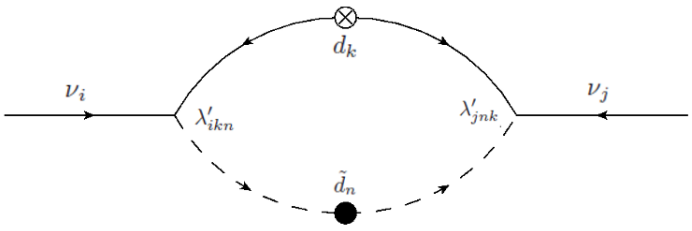

Figure 3.8: Squark-quark loop contribution to ν mass generation.

the following estimation, we ignored other contributions and assumed that ν mass generation mainly comes from the loop-diagram[9] in Figure 3.8. Reference [149] shows that the relation between neutrino mass matrix and trilinear coupling constants are as follows,

$$M^{\nu}_{ii'} = \frac{3}{16\pi^2}\lambda'_{ijk}\lambda'_{i'jk}[\sin(2\theta^k)m_{q^j} \times (\frac{\log(x_2^{jk})}{x_2^{jk}-1} + \frac{(x_2^{jk}-1)\log(x_1^{jk})}{x_1^{jk}-1(x_2^{jk}-1)}) + (j \leftrightarrow k)], \tag{3.25}$$

where

$$\begin{aligned}\sin(2\theta^k) &= 2m_{q^k}(A_k + \mu\tan\beta)\times \\ &\quad [(m^2_{\tilde{q}^k_L} - m^2_{\tilde{q}^k_R} - 0.34M_Z^2\cos(2\beta))^2 - 4(m_q^k(A_k+\mu\tan\beta))^2]^{-1/2}, \\ x_1^{jk} &= m^2_{q^j}/m^2_{\tilde{q}^k_1}, \quad x_2^{jk} = m^2_{q^j}/m^2_{\tilde{q}^k_2}.\end{aligned}$$

The definitions of $m^2_{\tilde{q}^k_1}$ and $m^2_{\tilde{q}^k_2}$ can be found in Ref. [149], while $m^2_{\tilde{q}^k_L}$ and $m^2_{\tilde{q}^k_L}$ in Ref. [129]. All of them are functions of m_0^2 (universal scalar mass) and $m_{1/2}^2$ (universal gaugino mass) [129].

We followed the assumptions in Ref. [149] and set up the values for different SUSY parameters, i.e.,

$\tan\beta \approx 20$,

$A_k = A_0 Y_k$, with $A_0 = 500$ GeV and Y_k is the Yukawa coupling for quarks,

$m_0 \approx m_{1/2} \gtrsim O(100)$GeV.

[9]Similar to the heavy sterile ν case, it is always expected that if RPV generates the light ν mass, the corresponding tree-level masses always dominate over the loop induced masses [147]. However, reference [148] showed that it is possible that the loop contribution exceeds the tree-level. In this thesis, we just simply adopt the conventional hypothesis that different approaches to ν mass generation do not compensate each other and thus we can estimate the limit of squark-quark loop contribution without knowing the others.

Since the values of η_λ and η_q depend on the values of m_0^2 and $m_{1/2}^2$, the universal scalar and gaugino mass are the key factors in our estimation. They are always supposed to be of the same order. In our calculation, we simply assumed $m_0^2 = m_{1/2}^2$ and then used Eq. (3.25) to get the limit of different λ'_{ijk}.

Since $(\beta\beta)_{0\nu}$-decay is only related to $\langle m_\nu \rangle = \sum_k (U_{ek})^2 m_k = M_{11}^\nu$, we rewrite Eq. (3.25) as

$$M_{11}^\nu = \frac{3}{16\pi^2}\lambda'_{1jk}\lambda'_{1jk}[\sin(2\theta^k)m_{q^j} \times (\frac{\log(x_2^{jk})}{x_2^{jk}-1} + \frac{(x_2^{jk}-1)\log(x_1^{jk})}{x_1^{jk}-1(x_2^{jk}-1)}) + (j \leftrightarrow k)]. \tag{3.25a}$$

In the rest of this section, we will use Eq. (3.25a) and estimate the contributions of "short-range trilinear $\not{R}_p$" and "long-range trilinear $\not{R}_p$" mechanisms and compare them with the standard light ν mechanism.

3.3.2 The short-range $\not{R}_p$

First, we concentrate on the discussion of short-range trilinear R-parity violation. The so-called "short-range $\not{R}_p$" mechanism means that at the quark level, the R-parity violating process arises from exchanging the heavy SUSY particles like gluinos, neutralinos, squarks (the left panel of Fig. 3.1), etc. All these processes involve only the λ'_{111} coupling constant. And among all these terms, the gluino exchange is supposed to dominate [150].

Since η_λ involves only λ'_{111}, we used Eq. (3.25a) to extract its limit and ignore the other coupling constants[10]. Eq. (3.25a) can be rewritten as

$$\begin{aligned} M_{11}^\nu &= \langle m_\nu \rangle \\ &\geq \frac{3}{16\pi^2}\lambda'_{111}\lambda'_{111}\times \\ &[\sin(2\theta^1)m_{q^1} \times (\frac{\log(x_2^{11})}{x_2^{11}-1} + \frac{(x_2^{11}+1)\log(x_1^{11})}{(x_1^{11}-1)(x_2^{11}-1)}) \times 2] \\ &= \lambda'^2_{111} C, \end{aligned} \tag{3.26}$$

where C is a parameter that depends on the value of m_0,

$$\begin{aligned} C = \frac{3}{16\pi^2}&[\sin(2\theta^1)m_{q^1}\times \\ &(\frac{\log(x_2^{11})}{x_2^{11}-1} + \frac{(x_2^{11}+1)\log(x_1^{11})}{(x_1^{11}-1)(x_2^{11}-1)}). \times 2]. \end{aligned}$$

Eq. (3.26) shows the relation between λ'_{111}, m_0 and the effective neutrino mass $\langle m_\nu \rangle$. Sub-

[10] Actually, there is no particular reason to ignore other λ'_{ijk}. On the contrary, if we use flavour symmetry to explain the fermion mass hierarchy, the contribution from λ'_{111} would be sub-dominant in the mass generation instead [151]. Here we just want to estimate the possible largest contribution to $(\beta\beta)_{0\nu}$-decay from short-range RPV mechanism.

stituting it into Eq. (3.2c), we get the constraint of η_λ,

$$\eta_\lambda \leq \frac{\pi\alpha_s}{6}\frac{(\langle m_\nu\rangle/C)}{G_F^2 m_{\tilde{d}_R}^4}\frac{m_{\rm p}}{m_{\tilde{g}}}\cdot[1+(\frac{m_{\tilde{d}_R}}{m_{\tilde{u}_L}})^2]^2. \tag{3.27}$$

Similar to the study of heavy neutrino mechanism, in $(\beta\beta)_{0\nu}$-decay, there may exist sizable contribution from short-range $\not{R}_p$, but the $\not{R}_p$ generated light ν mass has to be compatible with the neutrino experiments, i.e. $\lambda'^2_{111}C \leq \langle m_\nu\rangle \leq$ cosmology bound[11]. This will constrain the parameters λ'_{111} and m_0, and thus the maximum of η_λ is constrained as well [Eq. (3.27)]. However, about the estimation of λ'_{111}, we should keep in mind that λ'_{111} is related to $\sin(2\theta^k)$ [Eq. (3.25)], which depends on μ and $\tan\beta$, whose values are not confirmed yet. In Ref.[149], $\tan\beta$ is assumed to be 20. On the other hand, μ should be of the same order of sparticle masses [129]. In this thesis, we will follow these assumptions and analyse the value of λ'_{111} in different cases: $\mu = m_0$, 5 m_0 and 10 m_0.

Moreover, if short-range $\not{R}_p$ really dominates the $(\beta\beta)_{0\nu}$-decay, the contribution from η_λ should respect the current experimental bound and be larger than the future experimental sensitivity (just like the discussion of Fig. 3.6). This will further constrain the values of λ'_{111} and m_0. The allowed parameter regions (λ'_{111} – m_0) of dominant short-range $\not{R}_p$ contribution are shown in Figure 3.10 (left panel).

The discussion above just reveals the upper limit of η_λ, it is still possible that $\eta_\lambda \ll \eta_\nu$ and thus standard light ν mechanism dominates the process. Eq. (3.27) only shows the possible maximum of η_λ. It shows the possibility of short-range R-parity violation mechanism have significant contribution in the $(\beta\beta)_{0\nu}$-decay.

3.3.3 The long-range $\not{R}_p$

Besides the previous mechanism, the trilinear R-parity violation can also induce the $(\beta\beta)_{0\nu}$-decay by squark-neutrino mechanism [122], which suggests that the neutrino mediated $(\beta\beta)_{0\nu}$-decay originate from $\not{R}_p$ interactions. This mechanism is comparatively long-range as the intermediate particle is a light ν rather than gluinos. The LNV parameter for this "long-range (squark-neutrino) $\not{R}_p$" mechanism is η_q [Eq. (3.2d)].

By using the similar trick as before, the upper limit of η_q can be estimated and is related to the value of m_ν. Here we use the same assumption in the estimation of "short-range" contribution, λ'_{111} dominating among the trilinear coupling constants [12]. This means that

[11] Different with the constraints in *Section 3.2* , which just concerns the 1 generation ν mass correction from loop diagrams. In this section, Eq. (3.25) gives the whole ν mass matrix and Eq. (3.26) is particularly about $\langle m_\nu\rangle$. In the **Normal Hierarchy** $\langle m_\nu\rangle$ could be smaller than $\sqrt{\Delta m^2_\odot}$. Thus here the constraint is looser.

[12] According to ref [148], The maximum of $\lambda'_{112}\lambda'_{121}$ and $\lambda'_{113}\lambda'_{131} \gtrsim \mathrm{Max}(\lambda'^2_{111})$, thus we would just get the similar approximation if we assume $\lambda'_{112}\lambda'_{121}$ or $\lambda'_{113}\lambda'_{131}$ dominates in Eq. (3.2d).

Eq. (3.2d) changes to

$$\eta_q = \frac{\lambda'^2_{111}}{2\sqrt{2}G_F}[\sin 2\theta^d_{(1)}(\frac{1}{m^2_{\tilde{d}_1(1)}} - \frac{1}{m^2_{\tilde{d}_2(1)}})] \tag{3.29}$$

As showed in the previous subsection, $\lambda'^2_{111} \leq \langle m_\nu \rangle / C$, where

$$C = \frac{3}{16\pi^2}[\sin(2\theta^1) m_{q^1} \times (\frac{\log(x_2^{11})}{x_2^{11}-1} + \frac{(x_2^{11}+1)\log(x_1^{11})}{(x_1^{11}-1)(x_2^{11}-1)}). \times 2]$$

Thus the maximum of η_q is

$$\eta_q \leq \frac{\langle m_{\beta\beta} \rangle / C}{2\sqrt{2}G_F}[\sin 2\theta^d_{(1)}(\frac{1}{m^2_{\tilde{d}_1(1)}} - \frac{1}{m^2_{\tilde{d}_2(1)}})], \tag{3.30}$$

$$\text{while} \quad \langle m_\nu \rangle \geq \lambda'^2_{111} C.$$

Similar to the previous subsection, the constraint of neutrino mass should be satisfied, which means $\lambda'^2_{111} C \leq \langle m_\nu \rangle \leq$ cosmology bound. Also, the current limit and future sensitivities of $(\beta\beta)_{0\nu}$-decay experiments should be respected. Thus the parameters λ'_{111} and m_0 are constrained. The allowed regions of dominant contribution from long-range $\not{R}_p$ mechanism are plotted in the right panel of Fig. 3.9.

It is noteworthy that in Fig. 3.9, the colored areas on the left side are smaller than the right side, which means that "short-range $\not{R}_p$ " is more unlikely to dominate the $(\beta\beta)_{0\nu}$-decay. This is reasonable as short-range mechanism is expected to be smaller than long-range mechanism (the exchange particle is heavier in short-range $\not{R}_p$), thus short-range $\not{R}_p$ is more unlikely to have large contribution.

Moreover, different from Seesaw mechanism, the model of ν mass generation through R-parity violation is full of uncertainties and assumptions. For example, the values of m_0 (universal scalar mass) and $m_{1/2}$ (universal gaugino mass) are assumed to be equal for simplicity. Besides, in Eq. (3.25), the coupling A_k, the ratio of Higgs vacuum expectation values v_u and v_d, and the bilinear Higgs mixing parameter μ are not determined yet [148]. In this thesis, λ'_{ijk} are even assumed to be 0 if $i \neq 1$. Since the focus of this thesis is sterile neutrino, a lot of assumptions are made for the $\not{R}_p$ mechanism in this thesis. We just want to show the other mechanism which could have significant contribution to $(\beta\beta)_{0\nu}$-decay and even could effectively interfere with the standard light ν mechanism. Trilinear R-parity violation is mentioned in this thesis mainly because it could generate the light ν mass through loop diagrams and thus is not strongly suppressed. (We did not argue that the trilinear RPV must have large contributions in the $(\beta\beta)_{0\nu}$-decay.)

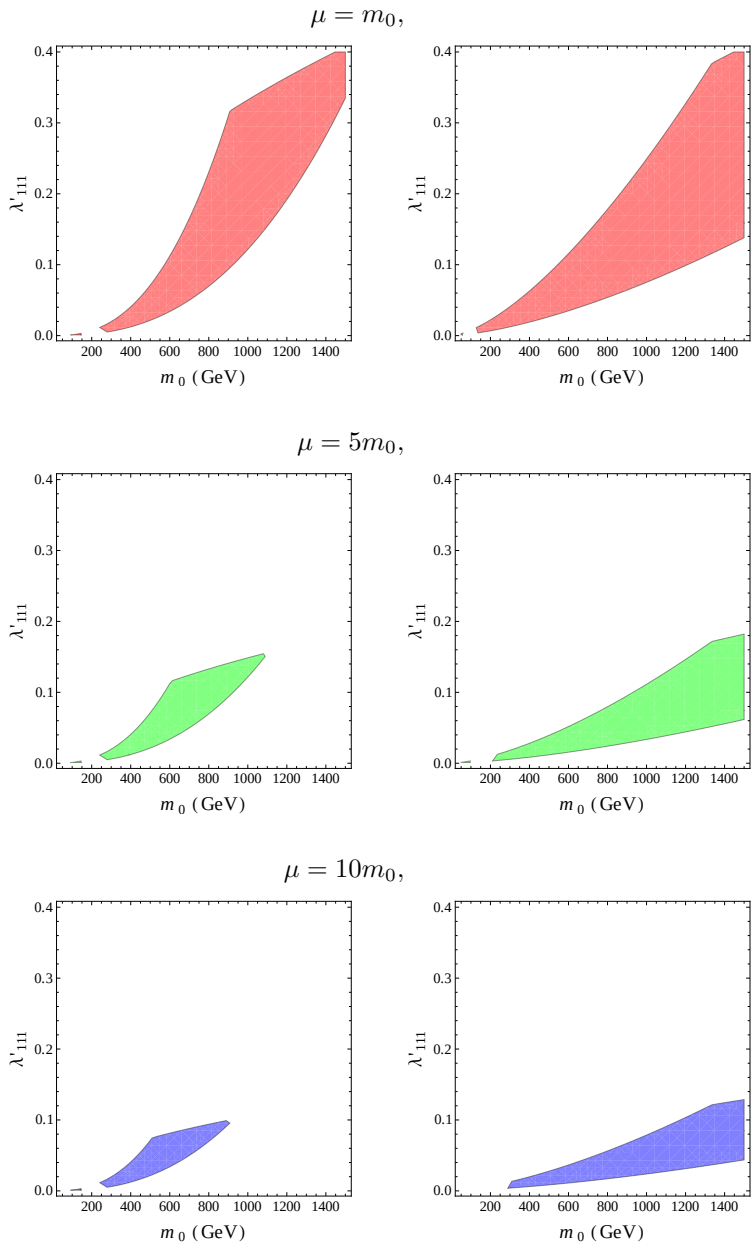

Figure 3.9: The allowed regions where dominant contributions from RPV (left, short-range; right, long-range) are between the bounds from current experimental results and the future sensitivity of $(\beta\beta)_{0\nu}$-decay experiments, i.e. 0.55 eV $\geq \langle m_{\beta\beta} \rangle \geq$ 50 meV , and the corresponding $\langle m_{\beta\beta} \rangle$ is compatible with the experiment results. The red, green and blue plots correspond to $\mu = m_0$, 5 m_0 and 10 m_0.

3.4 Summary

In this chapter, we briefly introduce the $(\beta\beta)_{0\nu}$-decay and four interesting mechanisms which can induce this process. Previously the exchange of light ν is assumed to be the leading mechanism, but we proved that heavy ν mechanism and trilinear RPV can also dominate this process. In the analysis of heavy ν mechanism, the typical Type-I Seesaw and Extended Seesaw were studied. The relation between ν mass generation and $(\beta\beta)_{0\nu}$-decay is discussed carefully and the importance of heavy sterile neutrino in these two issues are revealed. If Extended Seesaw is correct and TeV scale sterile neutrino is found in the future, the observation of Lepton Number Violating process at LHC will become more promising (as mentioned in *Chapter 2*). This chapter shows that it is possible that heavy ν mechanism (or RPV mechanisms) could be at the similar order as the traditional (light ν) mechanism. In the next chapter we will further tackle the possibility that they significantly cancel each other.

Chapter 4

The Possible Cancellation in $(\beta\beta)_{0\nu}$-decay

As stated in the previous chapter, it is important to determine the leading mechanism in $(\beta\beta)_{0\nu}$-decay and extract the values of the corresponding LNV parameters. However, it is also possible that the contributions from different mechanisms may be **of the same order**. As Eq. (3.1) shows, the decay rate is given by

$$\Gamma_i \equiv [T^{0\nu}_{1/2}]^{-1}_i = G_i \mid \eta_\nu \mathcal{M}_{\nu,i} + \eta_N \mathcal{M}_{N,i} + \eta_\lambda \mathcal{M}_{\lambda,i} + \eta_q \mathcal{M}_{q,i} \mid^2 .$$

In this equation, the LNV parameters η_ν, η_N, η_λ and η_q could have different signs or even be complex. Therefore, one can assume that these mechanisms destructively interfere with each other, which leads to the smallness of the decay rate. Actually, the absence of observation of $(\beta\beta)_{0\nu}$-decay further favours this assumption. For instance, the contributions from light neutrino and heavy neutrino mechanisms may effectively cancel each other and significantly reduce the decay rate of the process, as first considered in Ref. [152]. This may explain why the detection of neutrinoless double beta decay is absent in the current experiments and hints that even if neutrino is Majorana particle, future experiments may still fail to detect the signal of $(\beta\beta)_{0\nu}$-decay in some nuclei. This would become more interesting if "KArlsruhe TRItium Neutrino" (KATRIN) experiment [153, 154] measures $m_\nu > 0.2$ eV, but the measurements in $(\beta\beta)_{0\nu}$-decay experiments suggest that $\mid \langle m_\nu \rangle \mid$ should be smaller than 0.2 eV. In this case, the destructive interference in $(\beta\beta)_{0\nu}$-decay is likely to exist. In this chapter, we will continue to study the **Extended Seesaw** and **trilinear RPV** to determine whether it is possible that significant cancellations exist. We will further analyse how the cancellation assumption affects the current and future measurements of $(\beta\beta)_{0\nu}$-decay.

Here we discuss the cancellation effect in different cases, the cancellation between '**light**

neutrino and **heavy neutrino**', between '**light neutrino** and **short-range trilinear RPV**', and between '**light neutrino** and **long-range trilinear RPV**' mechanisms. We only discuss the cancellation between two mechanisms in each case in order to highlight the impact of destructive interferences. Similar considerations also apply in other mechanisms (e.g., extra-dimension).

4.1 The Possibility of Significant Cancellation

4.1.1 Cancellation between light and heavy ν mechanisms

As discussed in *Section 3.2*, through **Extended Seesaw**, the light neutrino mass can be generated at loop level and thus the heavy ν mechanism can contribute significantly to neutrinoless double beta decay. In this subsection, we assume that

$$\begin{aligned}\Gamma_i &= G_i \mid \eta_\nu \mathcal{M}_{\nu,i} + \eta_N \mathcal{M}_{N,i} \mid^2 \\ &= G_i |\frac{\delta M_L}{m_{\rm e}} \mathcal{M}_{\nu,i} - m_{\rm p} \frac{m_D^2 \mu'}{(m_D^2+\Lambda^2)^2} \mathcal{M}_{N,i}|^2. \\ &= G_i \mid A_{\rm light} + A_{\rm heavy} \mid^2 . \end{aligned} \tag{4.1}$$

The expression of the one-loop mass correction δM_L is referred to Eq. (3.20).
We assume that the contributions $A_{\rm light}$ and $A_{\rm heavy}$ destructively interfere with each other. To check whether an exact cancellation between "$A_{\rm light}$ and $A_{\rm heavy}$" can take place, similar to the plots in Fig. 3.8 (described the regions that heavy ν mechanism dominates the process), the parameters Λ, μ' and the Yukawa coupling Y must be constrained by different neutrino experiments. However, here the decay rate is defined as Eq. (4.1) rather than the approximation in Eq. (3.23), and now we are interested in the case that the decay rate (or the corresponding "$m_{\beta\beta}$") is smaller than the future experimental sensitivity[1]. This would lead to the failure of future measurements. Fig 4.1 shows that when Yukawa coupling Y = 0.01, 0.001, 10^{-4}, 10^{-5} and 10^{-6}, the decay-rate in Eq. (4.1) will be smaller than future experimental sensitivity in particular regions of Λ–μ' space.

Similar to the plots in *Chapter 3*, the position of the solid black line ($|A_{\rm light}| = |A_{\rm heavy}|$) is the same for different Yukawa couplings (since $A_{\rm light}$ and $A_{\rm heavy}$ are both proportional to Y^2 [146]), but this line depends on the ratio of the Nuclear Matrix Elements (NMEs). It means that it should be slightly different for different nuclei. However, for simplicity, here

[1]According to Ref.[27], the sensitivities of next-to-next generation experiments would be $\langle m_{\beta\beta}\rangle \simeq$ 27 - 41 meV. Here Fig. 4.1 conservatively requires that $\langle m_{\beta\beta}\rangle \leq$ 50 meV.

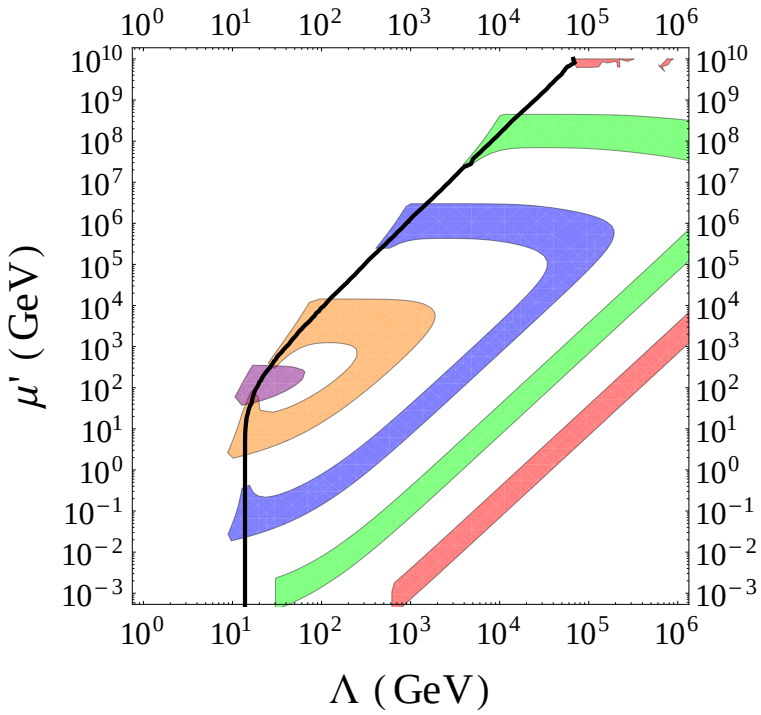

Figure 4.1: The allowed regions where combined contributions from heavy ν and standard light ν mechanisms are smaller than the future sensitivity, and the corresponding light ν mass and active-sterile ν mixing are compatible with the neutrino experiments. The red, green, blue, orange and purple plots correspond to Yukawa coupling = 0.01, 0.001, 10^{-4}, 10^{-5} and 3×10^{-6}. The solid black line represents when heavy ν contribution = light ν contribution, and the intersections between the black line and the colored areas are the regions that are phenomenologically interesting.

we assumed the ratio of M_N/M_ν is 100. The ratio of M_N/M_ν will slightly affect the location of the lines but would not make a significant difference to the plots. The exact values and ratios of the NMEs will be presented in the next section.

In Fig. 4.1, the colored areas correspond to those cases where the combined contributions from heavy ν and standard light ν mechanisms are smaller than the future sensitivity, but the smallnesses may also be a result from the lightness of neutrinos and the weak neutrino mixing. The intersections between the colored areas and the black line are the regions of interest in this study. These intersections imply that $|A_{\text{light}}| = |A_{\text{heavy}}|$ and at the same time $|A_{\text{light}} + A_{\text{heavy}}| <$ the future sensitivity. This corresponds to the possibility that we can not observe the $(\beta\beta)_{0\nu}$-decay due to the cancellation effect.

For Yukawa couplings smaller than 10^{-6}, the light neutrino masses generated at one loop

are smaller than $\sqrt{\Delta m^2_{\odot}}$; for Yukawa couplings larger than 10^{-2}, there are no intersections between the colored areas and the black line. Therefore the plots of other Yukawa couplings are not shown in Fig. 4.1.

In conclusion, in *Chapter 3* we showed that the heavy neutrino mechanism could have a large contribution toward $(\beta\beta)_{0\nu}$-decay. In that chapter, we further proved that a significant destructive interference or even an exact cancellation is possible in $(\beta\beta)_{0\nu}$-decay, and this would lead to the absence of observation in the future experiments. A more detailed analysis of the cancellation for different nuclei will be shown in *Section 4.2*.

4.1.2 Cancellation between light ν and $\not{R}_p$ mechanisms

As in the discussion on the heavy neutrino mechanism, here we assume that

$$\Gamma_i \equiv [T^{0\nu}_{1/2}]^{-1}_i = G_i \mid \eta_\nu \mathcal{M}_{\nu,i} + \eta_\lambda \mathcal{M}_{\lambda,i} \mid^2, \tag{4.2a}$$

$$\Gamma_i \equiv [T^{0\nu}_{1/2}]^{-1}_i = G_i \mid \eta_\nu \mathcal{M}_{\nu,i} + \eta_q \mathcal{M}_{q,i} \mid^2, \tag{4.2b}$$

and analyse the ranges in which λ'_{111} and m_0, the combined contribution from short-range (or long-range) $\not{R}_p$ and light ν mechanism[2], will be smaller than the future experimental sensitivities. The plots are shown in Fig. 4.2, which correspond to different values of μ (the relation between μ and λ'_{111} are noted in Eq. (3.25)).

Fig. 4.2 indicates that short-range (long-range) $\not{R}_p$ and standard light ν mechanisms can effectively cancel each other only in very fine-tuned areas. The small intersections between the colored areas and the black line represent the situations in which the short-range (long-range) $\not{R}_p$ contribution exactly cancels the light ν contribution. Again, this will lead to the absence of future measurements. Similar to the plots in Fig. 4.1, the location of the black line depends on the ratios of the NMEs, but we just assume $\mathcal{M}_\lambda = 100\mathcal{M}_\nu$ (or $\mathcal{M}_q = 100\mathcal{M}_\nu$ for the right panel). The phenomenological consequences will be discussed in detail in the next section.

It is noteworthy that in Fig. 4.2, the intersections on the left side are smaller than on the right side, which means that the cancellation between "short-range $\not{R}_p$ and light ν" is more fine-tuned than the cancellation between "long-range $\not{R}_p$ and light ν". This makes sense, since the short-range mechanism is expected to be smaller than the long-range mechanism (the exchange particle is heavier in short-range $\not{R}_p$); thus short-range $\not{R}_p$ is more unlikely to be at the same order of standard light ν mechanism.

[2]Here, $A_{active} \propto \delta M_L$ arises from trilinear $\not{R}_p$ loop diagrams, Fig. 3.8

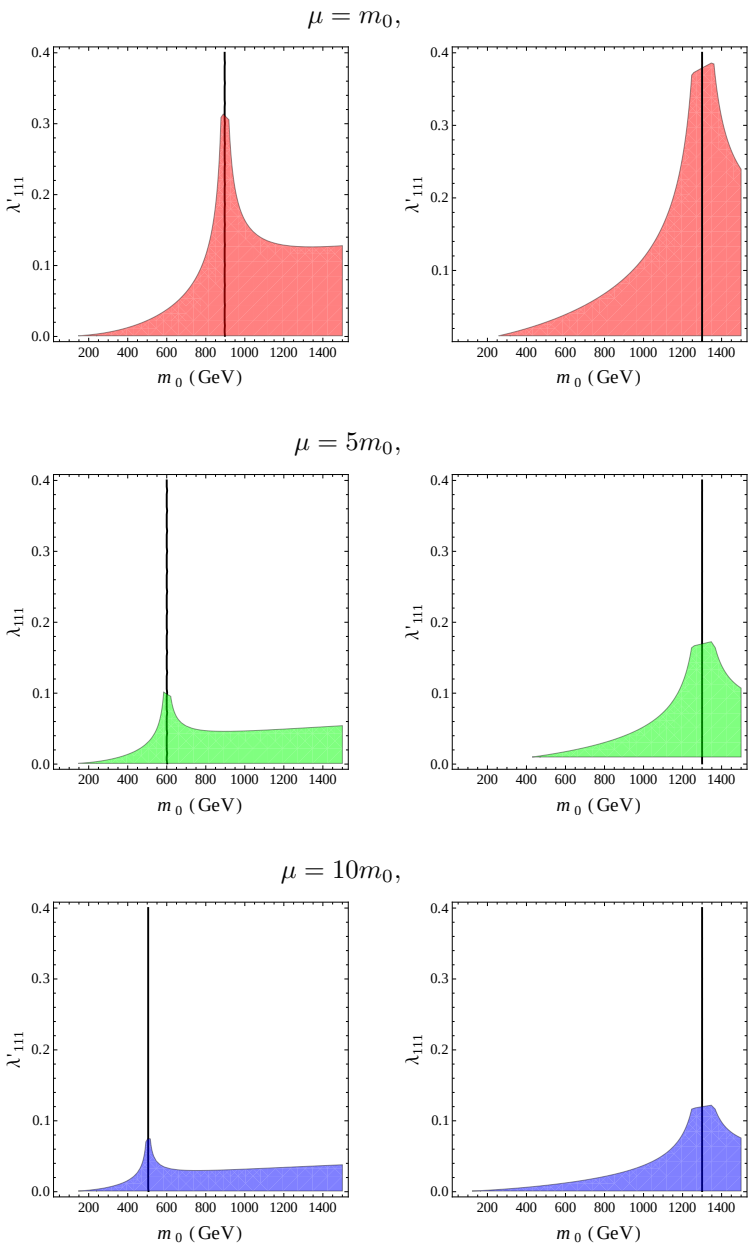

Figure 4.2: The allowed regions where combined contributions from RPV (left, short-range; right, long-range) and standard light ν mechanisms are smaller than the future sensitivity ($\langle m_{\beta\beta}\rangle \leq 50$ meV) of $(\beta\beta)_{0\nu}$-decay experiments, and the corresponding $\langle m_{\beta\beta}\rangle$ is compatible with the experiment results. The red, green and blue plots correspond to $\mu = m_0$, 5 m_0, 10 m_0. The solid black line represents when short-range (or long-range) RPV contribution = light ν contribution, and the intersections between the black line and the colored areas are the regions which are phenomenologically interesting.

4.2 The Cancellation Effect on Future Measurements

From the preceding sections, it is possible to argue that the "New Physics" mechanisms can be of the same order of the standard "light ν exchange" mechanism. In this section, we will quantitatively analyze the cancellation effects. But first, a precise evaluation of the nuclear matrix elements (NME) is necessary.

The evaluation of nuclear matrix elements suffers large uncertainties that in turn affect the predictions for the half-life time of the decay and the extraction of information on neutrino masses and mixing parameters from future measurements. They depend on the nuclear structure of the reaction, the adjustment of parameters like strength parameter 'g_{ph}, g_{pp}', the choice of the coupling constant g_A, the measurements of two-neutrino double beta decay and the exchange mechanism considered for the process [126, 131, 132].
In recent years, a wide effort has been devoted to the computation of the NME, using two main approaches: QRPA (quasiparticle random phase approximation) [132, 155] and NSM (nuclear shell model) [156, 157]. Encouragingly, the computed values tend to vary over a smaller range, despite large uncertainties.

In this thesis, the values of NMEs for all four mechanisms are taken from Ref. [128], where 8 variants of NMEs are listed, and each variant corresponds to different g_A values, *NN* potential and model space size. Since the ratio of the NMEs between the nuclei are similar for different variants (only the ratios of NMEs matter in our analysis, as shown in the following contents), and the discussion of 'different nuclei model and parameters' is beyond the scope of this thesis, here we present only the smallest and largest variants of NMEs in Ref. [128], as shown in Table 4.1.

All nuclear matrix elements were calculated under QRPA[3], since this approach keeps the uncertainties of NMEs largely under control [159]. The values of NME vary according to the species of nucleus. Table 4.1 shows the NMEs of four nuclei, which are the promising candidates in the future $(\beta\beta)_{0\nu}$-decay experiments.

It is interesting to note that in Table 4.1, $\mathcal{M}_N$, $\mathcal{M}_\lambda$ and $\mathcal{M}_q$ are much larger than $\mathcal{M}_\nu$. As Eq. (3.2b) shows, the contribution from heavy ν exchange is suppressed by the heavy ν masses. Similarly, the contributions from RPV mechanisms are also suppressed by the mass of SUSY particles. Previously, they were expected to be much smaller than the standard light ν mechanism. However, whenever the intermediate particles are heavy, the nuclear process becomes relatively short-range. The **finite nucleon size effect** must be taken into account

[3]In the Shell Model, it is difficult to construct all the intermediate nuclear states. However, in QRPA, the intermediate states of the nucleus are expressed as two quasiparticle states and then proper adjustments are made in the calculation. It has been shown that QRPA can handle great number of intermediate states. More details about QRPA are discussed in Refs. [117, 158]

and the calculation of the nuclear currents will be very different.

Table 4.1 The phase space factor and nuclear matrix elements for light, heavy neutrino exchange, short-range and long-range $\not{R}_p$ SUSY model.

	^{76}Ge	^{82}Se	^{100}Mo	^{130}Te
$G_i \times 10^{15}$ years [126]	7.93	35.2	57.3	55.4
Variant n.1 in [128]				
$\mathcal{M}_\nu$	3.85	3.59	3.62	3.29
$\mathcal{M}_N$	172	165	185	171
$\mathcal{M}_\lambda$	387	375	412	385
$\mathcal{M}_q$	396	379	405	382
Variant n.8 in [128]				
$\mathcal{M}_\nu$	5.82	5.66	5.15	4.70
$\mathcal{M}_N$	412	408	404	384
$\mathcal{M}_\lambda$	596	594	589	540
$\mathcal{M}_q$	728	720	691	641

Moreover, in these cases, the nucleons are coupled to the charged pions and this enhances the values of the corresponding nuclear matrix elements [160, 161, 121, 122]. At the nucleon level, there are two possible behaviours of the pions in flight between the nucleons. The first case is one pion mode: in the $(\beta\beta)_{0\nu}$-decay, one of the neutrons decays to a proton and two electrons and simultaneously produces a π^+, which is absorbed by another neutron and converts into a proton. The other scenario is the two pion mode: instead of π^+, the neutron produces a π^-. This π^- further decays into two electrons and one π^+. Again, the π^+ is absorbed by another neutron and converts into a proton. These two processes are shown in Fig. 4.3 (at the nucleon level).

Fig. 4.3 just illustrates the $(\beta\beta)_{0\nu}$-decay of pions in flight at nucleon level. More details about the process at the quark level are noted in *Appendix D*.

The nuclear matrix elements in Table 4.1 will be used to study whether it is possible to test the presence of destructive interference by combining the searches in different nuclei. In our analysis, the amplitude of $(\beta\beta)_{0\nu}$-decay for ^{76}Ge is assumed to be negligible (i.e., $\Gamma_{Ge} \sim 0$), due to interference between the two mechanisms and consequently, no signal for $(\beta\beta)_{0\nu}$-decay can be observed in this nucleus. The exact cancellation ($\Gamma_i \sim 0$) could also take place in other

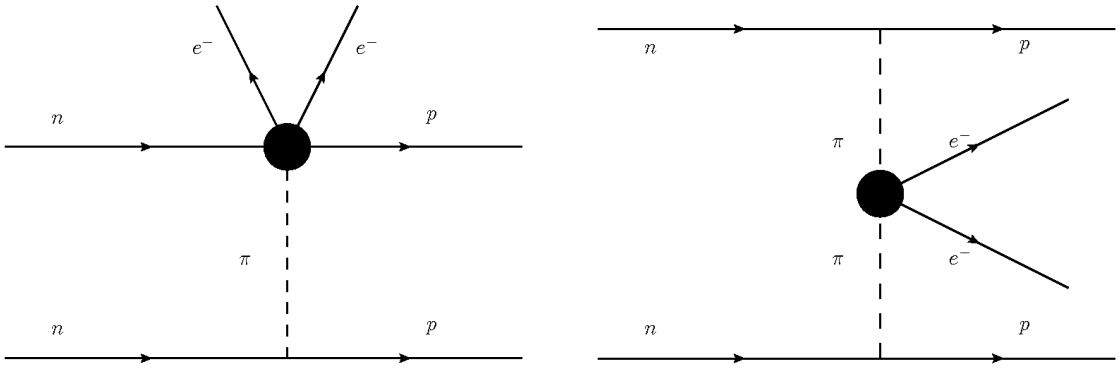

Figure 4.3: $(\beta\beta)_{0\nu}$-decay at the nucleon level. When the intermediate neutrinos (or SUSY particles like gluinos) are heavy, $(\beta\beta)_{0\nu}$-decay will be dominated by the pion exchange process. The left diagram represents one pion mode, while the right hand side is the two pion mode. The dark blobs denote the LNV vertices generated by the heavy sterile neutrinos (or trilinear R-parity violation).

nuclei and the corresponding analysis would be similar. Here we use ^{76}Ge as an example to show how the destructive interference will affect future measurements, since the experiments related to ^{76}Ge are most discussed in the last decade.

Based on this assumption, we calculate the amplitudes for other nuclei and test whether they are significantly different from zero.

The analysis will be performed in three different cases: i) The cancellation between light and heavy neutrino exchange mechanisms; ii) The cancellation between light neutrino and short-range $\not{R}_p$ mechanisms; and iii) The cancellation between light neutrino and long-range $\not{R}_p$ mechanisms.

4.2.1 Redefinition of $m_{\beta\beta}$

First, consider the interference between light and heavy neutrino mechanisms. Assume

$$\Gamma^{\nu N}_{Ge} = G_{Ge} \mid \eta_\nu M_{\nu,Ge} + \eta_N M_{N,Ge} \mid^2 \simeq 0, \tag{4.3}$$

$$\text{implying that } \eta_N = -\eta_\nu \times \frac{M_{\nu,Ge}}{M_{N,Ge}}. \tag{4.4}$$

Substituting Eq. (4.4) into the calculation of the amplitudes of other nuclei, the effective neutrino mass, $m_{\beta\beta}$, which will be measured by the future experiments and was previously

assumed to be simply $\sum_k^{\rm light}(U_{ek})^2 m_k$ of light neutrinos, should be redefined as

$$\begin{aligned} \mid m_{\beta\beta} \mid_i &= \mid \frac{m_e}{M_{\nu,i}}(\eta_\nu M_{\nu,i} - \eta_\nu \times \frac{M_{\nu,Ge}}{M_{N,Ge}} M_{N,i}) \mid, \\ &= \mid \langle m_\nu \rangle \times (1 - \frac{M_{\nu,Ge} \cdot M_{N,i}}{M_{N,Ge} \cdot M_{\nu,i}}) \mid . \end{aligned} \tag{4.5}$$

The $\mid m_{\beta\beta} \mid_i$ in L.H.S. of Eq. (4.5) is the value of "effective mass" expected to be observed in future experiments[4], while in R.H.S., $\langle m_\nu \rangle \equiv \sum_k^{\rm light}(U_{ek})^2 m_k$ is the effective light ν mass arising from the light ν mechanism. It follows immediately that if $\frac{M_{\nu,i}}{M_{\nu,Ge}} \neq \frac{M_{N,i}}{M_{N,Ge}}$, only partial cancellation will take place and $\mid m_{\beta\beta} \mid_i$ might be significantly different from 0.

Eq. (4.5) also manifests that despite the interference from heavy sterile neutrinos, the future measurement is still proportional to the effective light ν mass $\langle m_\nu \rangle$. The sensitivities of $\mid m_{\beta\beta} \mid_i$ of next-to-next generation experiments are expected to be around 27 - 41 meV [27]. Therefore, the value of $\langle m_\nu \rangle$ cannot be too small, otherwise the future experiments may not observe the process.

As mentioned in *Chapter 1*, the sign of Δm^2_{31} and the absolute neutrino mass scale [or the value of m_0, which is defined as $m_0 \equiv \min(m_1, m_2, m_3)$] is not determined yet, therefore, the ordering of the neutrino mass states is still unknown. There are three scenarios and they would give different values of $\langle m_\nu \rangle$ [162, 163].

(i) Normal Hierarchical Spectrum (NH), which indicates $m_0 = m_1 \ll m_2 \ll m_3$, $m_2 \simeq \sqrt{\Delta m^2_\odot}$, $m_3 \simeq \sqrt{\Delta m^2_{\rm A}}$. In this case,

$$\begin{aligned} |\langle m_\nu \rangle| &= |m_1 |U_{e1}|^2 + m_2 |U_{e2}|^2 e^{i\alpha_{21}} + m_3 |U_{e3}|^2 e^{i\alpha_{31}}| \\ &\simeq |(m_0 \cos^2\theta_\odot + e^{i\alpha_{21}} \sqrt{\Delta m^2_\odot + m_0^2} \sin^2\theta_\odot)\cos^2\theta_{13} + \sqrt{\Delta m^2_A + m_0^2} \sin^2\theta_{13} e^{i\alpha_{31}}| \end{aligned} \tag{4.6}$$

where α_{21} and α_{31} are the Majorana CPV phases.

(ii) Inverted Hierarchical Spectrum (IH), which indicates $m_0 = m_3 \ll m_1 \simeq m_2 \simeq \sqrt{\Delta m^2_{\rm A}}$. In this case,

$$\begin{aligned} |\langle m_\nu \rangle| &= |m_1 |U_{e1}|^2 + m_2 |U_{e2}|^2 e^{i\alpha_{21}} + m_3 |U_{e3}|^2 e^{i\alpha_{31}}| \\ &\simeq \sqrt{m_0^2 + \mid \Delta m^2_A \mid} \cos^2\theta_{13} (1 - \sin^2 2\theta_\odot \sin^2 \frac{\alpha_{21}}{2})^{1/2} \end{aligned} \tag{4.7}$$

(iii) Quasi-Degenerate Spectrum (QD), which indicates $m_0 = m_1 \simeq m_2 \simeq m_3 \gg \sqrt{\Delta m^2_{\rm A}}$, $m_0 \gtrsim 0.1$ eV. In this case,

$$\begin{aligned} |\langle m_\nu \rangle| &= |m_1 |U_{e1}|^2 + m_2 |U_{e2}|^2 e^{i\alpha_{21}} + m_3 |U_{e3}|^2 e^{i\alpha_{31}}| \\ &\simeq m_0 \mid \cos^2\theta_\odot + \sin^2\theta_\odot e^{i\alpha_{21}} \mid \end{aligned} \tag{4.8}$$

[4]Here we compare the measured "effective mass" rather than decay rates of different nuclei because the phase space factor G_i is not involved in Eq. (4.5). The cancellation effect of different nuclei would be obvious by comparing $\mid m_{\beta\beta} \mid_i$.

Obviously, $|\langle m_\nu \rangle|$ (NH) $<$ $|\langle m_\nu \rangle|$ (IH) $<$ $|\langle m_\nu \rangle|$ (QD). If the ν mass spectrum is *normal hierarchy*, then the corresponding $\mid m_{\beta\beta} \mid_i$ would be too small for the future measurement (even without the cancellation effect). More details about the relation between neutrino mass ordering and the $(\beta\beta)_{0\nu}$-decay are referred to Refs. [162, 163].

Similarly, we can evaluate $\mid m_{\beta\beta} \mid_i$ in the case of destructive interference between light ν and $\not{R}_p$ SUSY mechanisms. If the cancellation effect takes place between light ν and short-range $\not{R}_p$, then Eq. (4.4) and (4.5) will change to

$$\eta_\lambda = -\eta_\nu \times \frac{M_{\nu,Ge}}{M_{\lambda,Ge}}. \tag{4.9}$$

$$\mid m_{\beta\beta} \mid_i = \mid \langle m_\nu \rangle \times (1 - \frac{M_{\nu,Ge} \cdot M_{\lambda,i}}{M_{\lambda,Ge} \cdot M_{\nu,i}}) \mid . \tag{4.10}$$

If the cancellation effect takes place between light ν and long-range $\not{R}_p$, then Eq. (4.4) and (4.5) will change to

$$\eta_q = -\eta_\nu \times \frac{M_{\nu,Ge}}{M_{q,Ge}}. \tag{4.11}$$

$$\mid m_{\beta\beta} \mid_i = \mid \langle m_\nu \rangle \times (1 - \frac{M_{\nu,Ge} \cdot M_{q,i}}{M_{q,Ge} \cdot M_{\nu,i}}) \mid . \tag{4.12}$$

With Eqs. (4.5), (4.10) and (4.12), we can estimate the cancellation effect on the future measurements.

4.2.2 The future measurements

It was previously expected that the next-to-next generation experiments would observe $(\beta\beta)_{0\nu}$-decay if the ν mass spectrum was *inverted hierarchy* or *quasi-degenerate*. Therefore, we will first focus on the *inverted hierarchy* and *quasi-degenerate*. The range of $\langle m_\nu \rangle$ is assumed to be "0.01 eV (minimum of inverted hierarchy) - 1 eV (maximum of quasi-degenerate)". In Table 4.2, the expected values of $\mid m_{\beta\beta} \mid_i$, in the case of destructive interference between different mechanisms, are reported. Where $\mid m_{\beta\beta} \mid$(max) corresponds to the maximum of $\langle m_\nu \rangle$ in *quasi-degenerate*, $\mid m_{\beta\beta} \mid$(min) corresponds to the minimum of $\langle m_\nu \rangle$ in *inverted hierarchy*. The comparisons of the expected values of $\mid m_{\beta\beta} \mid_i$ and future experimental sensitivity (we take 50 meV as a conservative general assumption) are shown in Fig. 4.4. In Table 4.2 and Fig. 4.4, only the results corresponding to the NMEs of **Variant n.8** in Table 4.1 are shown, since the fuller study of different variants of NMEs lies outside the scope of this thesis (the NMEs of **Variant n.1** in Table 4.1 or other Variants in Ref.[128]

will lead to similar results, since the ratios of the the NMEs are similar).

Table 4.2 Expected values of $|m_{\beta\beta}|_i$ for different destructive interferences (assuming that $\Gamma_{\rm Ge} = 0$).

(eV)	^{76}Ge	^{82}Se	^{100}Mo	^{130}Te
	cancellation between heavy ν and light ν			
$\mid m_{\beta\beta} \mid$(max)	0	0.0183	0.108	0.154
$\mid m_{\beta\beta} \mid$(min)	0	1.83×10^{-4}	1.08×10^{-3}	1.54×10^{-3}
	cancellation between short $\not{R}_p$ and light ν			
$\mid m_{\beta\beta} \mid$(max)	0	0.0248	0.117	0.122
$\mid m_{\beta\beta} \mid$(min)	0	2.48×10^{-4}	1.17×10^{-3}	1.22×10^{-3}
	cancellation between long $\not{R}_p$ and light ν			
$\mid m_{\beta\beta} \mid$(max)	0	0.0170	0.0727	0.0903
$\mid m_{\beta\beta} \mid$(min)	0	1.70×10^{-4}	7.27×10^{-4}	9.03×10^{-4}

Table 4.2 and Fig. 4.4 reveal that if "exact cancellation" takes place in the decay of ^{76}Ge, then it is unlikely to observe any signals from the future experiments of ^{82}Se, since ^{76}Ge and ^{82}Se have similar values of NMEs. For ^{100}Mo and ^{130}Te, if the ν mass spectrum is quasi-degenerate, then observation is still possible. These results reflect that even if significant destructive interference really exists between various mechanisms in $(\beta\beta)_{0\nu}$-decay, the observation is still possible for certain nuclei, but it depends on the ν mass spectrum.

To show the dependence of ν mass spectrum and the cancellation effect more clearly, we reproduced the ν mass spectrum in Fig. 4.5 (corresponding to ^{82}Se) and Fig. 4.6 (corresponding to ^{130}Te). The cancellation effects between light ν and heavy ν mechanisms are shown (the cancellation effects between light ν and RPV mechanisms are similar). In Figs. 4.5 and 4.6, the $\mid m_{\beta\beta} \mid_i$ corresponding to traditional assumptions (light ν mechanism dominating the $0\nu\beta\beta$-decay), is also presented as a comparison [5].

The double beta decay of ^{82}Se is used as the first example, since under our assumption, the cancellation effect in this nuclei is most obvious.

Fig. 4.5 shows that due to the strong cancellation effect, the $\mid m_{\beta\beta} \mid_{^{82}Se}$ is almost two orders smaller than previously expected. Moreover, it is important to note that the intersections between the next-to-next generation sensitivity (red horizontal line) and the $\mid m_{\beta\beta} \mid_{^{82}Se}$ of destructive interference scenario (green solid lines) are inside the colored area, which is ruled

[5]The plots in Figs. 4.5 and 4.6 correspond to the up-to-date data for the oscillation parameters [164], including the most-updated measurement of large θ_{13} [15].

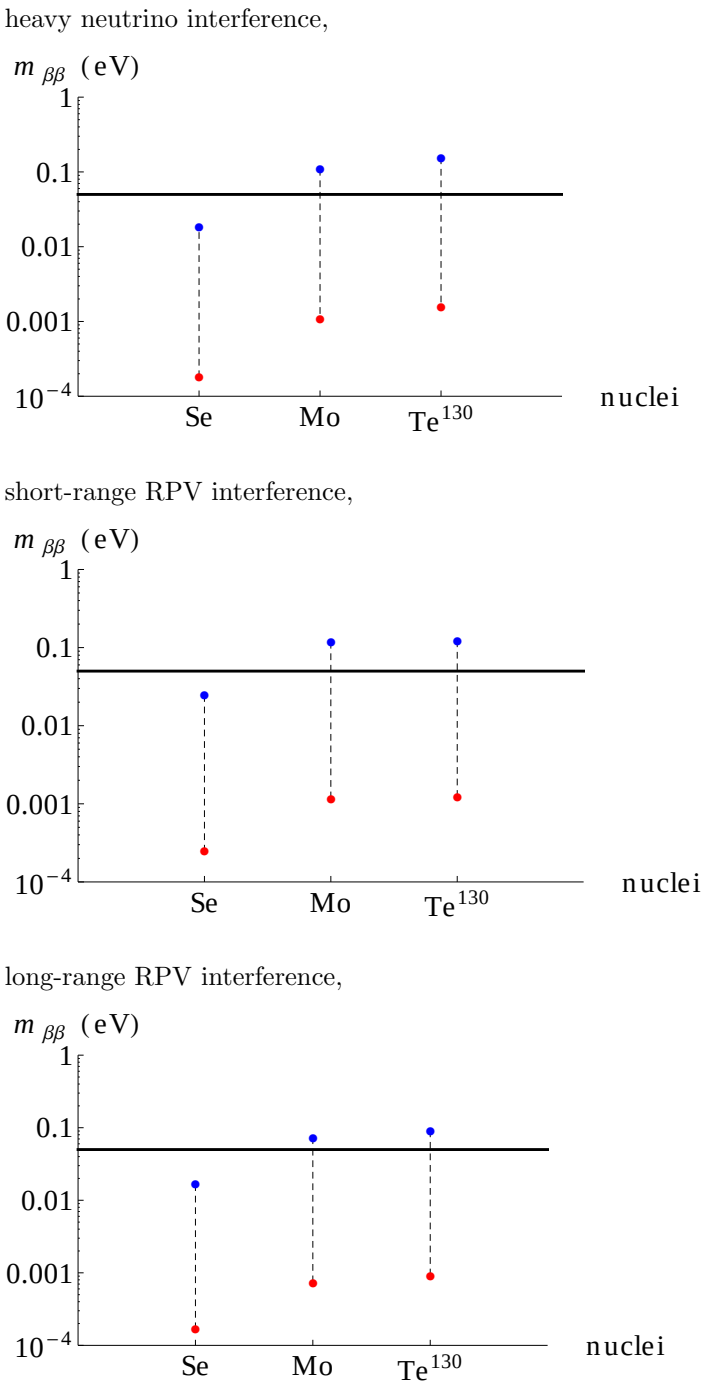

Figure 4.4: The expected values of $\mid m_{\beta\beta} \mid_i$ under the assumption of "exact cancellation" occurs in the decay of ^{76}Ge. The blue dots correspond to the result of 1 eV $\langle m_\nu \rangle$, while red dots correspond to 0.01 eV (refer to the text). The solid horizontal line represents the general sensitivity of next-to-next generation experiments (50 meV).

out by the cosmology result. This means that under our assumption, it would be impossible to observe the neutrinoless double beta decay of ^{82}Se in the next-to-next generation experiments.

However, we should keep in mind that the cancellation effect depends on the ratio of the NMEs and thus it should be different for different nuclei. The failure in one experiment does not lead to the absence of observations in all future experiments. For example, in the decay of ^{130}Te, the cancellation effect only reduces the $\mid m_{\beta\beta} \mid_{^{130}Te}$ a few times smaller than previously expected, as shown in Fig. 4.6.

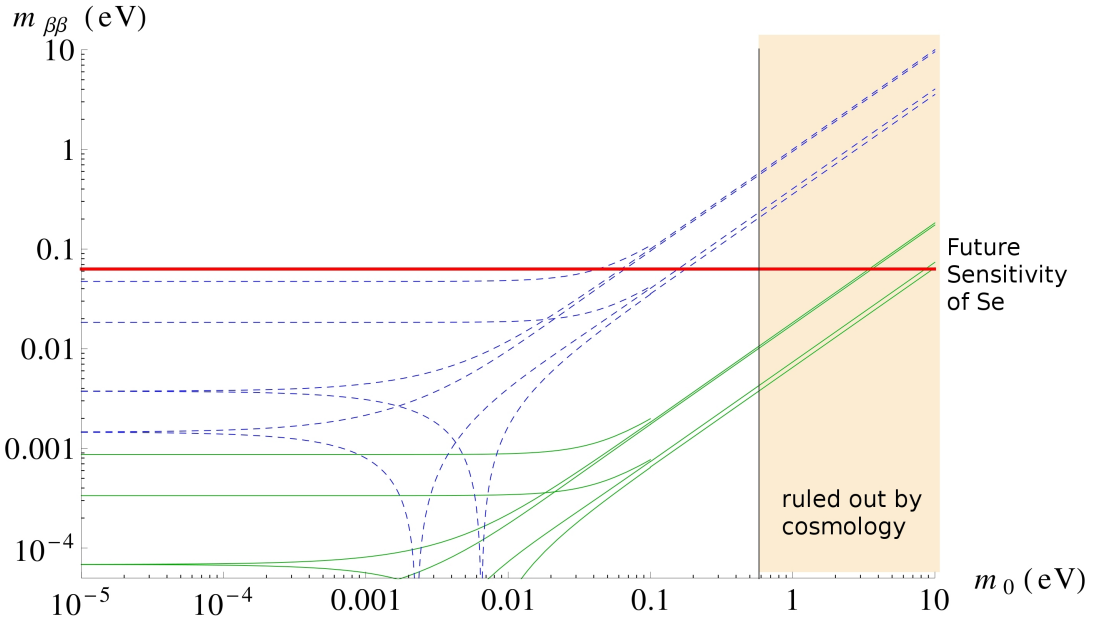

Figure 4.5: The expected values of $\mid m_{\beta\beta} \mid_{^{82}Se}$ corresponding to different ν mass spectra. The green solid curves correspond to the destructive interference between light ν and heavy ν mechanisms, while the blue dashed lines correspond to the traditional assumption (no interference, light ν dominating). The red horizontal line represents the general sensitivity of next-to-next generation of SuperNEMO experiment (63 meV [34, 27]). The colored area ($m_0 > 0.58$ eV) is the region that is ruled out by the cosmology result [135].

Fig. 4.6 shows that the cancellation effect in the decay of ^{130}Te is not as strong as the decay of ^{82}Se. This time, the intersections between the horizontal red line and the black solid lines do not lie in the the ruled out area. If the ν mass ordering is Quasi-Degenerate, or more specifically, m_0 is at the order of $O(1$ eV), the neutrinoless double beta decay is still detectable in the future experiment even though destructive interference exists. Therefore,

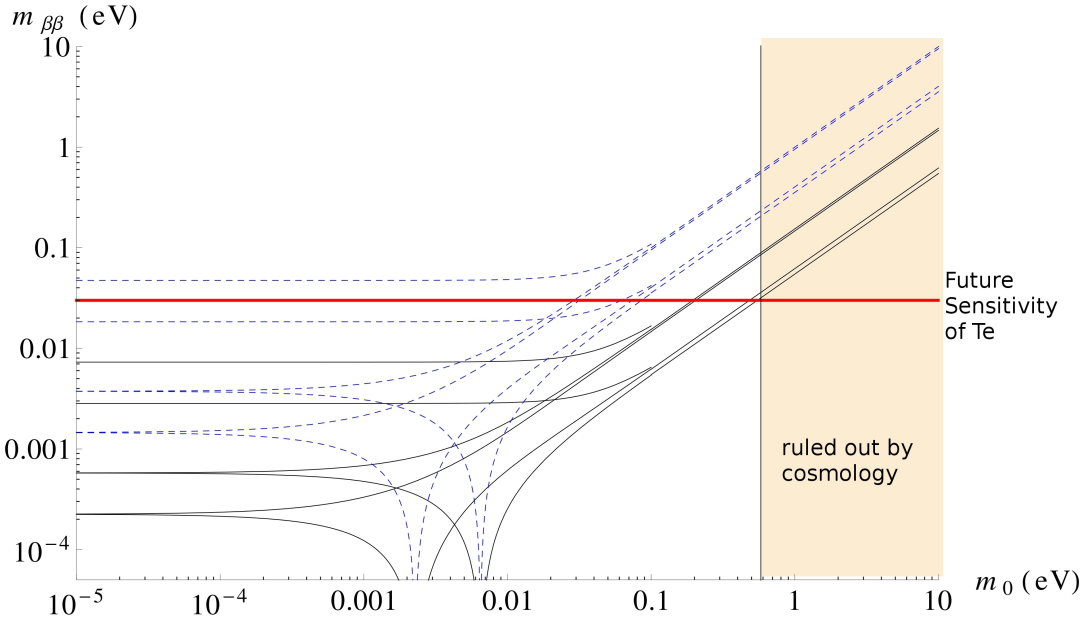

Figure 4.6: The expected values of $\mid m_{\beta\beta} \mid_{^{130}Te}$ corresponding to different ν mass spectra. The black solid curves correspond to the destructive interference between light ν and heavy ν mechanisms, while the blue dashed lines correspond to the traditional assumption (no interference, light ν dominating). The red horizontal line represents the general sensitivity of next-to-next generation of CUORE experiment (30 meV [30, 27]). The colored area ($m_0 >$ 0.58 eV) is the region that is ruled out by the cosmology result [135].

under our assumption, ^{130}Te is a good candidate for future measurements.

Furthermore, it is important to note that in both Fig. 4.5 and 4.6, even in the "no interference" circumstance, if the neutrino mass spectrum is with **normal hierarchy**, $(\beta\beta)_{0\nu}$-decay still cannot be observed in the next-to-next generation experiments. Thus, it is hard to distinguish if the absence of future observation comes from the cancellation effect or the insignificance of $\langle m_\nu \rangle$. However, in principle, the cancellation effect is different for different nuclei; it depends on the ratio of the nuclear matrix elements. If destructive interference really exists, $(\beta\beta)_{0\nu}$-decay is still expected to be observable in some certain nuclei. Thus, more experiments must be performed before making any conclusions.

4.2.3 The uncertainties of the nuclear matrix elements

The plots in Figs. 4.4 - 4.6 correspond to the NMEs of **Variant n.8** in ref. [128], which evaluated the NMEs under the quasiparticle random phase approximation (QRPA) [117]. However, the results in the previous subsection did not take the uncertainties of the NMEs into account. Ref. [128] offers eight variants of nuclear matrix elements, each corresponding to different g_A values, model space size and nucleon-nucleon potentials[6]. Since we focused on the cancellation effect in the previous subsection, it is safe to use one of the variants as an example because they all lead to similar NME ratios. However, if the precise values of the NMEs are not determined, we cannot accurately predict the values of the decay rate (even without interference).

If cancellation really exists, the decay-rate or expected value of $\mid m_{\beta\beta} \mid_i$ will be tiny. Thus the uncertainties of nuclear matrix elements will make a huge difference to our calculations. For the sake of simplicity, let us assume the uncertainties of all NMEs to be just 10%. Then for the destructive interference between light and heavy ν mechanisms, the uncertainty of $\mid m_{\beta\beta} \mid_i$ will become

$$\begin{aligned}\sigma^2(m_{\beta\beta,i}) =& \langle m_\nu \rangle [(\frac{M_{N,i}}{M_{N,Ge}M_{\nu,i}})^2 (0.1M_{\nu,Ge})^2 + (\frac{M_{\nu,Ge}}{M_{N,Ge}M_{\nu,i}})^2 (0.1M_{N,i})^2 \\ &+ (\frac{M_{\nu,Ge}M_{N,i}}{M_{N,Ge}M_{\nu,i}^2})^2 (0.1M_{\nu,i})^2 + (\frac{M_{\nu,Ge}M_{N,i}}{M_{N,Ge}^2 M_{\nu,i}})^2 (0.1M_{N,Ge})^2]. \end{aligned} \tag{4.13}$$

Fig. 4.4 shows that with the cancellation effect, the $(\beta\beta)_{0\nu}$-decay is highly unlikely to be observable. However, if the error of the maximum of $\mid m_{\beta\beta} \mid_i$ is taken into account, then the observation appears to be more promising. Considering Eq. (4.13), we reproduce Fig. 4.4; Fig. 4.7 shows that even the errors of NMEs are only 10%, the uncertainties of the $\mid m_{\beta\beta} \mid$

[6]Each variant of NMEs has an error of $\sigma(M) \sim O(10^{-1})$ [128].

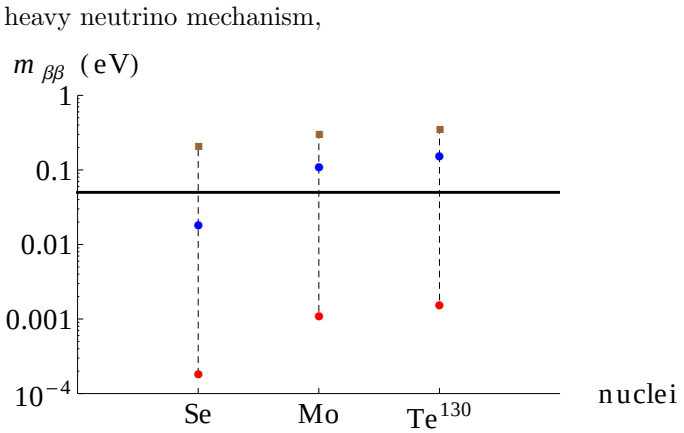

Figure 4.7: The expected values of $\mid m_{\beta\beta} \mid_i$, including the uncertainties of the nuclear matrix elements. The notations are basically the same as shown in Fig. 4.4, the only difference is that the brown square represents the values of "$\mid m_{\beta\beta} \mid$(max) + $\sigma(m_{\beta\beta})$".

would be large and even makes us unsure as to which nuclei would lead to strong cancellation effect. Hence a precise estimation of the NMEs is necessary, especially if destructive interference really exists.

The errors of the nuclear matrix elements come mainly from the adjustable nuclear parameters and the uncertainties of the nuclear model (if the Nuclear Shell Model [156, 157] is used to estimate the NMEs, it may enlarge the uncertainties [159]). One way to reduce the uncertainties of NMEs is by measuring the "two neutrino double beta decay" more precisely, to better estimate the values of nuclear parameters. Other ways to reduce the errors of the NMEs and calculate the correlation between different NMEs have also been discussed in Ref. [159]. Hopefully the future calculations of $(\beta\beta)_{0\nu}$-decay will be more precise.

4.3 Outline

In *Chapters 3 and 4*, we proved that the heavy ν mechanism and trilinear R-parity violation could have significant contributions to $(\beta\beta)_{0\nu}$-decay. Moreover, we suggested that the heavy ν mechanism (or RPV mechanisms) could effectively interfere with the contribution from light ν exchange. Due to the absence of observation, we suggested that the potential interference is destructive. In summary, we discussed the existence and the effect of destructive interferences among different mechanisms of neutrinoless double beta decay. For simplicity,

we only discussed the cancellation between two mechanisms, but it is straightforward to generalise the analysis to the interference between three or more mechanisms.

This chapter shows that destructive interference reduces the decay rate significantly and may lead to the failure in observing the signal of $(\beta\beta)_{0\nu}$ decay in the experiments and we have to choose the nuclei carefully for future measurements. For example, if exact cancellation takes place in the decay of ^{76}Ge, then future experiments corresponding to ^{82}Se may not observe any signal due to the similar ratios of NMEs. Meanwhile, ^{130}Te would be a good candidate for testing the LNV process.

Finally, besides the improvement of experimental sensitivity of $(\beta\beta)_{0\nu}$-decay, intense efforts should also be made on the theoretical study. We must determine the uncertainties of the NMEs under different mechanisms and reduce these uncertainties, otherwise even when we can measure the $(\beta\beta)_{0\nu}$-decay rates in experiments, we cannot extract much information about the effective ν mass, neutrino mass hierarchy, the details of heavy sterile neutrino (or the RPV parameters), etc.

Chapter 5

Search of the 4th Light Neutrino in LENF

Chapter 3 and 4 discussed the phenomenology of neutrinoless double beta decay, which is related to the heavy sterile neutrino. We have already shown that heavy sterile neutrino ($m_N > 100$ eV) is important in neutrino mass generation and neutrino nature studies. In this chapter, we are going to tackle the issue of light sterile neutrinos.

Over the last twenty years, evidence of neutrino oscillation has been collected from many experiments. Typically, neutrino oscillation is expected to be observed only among the three light active neutrinos. However, as mentioned in *Chapter 2*, light sterile neutrino(s) (around 0.1 - 10 eV) may exist and they could mix with the three active neutrinos. Hence, sterile neutrino(s) may also affect the neutrino oscillation measurements. Moreover, the hypothetical fourth light neutrino ν_s may also contribute to mass measurement in beta decay and neutrinoless double beta decay experiments [165]. For example, in the study of $(\beta\beta)_{0\nu}$-decay, the value of the effective mass $\langle m_\nu \rangle \equiv \sum_k^3 (U_{ek})^2 m_k$ has not been determined yet. If a sub-eV light sterile neutrino exists, it may also contribute to this process according to the light ν exchange model. Then the effective mass has to be rewritten as

$$\langle m_\nu \rangle = \sum_k^3 (U_{ek})^2 m_k + U_{e4}^2 \sqrt{\Delta m^2_{\text{sterile}}},$$

which may even be rewritten as $\langle m_\nu \rangle \simeq U_{e4}^2 \sqrt{\Delta m^2_{\text{sterile}}}$ if there are strong cancellations between the contributions from ν_1, ν_2 and ν_3. Therefore, the existence of the light sterile neutrino may also affect the measurement of the absolute neutrino mass scale.

To search the fourth light neutrino, it is necessary to measure its mixing between active neutrinos through the oscillation experiments. Nevertheless, these mixings are not expected to be large, since they are not observed in most of the neutrino experiments and the sterile

neutrinos only couple with active neutrinos.
Since the sterile neutrino mixing angles are supposed to be very small, to prove the existence of light sterile neutrinos, we need experiments with high precision. A Neutrino Factory (which is introduced in *Chapter 1*) can fulfill this requirement. In fact, other kinds of neutrino experiments can also study the sterile neutrino. However, there are a few motivations of using a Neutrino Factory to detect sterile neutrino oscillation: (i) **The high fluxes**: It can offer us high-statistics studies on Sterile Neutrino Mixing. (ii) **Backgrounds**: The ν beams in NF could be well controlled with very low backgrounds. (iii) **Matter effects**: The baseline of NF > 1000 km and it can help to enhance the matter effects.
In reference [166], the performance of high energy ($E_\mu = 25$ GeV) NF on measuring ν_s has been analyzed. Now we are going to tackle the possibility of using Low Energy Neutrino Factory (LENF) instead.
A neutrino factory with low energy ($E_\mu \leq 10$ GeV) has been proposed and discussed for a few years [56, 57, 58]. It has been shown that it can be compared with the high energy factory in measuring active neutrino parameters and there is a significant cost advantage.

Although a large number of studies have been made on sterile neutrinos, little is known about the sterile neutrino parameters and even the number of neutrino species. This chapter is intended to investigate how well can a Low Energy Neutrino Factory measure the light sterile neutrino. We will prove that, with optimizations of the setups of the flux and detector settings, the sensitivity of a **LENF** can be competitive with a **HENF**, and is better optimized for $\Delta m^2_{41} \sim 10^{-1} - 10^0$ eV^2.
We will discuss the oscillation channels and experimental setups for studying the Sterile Neutrino Oscillation. Our parameterization of the mixing matrix and the approximation of ν flavor conversion probabilities will be introduced. Then we will show the results of our simulation, which correspond to the '3+1' mass-scheme. The sensitivity of a LENF on measuring sterile neutrino mixing angles and the eV^2 scale Δm^2_{new} will be shown. Also, the recent interest of decoherence effect in Active-Sterile Neutrino Oscillation [167] will be discussed. It is interesting to notice that in a neutrino factory, the neutrino production region is not really pointlike. It will lead to decoherence in the oscillation and may affect the sensitivities of the measurement.

In this chapter, we will focus on the 4-ν framework. The number of light sterile neutrino may be more than one but it will be discussed in the next chapter.

5.1 Sterile Neutrino Oscillations

We first focus on the '3+1' framework. We assume that the nearly-sterile neutrino, ν_4, is much heavier than other massive states, implying that $\Delta m^2_{41} \gg |\Delta m^2_{31}| \gg \Delta m^2_{21} > 0$. The flavour and massive states are related by a 4×4 mixing matrix U as

$$\nu_\alpha = U_{\alpha i}\nu_i,$$

where $\alpha = e, \mu, \tau, s$ indicates the flavour states and $i = 1, \ldots 4$ the massive ones. Our parametrization of U follows Ref. [166] and is given by

$$U = R_{34}(\theta_{34}, 0)R_{24}(\theta_{24}, 0)R_{14}(\theta_{14}, 0)R_{23}(\theta_{23}, \delta_3)R_{13}(\theta_{13}, \delta_2)R_{12}(\theta_{12}, \delta_1), \tag{5.1}$$

where $R_{ij}(\theta_{ij}, \delta_k)$ are defined as:

$$[R_{ij}(\theta_{ij}, \delta_k)]_{p,q} = \begin{cases} \cos\theta_{ij} & p = q = i, j \\ 1 & p = q \neq i, j \\ \sin\theta_{ij}e^{-i\delta_k} & p = i; q = j \\ -\sin\theta_{ij}e^{i\delta_k} & p = j; q = i \\ 0 & \text{otherwise.} \end{cases}$$

Therefore, the mixing matrix elements are given by

$$\begin{cases} U_{e1} &= c_{12}c_{13}c_{14} \\ U_{e2} &= c_{13}c_{14}s_{12}e^{-i\delta_1} \\ U_{e3} &= c_{14}s_{13}e^{-i\delta_2} \\ U_{e4} &= s_{14} \end{cases}$$

$$\begin{cases} U_{\mu 1} &= -c_{23}c_{24}s_{12}e^{i\delta_1} - c_{12}[c_{24}s_{23}s_{13}e^{i(\delta_2-\delta_3)} + c_{13}s_{14}s_{24}] \\ U_{\mu 2} &= c_{12}c_{23}c_{24} - s_{12}e^{-i\delta_1}[c_{24}s_{23}s_{13}e^{i(\delta_2-\delta_3)} + c_{13}s_{14}s_{24}] \\ U_{\mu 3} &= c_{13}c_{24}s_{23}e^{-i\delta_3} - s_{13}s_{24}s_{14}e^{-i\delta_2} \\ U_{\mu 4} &= c_{14}s_{24} \end{cases}$$

$$\begin{cases} U_{\tau 1} &= s_{12}e^{i\delta_1}(c_{34}s_{23}e^{i\delta_3} + c_{23}s_{24}s_{34}) \\ & \quad -c_{12}[-c_{13}c_{24}s_{13}s_{34} + s_{13}e^{i\delta_2}(c_{23}c_{34} - s_{23}s_{24}s_{34}e^{-i\delta_3})] \\ U_{\tau 2} &= -c_{12}(c_{34}s_{23}e^{-i\delta_3} + c_{23}s_{24}s_{34}) \\ & \quad -s_{12}e^{-i\delta_1}[c_{13}c_{24}s_{14}s_{34} + s_{13}e^{i\delta_2}(c_{23}c_{34} - s_{23}s_{24}s_{34}e^{-i\delta_3}) \\ U_{\tau 3} &= -c_{24}s_{13}s_{14}s_{34}e^{-i\delta_2} + c_{13}((c_{23}c_{34} - s_{23}s_{24}s_{34}e^{-i\delta_3}) \\ U_{\tau 4} &= c_{14}c_{24}s_{34} \end{cases}$$

$$
\begin{cases}
U_{s1} &= s_{12}e^{i\delta_1}(c_{23}c_{34}s_{24} - s_{23}s_{34}e^{i\delta_3}) \\
&\quad -c_{12}(c_{13}c_{24}c_{34}s_{14} - s_{13}e^{i\delta_2}(c_{23}s_{34} + c_{34}s_{23}s_{24}e^{-i\delta_3})] \\
U_{s2} &= -c_{12}(c_{23}c_{34}s_{24} + s_{23}s_{34}e^{i\delta_3}) \\
&\quad -s_{12}e^{-i\delta_1}[c_{13}c_{24}c_{34}s_{14} - s_{13}e^{i\delta_2}(c_{23}s_{34} + c_{34}s_{23}s_{24}e^{-i\delta_3}) \\
U_{s3} &= -c_{24}c_{34}s_{13}s_{14}e^{-i\delta_2} - c_{13}((c_{23}s_{34} - c_{34}s_{23}s_{24}e^{-i\delta_3}) \\
U_{s4} &= c_{14}c_{24}c_{34}
\end{cases}
$$

where $c_{ij} \equiv \cos\theta_{ij}$, $s_{ij} \equiv \sin\theta_{ij}$.

Here, θ_{ij} are the mixing angles and δ_k correspond to the three Dirac CP phases present in the 4×4 mixing case. The Majorana phases are not included since they do not affect neutrino oscillations. With this parameterization, the neutrino flavor conversion probabilities can be derived. In the short-baseline experiments we are interested in, we have that $\Delta m^2_{41}L/4E \equiv \Delta_{41} \sim O(1)$, $\Delta m^2_{31}L/4E \ll 1$, $\Delta m^2_{21}L/4E \ll 1$ and matter-effects can be safely ignored. The oscillation probabilities $\mathrm{P}(\nu_a \to \nu_b) \equiv P_{ab}$ can be approximated as

$$
\begin{aligned}
P_{e,\mu} &= P_{\mu,e} = 4c^2_{14}s^2_{14}s^2_{24}\sin^2\Delta_{41}, \\
P_{e,\tau} &= 4c^2_{14}c^2_{24}s^2_{14}s^2_{34}\sin^2\Delta_{41}, \\
P_{\mu,\tau} &= 4c^4_{14}c^2_{24}s^2_{24}s^2_{34}\sin^2\Delta_{41}, \\
P_{\mu,\mu} &= 1 - c^2_{14}s^2_{24}[3 + 2c^2_{14}\cos^2(2\theta_{24}) - \cos^2(2\theta_{14})]\sin^2\Delta_{41}, \\
P_{e,e} &= 1 - 4c^2_{14}s^2_{14}\sin^2\Delta_{41}.
\end{aligned} \tag{5.2}
$$

From these formulas, we see that $P_{\mu\mu}$ and P_{ee} are the channels with leading order effects of sterile mixing angles, in particular s^2_{24} and s^2_{14}, while the appearance channels are proportional to at least the 4th order in the sterile mixing angles.

On the other hand, for the measurements in the far detector, the baseline is very long and $\Delta_{41} \gg 1$ and its effects are averaged out. In this limit, including matter effects which could be important, the conversion and survival probabilities are [166] [1]

[1] For a more accurate approximation of '3+1' flavor conversion probabilities in the far detector, please refer to [168].

$$
\begin{aligned}
P_{e,\mu} =& P_{e,\tau} = 2s_{13}^2\Delta_{31}^2\frac{\sin^2(\Delta_{31}-\Delta_e)}{(\Delta_{31}-\Delta_e)^2},\\
P_{e,e} =& 1-2s_{14}^2-4s_{13}^2\Delta_{31}^2\frac{\sin^2(\Delta_{31}-\Delta_e)}{(\Delta_{31}-\Delta_e)^2},\\
P_{\mu,\tau} =& \sin^2\Delta_{31}(1-8(s_{23}-\frac{1}{\sqrt{2}})^2-s_{24}^2-s_{34}^2)-c_{12}^2\Delta_{21}\sin(2\Delta_{31})-\\
& s_{24}s_{34}\sin(2\Delta_{31})[2\Delta_n\cos\delta_3-\sin\delta_3]-\\
& s_{13}^2\Delta_{31}\sin\Delta_{31}\frac{\Delta_{31}[\sin(\Delta_{31}-\Delta_e)+\sin(\Delta_e)]-2(\Delta_{31}-\Delta_e)\Delta_e\cos\Delta_{31}}{(\Delta_{31}-\Delta_e)^2},\\
P_{\mu,\mu} =& 1-2s_{24}^2-\sin^2\Delta_{31}(1-s_{24}^2-8(s_{23}-\frac{1}{\sqrt{2}})^2)+c_{12}^2\Delta_{21}\sin(2\Delta_{31})+\\
& 2s_{24}s_{34}\sin(2\Delta_{31})\Delta_n\cos\delta_3-\\
& 2s_{13}^2\Delta_{31}\cos\Delta_{31}\frac{(\Delta_{31}-\Delta_e)\Delta_e\sin(\Delta_{31})-\Delta_{31}\sin(\Delta_{31}-\Delta_e)\sin(\Delta_e)}{(\Delta_{31}-\Delta_e)^2}
\end{aligned}
\tag{5.3}
$$

where $\Delta_{31}\equiv\Delta m_{31}^2L/4E$, $\Delta_{e,n}=A_{e,n}L/4E$ describe the matter effects with $A_e\equiv 2\sqrt{2}G_Fn_e$, $A_n\equiv\sqrt{2}G_Fn_n$ [166], $n_{e,n}$ are the number density of electrons and neutrons, respectively. δ_3 is one of the CP phases as mentioned in Eq. (5.1)

One of the interesting differences between the oscillation probabilities at the near and far detector, Eqs. (5.2) and (5.3), is the measurement of θ_{34}, using the ν_τ channel. In the long-baseline limit, $P_{\mu\tau}$ depends at leading order on $\sin\theta_{34}$. This channel is in fact named *the discovery channel* for sterile ν [169]. While the τ appearance channels in the near detector (Eq. (5.2)) involve fourth order of θ_{i4}, in Eq. (5.3), $P_{\mu\tau}$ and $P_{\mu\mu}$ are only at second order of sterile mixing (θ_{i4}s are supposed to be small). Thus the measurement of θ_{34} relies on the far detector (1300 km far away from the source). In this case, the effects of large Δ_{41} average out, therefore the sensitivity to θ_{34} is almost constant for large Δm_{41}^2 (the plot will be shown in *Section 5.3*).

5.2 Ideal Experimental Setup

As sterile neutrino mixing has been discussed a lot in the past 10 years, the focus of this chapter is that how well can a Neutrino Factory measure the fourth neutrino. Previously ref [166] has done the simulation with a high energy factory, in the following, we will prove that, with optimisations of the setups of the flux and detector settings, the sensitivity of a **LENF**

can be competitive with a traditional high energy neutrino factory, and is better optimised for $\Delta m^2_{41} \sim 10^{-1} - 10^0$ eV^2.

We consider the LENF as proposed in Refs. [58, 166] which uses 4.5 GeV energy muons with 1.4×10^{21} useful muon decays per year, per polarity, running for 10 years and that has a baseline of 1300 km, corresponding to the distance between Fermilab and DUSEL. The flux in our simulation is more optimistic than that considered in Ref. [166] and in the IDS-NF (International Design Study neutrino factory) [170, 171], but it is a reasonable and feasible assumption according to Ref. [58]. In view of the large θ_{13} measured in T2K [17], MINOS [18], Daya Bay [15] and RENO [19], the baseline for the neutrino factory, as defined by the IDS-NF, has recently been reviewed and now considers muons with 10 GeV energies, a source-detector distance of 2000 km and 10^{22} muon decays per polarity in total. We will study the sensitivity of both setups, complemented by a near detector, in order to establish their sensitivity to sterile neutrinos and analyse the dependence of the physics reach on the muon energy.

The muons are stored and decay in a decay ring, for which we follow the design proposed in the IDS-NF, with a decay straight length of $l_p = 0.6$ km [170]. For muons with different energies it is expected that the decay ring can have different optimisations and correspondingly different decay straight length but for simplicity we will consider in both cases the same l_p. For the near detector located at 2 km from the end of the decay straight, For the detectors, two totally active scintillating detectors (TASD) are considered: one with 20 kton fiducial mass, located at 1300 km and the ND with a 50 tons mass, at a distance $L = 2$ km. For the near detector, geometry effects [172] are important as the length of the decay straight, l_p, cannot be ignored (Fig. 5.1). However, the typical calculation of the flux in Neutrino Factory, or the simulation software like GLoBES, always assume that the detectors are located far enough that the geometry effect can be neglected. In our simulation, we took these effect into consideration by using the effective baseline of near detector, $L_{\text{eff}} = \sqrt{L(L + l_p)} = 2.28$ km. More details about the geometry effect are referred to *Appendix E*.

5.2.1 Detector Properties

About the detector properties, for the sake of simplicity, it is assumed that the performance of both detectors is the same [58]: a constant energy resolution of $10\%E$, the efficiencies for muon (anti-)neutrino detection of 73% below 1 GeV and 94% above, for electron (anti-)neutrinos of 37% below 1 GeV and 47% above. The backgrounds to all channels are expected to arise mainly from charge misidentification and neutral current events and are taken to be at a level of 10^{-3} for muon appearance and disappearance channels, 10^{-2} for electron chan-

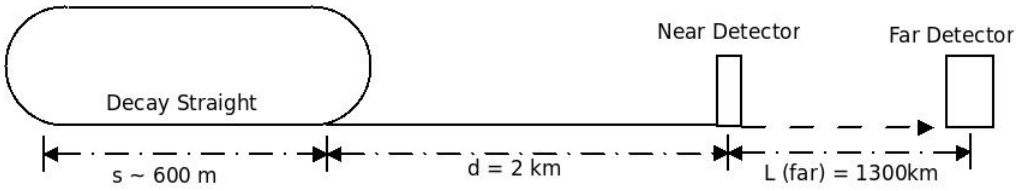

Figure 5.1: Schematic layout of the muon storage ring, near and far detector in our simulation (not to scale).

nels, in both detectors. More specifically, a level of 10^{-3} background in ν_μ channels means that we assume that 0.001 of all μ^-s are wrongly identified as μ^+ (charge misidentification), and also 0.001 of all un-oscillated events are wrongly counted as signal events (neutral current background).

It should be noted that the sensitivity of the setup would be very similar if using a different technology but with comparable performance, such as a magnetised LAr detector. We will show the different reach in *Subsection 5.3.4*. The magnetisation of a large volume is a great technological challenge. Ref. [61] has performed a detailed discussion about different technologies and difficulties of magnetisation of large detectors. However, small magnetised TASD or LAr detectors might be realisable in the not-far feature. Actually, a small LAr (around 600 tons) has already been tested to be able to operate in a magnetic field of 0.55 Tesla [173]. Ref. [174] further discusses the potential of large magnetised LAr detector. Moreover, experiments like MINERvA [175] and T2K also immerse the near detectors in a magnetic field [176, 177, 178, 179]. Since in our simulation, the scale of near detector is expected to be small (< 1 ktons), it is safe to assume that the near detector (TASD or LAr) operates in a magnetic field and is able to efficiently identify the charge of muons and electrons[2]. It is worth noting that due to the low neutrino energies, in particular for the 4.5 GeV LENF, an iron magnetised detector is not ideal as it has low efficiency at low energy and will not be considered in the present study.

5.2.2 Consideration of Oscillation Channels

Our most significant difference relative to the traditional neutrino factory analysis is the addition of ν_e appearance (platinum channel) and disappearance channels, since they are highly

[2]It has also been argued that a LENF could perform well even with non-magnetised detectors. The corresponding discussion is referred to Ref. [180]

sensitive to θ_{14}, which will be shown in *Subsection 5.3.1.* However, we should notice that the background and efficiency in ν_e channels are worse than those for ν_μ channels. This is due to the fact that it is more difficult to determine the electron momentum and charge due to their early showering [181], even in low-Z (namely, light nucleus) detectors such as TASD and LAr. Also, the separation of the pion background is challenging [58]. These effects lead to higher level of background and lower efficiencies in ν_e channels.

Besides the ν_e and ν_μ channels, we also test the contribution from ν_τ channels, mainly on measuring the angle θ_{34}. The technology considered in the previous literature to detect ν_τs is the Emulsion Cloud Chamber (ECC) detector. Due to the lack of ν_τ in the initial neutrino beam of neutrino factory, the detection of the ν_τ appearance channels would signal $\nu_e \to \nu_\tau$ [182] and/or $\nu_\mu \to \nu_\tau$ [169] oscillations. To detect the ν_e, $\nu_\mu \to \nu_\tau$ appearance signal, the right-sign muons, which are produced in the $\tau \to \mu$ decay, will be detected in coincidence with a τ decay vertex. These muons will be distinguished from the ν_μ disappearance muons. Thus, the τ detector would need both muon charge identification and τ vertex detection. The corresponding dominant backgrounds of this channel is from non-oscillated ν_e and $\bar{\nu_\mu}$ which produce charmed mesons that will eventually decay into wrong-sign muons and fake the detectors. More details about the background in ν_τ detection can be referred to Refs. [182, 183]. In our simulation, the values for the background and the efficiency of this channel are the same as the consideration in Ref.[166], i.e., 48% efficiency for the detection.
About the scale of the detector, we take the mass of the ECC detector to be 10 kt, twice the mass of the detector in Ref.[182], as an optimistic choice in order to enhance the poor sensitivity on θ_{34}. We put an ECC in the far detector only and we checked that including an ECC in the near detector configuration does not significantly enhance the sensitivity.

At the moment, detailed studies of the channels $\nu_e \to \nu_\tau$ and $\nu_\mu \to \nu_\tau$ in a Neutrino Factory have not been performed yet. In our simulation, the ECC-TASD hybrid is used, with the ECC measuring the ν_τ and TASD measuring ν_μ and ν_e. We simply assume that such a hybrid detector is achievable and it would be able to measure ν_τ, ν_μ and ν_e efficiently at the same time. However, due to the lack of the ν_τ disappearance channel and difficulties in detecting τ, the sensitivity of θ_{34} is very poor[3] compared with the measurements of θ_{14} and θ_{24}. The plots of sensitivities will be shown in the following section.
Moreover, it is important to note that, as $m_\tau \sim 1.8$GeV, neutrinos from 4.5 GeV muons do not have sufficient energy to efficiently produce τ. Therefore, in this thesis, the τ appearance

[3]Actually, the higher order terms in $P_{\mu\mu}$ and P_{ee} could have comparable contributions in the sensitivity of θ_{34}, since the event rates of disappearance channels are much higher.

channel will be studied only in relation to the 10 GeV Neutrino Factory.

5.2.3 Systematic Uncertainties

Systematic errors is the term used to include all non-random errors in the experiment. In neutrino oscillation experiments, there are many contributing factors that affect the measurements, such as the flux and cross-section uncertainties, the potential backgrounds, the energy calibration errors, and the energy threshold, resolution, uncertainty of the mass of detectors [184]. One of the advantages of the neutrino factory is that the neutrino flux from muon decay can be predicted to a great precision (an accuracy of better than 10^{-3} [61]), and so the systematic error associated with this measurement is relatively small.

On the other hand, the cross-section uncertainties are specific to the detector material and configuration and this error is likely to be the main systematic uncertainties in a Neutrino Factory [184]. Especially when the energy scale is between 500 MeV to 5 GeV, there are many interactions contributing, like quasi-elastic, single and multi pion productions, deep-inelastic scattering, etc. Thus the cross sections in NF always come with large uncertainties. Wide experimental effort are going to take place to measure these cross sections more precisely. For example, the cross section of charged current quasi-elastic interactions is closely related to the axial form factor which is measured in electron nucleus scattering. The experiments like MINERvA [175] and T2K [179] are expected to measure this form factor better and thus a better understanding on the quasi-elastic interaction could be achieved. About the single and multi pion productions, they are important background to the neutrino oscillation experiments. However, the knowledge of the resonance cross-section is difficult to model, and the nuclear re-interactions are difficult to measure in most of the neutrino experiments. It is suggested that with a powerful near detector which has good particle identification capabilities and momentum resolution (like the T2K experiment [179]), may be able to address the nuclear re-interactions measurements. More details about the uncertainties of the cross section can be found in Ref. [61].

In our study, the systematics errors are assumed to be 2% for the signal both in the far and near detectors. Meanwhile we assumed 1% background errors and negligible energy calibration errors. The effect of systematic errors and the ways of governing them will be discussed in *Subsection 5.3.2*.

5.3 Exclusion Limits From Our Simulations

As we will show in the following, a neutrino factory has an excellent sensitivity in measuring the sterile parameters and is a potential candidate for the study of sterile neutrinos.
In this section, we investigate the constraints to sterile mixing angles θ_{14} and θ_{24}. Since the measurement of θ_{34} mainly depends on the detection of ν_τ, and requires a higher energy for the muon beam. Thus we only discuss the θ_{34} limit in the 10 GeV case.
The best-fit values for the active neutrino oscillation parameters are taken to be: $\sin^2\theta_{12} = 0.3$, $\sin^2 2\theta_{13} = 0.092$[4], $\theta_{23} = 45°$, $\Delta m^2_{21} = 8 \times 10^{-5}$ eV^2, $|\Delta m^2_{31}| = 2.5 \times 10^{-3}$ eV^2. Δm^2_{31} is simply assumed to be positive but this choice does not impact on the results obtained and no CP-violation is considered. For the sterile oscillation parameters, the mixing is assumed to be negligible, i.e. all $\theta_{i4} = 0$, $\Delta m^2_{41} = 1$ eV^2, which corresponds to LSND result. All CP-phases are set to be 0.
We have used the GLoBES software [185, 186] to perform the numerical simulations of the low energy neutrino factory. GLoBES includes the oscillation of up to 6 sterile neutrino flavors and non-standard interactions. We have simulated various experimental configurations. In this section, we are going to investigate the constraints to sterile mixing angles θ_{14} and θ_{24}. Since the measurement of θ_{34} is supposed to depend on the detection of ν_τ, and it requires higher energy for the muon beam. Thus we only discuss the θ_{34} limit in the 10 GeV case.

With the experimental setup as mentioned previously, the event-rates of disappearance channels are also much bigger than other channels, as shown in Table 5.1

[4]All active oscillation parameters follow the assumptions in Ref.[58], except for θ_{13}, which is consistent with the updated result from the Daya-Bay experiment [15]. We also have tried to use smaller θ_{13} as previously assumed, and the results did not change significantly.

Table 5.1 The total event rates of different channels in the near detector (2km far away from the source), corresponding to different values of sterile mixing angles (assume $\theta_{i4} = \theta_{14} = \theta_{24}$)

For the 4.5 GeV LENF consideration (1.4×10^{22} muon decays per polarity in total) [58].

θ_{i4}	ν_e disapp	ν_e app	ν_μ disapp	ν_μ app	neutral current for ν_e	neutral current for ν_μ
0°	$\mathbf{9.980\times10^7}$	1.42	$\mathbf{1.161\times10^8}$	1.69	3.342×10^7	3.835×10^7
1°	$\mathbf{9.972\times10^7}$	31.39	$\mathbf{1.160\times10^8}$	30.37	3.342×10^7	3.835×10^7
5°	$\mathbf{9.781\times10^7}$	15291	$\mathbf{1.141\times10^8}$	15181	3.342×10^7	3.835×10^7
10°	$\mathbf{9.210\times10^7}$	233925	$\mathbf{1.086\times10^8}$	232544	3.342×10^7	3.835×10^7

For the 10 GeV IDS-NF consideration (10^{22} muon decays per polarity in total).

θ_{i4}	ν_e disapp	ν_e app	ν_μ disapp	ν_μ app	neutral current for ν_e	neutral current for ν_μ
0°	$\mathbf{7.501\times10^8}$	58.14	$\mathbf{8.324\times10^8}$	71.51	2.469×10^8	2.733×10^8
1°	$\mathbf{7.499\times10^8}$	201.67	$\mathbf{8.322\times10^8}$	232.37	2.469×10^8	2.733×10^8
5°	$\mathbf{7.450\times10^8}$	35532.6	$\mathbf{8.281\times10^8}$	40973	2.469×10^8	2.733×10^8
10°	$\mathbf{7.305\times10^8}$	520779	$\mathbf{8.160\times10^8}$	601833	2.469×10^8	2.733×10^8

Since we are going to test the hypothesis of no effect of extra sterile neutrinos, in this chapter we are interested in the scenario $\theta_{i4} \approx 0$. In this case, the energy distribution of events of various channels in the near detector are shown in Fig. 5.2,

Table 5.1 and Fig. 5.2 show that in the near detector, the event rates of disappearance channels are always much larger than the neutral current background[5] and the appearance channels. This is as expected from Eqs. (5.2). The survival probability are dominated by the first term, "1", thus $P_{\mu\mu}$ and P_{ee} are always much larger than other probabilities and the event rates of disappearance channels are abundant. The signals in the near detector mainly come from the disappearance channels and they provide excellent sensitivities on the sterile mixing parameters.

[5]The neutral current is one of important background in neutrino factory. This background is from the unoscillated ν beams, interacting with the detector through the process like '$\nu_\mu + n \to \nu_\mu + \pi^+ + \pi^- + \pi^0 + n$', '$\nu_e + p \to \nu_e + \pi^+ + n$', '$\nu_e + n \to \nu_e + \pi^- + p$', and the pions faking a muon or an electron in the detector. For more details about these backgrounds, please refer to Ref.[61].

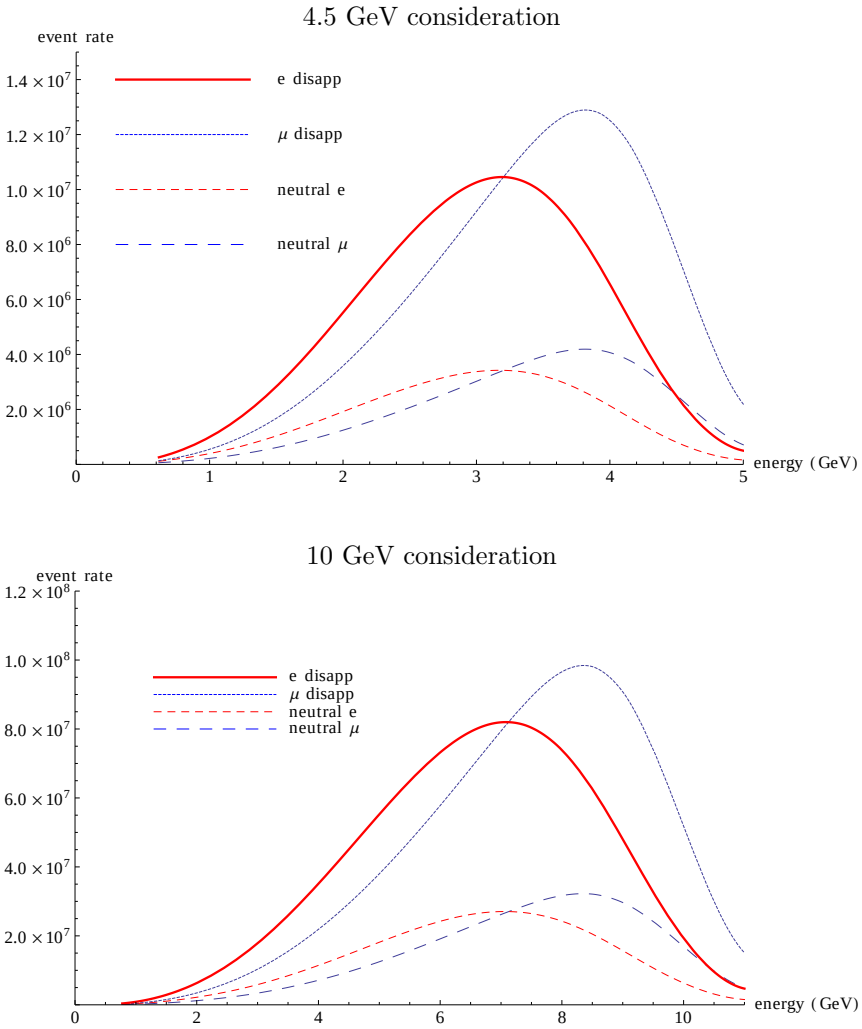

Figure 5.2: Energy distribution of events of different channels in the near detector. The upper plot corresponds to the previous LENF consideration in Ref. [58], and the lower plot corresponds to the updated IDS-NF consideration.

5.3.1 The Role of the Near Detector

As we are interested in large values of Δm^2_{41}, the oscillations driven by it will develop at short distances and the best sensitivity is provided by the near detector. In Fig. 5.3, we show the reach for Δm^2_{41} versus the two mixing angles θ_{14} and θ_{24} for both muon-energy setups with and without using the near detector.

As expected, the near detectors significantly improve the sensitivity for large Δm^2_{41}. The far detector is good at measuring small $\Delta \mathrm{m}^2_{41}$ but it cannot provide further detail of the sterile mixing if the Δm^2_{41} is large. As Eqs. (5.3) show, the probability formulas for long baseline (1300km) do not involve Δm^2_{41}. It is because the $\sin^2(\Delta m^2_{41} L/4E)$ will lead to fast oscillation when both L and Δm^2_{41} are large. In practice the detector resolution is finite and cannot measure such high frequency oscillation [168]. Thus in far detector the sterile ν oscillation is averaged out [6].

Moreover, Refs. [172, 184, 187] suggest that if a set of near detectors at different baselines is used, similar to the reactor experiments like Double CHOOZ and Daya Bay, the systematic errors can be well controlled. The 'further' near detector (where the oscillation averages out for large Δm^2_{41}) can measure the normalisation and contributes to reduce the impact of systematic errors. However, in our simulation, we just considered one near detector and one far detector, and assumed the effective systematic errors is 2% for both far and near detectors. More details about systematic errors will be discussed later.

We can see that with the near detector (which is located at a distance 2 km from the decay straight), the main peak of our measurement will be around 1 - 10 eV^2. If we put the near detector nearer the peak will be higher. It is interesting to investigate the effect of changing the location of ND. The sensitivities of different distances of ND are shown in the Fig. 5.4.

The plots in Fig. 5.4 suggest that reducing the distance between the ND and the decay-straight can effectively improve the sensitivity on large Δm^2_{41} but there are a few reasons forbidding the detector locating too near to the source. First of all, the geometry effects due to the finite length of the decay straight and the size of the near detector cannot be neglected, if the near detector is located at a distance < 1 km from the decay straight. If the distance of the ND $\sim O(100$ m), the corresponding ν_μ and ν_e flux distribution will be quite different to the FD and systematic errors would not cancel significantly limiting the

[6] If Δm^2_{41} is larger than 0.1 eV^2, then the measurements in near detector and disappearance channels will dominate in the simulation. However, if $\Delta m^2_{41} \sim \Delta m^2_{31}$, the appearance channels and measurements in far detector start to contribute largely. In this case the Eqs. (5.3) should be taken into account. The effects of appearance channels like $\nu_\mu \to \nu_e$, $\nu_\mu \to \nu_\tau$ can be referred to the CNGS experiment [183]

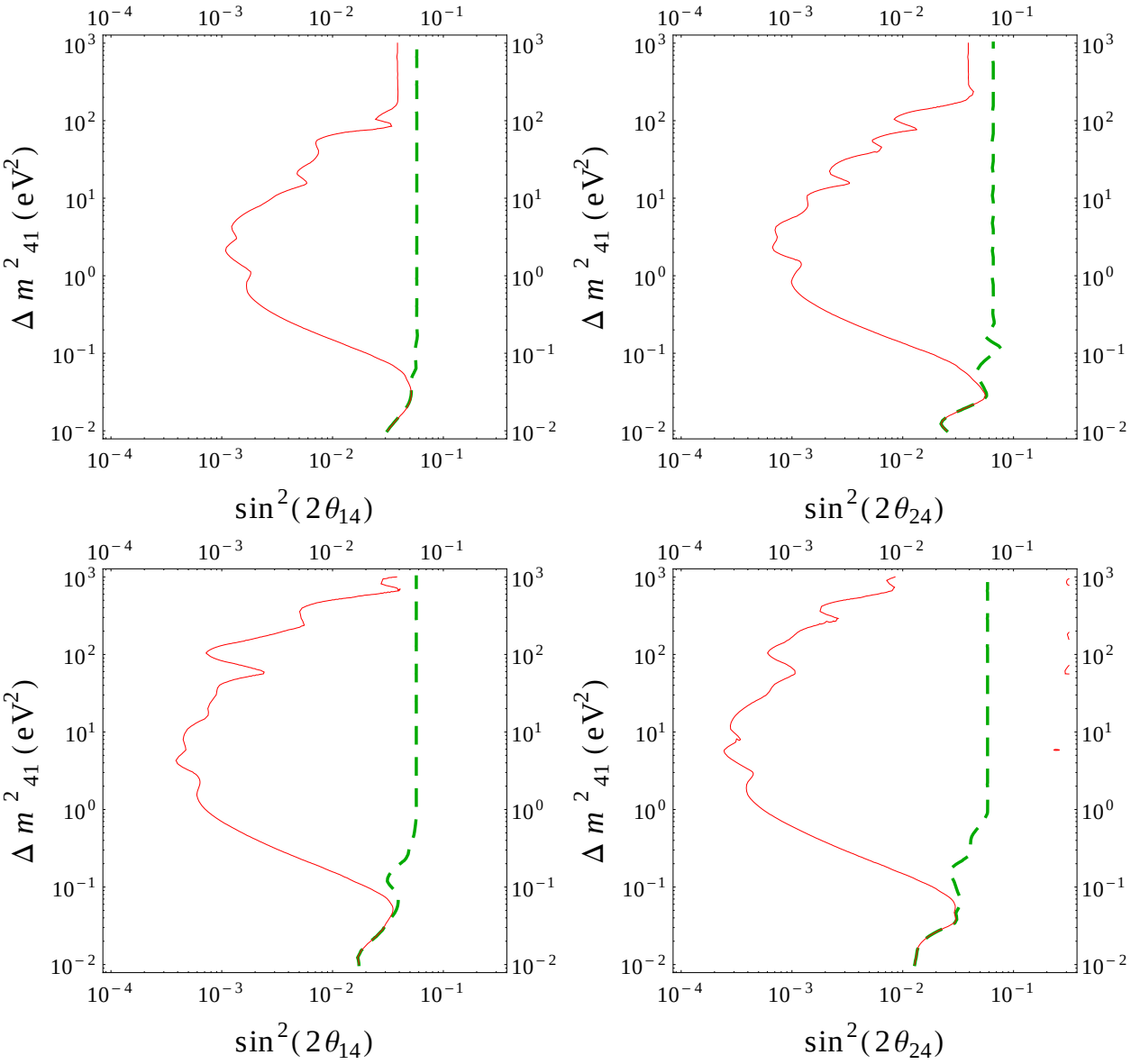

Figure 5.3: Sensitivity to $\sin^2 2\theta_{14}$–Δm^2_{41} (left) and $\sin^2 2\theta_{24}$–Δm^2_{41} (right) at 90% CL without (green dashed curves) and with (red solid curves) near detector. The upper pair of figures corresponds to the $E_\mu = 4.5$ GeV LENF and the lower pair to the updated IDS-NF consideration with $E_\mu = 10$ GeV.

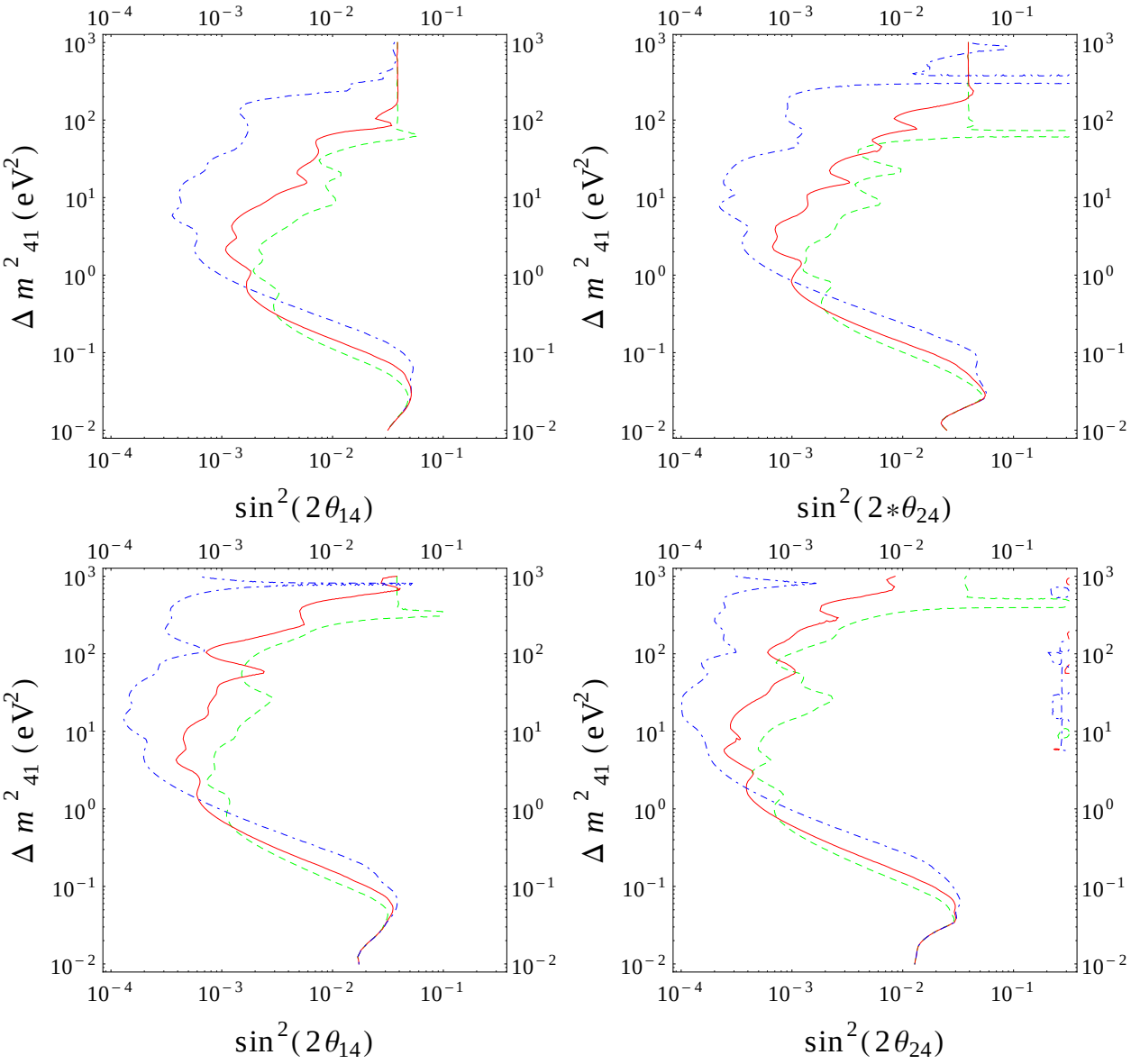

Figure 5.4: Sensitivity to $\sin^2 2\theta_{14}$–Δm^2_{41} (left) and $\sin^2 2\theta_{24}$–Δm^2_{41} (right) at 90% CL. Here the baseline of the FD is fixed to be 1300 km (upper pair) and 2000 km (lower pair), and the green-dashed (red-solid) [blue-dot-dashed] curve corresponds to a ND distance of $L = 4$ km (2 km) [0.5 km]. The upper pair of plots corresponds to the 4.5 GeV LENF in Ref. [58], and the lower pair to the current IDS-NF consideration.

physics reach [61], as shown later in Fig. 5.5. Moreover, if the baseline of the near detector is too short, it would also lead to decoherence effects, which will be discussed in *Section 5.4*. Since we are particularly interested in a sterile ν mass around 1 eV, we will chose the 2 km baseline as the default distance unless otherwise specified.

5.3.2 The Impact of Systematic Errors

As just mentioned, systematic errors would affect the sensitivities of a LENF. Systematic errors are involved in the calculation of χ^2, which is noted in *Appendix F*. (Larger systematic errors always lead to worse sensitivity.) The main systematic error in Neutrino Factory is due to the uncertainty of normalization of the signal events. These errors contains cross section errors, detector material properties, uncertainties of fiducial mass, detector normalization, etc, [184]. The effects of normalization errors on the sensitivities are shown in Fig. 5.5.

In a Neutrino Factory, the reason for a normalization error is due to the lack of the knowledge of cross section. Different to the reactor experiments, whose main systematic error come from the uncertainty of the flux, in a neutrino factory, the flux can be known at the 0.1% level through different monitoring devices [61]. (On the contrary, the leading systematic error of neutrino factory is the uncertainty of the cross section [184].) The energy regime of a LENF (a few GeV) involves several processes: single and multi-pion productions, quasi-elastic and deep inelastic scattering, etc, thus the knowledge of the cross section in neutrino factory is very limited and the systematic error is mainly due to the uncertainty of the cross section. An updated measurement of the processes just mentioned may provide a better knowledge of cross section, more detail can be referred to Ref. [61].
Besides, in reactor experiments like Double CHOOZ or Daya Bay, at least two identical near detectors at different baselines are used. In these experiments, any difference of event rates between different detectors must come from oscillation, not from uncertainties of cross sections, fluxes or efficiencies. Such a combination of NDs will control the cross section error to be smaller than 1%, since the measurements of the cross-section in different ND are correlated.

In this thesis, for simplicity, we just assumed one near detector and the corresponding systematic (normalization) error of 2%, uncorrelated between detectors, which follows the assumption in Ref. [58]. A better systematic treatment would require additional a combination of near detectors which are located at a few hundred meters far from the source, but this is beyond the scope of this study. More details can be referred to Ref. [172].

Fig. 5.5 shows that systematic errors (signal normalization) have a significant impact on

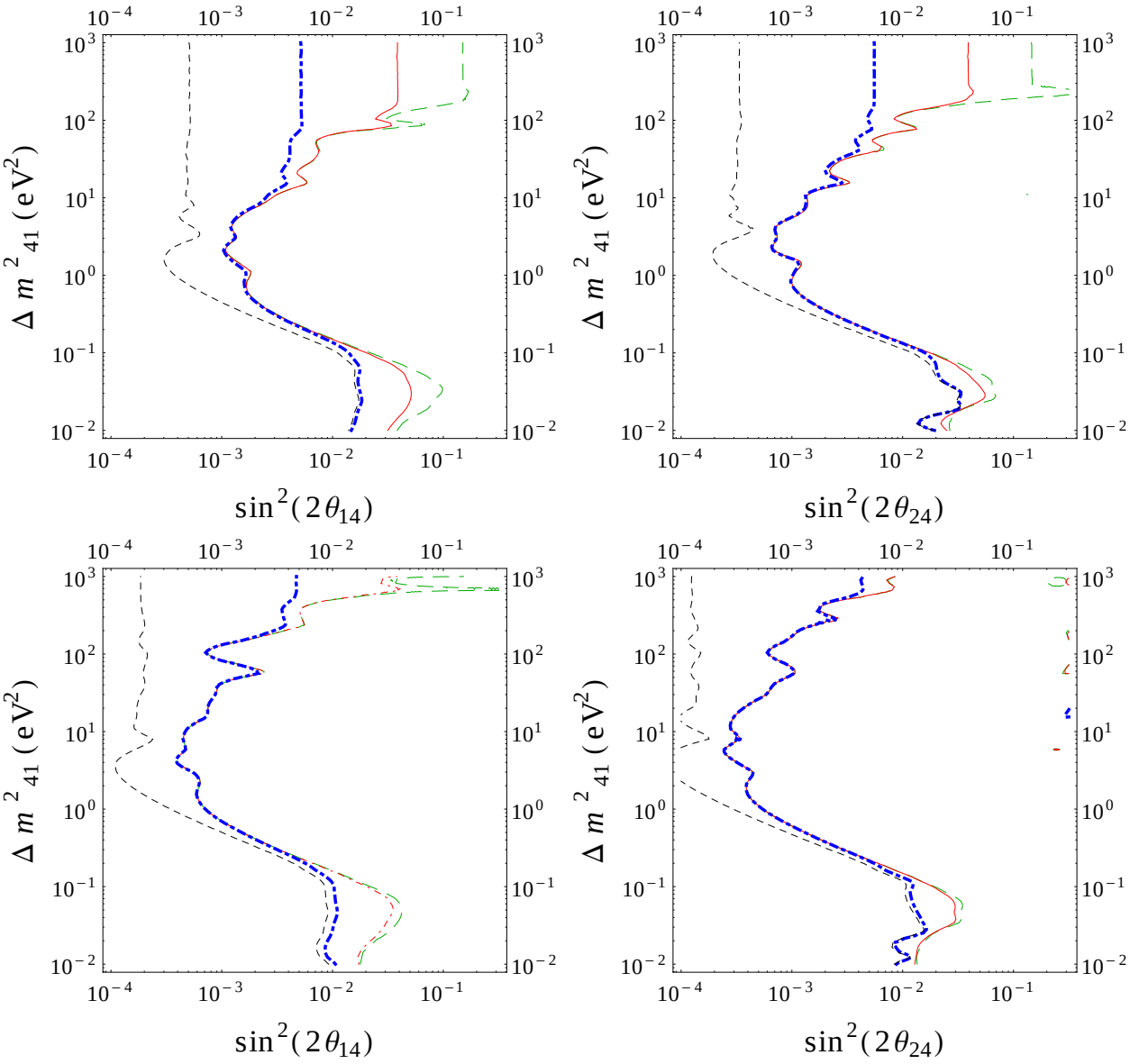

Figure 5.5: Sensitivity to $\sin^2 2\theta_{14}$–Δm^2_{41} (left) and $\sin^2 2\theta_{24}$–Δm^2_{41} (right) at 90% CL, with **10% (green), 2% (red), 0.2% (blue) and no (black) signal normalization errors**. The upper pair of plots corresponds to the 4.5 GeV LENF in Ref. [58], and the lower pair to the current IDS-NF consideration.

the sensitivities, especially at large Δm^2_{41}. Smaller systematic errors would lead to better sensitivity on mixing angles. However, it is remarkable that the errors only affect the sensitivity off the oscillation maximum. The peak of the sensitivities (corresponding to $\Delta m^2_{41} \sim$ a few eV^2) would not improve unless the systematic errors are reduced to smaller than 0.1%. If Δm^2_{41} is confirmed to be $\sim O(\text{eV}^2)$, even a 10% normalization error would still lead to sufficient sensitivities.

Besides the normalization error, the systematic errors also include energy calibration errors, background errors, but they are tested to be sub-dominant if the normalization errors are present. Thus we simply assumed these errors to be $\leq 1\%$ in our simulation and they are not discussed in this thesis.

5.3.3 The Effect of Energy Resolution

We also have studied the effect of the energy resolution, σ_E/E. In our simulation, we followed the optimistic scenario in Ref. [58] and assumed that the energy resolutions of both detectors are 10%. To show the effect of energy resolution, we compare our resolution consideration with other scenarios[7], $\sigma_E/E = 15\%$ and 30%, as shown in Fig. 5.6.

Comparing with the conservative scenario, $\sigma_E/E = 30\%$, our optimistic resolution consideration significantly improves the sensitivities. On the other hand, there are only slight differences between the '$\sigma_E/E = 15\%$' and '$\sigma_E/E = 10\%$' scenarios. With 15% energy resolution, it is expected that an excellent sensitivity to the sterile oscillation parameters can still be achieved in a LENF.

5.3.4 Comparing Liquid Argon Detector with TASD

The simulations in the previous subsection all correspond to the performance of a TASD for detecting both muon and electron neutrinos. As mentioned before, a Magnetized Iron Neutrino Detector (MIND) is not favoured in a LENF. Thus we consider a magnetised TASD in our simulation. However, there are still other options.

In the past few years, there have been discussions about constructing a large Liquid Argon Detector (LAr) [174, 180]. LAr is expected to have excellent resolution, background suppression and signal efficiency. If this kind of detector can be magnetized, it may enhance

[7]Previously, in Ref. [188], it was assumed that $\sigma_E/E = 15\%$. In order to show the effect of energy resolution, we further show one more conservative scenario, $\sigma_E/E = 30\%$.

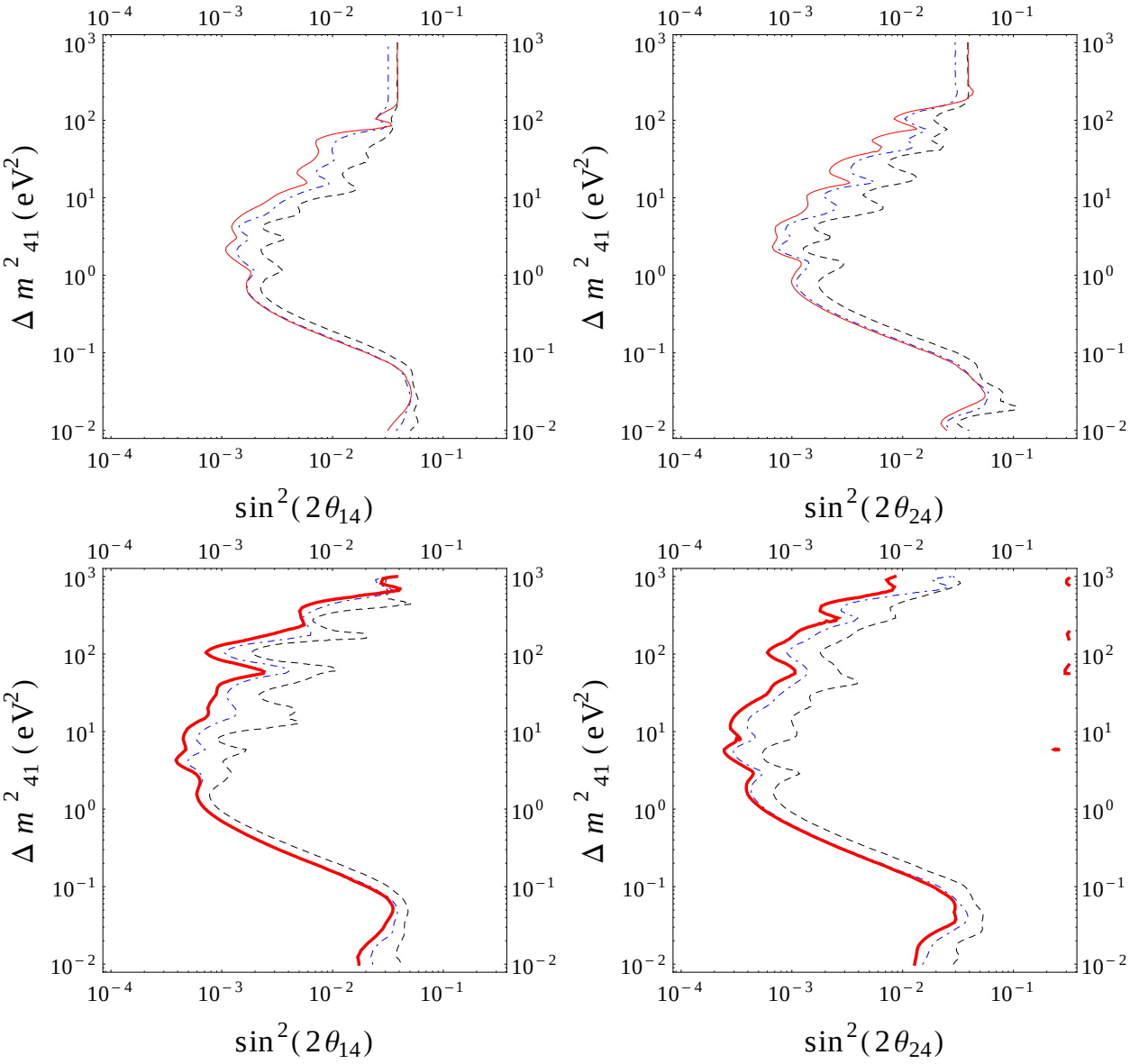

Figure 5.6: Sensitivity to $\sin^2 2\theta_{14}$–Δm^2_{41} (left) and $\sin^2 2\theta_{24}$–Δm^2_{41} (right) at 90% CL, with **10% (red, solid), 15% (blue, dot-dashed) and 30% (black, dashed)** energy resolution. The upper pair corresponds to the previous LENF consideration in Ref. [58], and the lower pair corresponds to the updated IDS-NF consideration.

the performance of neutrino factory. However, the scale of the detector is the main problem. In reality, there is concern about constructing a 100 kton-scale LAr. The issue of a large LAr has been extensively discussed in the literature [174, 189, 60].

Since, in our simulation of LENF, we do not require a large detector for the near detector (which dominates in our simulations), the concern about the detector scale is not a problem for us. In the following, we compare the performance of TASD and LAr as the detector in LENF.

We used the following Liquid Argon Detector settings to do the simulation [58, 190]:
(i) Background = 5×10^{-3} for the μ appearance and disappearance channels and 0.8 for the e appearance and disappearance channels.
(ii) Efficiencies: 80% on all channels.
(iii) Resolution = 10%E for non quasi-elastic events and 5% for quasi-elastic events.
(iv) Mass = 250 tons for the near detector. For consistency we have used a 100 kton magnetized detector for the far detector. However this does not impact significantly the results in the mass range of interest, $\Delta m^2_{41} > 10^{-1}$ eV^2 as the sensitivity is driven by the ND.
(v) Systematics errors: 5% for both far and near detectors.

The comparison between the TASD (Red) and the Liquid Argon Detector (Green) performance in the LENF are shown in Fig. 5.7.

It is obvious that the performance of a LAr is better than the one of the TASD, especially for the sensitivity to θ_{14}. This is because, in our scenario, the fiducial mass of the LAr is five times larger than the TASD (both the near detector and far detector) and this detector has an efficiency of 80% on all channels [190], instead of the efficiency of $e^{\pm}$ detection in TASD of only 37% below 1 GeV, and 47% above. If such a Liquid Argon Detector is achievable in the future, it could further improve the physics reach of the LENF.

5.3.5 Changing the Energy Scale

In this subsection, different muon energies will be discussed. For fixed baseline, higher muon energy is always expected to provide a better sensitivity. This is because, although the oscillation probability is $\sim \sin^2(\Delta m^2_{41}\mathrm{L}/4\mathrm{E})$, i.e. roughly $\propto 1/E^2$, the beam collimation $\propto E^2$ and the cross section $\propto E$, and the net effect on the sensitivity is roughly proportional to E.

Recently, the new consideration for a LENF has been proposed. According to the discus-

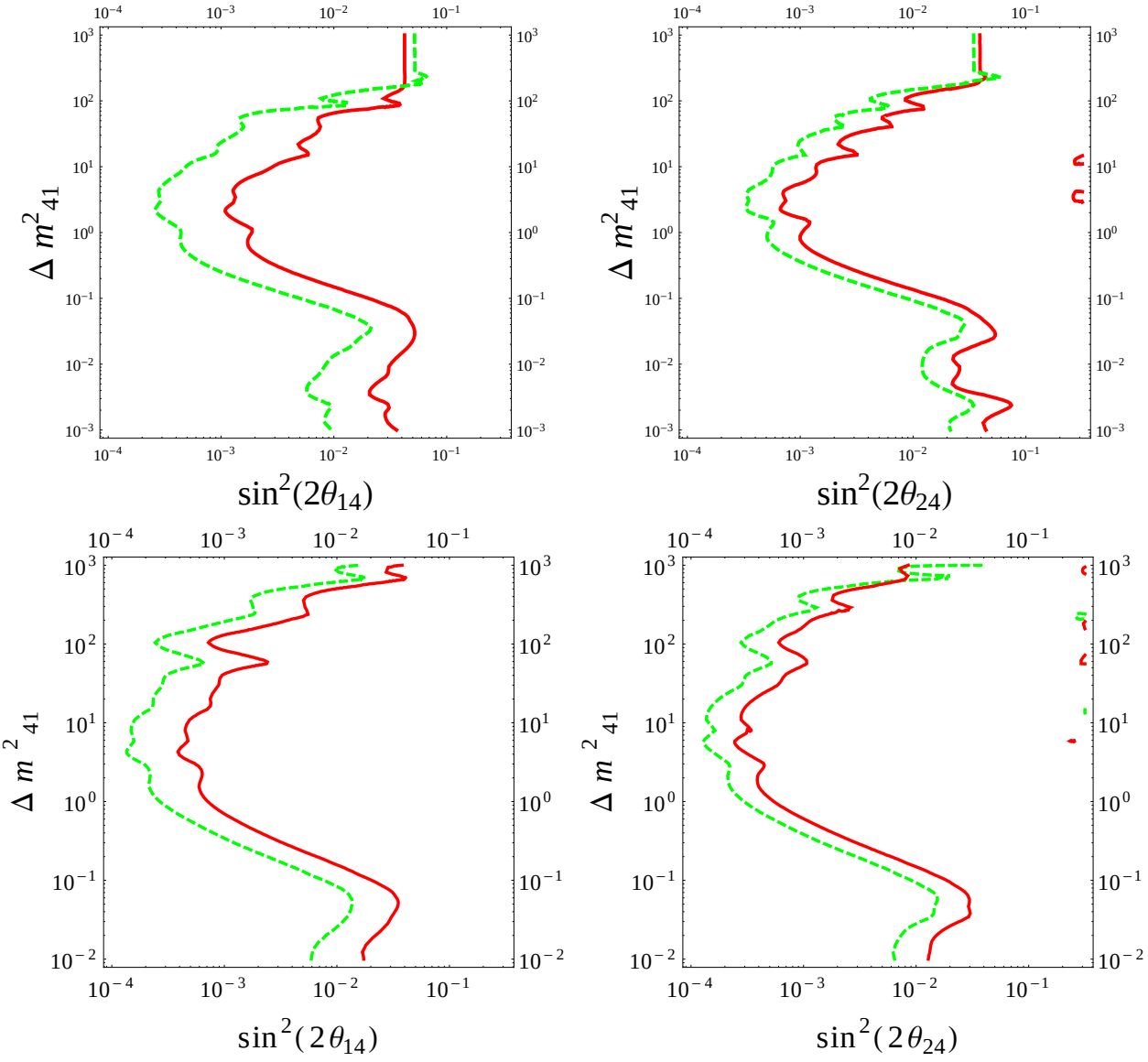

Figure 5.7: Sensitivity to $\sin^2 2\theta_{14}$–Δm^2_{41} (left) and $\sin^2 2\theta_{24}$–Δm^2_{41} (right) at 90% CL (4.5 GeV). The corresponding detectors are TASD (Red) and LAr (Green). The upper pair corresponds to the previous LENF consideration in Ref. [58], and the lower pair corresponds to the updated IDS-NF consideration.

sion from IDS-NF, the following setup of LENF is suggested as the ideal setup: 10 GeV muon beams are considered, with 1.0×10^{22} total useful muon decays per polarity [8], while the far detector is located at 2000 km from the source[9]. We compared this setup with our previous consideration for a LENF, which mainly followed the assumption in Ref. [58], and tested if the new consideration of IDS-NF would provide better sensitivity on measuring sterile ν. Moreover, a Very Low Energy Neutrino Factory (VLENF) has also been proposed recently [59, 187]. It is suggested that with a combination of very near detectors, a 2 GeV neutrino factory (with 1.0×10^{20} muon decays in total) would provide an excellent search of eV-scale sterile neutrinos. We have compared the performance of these different options in our choice of setup with a near detector at 2 km, see Fig. 5.8.

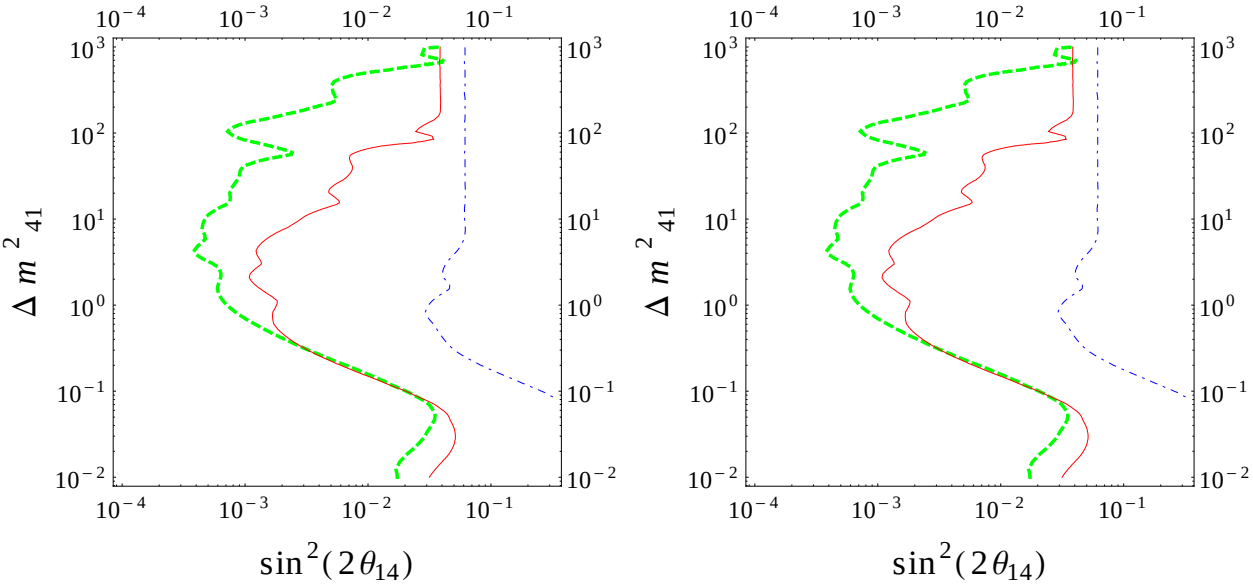

Figure 5.8: Sensitivity to $\sin^2 2\theta_{14}$–Δm^2_{41} (left) and $\sin^2 2\theta_{24}$–Δm^2_{41} (right) at 90% C.L. for different muon energies: 4.5 GeV with 1.4×10^{22} muon decays (red, solid line), 10 GeV with 1.0×10^{22} muon decays (green, dashed line) and 2 GeV with 1.0×10^{20} muon decays (blue, dot-dashed). All of them correspond to the simulation with a near detector at 2 km.

For the same distance of the near detector, the updated IDS-NF configuration, with a muon energy of 10 GeV would provide a much better sensitivity. However, the comparison above also shows that if Δm^2_{41} is just around O(eV) order, as for instance suggested by the Reactor Anomaly to be discussed in the following section, then the 4.5 GeV NF has a very good

[8] Similar to before, in our simulation in GLoBES, we set up the flux as 1.0×10^{21} useful muon decays per year, per polarity, running for 10 years in order to produce 1.0×10^{22} muons in total.

[9] Neither the detection of sterile neutrinos nor near detector is mentioned in this set-up, and thus we still locate the near detector at 2 km for this consideration.

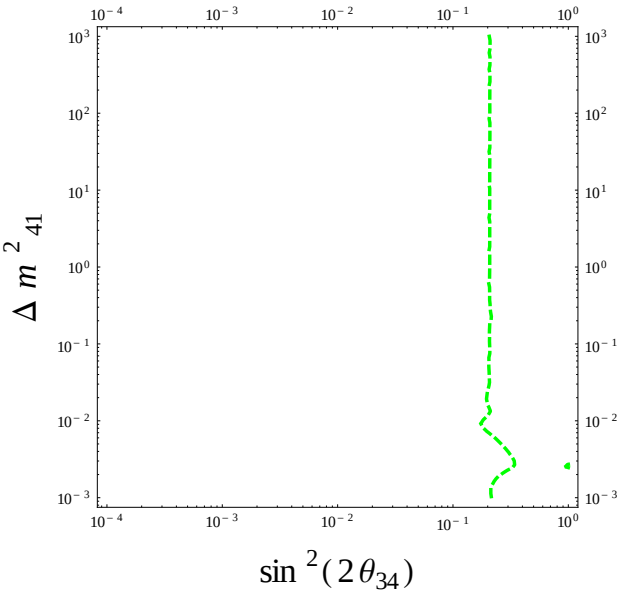

Figure 5.9: The sensitivity for $\sin^2 2\theta_{34}$–Δm^2_{41} at 90% CL, corresponding to the updated IDS-NF consideration (E = 10 GeV).

reach, down to 10^{-3} for $\sin^2 2\theta_{i4}$, $i = 1, 2$. If, in the future, there are hints that light sterile neutrinos are heavier than $O(10$ eV), then a 10 GeV or higher energy NF would be necessary.

Higher energy muons also allow to detect ν_τs, and thus provide sensitivity to θ_{34}, thanks to the far detector, as shown in Fig. 5.9 (but just with the appearance channel; thus the sensitivity is much worse than measuring θ_{14} and θ_{24}). Since the statistics at the far detector are much lower than at the ND and the ν_τ measurements are based on the appearance channels, the sensitivity for θ_{34} is very poor. In fact, we have also tried to add a Emulsion Cloud Chamber in the near detector, but the inclusion does not lead to any significant improvement of the sensitivities. Moreover, as the effect of large Δm^2_{41} is averaged out in the FD, the sensitivity of θ_{34} is almost constant with Δm^2_{41} [except when $\Delta m^2_{41} \approx \Delta m^2_{31}$. In this range, Eq. (5.3) also applies to Δm^2_{41} and thus θ_{34} is related to Δm^2_{41}, but such a small Δm^2_{41} is not our interest in this paper.]

Of course, increasing the energy can improve the study on sterile neutrino mixing; however, the comparison above also shows that if Δm^2_{41} is just around O(eV) order[10], then a 4.5 GeV NF is more than enough, since it can attain up to 10^{-3} for $\sin^2 2\theta$. We are convinced that

[10]That's also what the Reactor Anomaly suggested [63, 191], as we are going to discuss in *Chapter 6*.

a 4.5 GeV LENF can lead us to an excellent understanding of light sterile neutrino mixing. Besides, ν_e channels are difficult to use in higher energy, because electrons / positrons tend to shower early at high energies [192]. Therefore, in this thesis, we focus on the 4.5 GeV LENF.

If in the future, there are hints that light sterile neutrinos are heavier than $O(10\text{ eV})$, then a 10 GeV or higher energy NF is necessary.

5.4 Decoherence Effect

Recently, reference [167] studied the decoherence effect in the $\nu_\mu - \nu_s$ oscillation in the near detector of the MINOS experiment [193]. Their results suggest that if the energy difference of two mass eigenstates is **not** much smaller than the energy uncertainty of the initial pions (which are used to produce neutrinos in MINOS), then the partial decoherence may arise in the neutrino production. More specifically, in the MINOS experiment, since the length of the pion decay pipe (675 m) is comparable with the short-baseline of near detector, the conditions of coherent ν production is violated, which will suppress the oscillation effect of sterile neutrinos with 1 eV mass.

These decoherence effects are also relevant for a neutrino factory. Traditionally, the baseline of a neutrino factory is assumed to be over 1000 km, which is much longer than the length of a muon storage ring (600 m [172]) and it is a good approximation to consider the neutrino production as pointlike. However, in the study of sterile neutrino oscillation, as we have discussed earlier the near detector is crucial and the corresponding baseline is just a few kilometers, not much longer than the decay straight. Specifically in our simulation, the distance between decay straight and near detector is just 2 km, which means that the muon decay (or neutrino production) should not be considered as pointlike and the decoherence effect cannot be neglected.

A detailed discussion of the effect of muon lifetime on the coherence in neutrino oscillation can be found in Ref.[194]. Neutrino oscillations are observable because the flavor states are *coherent linear superpositions* of various mass states. This coherence requires that the energy uncertainties at ν production and detection (σ_E) are much larger than the energy difference of different ν mass eigenstates ΔE_{ij} [195]. If the neutrino production is not pointlike, the spatial uncertainty σ_x will be enlarged and thus σ_E will be reduced [11]. In this case, the condition $\sigma_E \gg \Delta E_{ij}$ and thus the coherence of mass states will be violated.

[11] $\sigma_E \sigma_x \simeq v_g$, where v_g is the average group velocity of the wave packets of different mass eigenstates [196].

In the near detector of a LENF, since L (length of baseline) $\approx l_p$ (the length of μ storage ring), l_p should be taken into account in the computation of the neutrino flux. In this case, neutrinos are produced incoherently and the effective survival probability depends on l_p and the decay rate of the muon in laboratory frame (Γ_μ). To leading order, the effective muon survival probability for '3+1' mass frame is given by [167]

$$\begin{aligned} P_{\mu\mu,\text{eff}} =& 1 - \frac{1}{2}\sin^2 2\theta_{24} + \frac{1}{2}\sin^2 2\theta_{24}\frac{\Gamma_\mu}{1-e^{-\Gamma_\mu l_p}}\int_0^{l_p} dx e^{-\Gamma_\mu x}\cos[\xi\Gamma_\mu(L-x)] \\ =& 1 - \frac{1}{2}\sin^2 2\theta_{24} + \frac{1}{2}\sin^2 2\theta_{24}\frac{1}{(1+\xi^2)(1-e^{-\Gamma_\mu l_p})}\cdot \\ & [\cos\phi_L + \xi\sin\phi_L - e^{-\Gamma_\mu l_p}(\cos(\phi_L-\phi_p) + \xi\sin(\phi_L-\phi_p))], \end{aligned} \tag{5.4}$$

where L is the baseline of near detector, the first two terms $(1 - \frac{1}{2}\sin^2 2\theta_{24})$ are the averaged probability, and

$$\begin{aligned} \Gamma_\mu &= \frac{\Gamma^0_\mu m_\mu}{E_\mu} = \frac{\alpha\Gamma^0_\mu m_\mu}{E_\nu} \quad (E_\nu = \alpha E_\mu, \quad \Gamma^0_\mu \text{ is the decay rate in rest-frame of } \mu) \\ \xi &= \frac{\Delta m^2_{41}}{2E_\nu\Gamma_\mu} = \frac{\Delta m^2_{41}}{2\alpha m_\mu \Gamma^0_\mu} \\ \phi_L &= \frac{\Delta m^2_{41} L}{2E_\nu} \\ \phi_p &= \frac{\Delta m^2_{41} l_p}{2E_\nu} \end{aligned} \tag{5.5}$$

Similarly the survival probability of ν_e is

$$\begin{aligned} P_{ee,\text{eff}} =& 1 - \frac{1}{2}\sin^2 2\theta_{14} + \frac{1}{2}\sin^2 2\theta_{14}\frac{1}{(1+\xi^2)(1-e^{-\Gamma_\mu l_p})}\cdot \\ & [\cos\phi_L + \xi\sin\phi_L - e^{-\Gamma_\mu l_p}(\cos(\phi_L-\phi_p) + \xi\sin(\phi_L-\phi_p))], \end{aligned} \tag{5.6}$$

It is interesting to notice that if ϕ_p and ξ are negligible, Eq. (5.1) and Eq. (5.6) will converge to $P_{\mu,\mu}$ and $P_{e,e}$ in Eqs. (5.2) (corresponding to θ_{14} or $\theta_{24} = 0$), which are the standard probability equations. We used Eqs. (5.4) and (5.6) as our user-defined probabilities and implemented them into GLoBES. Then we performed the simulation in the '3+1' mass scheme and compared the sensitivity with the previous studied case of no decoherence effects.

Fig. 5.10 shows that the decoherence effect will lead to certain loss of sensitivity, especially for large Δm^2_{41}. This is reasonable because large Δm^2_{41} will enlarge ϕ_p and thus enhance the decoherence effect. (The deficit in small Δm^2_{41} mainly comes from the interference with Δm^2_{31}. When Δm^2_{41} is small, we should also take Δm^2_{31} into account and Eq. (5.4), Eq. (5.6) would not be accurate enough. Our user-defined probability in this section is significant only when $\Delta m^2_{41} \gg \Delta m^2_{31}$.)

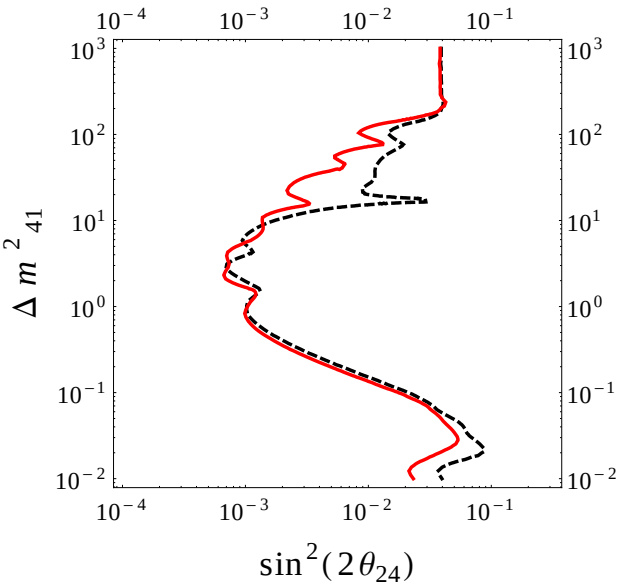

Figure 5.10: Sensitivity to $\sin^2 2\theta_{24}$–Δm^2_{41} at 90 % CL with and without considering decoherence effects. The red solid curve corresponds to the previous simulation, without considering the decoherence effect. The black-dashed curve corresponds to the decoherence effect in a LENF (wiht $l_p = 600$ m, the life-time of muon is 2.197×10^{-6} s in rest-frame).

In order to weaken the impact of the decoherence effect, the decoherence parameter has to be reduced. Differently from Ref. [167], the decoherence parameter in our case is ϕ_p rather than ξ. In MINOS, the decay length, $l_{\rm dec} = c\tau^0_\pi\gamma_\pi \sim 560$m, which is smaller than the corresponding l_p [167], thus most pions decay before reaching the end of the tunnel. Instead, in a LENF, $l_{\rm dec} = c\tau^0_\mu\gamma_\mu = 28$ km $\gg l_p$. In this limit, the ratio of the energy uncertainty of production, σ_E, to the energy difference of the various mass eigenstates, ΔE, is

$$\frac{\Delta E}{\sigma_E} \simeq \frac{\Delta m^2_{41} l_p}{2E_\nu} = \phi_p. \tag{5.7}$$

This means that, if ϕ_p is negligible compared to ϕ_L, the decoherence effect will be insignificant. Reducing the length of the muon storage ring, or increasing the muon energy or the distance of the near detector, which makes $\phi_L \gg \phi_p$, would significantly reduce the decoherence effect. However, in practice, applying these methods would be difficult, as the length of μ storage ring cannot be reduced dramatically without a significant loss of useful muon decays, and extending the baseline of ND will also lead to the loss of sensitivity (as discussed in the previous section). Ref. [195] suggests that in MINOS the detection of the muon would contribute to localize the pion decay and reduce the decoherence effects by making the neutrino production more pointlike. If the muon (in the case of LENF, should be electron)

produced in the pion decay is detected, then Eq. (5.4) would not apply, and the decoherence parameter no more depends on l_p, but the spatial width of the muon wave packet (which is expected to be much smaller than l_p, thus the decoherence effect is smaller). The detail of the calculation can be referred to [195].
Similarly, in a LENF, the detection of the electron from muon decay can be used to reduce the decoherence effect. Since the detection of the electron should be easier than detecting muon, in a LENF, it is expected to be able to eliminate the decoherence effect more effectively. In the future, more effort has to be devoted to the study and elimination of decoherence effects in sterile neutrino oscillation.

5.5 Summary

In this chapter, the light sterile neutrino oscillation has been discussed. We have studied the potential of a Low Energy Neutrino Factory with both far and near detectors in searching the sterile neutrino mixing. Our reference setup may be a little bit optimistic [58].
Since the measurement of light sterile neutrino mixing mainly depends on the near detector, we realized that the large detector is not required in our study, but the resolution, efficiencies and systematic errors of the detectors are more important. We have compared the simulations corresponding to TASD and LAr detectors, and our results showed that the performance of LAr are better.
We have also demonstrated what are the key factors in improving the sensitivity. We found out that the disappearance channels dominate in the near detector, since they are related to the leading order of θ_{i4}. On the other hand, increasing the resolution and efficiencies of the detectors, and reducing the systematic errors can significantly improve the sensitivity. With optimistic settings on these factors, the results of a LENF can be comparable to that of a HENF and we do not need to consume so much on the muon energy.

However, all the simulations in this chapter only consider one light sterile neutrino. As mentioned in *Chapter 2*, there may be more than one light sterile neutrinos. Actually, in the framework of '3+1', there is strong tension between the data from LSND, MiniBooNE, and the short baseline disappearance experiments [110]. In the last few years, there are more and more hints that suggest the '3+2' oscillation model provides a better description of the ν_s oscillation data compared to the '3+1' model [197, 66]. Moreover, in order to test the hypothesis of no effect of extra sterile neutrinos, in this chapter all the simulations only tested the scenario that "$\theta_{i4} \approx 0$".
Therefore, to make our analysis of "light sterile neutrino oscillation" more complete, in the

next chapter we will discuss the simulation for the '3+2' mass scheme. Furthermore, we will also perform the simulations for testing the scenario of "relatively large sterile mixing angles", which correspond to the best fit values from Ref. [191], a paper after the discovery of the **Reactor Anomaly**.

Chapter 6

'3+2' Mass Scheme and Reactor Anomaly

As mentioned in *Chapter 2*, MiniBooNE data suggested a non-observation of oscillation for neutrinos, despite the excess in the anti-neutrinos measurement. Moreover, there exists tension between the data from LSND, MiniBooNE and short-baseline experiments. The data from short baseline oscillation experiments also lead to a further constraint on the allowed region from LSND and MiniBooNE $\bar{\nu}$ signal. Although there are hints suggesting the existence of sterile neutrinos, there are also experimental results which disfavour the '3+1' (or even '3+2') oscillation hypothesis. However, the anomaly found by Ref. [63] suggests that previously the short-baseline reactor neutrino experiments, and also the MiniBooNE ν are misinterpreted.

In 2011, T.A.Mueller et al. [198] have provided new reactor antineutrino spectra and found a significant upward shift in the predicted fluxes. This result implies a weakening of existing reactor bounds on the absence of ν_e disappearance and suggests the existence of ν_s with $\Delta m^2_{\text{sterile}} \gtrsim 1$ eV^2 [63].

The re-evaluation of the antineutrino flux of the previous reactor experiments, which includes Bugey [103], Chooz [104], Palo Verde [199], etc, found an increase of the expected $\bar{\nu}$ rate by 3.5%. This would favor a small disappearance of $\bar{\nu}$ in the reactor neutrino experiments, and even an oscillation of the ν measurement in MiniBooNE [111]. Therefore, their results are compatible with the existence of sterile neutrinos. Fig. 6.1 illustrates the reactor antineutrino anomaly by displaying the goodness of fits of the "3 ν mixing hypothesis" and the "3+1 ν mixing hypothesis" [63].

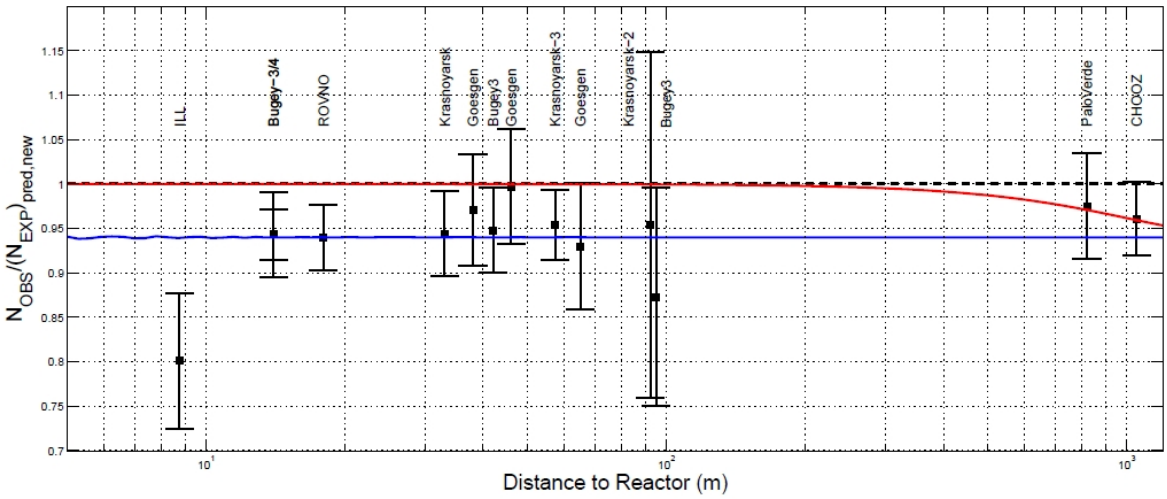

Figure 6.1: The ratio of observed event rates to expected event rates, which reveals the short baseline reactor antineutrino anomaly. The red line corresponds to 3 active neutrino mixing hypothesis with $\sin^2 2\theta_{13} = 0.06$. The blue line displays the fit of the hypothesis with a new neutrino mass state and a new $\Delta^2 m$. This figure is taken from Ref. [63] and detailed discussions of the plot can be found in this reference.

Although the increase of the flux has no significant effect on the solar parameter results, it significantly affects the results on testing the existence of sterile neutrinos from short-baseline experiments, as shown in Fig. 6.1. In this figure, the four neutrinos scenario clearly fits the data better. This illustrates that the impact of the reanalysis with the new antineutrino spectra flavours the existence of sterile neutrinos.

Since a LENF provides a more precise and higher statistics study on sterile neutrino mixing, it would be interesting to use a LENF to check the recent reactor anomaly. Moreover, a combined analysis [191] further favors '3+2' mixing scheme with $\Delta m^2_{41} \sim \Delta m^2_{51} \sim O(1\text{ eV})$. Giunti and Laveder also found that their global fit of reactor and short-baseline experiments favors the '3+2' scheme [68]. Besides, as mentioned in *Chapter 2*, it is suggested that the '3+2' scheme can provide a better fit to the LSND and MiniBooNE data [197, 66]. Thus in the following section, we are going to change our focus from '3+1' to '3+2'. In *Section 6.2* "the anomaly from recent Re-analysed Reactor Experiments" will be further studied.

6.1 '3+2' Mass Scheme

The accumulation of hints for the '3+2' neutrino mass scheme have been discussed in *Chapter 2*. In this section, we will focus on the simulations of two light sterile neutrino oscillations in LENF.

If we change the mixing scheme to 5 neutrinos scheme, our parameterization of U is re-defined as,

$$\begin{aligned} U =& R_{45}(\theta_{45},\delta_6)R_{35}(\theta_{35},\delta_5)R_{52}(\theta_{52},\delta_4)R_{51}(\theta_{51},0)R_{34}(\theta_{34},0)R_{24}(\theta_{24},0)R_{14}(\theta_{14},0) \\ & R_{23}(\theta_{23},\delta_3)R_{13}(\theta_{13},\delta_2)R_{12}(\theta_{12},\delta_1), \end{aligned} \tag{6.1}$$

The mixing matrix for '3+2' mass scheme is very complicated. Since the active states ν_e and ν_μ are most relevant in a Neutrino Factory, here only the mixing elements of U_{ei} and $U_{\mu i}$ are listed,

$$\begin{cases} U_{e1} &= c_{12}c_{13}c_{14}c_{15} \\ U_{e2} &= c_{13}c_{14}c_{15}s_{12}e^{-i\delta_1} \\ U_{e3} &= c_{14}c_{15}s_{13}e^{-i\delta_2} \\ U_{e4} &= c_{15}s_{14} \\ U_{e5} &= s_{15}, \end{cases}$$

$$\begin{cases} U_{\mu 1} &= -c_{23}c_{24}c_{25}s_{12}e^{i\delta_1} - c_{12}[c_{24}c_{25}s_{23}s_{13}e^{i(\delta_2-\delta_3)} + c_{13}(-c_{25}s_{14}s_{24} + c_{14}s_{15}s_{25}e^{-i\delta_4})] \\ U_{\mu 2} &= c_{12}c_{23}c_{24}c_{25} - s_{12}e^{-i\delta_1}[c_{24}c_{25}s_{23}s_{13}e^{i(\delta_2-\delta_3)} + c_{13}(-c_{25}s_{14}s_{24} + c_{14}s_{15}s_{25}e^{-i\delta_4})] \\ U_{\mu 3} &= c_{13}c_{24}c_{25}s_{23}e^{-i\delta_3} - s_{13}e^{-i\delta_2}(c_{25}s_{24}s_{14} + c_{14}s_{15}s_{25}e^{-i\delta_4}) \\ U_{\mu 4} &= c_{14}c_{25}s_{24} - s_{14}s_{15}s_{25}e^{-i\delta_3} \\ U_{\mu 5} &= c_{15}s_{25}e^{-i\delta_4}. \end{cases}$$

Also, the survival and conversion probabilities will change. In the near detector limit, their approximations are as following,

$$P_{\alpha,\alpha} = 1-4[(1-\mid U_{\alpha,4}\mid^2 - \mid U_{\alpha,5}\mid^2)\cdot(\mid U_{\alpha,4}\mid^2 \sin^2\Delta_{41} + \mid U_{\alpha,5}\mid^2 \sin^2\Delta_{51}) - \mid U_{\alpha,4}\mid^2 \mid U_{\alpha,5}\mid^2 \sin^2\Delta_{54}] \tag{6.2}$$

and

$$\begin{aligned} P_{\alpha,\beta} =& 4\mid U_{\alpha,4}\mid^2 \mid U_{\beta,4}\mid^2 \sin^2\Delta_{41} + 4\mid U_{\alpha,5}\mid^2 \mid U_{\beta,5}\mid^2 \sin^2\Delta_{51} + \\ & 8\mid U_{\alpha,4}\mid\mid U_{\beta,4}\mid\mid U_{\alpha,5}\mid\mid U_{\beta,5}\mid \sin\Delta_{41}\sin\Delta_{51}\cos(\Delta_{45}-\delta) \end{aligned} \tag{6.3}$$

where δ is the CP-phase as defined in Ref. [191]: $\delta = \arg(U^*_{\mu,5}U_{e,5}U_{\mu,4}U^*_{e,4})$, and Δ_{ij} is defined as $\Delta_{ij} = \Delta m^2_{ij}L/(4E)$.

Here, if we again assume $\theta_{i4} \approx \theta_{i5} \approx 0$, and all sterile CP-phases = 0, then expand Eq. (6.2) and (6.3) into leading order, the probability equations will be simplified as

$$P_{e,e} = 1 - 4(s_{14}^2 \sin^2\Delta_{41} + s_{15}^2 \sin^2\Delta_{51}), \tag{6.4}$$

$$P_{\mu,\mu} = 1 - 4(s_{24}^2 \sin^2\Delta_{41} + s_{25}^2 \sin^2\Delta_{51}), \tag{6.5}$$

and

$$P_{e,\mu} = P_{\mu,e} = 4s_{14}^2 s_{24}^2 \sin^2\Delta_{41} + 4s_{15}^2 s_{25}^2 \sin^2\Delta_{51} + 8s_{14}s_{24}s_{15}s_{25}\sin\Delta_{41}\sin\Delta_{51}\cos(\Delta_{45}). \tag{6.6}$$

In this case, the relation between θ_{i4} and Δm_{41}^2 (or θ_{i5} and Δm_{51}^2) are just similar to '3+1' mass-scheme (we can see in the leading order, the relations between θ_{i4} and Δm_{41}^2 are just the same as Eqs. (5.2)). Also, as shown in Eqs. (6.4) - (6.6), only the mixing angles θ_{14}, θ_{24}, θ_{15}, θ_{25} and the two $\Delta m_{\text{sterile}}^2$ can be measured, since they are related to the ν_μ and ν_e channels. The other sterile parameters will not be studied in this chapter.

Our results of simulation are as below:

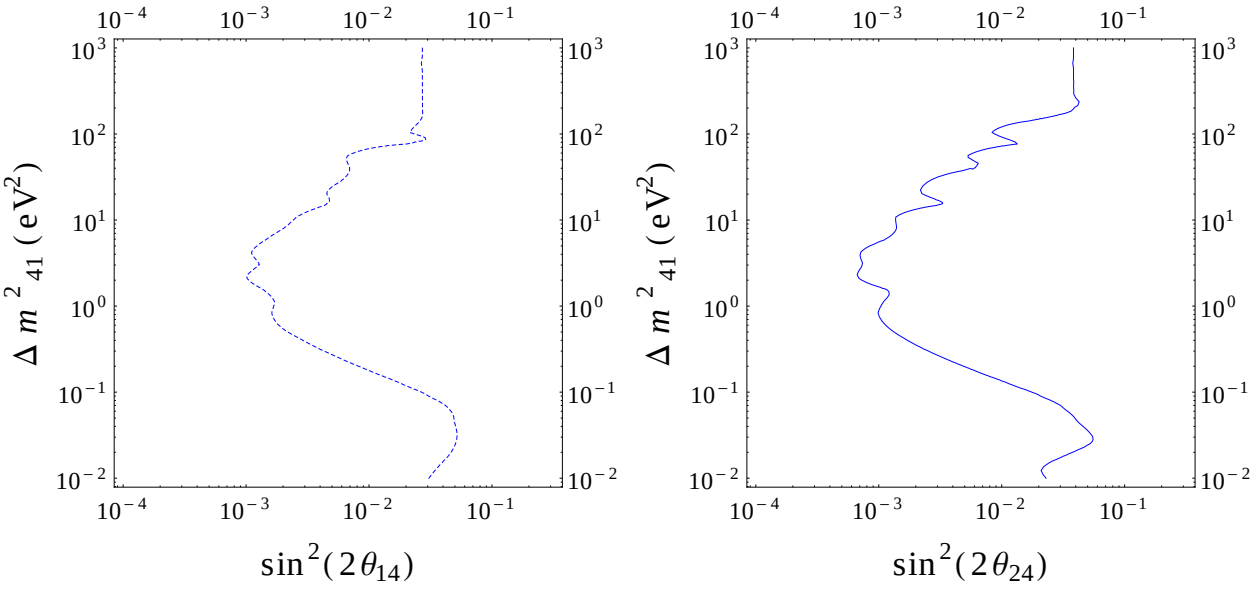

Figure 6.2: Sensitivity to $\sin^2 2\theta_{14}$–Δm_{41}^2 (left) and $\sin^2 2\theta_{24}$–Δm_{41}^2 (right) at 90% CL under '3+2' scheme (assuming $\theta_{i4} \approx \theta_{i5} \approx 0$).

The plot of θ_{15} - Δm_{51}^2 just provides a similar contour as $\sin^2 2\theta_{14}$–Δm_{41}^2, which is shown in Fig. 6.3.

We report in Fig. 6.2 and 6.3 the results of our simulations for the 3+2 scheme. If Δm_{41}^2 and Δm_{51}^2 are assumed to be of the same order, it is unlikely that the LENF will be able to distinguish the two mass squared differences as the probabilities have a similar dependence

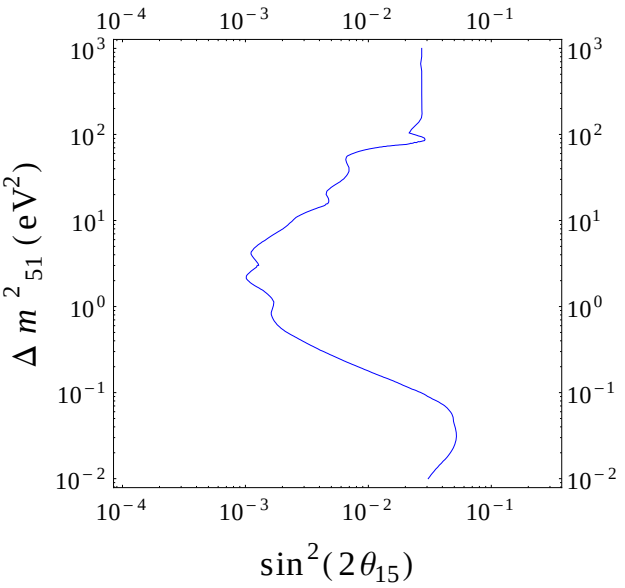

Figure 6.3: Sensitivity to $\sin^2 2\theta_{15}$–Δm^2_{51} at 90 % CL under '3+2' scheme (assuming $\theta_{i4} \approx \theta_{i5} \approx 0$).

to the two parameters. This degeneracy cannot be broken by the LENF and it would not be possible to distinguish this case from the 3+1 sterile mass scheme. However, this is not the case if the two masses are significantly different, leading to two different oscillatory patterns.

6.2 Comparison with Global Short-Baseline Neutrino Oscillation Data

As previously mentioned, Ref. [191] re-analysed the data from reactor experiments and other experiments and found that the sterile mixing angles can be relatively large. Afterwards, Ref. [68] also re-analysed the data and the '3+2' global fit in these two papers basically agree with each other. This further supports the reactor-anomaly and the existence of two sterile neutrinos, which also means that the values of the sterile mixing parameters need to be studied more precisely. This enhances the motivation of using a LENF to study sterile neutrino mixings. The results of Refs. [191] and [68] are shown in Table 6.1.

Table 6.1 Best fit values from Ref. [191] and Ref. [68] for the '3+2' mass scheme.

	Δm^2_{41} [eV^2]	$\lvert U_{e4} \rvert$	$\lvert U_{\mu 4} \rvert$	Δm^2_{51} [eV^2]	$\lvert U_{e5} \rvert$	$\lvert U_{\mu 5} \rvert$
Ref.[191]	0.47	0.128	0.165	0.87	0.138	0.148
Ref.[68]	0.9	0.130	0.134	1.60	0.130	0.08

In the previous simulation, the focus was on the lowest limit of the sterile mixing angles that a LENF can measure. Thus, in the simulation, $\theta_{sterile} = 0$ is assumed as the theoretical value for the calculation of χ^2. From now on, we study what precision a LENF could reach in measuring large values of the mixing angles and we take as reference the current best fit values from Ref. [191], see Table 6.1.

For the sake of simplicity, in all our simulations, the sterile CP-phases are assumed to be 0. The results for the mixing angles are shown in Fig. 6.4. It is obvious that the reach of the LENF is excellent, since the LENF can provide a much higher statistics study than reactor experiments. With the near detector, a LENF can constrain the parameters in a very small region if the mixing angles are large enough. Thus, it is a potential candidate to verify the results from the re-analysis of the reactor experiments.

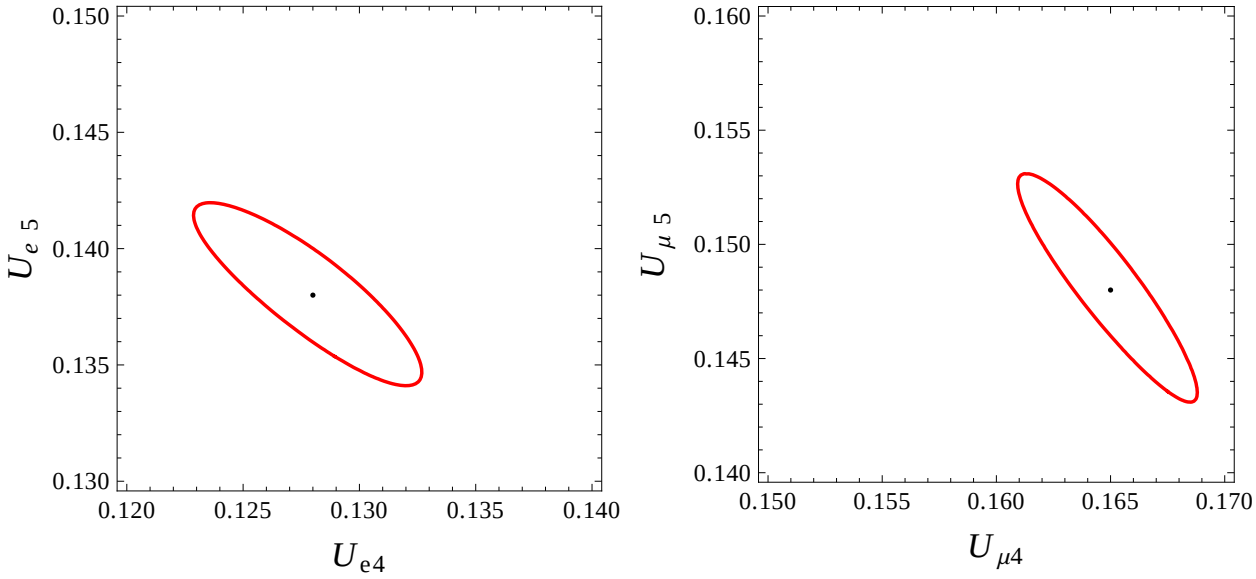

Figure 6.4: Sensitivity to U_{e4} vs U_{e5} (left) and $U_{\mu 4}$ vs $U_{\mu 5}$ (right) at 90 % C.L. in the '3+2' scheme. The black dot corresponds to the best-fit values from Ref. [191], reported in Table 6.1.

From Fig. 6.4, it is obvious the 90% CL contours from the LENF measurements are expected to be very constrained. This is reasonable, since the LENF can provide a higher-statistics study than reactor experiments. If the mixing angles are large enough, the probability equations [Eqs (6.4) - (6.6)] and also the χ^2 will become more sensitive to the change of θ_{i4}. With the near detector, LENF can constrain the sterile oscillation parameters in a very small region, thus it is a potential candidate to verify the results from the re-analysis of the reactor experiments.

As a further reference, the allowed regions in the Δm^2_{41} - Δm^2_{51} plane are presented in Fig. 6.5, where we compare the precision reachable at the LENF with the currently allowed region for the masses [191]. Comparing the 90% CL contours from the LENF simulation

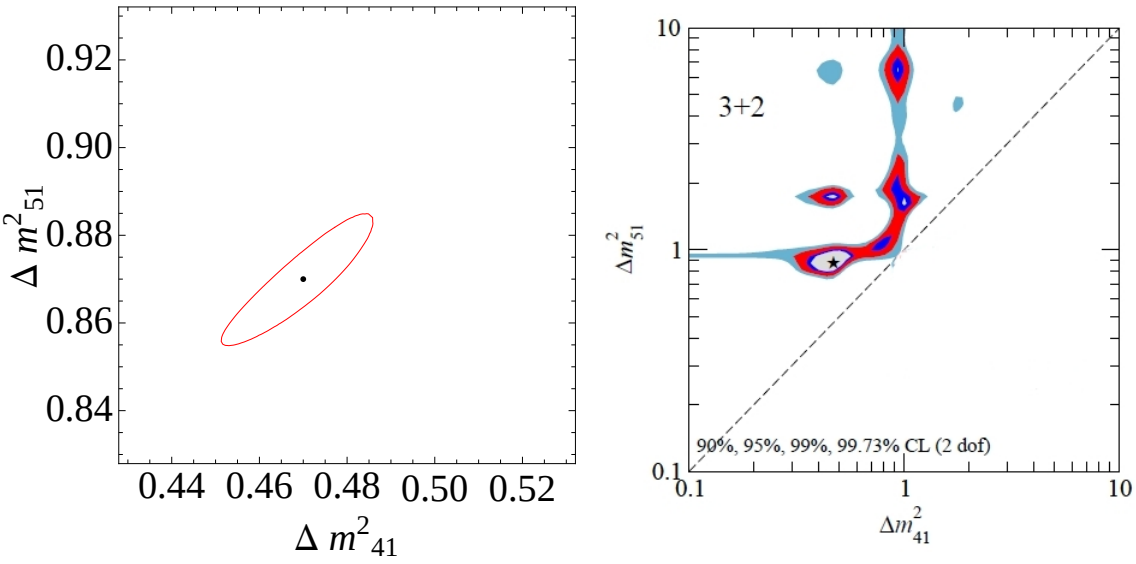

Figure 6.5: The 90% C.L. allowed values of Δm^2_{41} vs Δm^2_{51} for a future measurement at the LENF (left panel) compared to the current ones, (right panel), figure taken from Ref. [191]. The black dot (left panel) and the star (right panel) correspond to the best-fit values in Table 6.1.

(left panel of Fig. 6.5) and from Ref.[191] (the navy-blue area in right panel), the region constrained by the LENF is much smaller. This shows that LENF can further measure the two sterile Δm^2 with extremely high precision thanks to its large flux and higher energy.

If we enhance the energy scale to 10 GeV, which corresponds to the current IDS-NF consideration (as mentioned in the previous chapter), a more precise measurement could be achieved, as shown in Fig. 6.6

In a word, if the sterile mixing angles are as large as Ref. [191, 68] suggest ($U_{\alpha i} \approx 0.1$), then the sterile neutrino oscillation effects would be more obvious and the "Reactor Anomaly" will hopefully be further confirmed with higher statistics from a low energy neutrino factory.

6.3 Summary

In this chapter, the performance of a LENF on studying the '3+2' neutrino mass scheme has been discussed. We have shown that even if two light sterile neutrinos exist, with a near de-

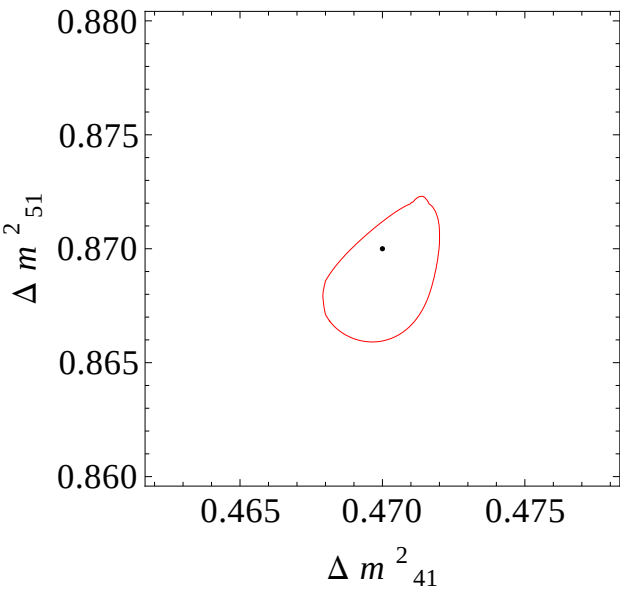

Figure 6.6: The 90% C.L. allowed values of Δm^2_{41} vs Δm^2_{51} for a future measurement at the 10 GeV LENF.

tector, a LENF is still powerful enough to search the light sterile ν mixings. Furthermore, we used the best fit values of the sterile oscillation parameters from Ref. [191] and re-performed the simulation. We found out that a LENF can constrain the sterile parameters in a very small range if the mixing angles (θ_{i4}) are as large as a recent global analysis of short-baseline experiments suggests [191, 68]. Therefore, a LENF is expected to be able to check the reactor antineutrino anomaly.

It is important to confirm the implication of the reactor antineutrino anomaly, as it is not necessarily caused by sterile neutrinos. After the reevaluation of reactor neutrino spectra performed by T.A.Mueller et al. [198], Huber also presented an independent analysis of the spectra [200]. His result is similar to the result from Ref. [198], but the origin of the anomaly is different. Huber studied the higher order corrections related to nuclear physics, which include the finite size corrections, weak magnetism [201] and found that the effect of these corrections on the antineutrino spectra could also lead to an upward shift in the predicted fluxes. Different to the conclusion from Ref. [63], Huber suggested that the reactor anomaly may be due to some not well understood nuclear physics, which means that it can be explained without the existence of sterile neutrinos. The existing reactor data still needs to be further analysed in order to extract the physics implication.

Therefore, to confirm the existence of sterile neutrinos and the best-fit values from a

global analysis of short-baseline experiments [191, 68], more experimental efforts have to be devoted. A LENF is one of the excellent candidates for this confirmation. Besides the LENF and short-baseline experiments, the eV-scale sterile neutrinos may also be tested through cosmology. Ref. [202] suggests that the Cosmic Microwave Background (CMB) measurements is compatible with one or two sterile neutrino species, and Ref. [203] reveals that Big-Bang nucleosynthesis can also provide the upper bound on the number of extra neutrino species. Hopefully in the future, more data about the search of sterile neutrino oscillations will be available.

Chapter 7

Conclusion

Neutrino physics has been making great progress during the past 15 years. Although neutrinos are the least known of all Standard Model elementary fermions, the first evidence of physics beyond Standard Model came from the discovery of neutrino oscillations. Neutrino physics has provided a window on physics beyond Standard Model. The neutrino experiments now underway or being prepared will improve our understanding on neutrino oscillations, masses and nature in many ways.

One of the interesting topics of neutrino physics beyond the Standard Model is the question of the existence *sterile neutrino*, which do not have the conventional weak interaction like normal active neutrinos. The idea of sterile neutrinos extends the study of neutrinos to a new area with many implications. The main goal of the physics study presented in this thesis has been to investigate the phenomenology of sterile neutrino at different mass scales, especially its impact on neutrinoless double beta decay and neutrino oscillations.

In *Chapter 1* we briefly introduce the background of neutrino physics, including neutrino oscillations, the implication of Majorana neutrinos, neutrino mass generation and various neutrino experiments. Then in *Chapter 2*, the sterile neutrino was introduced and discussed in the heavy and light mass regime. We have shown that heavy sterile neutrinos are crucial in neutrino mass generation models. Besides the mass of the heavy neutrino, its mixing with active neutrinos is also related to rich phenomena. It is suggested that the decay rates of pions, kaons, Z bosons, etc. depend on the mixing of heavy neutrinos. Moreover, the bounds on this mixing could also be achieved by the decay of heavy neutrino itself. There are a lot of theoretical and phenomenological works about the heavy neutrino mixing. On the other hand, light sterile neutrinos (0.1 - 10 eV) may lead to anomalies in oscillation experiments. At present, the 3-active neutrino scenario is consistent with most of the neutrino

experimental data, however, the results of the LSND and MiniBooNE experiments and the recent discovery of reactor anomaly suggest that light sterile neutrinos may exist. There are tensions between the data from different sterile neutrino experiments and new experiments with improved sensitivities are necessary in the study of neutrino oscillations.

Then in *Chapter 3 and 4*, we investigated neutrinoless double beta decay and four interesting mechanisms which can induce this process. Since the study of neutrinoless double beta decay is one of the main available probes of LNV, observing this process would be a remarkable physics result for the hunt for physics beyond the Standard Model in general.

Typically the exchange of light neutrinos is assumed to be the dominant contribution in $(\beta\beta)_{0\nu}$-decay, but in *Chapter 3* we proved that the heavy neutrino mechanism and trilinear R-parity violation could also dominate this process. We paid special attention to the heavy ν exchange, since the heavy sterile neutrino is also related to the Seesaw Mechanism. We carefully studied the typical Type-I Seesaw and Extended Seesaw (or Inverse Seesaw) models. In the analysis of the latter, we investigated the possibility of dominant loop-level neutrino mass generation, and checked how the experimental data constrain the parameters of the Extended Seesaw model and thus the contributions of heavy ν in $(\beta\beta)_{0\nu}$-decay. The light neutrino mass generation models and neutrinoless double beta decay have been connected and the importance of heave sterile neutrino in these two issues were revealed in this chapter. We demonstrated that heavy ν mechanism could dominate the $(\beta\beta)_{0\nu}$-decay, but only in very small parameter region.

Moreover, to make the analysis of $(\beta\beta)_{0\nu}$-decay more complete, we also investigated other potential leading mechanisms in $(\beta\beta)_{0\nu}$-decay, the short-range and long-range R-parity violating (RPV) ones. We revealed that trilinear R-parity violation can also induce the light neutrino mass through loop diagrams and thus theoretically the RPV mechanisms can also provide significant contributions to $(\beta\beta)_{0\nu}$-decay.

In *Chapter 4* we further investigated the possible interference and even cancellation between different mechanisms in $(\beta\beta)_{0\nu}$-decay. We took the nuclear matrix elements (NMEs) of different mechanisms into account, and showed that destructive interference could reduce the decay rate significantly and may lead to the failure in observing the signal of $(\beta\beta)_{0\nu}$-decay in the experiments. Therefore, the absence of observation in some of the future experiments do not prove that the neutrino is a Dirac particle. We have to check the decays of different isotope before making any conclusions. Furthermore, since the potential cancellation effect depends on the ratios of NMEs, the effect can be significantly different in various nuclei and we have to carefully choose the nuclei for future measurements.

Then in the second part of the thesis, we changed our focus to light sterile neutrinos. Although a lot of studies have been made on sterile neutrinos, little is known about the ν_s oscillation parameters. Since the sterile neutrino mixing angles are supposed to be very small, to prove the ν_s existence, experiments with high precision are necessary. In *Chapter 5 and 6*, we investigated the potential of a Low Energy Neutrino Factory (LENF) in searching for light sterile neutrino oscillations. In these two chapters, we showed the results of our simulation performed with the GLoBES software and suggest that a LENF is a powerful tool in measuring the light sterile neutrino parameters.

Chapter 5 only considered the oscillation with one light sterile neutrino. We have showed that the measurement of light sterile neutrino mixing mainly depends on the near detector, and we have investigated the key factors in improving the sensitivity, namely the impact of the near detector, systematic errors, energy scale, detector type (TASD or LAr), etc. We suggested that with optimistic settings for these factors, e.g. high fluxes (around 10^{22} muon decays in total), low systematic errors (2%), 10% resolution, a LENF could measure $\sin^2 2\theta_{i4}$ down to 10^{-3} (at 90 % CL). We believe that LENF could be a powerful tool in searching sterile neutrino oscillations.

Since there are more and more hints suggesting that the 3+2 oscillation model provides a better description of the experimental data, we further discussed the performance of a LENF on studying the 3+2 neutrino mass scheme in *Chapter 6*. Moreover, we discussed the reactor antineutrino anomaly and compared our LENF simulation with the current global fit of neutrino oscillation data (after the discovery of the reactor anomaly). We showed that the LENF can constrain the sterile oscillation parameters in very small regions. Therefore, it is an excellent candidate to confirm the reactor anomaly, and measure the sterile parameters with much smaller errors compared to the results of a global analysis of short-baseline experiments. Hopefully in the future, more evidence on the existence and number of light sterile neutrinos can be achieved.

In the future, if Lepton Number Violation is observed or the existence of sterile neutrinos is confirmed, neutrino physics will cause a great excitement and it may be able to answer unsolved problems in particle physics which even the LHC can not address.

Appendix A

Neutrino Oscillation Formulation

In *Section 1.1*, the flavor eigenstates are shown to be connected with the mass eigenstates by the mixing matrix U:

$$\mid \nu_\alpha\rangle(t) = \sum_k U_{\alpha k} e^{-iE_k t} \mid \nu_k\rangle, \tag{A.1}$$

where α denotes neutrino flavors, k denotes the mass eigenstates labels, E_k is the energy of mass-state k. U is a unitary matrix with $UU^\dagger = 1$. Based on this equation, the transition amplitude to the other flavor state $\mid \nu_\beta\rangle$ is given by

$$\langle \nu_\beta \mid \nu_\alpha\rangle(t) = \sum_k U_{\alpha k} U^\dagger_{k\beta} e^{-iE_k t}, \tag{A.2}$$

Obviously if $t = 0$, which means transitions does not take place, then $\langle \nu_\beta \mid \nu_\alpha\rangle = \delta_{\alpha\beta}$ since U is unitary.

For neutrino, $E_k = \sqrt{p^2 + m_k^2} \simeq p + m_k^2/2p \simeq p + m_k^2/2E$, and relativistic approximation applies, i.e. $t \simeq L$[1]. Therefore

$$\begin{aligned}\langle \nu_\beta \mid \nu_\alpha\rangle(L) &= \sum_k U_{\alpha k}(U^\dagger)_{k\beta} \exp(-i(p + m_k^2/2E)L) \\ &= \sum_k U_{\alpha k} U^*_{\beta k} \exp(-i(p + m_k^2/2E)L).\end{aligned}$$

The transition probability is then given by

$$\begin{aligned}P_{\nu_\alpha \to \nu_\beta} &= |\langle \nu_\beta \mid \nu_\alpha\rangle|^2 \\ &= \sum_{k,j} U_{\alpha k} U^*_{\beta k} U^*_{\alpha j} U_{\beta j} \exp(-i(p + m_k^2/2E)L) \exp(i(p + m_j^2/2E)L) \\ &= \sum_{k,j} U_{\alpha k} U^*_{\beta k} U^*_{\alpha j} U_{\beta j} \exp(-i\frac{\Delta m_{kj}^2 L}{2E}),\end{aligned}$$

[1]In reality, the propagation time t is not measured in the experiments. What is know is the distance L between the source and detector. Thus in the calculations, it is necessary to change t to L

where $\Delta m^2_{kj} = m^2_k - m^2_j$ is the neutrino mass square difference, and $\Phi \equiv \dfrac{\Delta m^2_{kj} L}{2E}$ is the oscillation phase, describing the oscillation effect. Using the unitarity relation, $UU^\dagger = 1 \Leftrightarrow \sum_k U_{\alpha k} U^*_{\beta k} = \delta_{\alpha\beta}$, the probability equation can be further simplified as

$$
\begin{aligned}
P_{\nu_\alpha \to \nu_\beta} &= \sum_k |U_{\alpha k}|^2 |U^*_{\beta k}|^2 + 2 \sum_{k>j} U_{\alpha k} U^*_{\beta k} U^*_{\alpha j} U_{\beta j} \exp(-i \frac{\Delta m^2_{kj} L}{2E}) \\
&= (|\sum_k U_{\alpha k} U^*_{\beta k}|^2 - 2\mathrm{Re}[\sum_{k>j} U_{\alpha k} U^*_{\beta k} U^*_{\alpha j} U_{\beta j}]) + \\
&\{2 \sum_{k>j} \mathrm{Re}[U_{\alpha k} U^*_{\beta k} U^*_{\alpha j} U_{\beta j}] \cdot \mathrm{Re}[\exp(-i \frac{\Delta m^2_{kj} L}{2E})] \\
&+ 2(i \cdot i) \sum_{k>j} \mathrm{Im}[U_{\alpha k} U^*_{\beta k} U^*_{\alpha j} U_{\beta j}] \cdot \mathrm{Im}[\exp(-i \frac{\Delta m^2_{kj} L}{2E})]\} \qquad (P_{\alpha\beta} \text{ must be real.}) \\
&= \delta^2_{\alpha\beta} - 2 \sum_{k>j} \mathrm{Re}[U_{\alpha k} U^*_{\beta k} U^*_{\alpha j} U_{\beta j}](1 - \cos(\frac{\Delta m^2_{kj} L}{2E})) - 2 \sum_{k>j} \mathrm{Im}[U_{\alpha k} U^*_{\beta k} U^*_{\alpha j} U_{\beta j}](-\sin \frac{\Delta m^2_{kj} L}{2E}) \\
&= \delta_{\alpha\beta} - 4 \sum_{k>j} \mathrm{Re}[U_{\alpha k} U^*_{\beta k} U^*_{\alpha j} U_{\beta j}] \sin^2(\frac{\Delta m^2_{kj} L}{4E}) + 2 \sum_{k>j} \mathrm{Im}[U_{\alpha k} U^*_{\beta k} U^*_{\alpha j} U_{\beta j}] \sin(\frac{\Delta m^2_{kj} L}{2E}).
\end{aligned}
\tag{A.3}
$$

The oscillation probabilities of channels with $\alpha \neq \beta$ are transition probabilities; while the probabilities of the channels with $\alpha = \beta$ are survival probabilities, in this case, $U_{\alpha k} U^*_{\beta k} U^*_{\alpha j} U_{\beta j} = |U_{\alpha k}|^2 |U_{\alpha j}|^2$ is real, the last term in Eq. (A.3) vanishes, thus

$$
P_{\alpha\alpha} = 1 - 4 \sum_{k>j} |U_{\alpha k}|^2 |U_{\alpha j}|^2 \sin^2(\frac{\Delta m^2_{kj} L}{4E})
$$

The unitary mixing matrix U, is called the Pontecorvo-Maki-Nakagawa-Sakata (PMNS) matrix [13]. It converts the neutrinos from flavor eigenstates into mass eigenstates. In the case of two Dirac neutrinos, U is simply given by

$$
U = \begin{pmatrix} \cos\theta & \sin\theta \\ -\sin\theta & \cos\theta \end{pmatrix}.
$$

In the case of three active Dirac neutrinos, U is given by

$$\begin{aligned} U &= U_{23}U_{13}U_{12} \\ &= \begin{pmatrix} 1 & 0 & 0 \\ 0 & c_{23} & s_{23} \\ 0 & -s_{23} & c_{23} \end{pmatrix} \begin{pmatrix} c_{13} & 0 & s_{13}e^{\pm i\delta} \\ 0 & 1 & 0 \\ -s_{13}e^{\mp i\delta} & 0 & c_{13} \end{pmatrix} \begin{pmatrix} c_{12} & s_{12} & 0 \\ -s_{12} & c_{12} & 0 \\ 0 & 0 & 1 \end{pmatrix} \\ &= \begin{pmatrix} c_{12}c_{13} & s_{12}c_{13} & s_{13}e^{\pm i\delta} \\ -s_{12}c_{23} - c_{12}s_{23}s_{13}e^{\mp i\delta} & c_{12}c_{23} - s_{12}s_{23}s_{13}e^{\mp i\delta} & s_{23}c_{13} \\ s_{12}s_{23} - c_{12}c_{23}s_{13}e^{\mp i\delta} & c_{12}s_{23} - s_{12}c_{23}s_{13}e^{\mp i\delta} & c_{23}c_{13} \end{pmatrix}, \end{aligned} \tag{A.4}$$

where $s_{ij} = \sin\theta_{ij}$, $c_{ij} = \cos\theta_{ij}$, δ is the Dirac CP-phase (the upper sign corresponds to neutrino and lower sign to anti-neutrino). CP violation takes place if δ does not equal to 0 or π. Notice that δ does not appear in the case of two neutrinos. This is because CP violation only exists in the mixing between more than two families [204].
If neutrinos are Majorana particles, there will be two more CP-phases (Majorana phases). The equation above will become

$$\begin{aligned} U &= U_{23}U_{13}U_{12}V_{\text{Majorana}} \\ &= \begin{pmatrix} c_{12}c_{13} & s_{12}c_{13} & s_{13}e^{i\delta} \\ -s_{12}c_{23} - c_{12}s_{23}s_{13}e^{-i\delta} & c_{12}c_{23} - s_{12}s_{23}s_{13}e^{-i\delta} & s_{23}c_{13} \\ s_{12}s_{23} - c_{12}c_{23}s_{13}e^{-i\delta} & c_{12}s_{23} - s_{12}c_{23}s_{13}e^{-i\delta} & c_{23}c_{13} \end{pmatrix} \begin{pmatrix} e^{-i\phi_1} & 0 & 0 \\ 0 & e^{-i\phi_2} & 0 \\ 0 & 0 & 1 \end{pmatrix}. \end{aligned} \tag{A.5}$$

However, the phases ϕ_1 and ϕ_2 will not play any roles in neutrino oscillations. They can only be detected through Lepton Number Violation processes, such like neutrinoless double beta decay.

Moreover, the number of CP-phases also depends on the species of neutrinos. If there exist sterile neutrinos, there will be extra CP-phases in Eq. (A.5). For example, if there exist n generations of Dirac neutrinos, then the number of physical phases is [25]

$$n^2 - \frac{n(n-1)}{2} - (n-1) - n = \frac{(n-1)(n-2)}{2}. \tag{A.6}$$

It is noteworthy that when $n = 2$, the number of physical phases = 0. Again this shows that we cannot see CP-violation in the simplified two neutrino mixing scenario; On the other hand, for n generations of Majorana neutrinos, the number of phases is

$$n^2 - \frac{n(n-1)}{2} - n = \frac{n(n-1)}{2}. \tag{A.7}$$

Eqs. (A.6) and (A.7) show that there are always $(n-1)$ more physical phases in the scenario with Majorana neutrinos[2]. Basically it is because in the case of Dirac neutrino, there are phases which are arbitrary and can be absorbed by the neutrino wave function. This means that these phases cannot be observed and they are non-physical. However, if neutrinos are Majorana particle, due to the Majorana condition, these phases are not arbitrary and cannot be absorbed. They are physical and can be observed in LNV processes. More detailed discussion about the CP-phases are noted in Refs. [25, 208].

In the case of the '3+1' mass scheme, there will be two more Dirac CP-phases, the corresponding mixing matrix is shown in *Chapter 5*.

[2]Therefore, if neutrinos are Majorana particle, the CP violation effects are observable even $n = 2$ [205, 206, 207].

Appendix B

The Calculation Of The Standard $(\beta\beta)_{0\nu}$-Decay Process

The effective operator for neutrinoless double beta decay is

$$\hat{O} = 2G_F^2(\bar{e}_L\gamma_\mu\nu_L)(-\bar{\nu_L^c}\gamma_\nu e_L^c) \times J^\mu J^\nu, \tag{B.1}$$

where J is the nucleon current [118, 155].

$$J^\mu = \bar{\Psi}\tau_+[g_V(k^2)\gamma^\mu - ig_M(k^2)\frac{\sigma^{\mu\nu}}{2m_p}k_\nu - g_A(k^2)\gamma^\mu\gamma_5 + g_P(k^2)k^\mu\gamma_5]\Psi,$$

where τ is the isospin operator, Ψ represents the nucleon field. In the non-relativistic limit, this current can be rewritten as

$$J^\mu(\vec{x}) = \sum_\alpha(\tau_+)_\alpha[g^{\mu 0}J_\alpha^0(\vec{k}^2) - g^{\mu i}J_\alpha^i(\vec{k}^2)]\delta(\vec{x} - \vec{x_\alpha}), \quad i = 1, 2, 3, \tag{B.2}$$

$$\text{with } J_\alpha^0(\vec{k}^2) = g_V(\vec{k}^2),$$

$$J_\alpha^k(\vec{k}^2) = ig_M(\vec{k}^2)\frac{\vec{\sigma_\alpha} \times \vec{k}}{2m_p} + g_A(\vec{k}^2)\vec{\sigma_\alpha} - g_P(\vec{k}^2)\frac{\vec{k}(\vec{\sigma_\alpha} \cdot \vec{k})}{2m_p},$$

where $\sum_\alpha$ means a sum over all nucleons of the nucleus. $\vec{x_\alpha}$ is the coordinate of the αth nucleon. In the the non-relativistic limit, the form factors g_V, g_M, g_A, g_P are given by

$g_V(\vec{k}^2) = g_V(0)/(1 + \vec{k^2}/\Lambda_V^2)^2$,

$g_M(\vec{k}^2) = (\mu_p - \mu_n)g_V(\vec{k}^2)$,

where $(\mu_p - \mu_n) = 3.70$, $\quad \mu_p, \mu_n$ denote proton and neutron anomalous magnetic moment,

$g_A(\vec{k}^2) = g_A(0)/(1 + \vec{k^2}/\Lambda_A^2)^2$,

$g_P(\vec{k}^2) = [2m_p g_A(\vec{k}^2)/(\vec{k}^2 + m_\pi^2)](1 - m_\pi^2/\Lambda_A^2)$,

where $\Lambda_V = 0.85$ GeV, $\Lambda_A = 1.09$ GeV, and m_π is the mass of pion[1].

With the effective operator $\hat{O}$ [Eq. (B.1)], the corresponding amplitude of $(\beta\beta)_{0\nu}$-decay is given by (corresponding to light ν contribution only, refer to Chapter 3)

$$M = -2G_F^2(\bar{e}_L\gamma_\mu\nu_L)(-\bar{\nu_L^c}\gamma_\nu e_L^c)\times\int\int < f|J^\mu(x)J^\nu(y)|i > \exp(-iP_1x - iP_2y)d^4xd^4y, \quad \text{(B.3)}$$

where G_F is the Fermi coupling constant; P_1 and P_2 are the momentum of the emitted electrons; $J^\mu(x)$ is defined in Eq. (B.2); $|f>$ and $|i>$ are the final and initial nuclear states. Eq. (B.3) shows that the amplitude involves the Majorana mass term of neutrino: $\nu_L\bar{\nu_L^c}$ and it will lead to the effective neutrino mass $\langle m_\nu \rangle$.
In Eq. (B.3), $(\bar{e}_L\gamma_\mu\nu_L)(-\bar{\nu_L^c}\gamma_\nu e_L^c)$ yields the leptonic part $L_{\mu\nu}$,

$$\begin{aligned}
L_{\mu\nu} &= \int \frac{d^4k}{(2\pi)^4}[\overline{\frac{1-\gamma_5}{2}u(P_1)}]\gamma_\mu\sum_j\frac{U_{ej}^2m_j}{k^2-m_j^2}\frac{1-\gamma_5}{2}\gamma_\nu[\frac{1-\gamma_5}{2}v(P_2)]e^{ik(x-y)} \\
&= \int \frac{d^4k}{(2\pi)^4}\bar{u}(P_1)\gamma_\mu\sum_j\frac{U_{ej}^2m_j}{k^2-m_j^2}\frac{1-\gamma_5}{2}\gamma_\nu v(P_2)e^{ik(x-y)} \\
&= \bar{u}(P_1)\gamma_\mu\gamma_\nu\frac{1+\gamma_5}{2}v(P_2)\int\frac{d^3k}{(2\pi)^3}\sum_j\frac{U_{ej}^2m_j}{k^2-m_j^2}\exp(i\vec{k}\cdot(\vec{x}-\vec{y}))\int\frac{dk^0}{2\pi}\exp(ik_0(x_0-y_0)) \\
&= AB\int\frac{d^0k}{2\pi}\exp(ik_0(x_0-y_0))
\end{aligned}$$

$$\begin{aligned}
\text{where} \quad A &= \bar{u}(P_1)\gamma_\mu\gamma_\nu\frac{1+\gamma_5}{2}v(P_2) \\
&= \bar{u}(P_1)g_{\mu\nu}\frac{1+\gamma_5}{2}v(P_2) \\
B &= \int\frac{d^3\vec{k}}{(2\pi)^3}\sum_j\frac{U_{ej}^2m_j}{k^2-m_j^2}\exp(i\vec{k}\cdot(\vec{x}-\vec{y})) \\
&= \int\frac{d^3\vec{k}}{(2\pi)^3}\sum_j\frac{U_{ej}^2m_j}{k^2-m_j^2}e^{i\vec{k}\vec{r}}, \qquad \text{(B.4)}
\end{aligned}$$

where $\vec{r} = \vec{x} - \vec{y}$ is relative distance of the two nucleons. The value of r is related to the typical neutrino momentum

$$< \vec{k} > \sim \frac{1}{\vec{r}} \sim 100 \text{ MeV}.$$

On the other hand, in Eq. (B.3), $< f|J^\mu(x)J^\nu(y)|i >$ is the hadronic current. It is related to the nuclear matrix elements and phase space factor in the decay rate, and its value depends

[1]These form factors weaken the coupling for large transferred momentum (k), which means that the nucleons in the $(\beta\beta)_{0\nu}$-decay are not allowed for getting too close. If the exchange particle is light neutrino, the transferred momenta is much smaller than Λ_V, Λ_A, thus the form factors are approximated as constants in our calculation.

on the nuclear species.

Among all terms in the amplitude, the integral B is important for neutrino physics, which can be further rewritten as

$$\begin{aligned} B &= \sum_j U_{ej}^2 m_j \int_0^\infty \frac{d \mid \vec{k} \mid}{(2\pi)^3} 2\pi \frac{\vec{k}^2}{k^2 - m_j^2} \int_{-1}^{1} d(\cos\theta) \exp(i \mid \vec{k} \mid\mid \vec{r} \mid \cdot\cos\theta) \\ &= \sum_j U_{ej}^2 m_j \cdot \frac{1}{4\pi^2 r} \int_0^\infty d \mid \vec{k} \mid \frac{\mid \vec{k} \mid \sin(\mid \vec{k} \mid\mid \vec{r} \mid)}{k^2 - m_j^2} \end{aligned} \tag{B.5}$$

the denominator $k^2 - m_j^2 = k_0^2 - \vec{k}^2 - m_j^2$, where k_0 is the virtual neutrino energy, from the energy conservation,

$$\mid k_0 \mid = \mid < E > - E_i + E_e \mid .$$

Where $< E >$ is the average energy of the intermediate states between the initial and final nuclei in the decay; E_i is the energy of the initial nucleus, E_e is the energy of one of the emitted electrons. It is noteworthy that in $(\beta\beta)_{0\nu}$-decay, $\mid < E > - E_i + E_e \mid$ is expected to be much smaller than $\sqrt{\vec{k}^2 - m_j^2}$ [25, 209], which means $k_0^2 \ll \vec{k}^2 + m_j^2$, hence Eq. (B.5) can be further simplified as

$$\begin{aligned} B &= \sum_j U_{ej}^2 m_j \cdot \frac{1}{4\pi^2 r} \int_0^\infty d \mid \vec{k} \mid \frac{\mid \vec{k} \mid \sin(\mid \vec{k} \mid\mid \vec{r} \mid)}{\mid \vec{k} \mid^2 + m_j^2} \\ &= \sum_j U_{ej}^2 m_j \cdot \frac{1}{4\pi^2 r} \cdot \frac{\pi}{2} \exp(-m_j \mid \vec{r} \mid). \end{aligned} \tag{B.6}$$

If $(\beta\beta)_{0\nu}$-decay is induced by the active light neutrinos, all m_j are expected to be much smaller than the typical neutrino momentum, 100 MeV, which means that $m_j \ll \frac{1}{|\vec{r}|}$. Therefore the exponential in Eq. (B.6) just reduces to 1, and the only dependence of B on the neutrino mass m_j is only the term $\sum_j U_{ej}^2 m_j$. Thus, in the standard light ν exchange assumption, the amplitude of $(\beta\beta)_{0\nu}$-decay is

$$\begin{aligned} M \propto B = \sum_j U_{ej}^2 m_j \cdot \frac{1}{4\pi^2 r} \cdot \frac{\pi}{2}, \\ \text{Therefore } M \propto \sum_j U_{ej}^2 m_j = < m_\nu > . \end{aligned} \tag{B.7}$$

The Eq. (B.3) hence can be rewritten as

$$\begin{aligned}
M =& -2G_F^2 A \sum_j U_{ej}^2 m_j \cdot \frac{1}{8\pi r} \cdot \int \frac{d^0k}{2\pi} \exp(ik_0 r_0) \times \\
& \int\int < f|J^\mu(x)J^\nu(y)|i > \exp(-iP_1x - iP_2y) d^4x d^4y \\
\Gamma \propto M^2 =& 4G_F^4 A^2 | < m_\nu > |^2 \cdot \frac{1}{8\pi r} \cdot \int \frac{d^0k}{2\pi} \exp(ik_0 r_0) \times \\
& \int\int < f|J^\mu(x)J^\nu(y)|i > \exp(-iP_1x - iP_2y) d^4x d^4y \\
\text{where} \quad A^2 =& |\bar{u}(P_1) g_{\mu\nu} \frac{1+\gamma_5}{2} v(P_2)|^2 \\
=& \mathrm{Tr}(\not{P}_1 \frac{1+\gamma_5}{2} \not{P}_2 \frac{1+\gamma_5}{2}) \\
=& \mathrm{Tr}(\not{P}_1 (\frac{1+\gamma_5}{2})^2 \not{P}_2) = \mathrm{Tr}(\frac{\not{P}_1 \cdot \not{P}_2}{2}) = 2(P_1 \cdot P_2) \\
\therefore \Gamma \propto M^2 =& | < m_\nu > |^2 \cdot [8G_F^4 (P_1 \cdot P_2) \cdot \frac{1}{8\pi r} \cdot \int \frac{d^0k}{2\pi} \exp(ik_0 r_0) \times \\
& \int\int < f|J^\mu(x)J^\nu(y)|i > \exp(-iP_1x - iP_2y) d^4x d^4y].
\end{aligned}$$

The calculation of the terms in the middle bracket [ ] involves nuclear current and depends on the nuclear model. Since nuclear physics is outside the scope of this thesis, here we just show the last result of the decay rate as

$$\begin{aligned}
\Gamma &= G| < m_\nu > \cdot \frac{1}{m_e^2} M_\nu|^2 \\
&= G|\eta_\nu M_\nu|^2, \qquad \text{(B.8)}
\end{aligned}$$

where $\eta_\nu = | < m_\nu > /m_e|^2$, m_e is the mass of electron. G is the phase space factor and M_ν is the nuclear matrix element (NME). The last two terms are nuclear parameters and their values depend on the nuclei chosen for the experiments.

A more detailed calculation of the decay rate of $(\beta\beta)_{0\nu}$-decay can be referred to Refs. [26, 209] or Chapter 7 of Ref. [25]. However, these calculations are just for the light ν exchange. If the ν mass (or, m_j in the calculation above) is larger than 100 MeV, the approximations in these references are not applicable. $(\beta\beta)_{0\nu}$-decay would become a short-range process as the exchange particle is heavy (which means $\mid \vec{r} \mid$ in the calculation above would become smaller). In this case the nucleons cannot be seen as point-like and we have to consider the **finite nucleon size effect** [119]. This means that in the nucleon current, the form factors are not constants , but depend on the transferred momentum (as defined above).
Moreover, it is important that if the exchange particle is heavy ν, $m_j \gg |\vec{k}|$. Thus Eq. (B.6)

should be rewritten as

$$B \approx \sum_j U_{ej}^2 m_j \cdot \frac{1}{4\pi^2 r} \int_0^\infty d \mid \vec{k} \mid \frac{\mid \vec{k} \mid \sin(\mid \vec{k} \mid\mid \vec{r} \mid)}{m_j^2} \cdot \frac{1}{(1+k^2/\Lambda_A^2)^4},$$

(the last factor $\frac{1}{(1+k^2/\Lambda_A^2)^4}$ comes from the form factors and we assumed that $\Lambda_V \approx \Lambda_A \approx 0.85$ GeV)

$$\therefore M \propto B \propto (\sum_j V_{ej}^2 m_j) \cdot \frac{1}{m_j^2} = \sum_j (V_{ej}^L)^2 \frac{1}{m_j}, \tag{B.9}$$

which agrees with Eq. (3.2 b) in this thesis. More detail about the heavy neutrino mechanism can be referred to Refs. [118, 119].

Appendix C

Two Neutrino Double Beta Decay

Besides the neutrinoless mode, there is also another double beta decay mode, which is called $(\beta\beta)_{2\nu}$-decay:

$$(\mathrm{A,Z}) \rightarrow (\mathrm{A,Z+2}) + 2\ \mathrm{e}^- + 2\ \bar{\nu}_e.$$

This process is is allowed in Standard Model and has already been observed [45]. (Thus it is not of interest in this thesis.) It is included in the Appendix as a reference because it is parallel to neutrinoless mode both experimentally and theoretically. The measurements of $(\beta\beta)_{2\nu}$ decay rates are connected with experimental determinations of the nuclear matrix elements related to neutrinoless mode [131, 47]. Although the $(\beta\beta)_{2\nu}$ decay does not provide direct information on the nuclear matrix elements for the neutrinoless mode, it may serve as a diagnostic tool for the nuclear model and the adjustable parameters used to calculate the $(\beta\beta)_{0\nu}$-decay nuclear matrix elements. Thus this process is worthy of study. The corresponding diagram for this two neutrino process is shown in Fig. C.1.

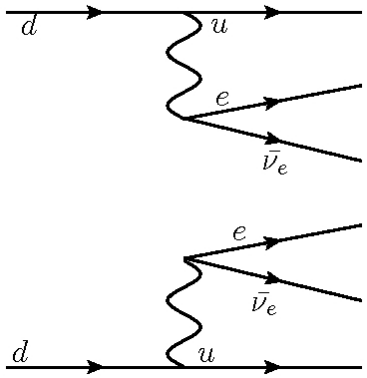

Figure C.1: The diagram of two neutrinos double beta decay

Similar to the neutrinoless double beta decay, the amplitude of the two neutrino mode is given by

$$M = -2G_F^2(\bar{e}_L\gamma_\mu\nu_L)(-\bar{\nu_L^c}\gamma_\nu e_L^c)\times\int\int < f|J^\mu(x)J^\nu(y)|i > \exp(-i(P_1+K_1)x-i(P_2+K_2)y)d^4xd^4y, \tag{C.1}$$

where the notation is basically the same as *Appendix B*, except K_1 and K_2 represent the 4-momenta of the two emitted anti-neutrinos. The detail of the calculation can be referred to Refs. [26, 25, 117]. The decay rate of this process can be written as

$$\Gamma_i = G_i^{2\nu}|M_i^{2\nu}|^2, \tag{C.2}$$

where i represents the nuclear species. $G^{2\nu}$ and $M^{2\nu}$ are the common phase space factor and nuclear matrix element, corresponding to the two neutrinos mode. Notice that the equation above does not involve any lepton number violating (LNV) parameters. Since this process is not suppressed by the LNV parameter, which is expected to be small for respecting the lepton symmetry, the corresponding decay rate is much larger than neutrinoless mode[1]. In reality, the various modes of double beta decay are separated by the differences in their electron sum energy spectrum. The electron sum energy spectra for the two neutrinos mode and the neutrinoless mode are shown in Fig. C.2 [210].

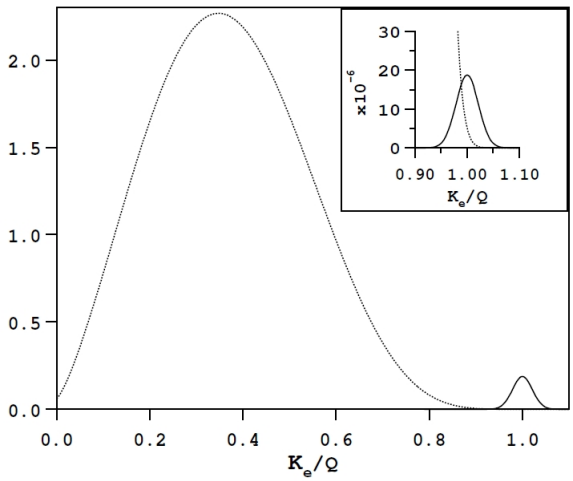

Figure C.2: The spectra of the sum of the electron kinetic energies K_e. Q corresponds to the value of the endpoint. Notice that the neutrinoless mode is normalized to 10^{-2} (10^{-6} in the figure inset). This figure shows that the decay rate of $(\beta\beta)_{0\nu}$-decay is expected to be much smaller than $(\beta\beta)_{2\nu}$-decay.

[1]Generally, the decay rate of two neutrinos mode is expected to be at least 1000 times larger than neutrinoless mode.

Notice that if the experimental resolution is poor, the $(\beta\beta)_{2\nu}$ tail in Fig C.2 would extend up to the $(\beta\beta)_{0\nu}$ peak region and become part of the background. Although the spectrum of $(\beta\beta)_{2\nu}$ is expected to has less effect near the endpoint energy Q. Since the decay rate of $(\beta\beta)_{2\nu}$ is much larger than $(\beta\beta)_{0\nu}$, high energy resolution is necessary to distinguish these two different modes in the experiments. Therefore $(\beta\beta)_{2\nu}$-decay is a potential background in the search of neutrinoless double beta decay. Observing $(\beta\beta)_{2\nu}$-decay not only contributes to constrain the nuclear models for evaluation of neutrinoless double beta decay, but also necessary for the background suppression in the search of the neutrinoless mode.

Appendix D

Pions In Flight Between The Two Interacting Nucleons In $(\beta\beta)_{0\nu}$-Decay

Chapter 4 mentioned that the pionic contribution to neutrinoless double beta decay could enhance the nuclear matrix elements (NMEs) of heavy neutrino exchange, and R-parity violation mechanism [160, 161, 121, 122]. Fig. 4.3 shows the 1 π mode and 2 π mode at the nucleon level. The diagrams in Fig. D.1 illustrate the 1 π processes at the quark level.

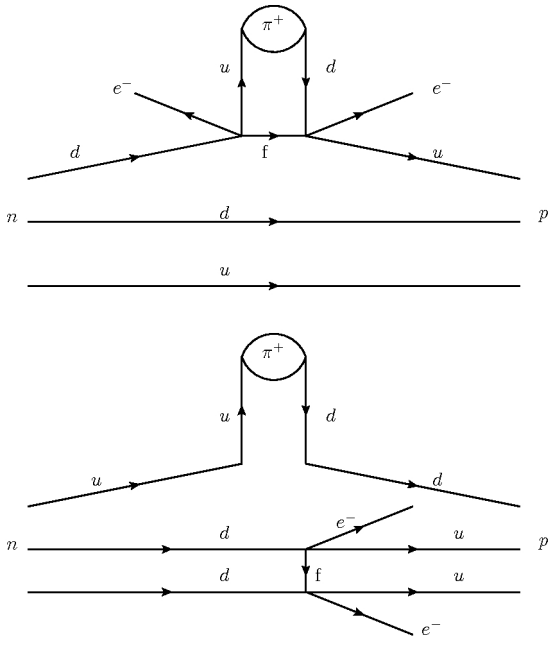

Figure D.1: Two possibilities of 1π exchange in the $(\beta\beta)_{0\nu}$-decay at quark level. In these two diagrams, f stands for a heavy fermion, it could be a heavy sterile neutrino, gluino or other SUSY particles.

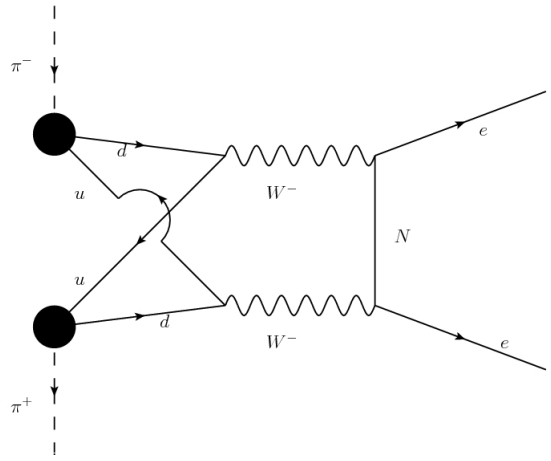

Figure D.2: The 2π exchange in the $(\beta\beta)_{0\nu}$-decay at quark level. Here only the exchange of heavy neutrinos is shown. The diagrams for R-parity violation mechanisms are similar, with intermediate gluinos or other SUSY particles.

Fig. D.1 and D.2 are important only when the intermediate particles are very massive. If the exchange particle is lighter than the pions (such as light active neutrinos and light sterile neutrinos), the charged pions exchange cannot dominate, and there would be no enhancement of the corresponding nuclear matrix element.

Exchanging the virtual mesons could enhance the amplitude of $(\beta\beta)_{0\nu}$-decay, because in this case, the quarks in the mesons (not the quarks in the nucleons) undergo the $\not{R}_p$ SUSY transition. This means that in the decay process, the two nucleons would not get too close and thus the process would not be suppressed by the 'nucleon repulsion'. Otherwise the finite nucleon size effect have to be taken into account and the corresponding NMEs will be suppressed by extra terms like $\dfrac{1}{[1-(q^2/\Lambda_A^2)]^2}$.

The exchanging virtual mesons are not necessarily pions, but other heavier mesons are expected to be suppressed by heavier masses. Therefore the pions exchange dominates the process.

Appendix E

Geometric Treatment Of The Near Detector

The geometry effect and the calculations of the near detector flux are described in detail in Ref. [172]. Here we just briefly introduce the geometric effect and the derivation of an effective near detector baseline ($L_{\text{eff}} = \sqrt{d(d+s)}$), which is part of the calculations in Ref. [172]

As shown in Fig. E.1, the length of the decay straight should not be neglected for the near detector measurements. This figure reveals that the actual baseline L is the distance between the production point and near detector, which means $d \leq L \leq d + s$. For the far detector, $L \approx d$, but this approximation is not suitable for the near detector.

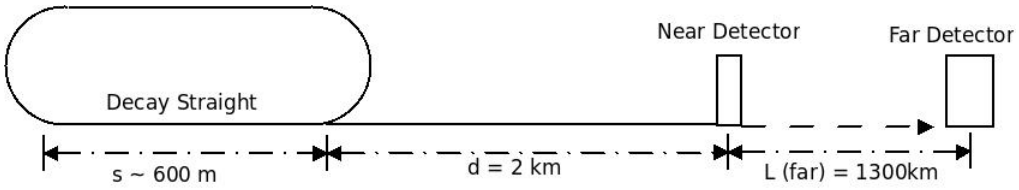

Figure E.1: Schematic layout of the muon storage ring, near and far detector in our simulation (not to scale).

Furthermore, if the near detector is very close to the decay straight, it should experience the beam divergence, which is not taken into account in the simulation of far detector. This means that the beam axis is not necessarily the same as the direction pointing towards the detector.

In the laboratory frame, the differential decay rates of an unpolarized muon, boosted along

the muon momentum vector, are given by the following expressions [211, 212]:

$$\frac{d^2\Gamma}{dE_{\nu_\mu}d\cos\theta} = \frac{G_F^2}{24\pi^3}E_\mu(1-\beta\cos\theta)E_{\nu_\mu}^2[3m_\mu - 4\frac{E_\mu}{m_\mu}E_{\nu_\mu}(1-\beta\cos\theta)], \tag{E.1}$$

$$\frac{d^2\Gamma}{dE_{\nu_e}d\cos\theta} = \frac{G_F^2}{4\pi^3}E_\mu(1-\beta\cos\theta)E_{\nu_e}^2[m_\mu - 2\frac{E_\mu}{m_\mu}E_{\nu_e}(1-\beta\cos\theta)], \tag{E.2}$$

where $\beta = \sqrt{1-m_\mu^2/E_\mu^2}$, m_μ is the muon rest mass. θ is the angle between the beam axis and the direction pointing towards the detector.

The number of neutrino events produced in the detector is related to the decay rates in the equations above, which is given by

$$\frac{dN}{dE} \propto \frac{1}{A_{\rm Det}}\int_0^{\theta_{\rm max}} \frac{d^2\Gamma}{dE_\nu d\cos\theta}\sin\theta d\theta, \tag{E.3}$$

where $\theta_{\rm max} \simeq r/L \ll 1$ (r is the detector radius, L is the distance between the production point and the near detector), $A_{\rm Det}$ is the area of the detector. For the sake of simplicity, we assume that $A_{\rm Det} = \pi r^2$. It is important to note that if the source of the Neutrino Factory can be considered as point-like, (i.e., $L \gg s$), the point-source approximation is applicable,

$$\frac{d^2\Gamma}{dE_\nu d\cos\theta}(\cos\theta) \simeq \frac{d^2\Gamma}{dE_\nu d\cos\theta}|_{\theta=0} \quad \text{which is independent of } \theta. \tag{E.4}$$

This means that

$$\begin{aligned}
\frac{dN}{dE}_{\rm point} &\propto \frac{1}{A_{\rm Det}}\int_0^{\theta_{\rm max}} \frac{d^2\Gamma}{dE_\nu d\cos\theta}|_{\theta=0}\sin\theta d\theta, \\
&= \frac{1}{\pi r^2}\frac{d^2\Gamma}{dE_\nu d\cos\theta}|_{\theta=0}\int_0^{\theta_{\rm max}}\sin\theta d\theta, \\
&= \frac{1}{\pi r^2}\frac{d^2\Gamma}{dE_\nu d\cos\theta}|_{\theta=0}(1-\cos\theta_{\rm max}), \\
&\simeq \frac{1}{\pi r^2}\frac{d^2\Gamma}{dE_\nu d\cos\theta}|_{\theta=0}\frac{1}{2}(\frac{r}{L})^2 \quad (\theta_{\rm max} \simeq r/L \ll 1), \\
&= \frac{1}{2\pi L^2}\frac{d^2\Gamma}{dE_\nu d\cos\theta}|_{\theta=0}.
\end{aligned} \tag{E.5}$$

This is also the number of events used in GLoBES. To show how the geometric effect affects the simulations in GLoBES, we rewrite the general result in Eq. (E.3) in terms of $\frac{dN}{dE}_{\rm point}$ [Eq. (E.5)],

$$\frac{dN}{dE} = \frac{dN}{dE}_{\rm point}(\frac{A_{\rm eff}}{A_{\rm Det}}), \tag{E.6}$$

$$\text{where } A_{\rm eff} = [2\pi L^2/(\frac{d^2\Gamma}{dE_\nu d\cos\theta}|_{\theta=0})]\int_0^{\theta_{\rm max}} \frac{d^2\Gamma}{dE_\nu d\cos\theta}\sin\theta d\theta, \tag{E.7}$$

$A_{\rm eff}$ is the effective surface area which takes into account the angular dependence of the neutrino flux. $A_{\rm eff}$ is not necessarily equal to $A_{\rm Det}$ if we consider the beam divergence. The ratio $A_{\rm eff}/A_{\rm Det}$ shows how much of the beam is captured compared to the on-axis flux. If the baseline (L) of the detector is large enough, $A_{\rm eff} \approx A_{\rm Det}$.

The previous calculations do not take the length of the decay straight (s) into account. Since $\frac{dN}{dE}$ depends on L ($d \leq L \leq d+s$), we should average over $\frac{dN}{dE}$,

$$\begin{aligned}\frac{dN}{dE}_{\rm avg} &= \frac{1}{s}\int_d^{d+s} \frac{dN}{dE} dL, \\ &= \frac{1}{s}\int_d^{d+s} \frac{dN}{dE}_{\rm point} (\frac{A_{\rm eff}}{A_{\rm Det}}),\end{aligned}$$

Eq. (E.5) shows that $\frac{dN}{dE}_{\rm point}(L) = 1/L^2 \times$ constant, thus the equation above can be rewritten as

$$\frac{dN}{dE}_{\rm avg} = \frac{dN}{dE}_{\rm point}(L_{\rm eff}, E)\frac{L_{\rm eff}^2}{s}\int_d^{d+s} \frac{1}{L^2}(\frac{A_{\rm eff}}{A_{\rm Det}}), \tag{E.8}$$

where $\frac{dN}{dE}_{\rm point}(L_{\rm eff}, E)\frac{L_{\rm eff}^2}{L^2} = \frac{dN}{dE}_{\rm point}(L)$.

$L_{\rm eff}$ is defined as the effective baseline. In the case that s is negligible, $\frac{dN}{dE}_{\rm avg} \approx \frac{dN}{dE}_{\rm point}(L_{\rm eff}, E)$. This means that $L_{\rm eff}$ should satisfy the following equation,

$$\begin{aligned}&\frac{L_{\rm eff}^2}{s}\int_d^{d+s} \frac{1}{L^2}(\frac{A_{\rm eff}}{A_{\rm Det}}) = 1, \\ &\frac{L_{\rm eff}^2}{s}\int_d^{d+s} \frac{1}{L^2}\cdot 1 = 1 \qquad (A_{\rm eff} = A_{\rm Det} \text{ when } s \text{ is negligible}), \\ &\therefore L_{\rm eff} = \sqrt{d(d+s)}\end{aligned} \tag{E.9}$$

The calculations in this appendix show that when the geometry effect is taken into account, the effective baseline $L_{\rm eff}$ and the ratio of $A_{\rm eff}/A_{\rm Det}$ are necessary for the simulation. However, in our simulation, we assumed that the near detector is located at 2 km far from the source. According to Ref. [172], it is safe to assume $A_{\rm eff}/A_{\rm Det} = 1$ at this distance. Therefore, in our simulation, we simply changed the baseline of near detector from L to $L_{\rm eff}$, which means that we input $\sqrt{2(2+0.6)} = 2.28$ km rather than 2 km in GLoBES.

Appendix F

Simulation Technique

In order to investigate the performance of future experiments, a simulation of their properties is necessary. All the simulations described in this thesis are done by a software package called General Long Baseline Experiment Simulator (GLoBES) [185, 186]. With the help of this program, a user can specify the information of the source and the detector in the 'experiment files': the flux and running time for the source description; the energy resolution, channels, mass, efficiency, background, etc. for the description of the detector [1]. In addition, the baseline and matter profile type should also be specified in the 'experiment files'. These information will be used by GLoBES to simulate the production, oscillation and detection process in an oscillation experiment. It must be noted that the default code of GLoBES could not describe the geometry effect, and consider the neutrino source and detection as point-like. To study the geometry and decoherence effects, the code has to be edited.

Before performing the simulation, the user must specify true values for all the oscillation parameters from which the oscillation probabilities are calculated. From these probabilities and the source information, the rates of all the specified channels are evaluated. These rates are called *true rates*. It is noteworthy that since the neutrino cannot be directly observed and only the secondary particles are detected in the experiments, the well-defined energy of the incident ν is interpreted as a distribution of possible energy range. This means that each true event is transformed by the detector properties which maps onto a reconstructed event. Finally, the measurement would read the *reconstructed rates* instead of the *true rates*.

Therefore, in order to derive the true values of the oscillation parameters from the *reconstructed rates*, GLoBES performs a statistical parameter estimation test where users define how many parameters and in which range the parameters are to be constrained. The corre-

[1] In our simulations, we simply used the default cross-section files that come with the GLoBES package, but users can use the user-defined cross-section files as well.

sponding chi-squared (χ^2) will be minimised with respect to certain oscillation parameters[2]. In the simulation of neutrino factory, the total χ^2 should be given by [172]

$$\chi^2 = \min_{a_i} \sum_{D,C} \chi^2_{D,C}(\text{oscillation parameters}, a_i) + \chi^2_{\text{Pull}}(a_i), \tag{F.1}$$

where $\chi^2_{D,C}$ correspond to the χ^2 for different detectors (D) and channels (C) and should be Poissonian,

$$\chi^2_{D,C}(\text{oscillation parameters}, a_i) = \sum_{j}^{\text{bins}} 2[T^j_{D,C} - O^j_{D,C} + O^j_{D,C} \cdot \ln(\frac{O^j_{D,C}}{T^j_{D,C}})], \tag{F.2}$$

where the values of $T^j_{D,C}$ and $O^j_{D,C}$ depend on the oscillation parameters and a_i. a_i are the the nuisance parameters, which are varied in the minimization process and describe the dependence of the event rates on the various sources of systematical errors. On the other hand, $\chi^2_{\text{Pull}}(a_i)$ is given by

$$\chi^2_{\text{Pull}}(a_i) = \sum_i (\frac{a_i^2}{\sigma^2_{a_i}}). \tag{F.3}$$

$\sigma^2_{a_i}$ correspond to different systematical errors which are considered in the simulation. More details of the systematic and statistical treatment can be referred to the user-manual of GLoBES [213].

[2]Ideally, a minimisation should be performed over all parameters except those which are being constrained. However, it would be very time-consuming to perform such a complicated multi-parameter minimisation, especially in the sterile oscillation there are so many oscillation parameters. Thus in our work, the minimisations were performed only over the most relevant parameters.

List of Figures

Bibliography

[1] Y.Fukuda et al. Evidence for oscillation of atmospheric neutrinos. *Phys.Rev.Lett*, 81:1562–1567, 1998, arXiv:hep-ex/9807003.

[2] Y.Fukuda et al. Solar neutrino data covering solar cycle 22. *Phys.Rev.Lett*, 77:1683–1686, 1996.

[3] R.Becker-Szendy et al. Search for muon neutrino oscillations with the irvine-michigan-brookhaven detector. *Phys.Rev.Lett*, 69:1010–1013, 1992.

[4] M.Sanchez et al. Measurement of the l/e distributions of atmospheric ν in soudan 2 and their interpretation as neutrino oscillations. *Phys.Rev.D*, 68(113004), 2003, arXiv:hep-ex/0307069.

[5] B.T.Cleveland et al. Measurement of the solar electron neutrino flux with the homestake chlorine detector. *Astrophys.J*, 496:505–526, 1998.

[6] J.N.Abdurashitov et al. Measurement of the solar neutrino capture rate by the russian-american gallium solar neutrino experiment during one half of the 22-year cycle of solar activity. *J.Exp.Theor.Phys*, 95:181–193, 2002, astro-ph/0204245.

[7] W.Hampel et al. GALLEX solar neutrino observations: results for GALLEX IV. *Phys.Lett.B*, 447:127–133, 1999.

[8] S.Ahmed et al. Measurement of the total active 8b solar neutrino flux at the sudbury neutrino observatory with enhanced neutral current sensitivity. *Phys.Rev.Lett*, 92(181301), 2004, arXiv:nucl-ex/0309004.

[9] B.Pontecorvo. Mesonium and antimesonium. *Sov.Phys. JETP*, 6:429, 1957.

[10] C.Athanassopoulos et al. [LSND Collaboration]. Evidence for $\bar{\nu_\mu} \to \bar{\nu_e}$ oscillations from the lsnd experiment at the los alamos meson physics facility. *Phys.Rev.Lett.*, 77:3082, 1996.

[11] A.Aguilar et al. [LSND Collaboration]. Evidence for neutrino oscillations from the observation of $\bar{\nu_e}$ appearance in a $\bar{\nu_\mu}$ beam. *Phys.Rev.D*, 64(112007), 2001.

[12] D.G. Charlton. Lep, slc and the standard model. arXiv:hep-ex/0211003.

[13] M.Nakagawa Z.Maki and S.Sakata. Remarks on the unified model of elementary particles. *Prog.Theor.Phys.*, 28:870–880, 1962.

[14] A.Marrone D.Montanino A.Palazzo G.L.Fogli, E.Lisi and A.M.Rotunno. Global analysis of neutrino masses, mixings and phases: entering the era of leptonic cp violation searches. arXiv:1205.5254.

[15] E.P.An et al. Observation of electron-antineutrino disappearance at daya bay. arXiv:1203.1669.

[16] R.N.Mohapatra et al. Theory of neutrinos. arXiv:hep-ph/0412099.

[17] M.Khabibullin. Latest oscillation results from T2K. arXiv:1111.0183.

[18] P.Adamson et al. [MINOS Collaboration]. Improved search for muon-neutrino to electron-neutrino oscillations in MINOS. arXiv:1108.0015 [hep-ex].

[19] [RENO Collaboration] J.K.Ahn et al. Reno: An experiment for neutrino oscillation parameter θ_{13} using reactor neutrinos at yonggwang. 2010, arXiv:1003.1391.

[20] H.Minakata. If theta(13) is large, then what? arXiv:1110.4237.

[21] W.Grimus and L.Lavoura. Models of maximal atmospheric neutrino mixing. arXiv:hep-ph/0310050.

[22] S.Choubey. Probing the neutrino mass matrix in next generation neutrino oscillation experiments. arXiv:hep-ph/0509217.

[23] M.Ratz D.Wright K.Dick, M.Lindner. Leptogenesis with dirac neutrinos. *Phys.Rev.Lett*, 84:4039–4042, 2000.

[24] J.Schechter and J.W.F.Valle. Neutrinoless double beta decay in $SU(2)U(1)$ theories. *Phys.Rev.D*, 25:2951, 1982.

[25] T.Yanagida M.Fukugita. Physics of Neutrinos and Application of Astrophysics. *(text book)*, 2003.

[26] T.Kotani M.Doi and E.Takasugi. Double beta decay and majorana neutrino. *Prog.Theor.Phys.Suppl.*, 83:1, 1985.

[27] M.Sorel P.Ferrario F.Monrabal J.Munoz-Vidal P.Novella A.Poves J.J.Gomez-Cadenas, J.Martin-Albo. Sense and sensitivity of double beta decay experiments. arXiv:1010.5112.

[28] I.Abt et al. A new 76ge double beta decay experiment at lngs. arXiv:hep-ex/0404039.

[29] M. Barnab Heider et al. Operation of a gerda phase i prototype detector in liquid argon and nitrogen. arXiv:0812.3976.

[30] F.Alessandria et al. Sensitivity of cuore to neutrinoless double-beta decay. arXiv:1109.0494.

[31] on behalf of the CUORE collaboration Monica Sisti. From cuoricino to cuore: Investigating neutrino properties with double beta decay. *J.Phys.Conf.Ser.*, 203:012069, 2010.

[32] The Majorana collaboration. White paper on the majorana zero-neutrino double-beta decay experiment. arXiv:nucl-ex/0311013.

[33] S. Elliott et al. The majorana project. *J.Phys.Conf.Ser.*, 173:012007, 2009.

[34] Yu.A. Shitov et al. NEMO/SuperNEMO Collaboration. A search for neutrinoless double beta decay: from NEMO-3 to SuperNEMO. arXiv:1006.4775.

[35] R.Arnold et al. Probing new physics models of neutrinoless double beta decay with SuperNEMO. arXiv:1005.1241.

[36] A.Dolgolenko G.Giannini G.Gratta P.Picchi A.Piepke F.Pietropaolo-P.Vogel J-L.Vuilleumier Y-F.Wang O.Zeldovich M.Danilov, R.DeVoe. Detection of very small neutrino masses in double-beta decay using laser tagging. *Phys.Lett.*, B480:12, 2000.

[37] Nicole Ackerman on behalf of the EXO Collaboration. Status of exo-200. arXiv:0909.1826.

[38] P.B.Pal R.N.Mohapatra. Massive Neutrinos in Physics and Astrophysics. *(text book)*, 2004.

[39] R.N.Mohapatra and G.Senjanovic. Neutrino mass and spontaneous parity nonconservation. *Phys.Rev.Lett*, 44:912, 1980.

[40] T.Yanagida. *Proc. Workshop on the Unified Theory and Baryon Number in the Universe*, (KEK report 79-18):95, 1979.

[41] W.Konetschny and W.Kummer. Nonconservation of total lepton number with scalar bosons. *Phys.Lett.B*, 70:433, 1977.

[42] T.P.Cheng and L-F.Li. Neutrino masses, mixings, and oscillations in SU(2)U(1) models of electroweak interactions. *Phys.Rev.D*, 22:2860, 1980.

[43] X.G.He R.Foot, H.Lew and G.C.Joshi. See-saw neutrino masses induced by a triplet of leptons. *Z.Phys.C*, 44:441, 1989.

[44] E.Ma. Pathways to naturally small neutrino masses. *Phys.Rev.Lett*, 81:1171, 1998, arXiv:hep-ph/9805219.

[45] A.S.Barabash. Double beta decay: present status. *Phys.Atom.Nucl.*, 73, 162-178, arXiv:0807.2948.

[46] M. Auger et al. Search for Neutrinoless Double-Beta Decay in ^{136}Xe with EXO-200. 2012, arXiv:1205.5608.

[47] V.A.Rodin P.Vogel F.Simkovic, A.Faessler and J.Engel. Anatomy of nuclear matrix elements for neutrinoless double-beta decay. *Phys.Rev.C*, 77:045503, 2008.

[48] H.V.Klapdor-Kleingrothaus et al. Search for neutrinoless double beta decay with enriched 76ge in gran sasso 19902003. *Phys.Lett.B*, 586:198, 2004.

[49] A.M. Bakalyarov et al. Results of the experiment on investigation of Germanium-76 double beta decay. experimental data of Heidelberg-Moscow collaboration November 1995 - August 2001. 2005.

[50] F.Vissani A.Strumia. Implications of neutrino data circa 2005. *Nucl.Phys.B*, 726:294–316, 2005.

[51] M.Altmann et al. GNO solar neutrino observations: results for GNO I. *Phys.Lett.B*, 490:16–26, 2000, hep-ex/0006034.

[52] D.G.Michael et al. MINOS Collaboration. Observation of muon neutrino disappearance with the minos detectors in the numi neutrino beam. *Phys.Rev.Lett*, 97(191801), 2006, arXiv:hep-ex/0607088.

[53] F.Ardellier et al. Letter of intent for double-chooz: a search for the mixing angle theta13. 2004, arXiv:hep-ex/0405032.

[54] W.Wang for DayaBay collaboration. The hunt for theta13 at the daya bay nuclear power plant. 2009, arXiv:0910.4605.

[55] K.Eguchi et al. First results from kamland: Evidence for reactor anti-neutrino disappearance. *Phys.Rev.Lett.*, 90:021802, 2003, arXiv:hep-ex/0212021.

[56] S.Pascoli S.Geer, O.Mena. Low energy neutrino factory for large θ_{13}. *Phys.Rev.D*, 75(093001), 2007.

[57] S.Geer O.Mena S.Pascoli A.Bross, M.Ellis. Neutrino factory for both large and small θ_{13}. *Phys.Rev.D*, 77(093012), 2008.

[58] M.Ellis E.F.Martinez T.Li S.Pascoli A.Bross, S.Geer and O.Mena. The multi-channel low energy neutrino factory. arXiv:0911.3776.

[59] A.D.Bross J.H.Cobb, C.D.Tunnell. Sensitivity to ev-scale neutrinos of experiments at a very low energy neutrino factory. 2011.

[60] T.Kobayashi A.Marchionni A.Meregaglia T.Maruyama K.Nishikawa A.Rubbia A.Badertscher, T.Hasegawa. A possible future long baseline neutrino and nucleon decay experiment with a 100 kton liquid argon tpc at okinoshima using the j-parc neutrino facility. arXiv:0804.2111.

[61] T.Abe et al. Detectors and flux instrumentation for future neutrino facilities. arXiv:0712.4129.

[62] P. Kyberd et al. nuSTORM - Neutrinos from STORed Muons: Letter of Intent to the Fermilab Physics Advisory Committee. 2012, arXiv:1206.0294.

[63] Th.Lasserre Th.A.Mueller D.Lhuillier M.Cribier G.Mention, M.Fechner and A.Letourneau. The reactor antineutrino anomaly. *Phys.Rev.D*, 83(073006), 2011, arXiv:1101.2755.

[64] Carlo Giunti. Phenomenology of Sterile Neutrinos. 2011, arXiv:1110.3914.

[65] A.A.Aguilar-Arevalo et al. [MiniBooNE Collaboration]. Search for electron neutrino appearance at the $\delta m^2 \sim 1ev^2$ scale. *Phys.Rev.Lett.*, 98(231801), 2007.

[66] M.Maltoni and T.Schwetz. Sterile neutrino oscillations after first Miniboone results. arXiv:0705.0107.

[67] K.N. Abazajian, M.A. Acero, S.K. Agarwalla, A.A. Aguilar-Arevalo, C.H. Albright, et al. Light Sterile Neutrinos: A White Paper. 2012, arXiv:1204.5379.

[68] M.Laveder C.Giunti. 3+1 and 3+2 sterile neutrino fits. arXiv:1107.1452.

[69] M.Shaposhnikov T.Asaka. The msm, dark matter and baryon asymmetry of the universe. arXiv:hep-ph/0505013.

[70] R.E.Shrock. New tests for and bounds on neutrino masses and lepton mixing. *Phys.Lett.B*, 96:159, 1980.

[71] S.Pascoli B.Zhang A.Atre, T.Han. The search for heavy majorana neutrinos. *JHEP*, 0905:030, 2009, [arXiv:0901.3589].

[72] Amitava Datta and Apostolos Pilaftsis. Revealing the Majorana nature of heavy neutrinos via a heavy Higgs boson. *Phys.Lett.*, B278:162–166, 1992.

[73] R.E. Shrock. New tests for and bounds on neutrino masses and lepton mixing. *Phys.Lett.B*, 96:159, 1980.

[74] D. I. Britton, S. Ahmad, D. A. Bryman, R. A. Burnham, E. T. H. Clifford, P. Kitching, Y. Kuno, J. A. Macdonald, T. Numao, A. Olin, J. M. Poutissou, and M. S. Dixit. Improved search for massive neutrinos in $\pi^+ \to e^+\nu$ decay. *Phys. Rev. D*, 46:R885–R887, Aug 1992.

[75] T. Yamazaki, T. Ishikawa, Y. Akiba, M. Iwasaki, K.H. Tanaka, et al. Search for Heavy Neutrinos in Kaon Decay. *Conf.Proc.*, C840719:262, 1984.

[76] F. Bergsma et al. [CHARM collaboration]. A search for decays of heavy neutrinos in the mass range 0.5 gev to 2.8 gev. *Phys.Lett.B*, 166:473, 1986.

[77] G. Bernardi, G. Carugno, J. Chauveau, F. Dicarlo, M. Dris, et al. Further limits on heavy neutrino couplings. *Phys.Lett.*, B203:332, 1988.

[78] J. Badier et al. MASS AND LIFETIME LIMITS ON NEW LONGLIVED PARTICLES IN 300-GeV/c pi- INTERACTIONS. *Z.Phys.*, C31:21, 1986.

[79] P. Abreu et al. [DELPHI collaboration]. Search for neutral heavy leptons produced in z decays. *Z.Phys.C*, 74:57, 1997.

[80] O. Adriani et al. [L3 collaboration]. Search for isosinglet neutral heavy leptons in z_0 decays. *Phys.Lett.B*, 295:371, 1992.

[81] Shaouly Bar-Shalom, Gad Eilam, Tao Han, and Amarjit Soni. Charged Higgs Boson Effects in the Production and Decay of a Heavy Majorana Neutrino at the CERN LHC. *Phys.Rev.*, D77:115019, 2008, arXiv:0803.2835.

[82] A. Pilaftsis. Heavy neutrino effects on tau lepton decays. *Mod.Phys.Lett.*, A9:3595–3604, 1994, arXiv:hep-ph/9410412.

[83] S.N. Gninenko. Constraints on sub-GeV hidden sector gauge bosons from a search for heavy neutrino decays. *Phys.Lett.*, B713:244–248, 2012, arXiv:1204.3583.

[84] F.Vissani M.Mitra, G.Senjanovic. Neutrinoless double beta decay and heavy sterile neutrinos. arXiv:1108.0004.

[85] Z.Xing and S.Zhou. Multiple seesaw mechanisms of neutrino masses at the tev scale. 2009, arXiv:0906.1757.

[86] Z.Lu S.Kovalenko and I.Schmidt. Lepton number violating processes mediated by majorana neutrinos at hadron colliders. 2009, arXiv:0907.2533.

[87] J.A.Aguilar-Saavedra F.del Aguila. Electroweak scale seesaw and heavy dirac neutrino signals at lhc. 2009, arXiv:0809.2096.

[88] Joern Kersten and Alexei Yu. Smirnov. Right-Handed Neutrinos at CERN LHC and the Mechanism of Neutrino Mass Generation. *Phys.Rev.*, D76:073005, 2007, arXiv:0705.3221.

[89] Abdesslam Arhrib, Borut Bajc, Dilip Kumar Ghosh, Tao Han, Gui-Yu Huang, et al. Collider Signatures for Heavy Lepton Triplet in Type I+III Seesaw. *Phys.Rev.*, D82:053004, 2010, arXiv:0904.2390.

[90] C.S.Kim S.K.Kang. Extended double seesaw model for neutrino mass spectrum and low scale leptogenesis. *Phys.Lett*, B646:248, 2007.

[91] R.Pittau F.del Aguila, J.A.Aguilar-Saavedra. Heavy neutrino signals at large hadron colliders. *JHEP*, 0710:047, 2007, arXiv:hep-ph/0703261.

[92] O.Kittel J.A.Aguilar-Saavedra, F.Deppisch and J.W.F.Valle. Flavour in heavy neutrino searches at the lhc. arXiv:1203.5998.

[93] M.G. Haehnelt S. Matarrese-A. Riotto M. Viel, J. Lesgourgues. Constraining warm dark matter candidates including sterile neutrinos and light gravitinos with WMAP and the Lyman-α forest. *Phys.Rev.D*, 71(063534), 2005.

[94] George M. Fuller, Alexander Kusenko, and Kalliopi Petraki. Heavy sterile neutrinos and supernova explosions. *Phys.Lett.*, B670:281–284, 2009, arXiv:0806.4273.

[95] A.D. Dolgov. Neutrinos in cosmology. *Phys.Rept.*, 370:333–535, 2002, arXiv:hep-ph/0202122.

[96] T.Hambye S.Palomares-Ruiz C.Boehm, Y.Farzan and S.Pascoli. Are small neutrino masses unveiling the missing mass problem of the universe? arXiv:hep-ph/0612228.

[97] Matteo Viel, Julien Lesgourgues, Martin G. Haehnelt, Sabino Matarrese, and Antonio Riotto. Can sterile neutrinos be ruled out as warm dark matter candidates? *Phys.Rev.Lett.*, 97:071301, 2006, arXiv:astro-ph/0605706.

[98] Y.F.Li and Z.Xing. Neutrinos as hot or warm dark matter. arXiv:1110.2293.

[99] J.Gluza and M.Zralek. Physics of heavy neutrinos. *Acta Phys.Polon.B*, 27:1557–1568, 1996, arXiv:hep-ph/9605354.

[100] S.H.Hansen. Heavy sterile neutrinos - what they can be and what they can't. arXiv:astro-ph/0011526.

[101] A.Strumia. Interpreting the lsnd anomaly: sterile neutrinos or cpt-violation or...? arXiv:hep-ph/0201134.

[102] M.A.Tortola-J.W.F.Valle M. Maltoni, T.Schwetz. Status of global fits to neutrino oscillations. arXiv:hep-ph/0405172.

[103] Y.Declais et al. Study of reactor antineutrino interaction with proton at bugey nuclear power plant. *Phys. Lett. B*, 338:383, 1994.

[104] M.Apollonio et al. Limits on neutrino oscillations from the chooz experiment. *Phys. Lett. B*, 466:415, 1999.

[105] F. Dydak, G.J. Feldman, C. Guyot, J.P. Merlo, H.J. Meyer, et al. A Search for Muon-neutrino Oscillations in the Delta m**2 Range 0.3-eV**2 to 90-eV**2. *Phys.Lett.*, B134:281, 1984.

[106] B. Armbruster et al. Upper limits for neutrino oscillations muon-anti-neutrino to electron-anti-neutrino from muon decay at rest. *Phys.Rev.*, D65:112001, 2002, arXiv:hep-ex/0203021.

[107] P. Astier et al. Search for $\nu_\mu \to \nu_e$ oscillations in the NOMAD experiment. *Phys.Lett.*, B570:19–31, 2003, arXiv:hep-ex/0306037.

[108] Michel Sorel, Janet M. Conrad, and Michael Shaevitz. A Combined analysis of short baseline neutrino experiments in the (3+1) and (3+2) sterile neutrino oscillation hypotheses. *Phys.Rev.*, D70:073004, 2004, arXiv:hep-ph/0305255.

[109] A.A.Aguilar-Arevalo et. al. [MiniBooNE Collaboration]. arXiv:1007.1150.

[110] T.Schwetz E.Akhmedov. Event excess in the miniboone search for $\bar{\nu_\mu} \to \bar{\nu_e}$ oscillations. *JHEP*, 1010:115, 2010, arXiv:1007.4171.

[111] A.A. Aguilar-Arevalo et al. A Combined $\nu_\mu \to \nu_e$ and $\bar{\nu}_\mu \to \bar{\nu}_e$ Oscillation Analysis of the MiniBooNE Excesses. 2012, arXiv:1207.4809.

[112] R.R.Volkas. Introduction to sterile neutrinos. *Progress in Particle and Nuclear Physics*, 48:161–174, 2002.

[113] R.N.Mohapatra Z.Berezhiani. Reconciling present neutrino puzzles: Sterile neutrinos as mirror neutrinos. *Phys.Rev.D*, 52:6607, 1995.

[114] R.N.Mohapatra. Connecting bimaximal neutrino mixing to a light sterile neutrino. *Phys.Rev.D*, 64(091301), 2001.

[115] U.Sarkar. Importance of neutrinoless double beta decay. arXiv:0712.2690.

[116] J.Suhonena O.Civitarese. Light-neutrino mass spectrum, nuclear matrix elements, and the observability of neutrinoless double beta decay. *Nucl.Phys.A*, 729:867, 2003.

[117] A.Faessler and F.Simkovic. Double beta decay. *J.Phys.G*, 24:2139, 1998.

[118] J.D.Vergados F.Simkovic, G.Pantis and A.Faessler. Additional nucleon current contributions to neutrinoless double beta decay. *Phys.Rev.C*, 60(055502), 1999.

[119] J.D.Vergados. A limit on the neutrino masses from double beta decay. *Physics Letters*, 109B:96, 1982.

[120] S.G.Kovalenko M.Hirsch, H.V.Klapdor-Kleingrothaus. Supersymmetry and neutrinoless double beta decay. *Phys. Rev. D*, 53:13291348, 1996.

[121] F.Simkovic A.Faessler, S.Kovalenko and J.Schweiger. Dominance of pion exchange in r-parity-violating supersymmetric contributions to neutrinoless double beta decay. *Phys.Rev.Lett.*, 78:183, 1997.

[122] S.Kovalenko A.Faessler, T.Gutsche and F.Simkovic. Pion dominance in RPV SUSY induced neutrinoless double beta decay. arXiv:0710.3199.

[123] E.Bender K.Muto and H.V.Klapdor. Nuclear structure effects on the neutrinoless double beta decay. *Z.Phys.A*, 334:187, 1989.

[124] H.Pas G.Bhattacharyya, H.V.Klapdor-Kleingrothaus and A.Pilaftsis. Neutrinoless double beta decay from singlet neutrinos in extra dimensions. arXiv:hep-ph/0212169.

[125] A.V.Borisov A.Ali and D.V.Zhuridov. Neutrinoless double beta decay: Electron angular correlation as a probe of new physics. arXiv:hep-ph/0606072.

[126] S.R.Elliott V.M.Gehman. Multiple-isotope comparison for determining neutrinoless double-beta decay mechanisms. arXiv:hep-ph/0701099.

[127] E.Lisi G.L.Fogli and A.M.Rotunno. Probing particle and nuclear physics models of neutrinoless double beta decay with different nuclei. arXiv:0905.1832.

[128] E.Lisi A.M.Rotunno F.Simkovic A.Faessler, G.L.Fogli. Multi-isotope degeneracy of neutrinoless double beta decay mechanisms in the quasi-particle random phase approximation. arXiv:1103.2504.

[129] S.P.Matrin M.Drees. Implications of SUSY model building. arXiv:hep-ph/9504324.

[130] S.Kovalenko A.Faessler and F.Simkovic. Pions in nuclei and manifestations of supersymmetry in neutrinoless double beta decay. *Phys.Rev.D*, 58(115004), 1998.

[131] A.Faessler V.A.Rodin, F.Simkovic and P.Vogel. Assessment of uncertainties in qrpa neutrinoless double beta decay nuclear matrix elements. *Nuclear Physics A*, 766:107–131, 2006.

[132] A.Faessler V.A.Rodin, F.Simkovic and P.Vogel. Uncertainty in the neutrinoless double-beta decay nuclear matrix elements. *Phys.Rev.C*, 68(044302), 2003.

[133] S.T.Petcov A.Ibarra, E.Molinaro. Tev scale see-saw mechanisms of neutrino mass generation, the majorana nature of the heavy singlet neutrinos and $\beta\beta$-decay. arXiv:1007.2378.

[134] Miha Nemevsek, Fabrizio Nesti, Goran Senjanovic, and Vladimir Tello. Neutrinoless Double Beta Decay: Low Left-Right Symmetry Scale? 2011, arXiv:1112.3061.

[135] E.Komatsu et al. Seven-year wilkinson microwave anisotropy probe (wmap) observations: Cosmological interpretation. arXiv:1001.4538.

[136] J.Lopez-Pavon J Menendez M.Blennow, E.Fernandez-Martinez. Neutrinoless double beta decay in seesaw models. arXiv:1005.3240.

[137] D.P.George M.Duerr and K.L.McDonald. Neutrino mass and $\mu \to e + \gamma$ from a mini-seesaw. arXiv:1105.0593.

[138] S.Kovalenko A.Faessler. arXiv:hep-ph/9712535.

[139] J.W.F.Valle R.N.Mohapatra. Neutrino mass and baryon-number nonconservation in superstring models. *Phys.Rev.D*, 34:1642–1645, 1986.

[140] D.Hernandez P.Hernandez M.B.Gavela, T.Hambye. Minimal flavour seesaw models. *JHEP*, 0909:038, 2009, arXiv:0906.1461.

[141] A.Zee. A theory of lepton number violation and neutrino majorana masses. *Phys.Lett.*, B93:389, 1980.

[142] W.Grimus and H.Neufeld. Radiative neutrino masses in an $SU(2) \times U(1)$ model. *Nucl.Phys*, B325:18, 1989.

[143] Carlos E. Yaguna D. Aristizabal Sierra. On the importance of the 1-loop finite corrections to seesaw neutrino masses. arXiv:1106.3587.

[144] L.Lavoura W.Grimus. One-loop corrections to the seesaw mechanism in the multi-higgs-doublet standard model. *Phys.Lett.B*, 546:86–95, 2002.

[145] A.Pilaftsis. Radiatively induced neutrino masses and large higgs-neutrino couplings in the standard model with majorana fields. *Z.Phys.C*, 55:275–282, 1992.

[146] C.Wong S.Pascoli, J.Lopez-Pavon. in preparation.

[147] B.C.Allanach and C.H.Kom. Bilinear r-parity violation in neutrinoless double beta decay. arXiv:0712.0852.

[148] S.Grab H.K.Dreiner, M.Hanussek. Bounds on R-parity violating couplings at the grand unification scale from neutrino masses. arXiv:1005.3309.

[149] W.A.Kaminski M.Gozdz and F.Simkovic. Neutrino mass in gut constrained supersymmetry with R-parity violation in light of neutrino oscillations. *PhysRevD*, 70(095005), arXiv:hep-ph/0412171.

[150] F.Simkovic A.Wodecki, W.A.Kaminski. Grand unified theory constrained supersymmetry and neutrinoless double beta decay. *Phys.Rev.D*, 60(115007), 1999.

[151] R.Barbier et al. R-parity-violating supersymmetry. *Physics Reports*, 420:1–195, 2005.

[152] S.T.Petcov A.Halprin and S.P.Rosen. Effects of light and heavy majorana neutrinos in neutrinoless double beta decay. *Phys.lett*, 125B:335–338, 1983.

[153] E.Otten. *Hyperfine Interactions*, 196:Issue 1, 3 – 23, 2010.

[154] F.M.Frankle. Katrin: an experiment to determine the neutrino mass. arXiv:1110.0087.

[155] Osvaldo Civitarese Jouni Suhonena. Weak-interaction and nuclear-structure aspects of nuclear double beta decay. *Phys.Rep*, 300:123, 1998.

[156] P.Vogel. Nuclear physics aspects of double beta decay. arXiv:0807.2457.

[157] E. Caurier F. Nowacki J. Menndez, A. Poves. Disassembling the nuclear matrix elements of the neutrinoless double beta decay. arXiv:0801.3760.

[158] G. Pantis, F. Šimkovic, J. D. Vergados, and Amand Faessler. Neutrinoless double beta decay within the quasiparticle random-phase approximation with proton-neutron pairing. *Phys. Rev. C*, 53:695–707, Feb 1996.

[159] E.Lisi V.Rodin A.M.Rotunno F.Simkovic A.Faessler, G.L.Fogli. Quasiparticle random phase approximation uncertainties and their correlations in the analysis of neutrinoless double beta decay. arXiv:0810.5733.

[160] J.D.Vergados. The neutrinoless double beta decay from a modern perspective. *Physics Reports*, 361:1–56, 2002.

[161] A.Faessler J.D.Vergados and H.Toki. Pionic contribution to neutrinoless double beta decay. 2009.

[162] S.T.Petcov S.Pascoli and T.Schwetz. The absolute neutrino mass scale, neutrino mass spectrum, majorana cp-violation and neutrinoless double-beta decay. arXiv:hep-ph/0505226.

[163] S.Pascoli and S.T.Petcov. Majorana neutrinos, neutrino mass spectrum and the $\langle m \rangle \sim$ 0.001 ev frontier in neutrinoless double beta decay. *Phys.Rev.D*, 77(113003), 2008, arXiv:0711.4993.

[164] A.Marrone A.Palazzo G.L.Fogli, E.Lisi and A.M.Rotunno. Evidence of $\theta_{13} > 0$ from global neutrino data analysis. arXiv:1106.6028.

[165] M.Laveder C.Giunti. Short-baseline electron neutrino disappearance, tritium beta decay, and neutrinoless double-beta decay. *Phys.Rev.D*, 82(053005), 2010.

[166] W.Winter D.Meloni, J.Tang. Sterile neutrinos beyond lsnd at the neutrino factory. arXiv:1007.2419.

[167] D.Hernandez and A.Yu.Smirnov. Active to sterile neutrino oscillations: Coherence and MINOS results. arXiv:1105.5946.

[168] A.Dighe and S.Ray. Signatures of heavy sterile neutrinos at long baseline experiments. arXiv:0709.0383.

[169] J.Lopez-Pavon D.Meloni O.Yasuda A.Donini, K.Fuki. The discovery channel at the neutrino factory: $\nu_\mu \to \nu_\tau$ pointing to sterile neutrinos. arXiv:0812.3703.

[170] International Design Study of Neutrino Factory, http://www.ids-nf.org.

[171] IDS-NF Steering Group. 2008, IDS-NF-Baseline-2007/1.0.

[172] W.Winter J.Tang. Physics with near detectors at a neutrino factory. *Phys.Rev.D*, 80(053001), 2009, arXiv:0903.3039.

[173] A.Meregaglia A.Muller A.Rubbia A.Badertscher, M.Laffranchi. First results from a Liquid Argon time projection chamber in a magnetic field. *Nucl.Instrum.Meth.A*, 555:294, 2005, arXiv:physics/0505151.

[174] A.Rubbia. Underground neutrino detectors for particle and astroparticle science: the giant liquid argon charge imaging experiment (glacier). *J.Phys.Conf.Ser.*, 171(012020), 2009.

[175] on behalf of the MINERvA collaboration K.S.McFarland. MINERvA: A dedicated neutrino scattering experiment at NuMI. arXiv:physics/0605088.

[176] Minerva Collaboration (Fermilab E938). Proposal to perform a high-statistics neutrino scattering experiment using a fine-grained detector. arXiv:hep-ex/0405002.

[177] D.G.Brook-Roberge for the T2K Collaboration. Neutrino interaction measurements using the T2K near detectors. arXiv:1109.6728.

[178] Y.Kudenko (Representing the T2K Collaboration). The near neutrino detector for the T2K experiment. arXiv:0805.0411.

[179] D. Karlen. Near detectors for the T2K experiment. *Nucl.Phys.Proc.Suppl.*, 159:91–96, 2006.

[180] T.Schwetz P.Huber. A low energy neutrino factory with non-magnetic detectors. arXiv:0805.2019.

[181] M.Apollonio et al. (CERN working group on oscillation physics at the Neutrino Factory). Oscillation physics with a neutrino factory. arXiv:hep-ph/0210192.

[182] D.Autiero et al. The synergy of the golden and silver channels at the neutrino factory. *Eur.Phys.J.C*, 33:243, 2004.

[183] D.Meloni P.Migliozzi F.Terranova A.Donini, M.Maltoni. Sterile neutrinos at the CNGS. arXiv:0704.0388.

[184] W.Winter C.Giunti, M.Laveder. Short-baseline electron neutrino disappearance at a neutrino factory. arXiv:0907.5487.

[185] W.Winter P.Huber, M.Lindner. Simulation of long-baseline neutrino oscillation experiments with globes. arXiv:hep-ph/0407333.

[186] M.Lindner M.Rolinec P.Huber, J.Kopp and W.Winter. New features in the simulation of neutrino oscillation experiments with globes 3.0. arXiv:hep-ph/0701187.

[187] W.Winter. Optimization of a very low energy neutrino factory for the disappearance into sterile neutrinos. arXiv:1204.2671.

[188] P. Huber, M. Lindner, and W. Winter. Superbeams vs. neutrino factories. *Nuclear Physics B*, 645:3–48, November 2002, arXiv:hep-ph/0204352.

[189] T.Schwetz. Physics potential of future atmospheric neutrino searches. arXiv:0812.2392.

[190] D.Marfatia V.Barger, P.Huber and W.Winter. Which long-baseline neutrino experiments are preferable? *Phys.Rev.D*, 76(053005), 2007.

[191] T.Schwetz J.Kopp, M.Maltoni. Are there sterile neutrinos at the ev scale? arXiv:1103.4570.

[192] M.Rolinec W.Winter P.Huber, M.Lindner. Optimization of a neutrino factory oscillation experiment. arXiv:hep-ph/0606119.

[193] P.Adamson et al. [MINOS Collaboration]. Active to sterile neutrino mixing limits from neutral-current interactions in minos. *Phys.Rev.Lett.*, 107:2011, 011802, arXiv:1104.3922.

[194] S.Mohanty W.Grimus, P.Stockinger. Field-theoretical approach to coherence in neutrino oscillations. *Phys. Rev. D*, 59(013011), 1998.

[195] A.Yu.Smirnov E.Kh.Akhmedov, D.Hernandez. Neutrino production coherence and oscillation experiments. arXiv:1201.4128.

[196] Mikael Beuthe. Oscillations of neutrinos and mesons in quantum field theory. *Phys.Rept.*, 375:105–218, 2003, hep-ph/0109119.

[197] J.M.Conrad M.H.Shaevitz G.Karagiorgi, Z.Djurcic and M.Sorel. Viability of $\Delta m^2 \sim 1$ ev^2 sterile neutrino mixing models in light of MiniBooNE electron neutrino and antineutrino data from the Booster and NuMI beamlines. *Phys.Rev.D*, 80(073001), 2009, arXiv:0906.1997.

[198] Th.A. Mueller, D. Lhuillier, M. Fallot, A. Letourneau, S. Cormon, et al. Improved Predictions of Reactor Antineutrino Spectra. *Phys.Rev.*, C83:054615, 2011, 1101.2663.

[199] F.Boehm et al. Final results from the palo verde neutrino oscillation experiment. *Phys. Rev. D*, 64(112001), 2001, arXiv:hep-ex/0107009.

[200] Patrick Huber. On the determination of anti-neutrino spectra from nuclear reactors. *Phys.Rev.*, C84:024617, 2011, 1106.0687.

[201] Murray Gell-Mann. Test of the Nature of the Vector Interaction in beta Decay. *Phys.Rev.*, 111:362–365, 1958.

[202] Elena Giusarma, Martina Corsi, Maria Archidiacono, Roland de Putter, Alessandro Melchiorri, et al. Constraints on massive sterile neutrino species from current and future cosmological data. *Phys.Rev.*, D83:115023, 2011, 1102.4774.

[203] Gianpiero Mangano and Pasquale D. Serpico. A robust upper limit on $N_{\rm eff}$ from BBN, circa 2011. *Phys.Lett.*, B701:296–299, 2011, 1103.1261.

[204] M.Kobayashi and T.Maskawa. Cp-violation in the renormalizable theory of weak interaction. *Prog.Theor.Phys.*, 49:652–657, 1973.

[205] J. Schechter and J.W.F. Valle. Neutrino masses in SU(2) $\times$ U(1) theories. *Phys.Rev.D*, 22:2227–2235, 1980.

[206] J. Hoek S.M. Bilenky and S.T. Petcov. On the oscillations of neutrinos with dirac and majorana masses. *Phys.Lett.B*, 94:495–498, 1980.

[207] H. Nishiura K. Okuda M. Doi, T. Kotani and E. Takasugi. Cp violation in majorana neutrinos. *Phys.Lett.B*, 102:323–326, 1981.

[208] J. Schechter and J.W.F. Valle. Neutrino-oscillation thought experiment. *Phys.Rev.D*, 23:1666–1668, 1981.

[209] S.M.Bilenky and S.T.Petcov. Massive neutrinos and neutrino oscillations. *Rev.Mod.Phys.*, 59:671–754, 1987.

[210] S.R.Elliot and P.Vogel. Double beta decay. arXiv:hep-ph/0202264.

[211] S.Geer. Neutrino beams from muon storage rings: Characteristics and physics potential. *Phys.Rev.D*, 57:6989, 1998, arXiv:hep-ph/9712290.

[212] M.B.Gavela J.J.Gomez Cadenas P.Hernandez O.Mena S.Rigolin A.Cervera, A.Donini. Golden measurements at a neutrino factory. *Nucl.Phys.B*, 579:17, 2000, arXiv:hep-ph/0002108.

[213] M.Lindner M.Rolinec W.Winter P.Huber, J.Kopp. http://www.mpi-hd.mpg.de/personalhomes/globes/index.html.